ADVANCED MASTERS IN STRUCTURAL ANALYSIS
OF MONUMENTS AND HISTORICAL CONSTRUCTIONS

Master's Thesis

Enrique del REY CASTILLO

Parametric Study of a Historical Masonry Building Subjected to Seismic Loading

This Masters Course has been funded with support from the European Commission. This publication reflects the views only of the author, and the Commission cannot be held responsible for any use which may be made of the information contained therein.

Portugal | 2012

DECLARATION

Name:	Enrique del Rey Castillo
Email:	Enrique.rey.castillo@gmail.com

Title of the Msc Dissertation:	Parametric study of a historical masonry building subjected to seismic loading.
Supervisor(s):	Paulo B. Lourenço
Year:	2011/2012

I hereby declare that all information in this document has been obtained and presented in accordance with academic rules and ethical conduct. I also declare that, as required by these rules and conduct, I have fully cited and referenced all material and results that are not original to this work.

I hereby declare that the MSc Consortium responsible for the Advanced Masters in Structural Analysis of Monuments and Historical Constructions is allowed to store and make available electronically the present MSc Dissertation.

University:	Universidade do Minho
Date:	July 17th, 2012
Signature:	_____

Le quiero dedicar ésta tesis, fruto de varios meses de duro trabajo, a mi familia, a mis amigos (esos que se pueden contar con los dedos de una mano) y al azar, por haber nacido donde he nacido y haberme criado bajo las condiciones en que me he criado. Pero le quiero agradecer especialmente a mis padres su apoyo incondicional, siempre y a todos los niveles.

ABSTRACT

Earthquakes are one of the natural hazards that have caused more losses to the mankind. Besides countless human lives, earthquakes have destroyed buildings and even cities in many places and civilizations around the world. However, the nature and origin of earthquakes, as well as their effect in built structures, have been studied in detail only recently. An important factor that influenced the progress of this science is the development of computing, which allowed to carry out complex calculations. In parallel to that, many researches have been done in the last years aimed at understanding and reproducing the effects of earthquakes in built structures.

Thanks to the combination of new methods of structural analysis and powerful computing resources, accurate approaches of the behavior of a specific structure can be done nowadays. The two more widely used structural analysis methods are adopted in this thesis, namely Pushover Analysis and Time Integration Analysis. The Finite Element Method (FEM) is used to model a case study and to discuss the obtained results in detail.

The case study is a ‘‘Gaioleiro’’ building, a traditional stone masonry typology used mainly in Lisbon, Portugal, between the 19th and 20th century. The study of this building started years ago with a shaking table test carried out by the National Laboratory of Civil Engineering in Lisbon (LNEC), together with University of Minho. Subsequently, a FEM model was calibrated by other authors according to the results obtained in this test.

The present thesis starts with a brief introduction, some basic background about seismic engineering and a brief description of the adopted FEM model. Then the results obtained for the model with Pushover and Time History Analyses are discussed, with the aimed to contribute for the validation and application of pushover analysis in the seismic assessment of historical masonry buildings without box behavior. The main body of the thesis includes a sensitivity analysis intended to assess the influence of the material properties in the behavior of the structure, as well as the impact of rigid diaphragm floor structures and the load pattern distribution in the response of the building. The sensitivity analysis is performed for both Pushover and Time History Analyses, in order to discuss the objectivity of the results.

RESUMO

Estudo paramétrico de um edifício de alvenaria histórica submetido a ações sísmicas

Os terremotos são um dos perigos naturais que causaram mais perdas para a humanidade. Além de inúmeras vidas humanas, os terremotos destruíram edifícios e até cidades em muitos lugares e civilizações ao redor do mundo. No entanto, a natureza e a origem de sismos, bem como o seu efeito em estruturas construídas, têm sido estudadas em detalhe apenas recentemente. Um fator importante que influenciou o progresso desta ciência é o desenvolvimento da computação, o que permitiu a realização de cálculos complexos. Em paralelo a isso, muitas investigações têm sido feitas nos últimos anos que visam compreender e reproduzir os efeitos de terremotos em estruturas construídas.

Graças à combinação de novos métodos de análise estrutural e recursos computacionais poderosos, as abordagens precisas do comportamento de uma estrutura específica podem ser feitas hoje em dia. Os dois métodos de análise estrutural mais utilizados são adotados nesta tese, a saber a Análise Pushover e Análise dinâmica com integração no tempo. O Método dos Elementos Finitos (MEF) é usado para modelar um estudo de caso com estas técnicas e discutir os resultados obtidos em detalhe.

O caso de estudo é um edifício gaioleiro, uma tipologia tradicional de alvenaria de pedra usado principalmente em Lisboa, Portugal, entre os séculos XIX e XX. O estudo deste edifício começou há alguns anos com um ensaio de mesa sísmica realizado pelo Laboratório Nacional de Engenharia Civil, em Lisboa (LNEC), em conjunto com a Universidade do Minho. Subsequentemente, um modelo MEF foi calibrado por outros autores de acordo com os resultados obtidos neste teste.

A presente tese começa com uma breve introdução, algumas informações básicas sobre engenharia sísmica e uma breve descrição do modelo MEF adotado. Em seguida, os resultados obtidos para o modelo com Análises Pushover e com integração no tempo são discutidos, com o objetivo de contribuir para a validação e aplicação de análise avançada na avaliação sísmica de edifícios históricos de alvenaria sem comportamento do tipo caixa. O corpo principal da tese inclui uma análise de sensibilidade destinada a avaliar a influência das propriedades do material no comportamento da estrutura, bem como o impacto da rigidez da de diafragma do pavimento e do padrão de distribuição de carga na resposta do edifício. A análise de sensibilidade é realizada tanto para Pushover como para a integração no tempo, a fim de discutir a objetividade dos resultados.

RESUMEN

Estudio paramétrico de un edificio histórico de albañilería sometido a cargas sísmicas.

Los terremotos son uno de los fenómenos naturales que han causado más pérdidas en la historia de la humanidad. Aparte de incontables vidas humanas, los terremotos han destruido edificios e incluso ciudades enteras en muchos lugares y civilizaciones diferentes alrededor del mundo. Sin embargo, la naturaleza y origen de los terremotos, así como su efecto en las estructuras, han sido estudiados en detalle solo en tiempos recientes. Un factor importante que ha influido en el progreso de esta rama de la ingeniería es el desarrollo de la informática, que ha permitido llevar a cabo cálculos complejos. En paralelo a esto, muchas investigaciones han sido realizadas en los últimos años, enfocadas a comprender y reproducir los efectos de los terremotos en las estructuras.

Gracias a la combinación de nuevos métodos de análisis estructural y potentes recursos computacionales, aproximaciones precisas del comportamiento de una estructura específica ante cargas estáticas y dinámicas pueden ser realizados actualmente. Los dos métodos de análisis estructural más ampliamente usados en el campo académico son adoptados en esta tesis, a saber; análisis de Pushover y análisis de tiempo-historia. El método de elementos finitos (MEF) es usado para modelar el objeto de estudio y discutir en detalle los resultados obtenidos.

El objeto de estudio es un edificio ‘‘Gaioleiro’’, una tipología tradicional basada en albañilería de piedra y usada principalmente en Lisboa, Portugal, entre los siglos 19 y 20. El estudio de este edificio comenzó hace años con un ensayo realizado en una mesa de vibración por el Laboratorio Nacional de Ingeniería Civil (LNEC) en Lisboa, junto con la Universidad de Minho. Posteriormente, un modelo realizado con el método de elementos finitos fue calibrado por otros autores de acuerdo con los resultados obtenidos en este ensayo.

La presente tesis comienza con una breve introducción, algunos conocimientos básicos sobre ingeniería sísmica y una breve descripción del modelo adoptado. Los resultados obtenidos con el análisis de Pushover y de tiempo-historia son analizados y discutidos. El principal objetivo de este análisis es la contribución en la validación y aplicación del análisis de Pushover en la valoración sísmica de edificios históricos de albañilería sin comportamiento de ‘‘caja’’. El cuerpo principal de la tesis incluye un análisis de sensibilidad con el objeto de evaluar la influencia de las propiedades de los materiales en el comportamiento de la estructura, así como el impacto que diafragmas rígidos y diferentes patrones de distribución de cargas pueden tener en la respuesta del edificio. El análisis de sensibilidad es llevado a cabo para ambos análisis, los de Pushover y de tiempo-historia para discutir la objetividad de los resultados.

TABLE OF CONTENTS

Chapter 1

Introduction

1.1 Masonry and Earthquakes

Masonry is a construction technique used for centuries all over the world, from Europe to Asia, as well as in Africa or America. In places where stone was available the buildings started to be made just placing one stone over another without any mortar. The stones could be placed just as found in nature, but later on, when carving tools were developed, stones were dressed to assure a better adjustment. As man started to find out how to use clay, lime or other mortars, masonry evolved to more sophisticated arrangements, bonding the units with these mortars. In places where stone was not available, construction techniques were slightly different. The units needed to be made by man, usually mixing mud and straw, and letting the mix to dry at the sun. It was common to use the same mud as mortar in the joints. This earth based technique is still much in use today in developing countries. The third big family of masonry techniques is the one made by using clay brick fired in ovens. Again different kind of mortars can be used in the joints, made with clay, cement, lime, glue, etc. To summarize, the evolution of humanity is connected to the history of architecture and of the materials used to build, (Musgrove and Fletcher, 1987), (Davey, 1961).
Nowadays there is a large range of materials and construction techniques available in the market. Some examples of masonry are shown in Figure 1, (Roca, P et all, 1998) In the case study the units are granite stone and the joints are made with lime mortar.

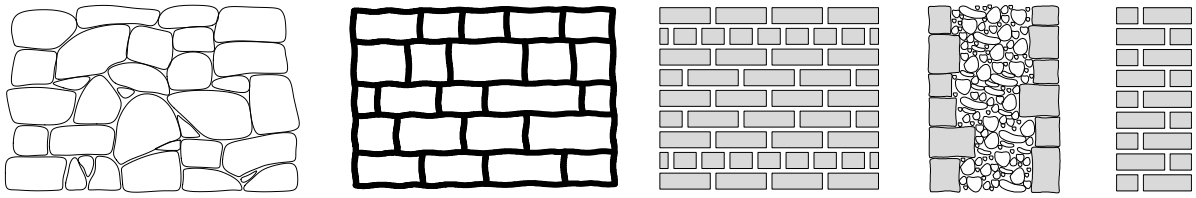

Figure 1 - Different masonry bond: (a) bond in the wall face; (b) internal structure.

The seismic performance of masonry structures is related with many characteristic of the materials, as well as the quality of the workmanship and the structural configuration. The seismic performance of stone masonry construction is generally very poor. The main reason is the low tensile strength of the masonry and the poor bond provided by the irregular units. Timber roof and floor structures are usually light and they do not induce large additional seismic forces, in contrast to masonry that is rather heavy. However, the connections and horizontal structures are not very stiff and thus the structures are flexible and are not able to form a rigid diaphragm; there is not box behaviour. Several researches have been done already regarding the behaviour of flexible-rigid diaphragms. Some examples can be seen in (Brignola et al. 2008, Yi 2004, Paquette and Bruneau 2000, Tomaževic et al. 1996 and Lutman 2011)

A “Gaioleiro” building is a traditional stone masonry typology used between the middle of the 19th century and the beginning of the 20th century, in the Lisbon (Portugal). The development of the city in the middle of the 19th century attracted many constructors from small villages, who extrapolated the methods from one or two storey buildings to these four or five storey buildings, Construir Portugal (2012). These buildings are part of the transition period from the ‘pombalino’ buildings, with anti-seismic practices as timber frames in the walls, and the modern reinforced concrete frame buildings, (Lourenço, Mendes, et al. 2011, Ramos and Paulo B Lourenço 2004). Many examples of these buildings remain in use nowadays, as shown in Figure 2, (Mendes and P.B. Lourenço 2009)
Their typology is usually based on masonry walls with timber floors and roof. The external walls are, usually, in rubble limestone masonry with lime mortar. A key feature regarding the seismic assessment of these building is the fact that the connection between walls and floors is very weak.

Figure 2 - Examples of “Gaioleiro” buildings, Lisbon, Portugal.

Lisbon is located in a region of moderate seismicity and suffered a catastrophic earthquake in 1755. An earthquake is the result of the release of energy in the crust of the earth, originating, basically, due to two factors; volcanic activity and tectonic drifts. Earthquakes due to volcanic activity are usually weak, so the most important earthquakes to take into account are the ones produced by tectonic drifts. Tectonic plates are in constant drift. When two tectonic plates are drifting against each other all the energy used to move these plates is stored in the material where the two plates contact. This energy is stored till it reaches a certain limit, which the material is able to bear. Then, the two plates moves and this energy is suddenly released, causing seismic waves.
A map with the frequency of earthquakes in the years between 1963 and 1998 is shown in Figure 3, Digital Tectonic Activity Map (2012), with the main faults between tectonic plates. In places where there is higher concentration of earthquakes the tectonic plates are pushing against each other. If the concentration is not so high it means the tectonic plates are moving apart.

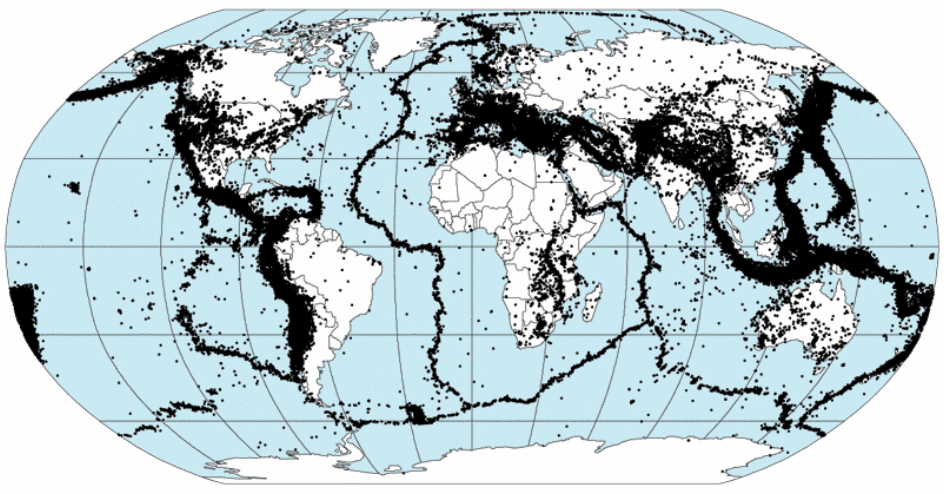

Figure 3 - Map of earthquake concentration between 1963 and 1998.

The point where this energy is released is called hypocentre. As shallower the hypocentre is the more damage it causes to buildings. From the hypocentre the seismic waves travel through the earth. The point just above the hypocentre is called epicentre, and it is in the surface of the earth. In this surface the earthquakes cause horizontal and vertical waves, which affect to the structures in different ways, Oliveira (2012).

1.2 Contents of the thesis

The main goal of the thesis is to contribute in the validation and application of pushover analyses in the seismic assessment of historic masonry structures. To achieve this objective the thesis has been divided in two different parts. In the first part a parametric study is performed to compare the results between pushover analysis and time history analysis. A thorough sensitivity analysis of the parameters involved is carried out in order to evaluate their influence in the results. As an example, the influence of stiffness of the floor diaphragm in the global behaviour is assessed. In the second part pushover analyses are performed considering force based and displacement based approaches for the mass distribution. Within these two possibilities of performing pushover analysis, also different usual load patterns are applied: the typical mass proportional, inverted triangle and first mode proportional. Besides these load patterns, innovative load patterns are applied as well, namely adaptive modal and multimodal.

The thesis starts with some basic concepts about seismicity, as well as a description of the different analysis techniques used in the subsequent chapters. Afterwards a description of the case study is given, with a brief description of the process followed to calibrate the model. The description includes

the characteristics of the finite element model, the properties of the materials and the loads, both for static and dynamic loads.

The main body of the thesis starts thereafter, with the parametric study, i.e. the comparison between pushover analysis and time history analysis, as well as the discussion of the influence of different parameters in the final results. Then, a comparison between different load patterns for pushover methods is carried out, with a distinction between force based and displacement based but also between the different load patterns to apply in the model.

Finally, conclusion and suggestions for future works completes the thesis.

Chapter 2

Seismic analysis

Abstract

This chapter provides a brief review about seismic behaviour and basic knowledge about seismic analysis. Afterwards the main analysis techniques to be used in the thesis are introduced, namely nonlinear static and nonlinear dynamic analyses. Besides a brief explanation on how the techniques work and some of their advantages and disadvantages are highlighted. In the last part of the chapter, the concept of safety assessment is addressed and descriptions of the different pushover methods to be used are given, together with a discussion on the load patterns later used in the pushover analyses.

2.1 State of the art

Earthquakes have caused countless losses in the humanity history. Besides the earthquake itself, seismic waves can cause several different natural disasters such as land sliding, floods, tsunamis or fires. However, this thesis is focused in the effect of earthquake in structures, i.e. how the ground motion due to the earthquake affects a specific building. Earthquakes have affected the built heritage from the beginning of the history. The earliest cultures in Middle East had already some kind of anti-seismic construction techniques. These construction techniques and others developed in different civilizations have been employed in many parts of the world and in different times. But there is a common feature: all of them were based in the experience of the builders and the trial and error method.

In recent times several researches have been carried out regarding the nature, origin, and effects of earthquakes in the built heritage. Several factors have influenced this development, mainly from two sources. The first one and most obvious is the progress of the science, which allowed to carry out more advanced calculations (especially with the introduction of computing), more complex and higher buildings and, at the same time, build them in a safer a more economical way. The second source is related with the advance of the society itself, which gives a higher value for human life and provides more understanding and appreciation of the value of ancient buildings as a source of knowledge and a cultural heritage. A new branch of the structural analysis science was born and is growing day by day: seismic analysis. The aim of this science is to understand and explain the seismic behaviour of the buildings. The seismic behaviour, or seismic response of a building, is a complex science which depends on many factors. Thus, there are several research fields involved in this process; computational engineering, structural engineering, material engineering, soil engineering, seismic engineering, etc.

In a simplified way, the building features that influence more the response of the building to an earthquake are, basically, the construction techniques, the material properties and structural configuration. In this paper the construction techniques and structural configuration are fixed, as only one case study is analysed. Thus, only possible changes in the material properties will be assessed, regarding their influence in the structural behaviour of a given earthquake. Besides the building features, the influence of the applied load is assessed as well.

Vibration modes or modes of response are oscillation systems with a pattern of motion in which all parts of the system move sinusoidally with the same frequency and with a fixed phase relation i.e. how the building will move depending on its structural configuration. Modes of response do not depend on the load the building is subjected to. Even simple buildings usually have too many modes of response and they need not to be all taken into account. Usually, only the first ones are important and have relevant influence in the final response of the building. Thus, only the first modes of response are often

used in the calculations of the building response. Figure 4 shows examples of the first three modes of response of a Gaioleiro building, (Mendes et al. 2010): 1st mode is transversal, 2nd mode is rotational and 3rd mode is longitudinal.

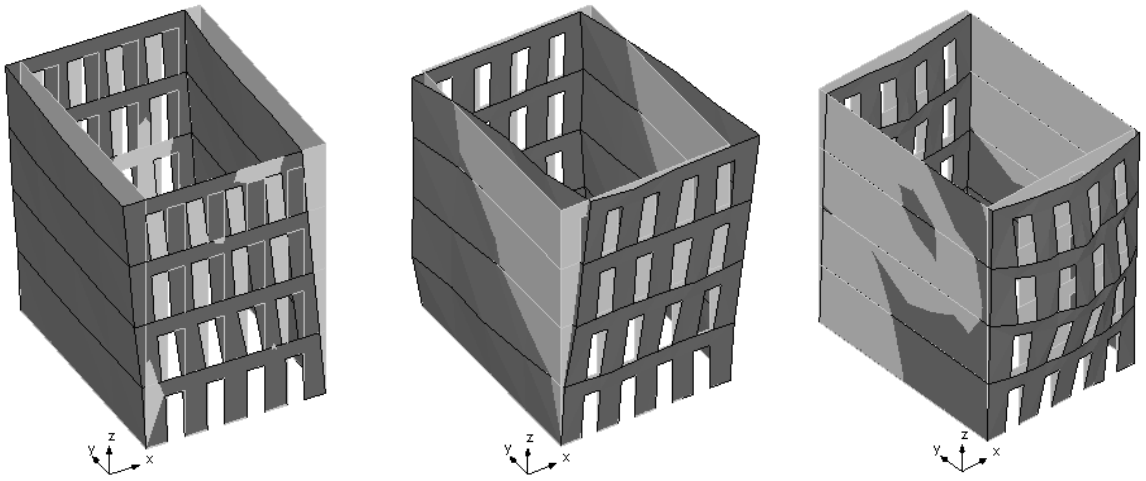

1st Mode [4.93 Hz] 2nd Mode [8.45 Hz] 3rd Mode [12.08 Hz]

Figure 4 - First three modes of response for a Gaioleiro building.

Macro-block analysis consists of dividing the model into several rigid blocks, which have a common feature or behaviour. This method is a simplification of the actual performance of the building and the number of blocks to divide the building depends on the behaviour predicted to occur in the case study. For masonry structures under seismic loading, in most cases collapse occurs with loss of equilibrium in masonry portions or blocks. The verification for these mechanisms has a meaning if a certain monolithic behaviour within the blocks themselves is guaranteed i.e. if the blocks remain together.

There are two types of local mechanisms in masonry building; perpendicular to the plane of the wall (out of plane) or parallel of the plane of the wall (in plane). The first type of mechanisms is more common in historical buildings since the tensile performance of the masonry is poor and connections are poor.

Two examples of mechanisms of macro block analysis are shown in the Figure 5. In the case (a) a tower is falling apart of the rest of the building. In the case (b) the whole façade overturns and separates from the main body of the building, (Lourenço et al. 2011). This method of analysis is recommended for assessment and design, but requires a good definition of the possible failure mechanisms. This might be a difficult challenge in many practical applications.

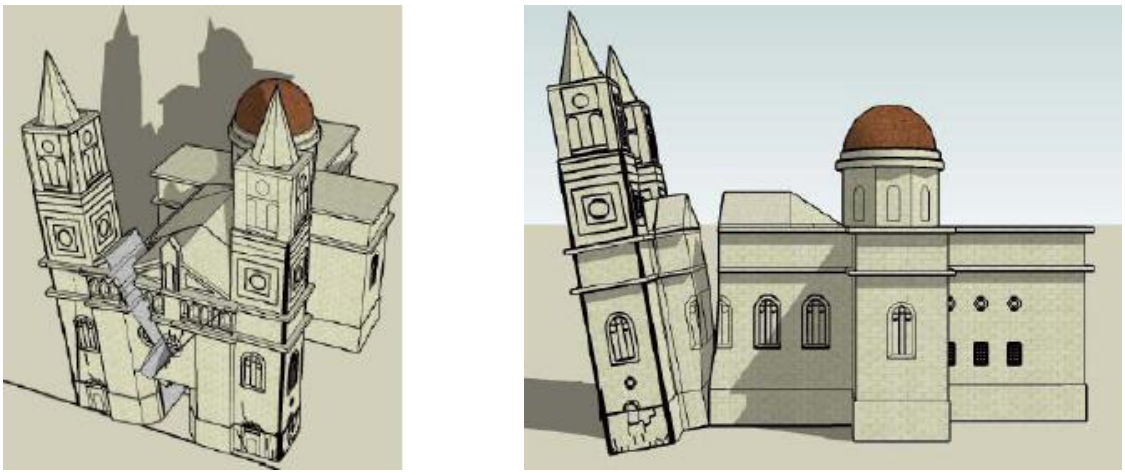

(a) (b)

Figure 5 - Examples of mechanisms due to block analysis. (a) overturning of the bell towers and (b) overturning of the main façade.

Non-linear static analysis is usually required for existing masonry structures because the response is expected to be controlled by the inelastic properties. Pushover methods usually assume that the seismic behaviour depends only in the fundamental mode, and that this mode does not change when the structure yields. For historical buildings, higher modes can be important for the final behaviour or significant torsional irregularities can be present in the building, meaning that pushover methods can provide unrealistic results. Still, this is a much used technique in the seismic assessment of masonry buildings.

In static analysis (pushover) horizontal forces are applied, without dynamic effects, incrementally to define a capacity curve. This process can be combined with a demand curve such as an equivalent response spectrum, reducing thus the problem to a single degree of freedom one, (PAN and Ohsaki 2006). This procedure is based on the assumption that the response is controlled by the elastic fundamental mode and that the mode shape remains unchanged after the structure yields, (Krawinkler and Seneviratna 1998). To perform this analysis the gravity loads have to be constant and the horizontal loads are increased monotonically. According to (CEN 2003a, 2003b), at least two distributions of the lateral loads should be applied:

- a “uniform” pattern, based on lateral forces that are proportional to mass regardless of elevation (uniform response acceleration);
- a “modal” pattern, proportional to lateral forces consistent with the lateral force distribution in the direction under consideration determined in elastic analysis (in accordance with lateral force method or modal response spectrum analysis).

Besides these two load patterns that the (CEN 2003a, 2003b) defines as compulsory, three other load patterns will be used in this thesis. One of them is the inverted triangular pattern, which is well known and represents an approximation of the first mode of response. The other two load patterns used, adaptive modal pattern and multimodal pattern, have been proposed more recently and have been scarcely used, particularly for masonry structures is limited. These load patterns will be explained in detail in the Section 3.4.

After applying the incremental loading, the relation between the shear force at the base and a control displacement at the top has to be determined for values in a range between zero and 150% of the target displacement. The target displacement is the maximum displacement that the structure is able to bear, obtained from the elastic response spectrum of an equivalent SDOF system. Since the target displacement is not available in the case study, its value depends on the calculation. However, the displacement for each assumption is big enough to assure that the results are valid. The relation between shear force and displacement is the so-called ‘‘capacity curve’’, which is basically the response of the structure. Each point of the capacity curve represents an effective and equilibrated stress-state of the structure, i.e. a deformation shape which corresponds to the applied external lateral loads, (Antoniou and Pinho 2009). Besides the capacity curve, it is possible to obtain the collapse mechanisms and different values of quantities, such as maximum displacements, maximum stresses, etc. Figure 6 shows examples of capacity curves for a structure with different materials, (Jianguo et all 2006).

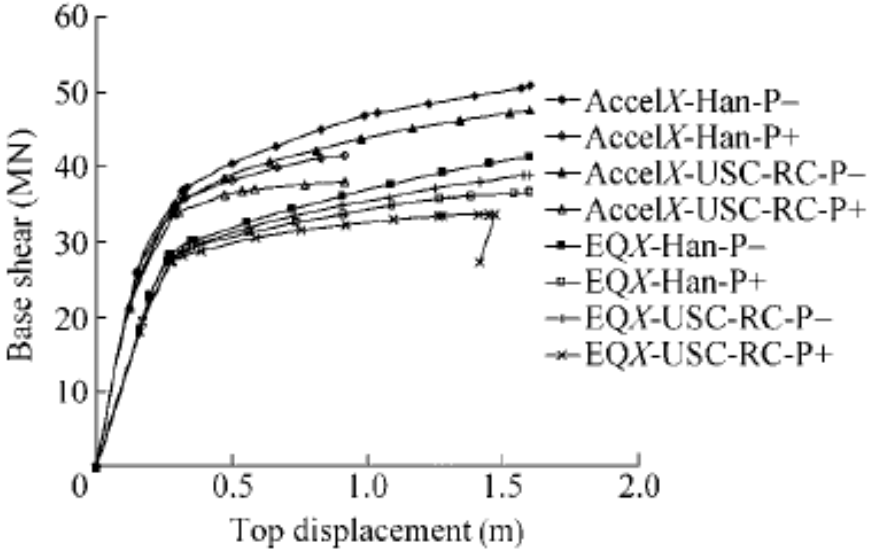

Figure 6 - Capacity curves for a structure with different materials.

In *non-linear dynamic analysis* (time integration) the earthquake accelerograms are given as external actions which duration is the same than the duration of earthquake itself. The structure is thus considered with dynamic properties, which change throughout time. This method is based on the equation of motion, shown in Eq. (1);

$$m\ddot{u} + c\dot{u} + ku = p(t) \tag{1}$$

Where;

m is the mass and $\ddot{u}$ is the acceleration

c is the damping and $\dot{u}$ is the velocity

k is the stiffness and u the is displacement

p is the external force and t is the time step

A time step needs to be selected and the initial conditions need to be given. Then the acceleration, velocity and displacement are calculated step by step based on these assumptions. Thus, it is possible to obtain the values of acceleration, velocity and displacement during the duration of the earthquake.

Time history analysis is the most accurate method for assessing the response of structures subjected to earthquake actions. However, such type of analysis has also difficulties or drawbacks, particularly for what concerns application in a design office context. The first inconvenience, as it is said in (Bommer and Acevedo 2004), is to find a specific ground motion compatible with the seismic hazard spectrum for the place where the case study is located. Nonlinear time-history analyses are also computationally demanding and require much time for the calculation and for analysing the results obtained. To run this kind of calculations, powerful computers are also usually needed. Usually, preliminary simpler analyses, such as modal and static analyses, are run to allow a first check of the model, (Antoniou and Pinho 2009). Usually several different earthquake records need to be used, assuming the results as the average of the most conservation response. For a low number of records, the value of E_d is the most unfavourable of the response quantity among the analyses. E_d is the design value of the action effect due to the seismic effect. This value should be lower than R_d, which is the design resistance value of the element and depends on the material used.

Parametric studies are particularly relevant and have several aims because of the scarce use of time history analysis and the potential effect of changing the control parameters. To start a parametric study some assumptions are required. First of all the parameters to change and their ranges must be defined. Once the parameters for use in the simulation and their ranges have been established it is convenient to set up various possible parametric configurations. The first parameter to be changed here is the stiffness of the floor panels, to evaluate the influence of rigid diaphragm floor structure in the actual behaviour of the structure. The second parameter is the damping ratio. For masonry several

other parameters are assessed, namely the modulus of elasticity assessed, tensile strength and tensile fracture energy. All these parameters are explained in detail in the Section 3.3.

2.2 Safety assessment

Safety assessment is a very important part of the design of new structures because it ensures the integrity of the construction and saves human lives. In the case of ancient construction, it also preserves the architectural and cultural heritage. Seismic safety assessment is a compulsory evaluation established in the (CEN 2003a, 2003b), which aims at determining the expected collapse mechanism and the building lateral strength and displacement capacity. The building integrity has to be verified at the relevant limit states;

- Ultimate limit state: under the design seismic action (probability of exceedance of 10% in 50 years) the buildings are heavily damaged, both in structural and non-structural elements. The buildings have to keep residual resistance, lateral stiffness and the whole bearing capacity with reference to the vertical loads. Collapse of the building is not allowed.
- Damage limitation state: under the seismic actions with lower return period (probability of exceedance of 50% in 50 years) the buildings cannot be heavily damaged. Structural damage is limited.

Pushover methods are used to perform the safety assessment. They can be divided in force based methods and displacement based methods. Within each method there are different ways to apply the force; mass proportional, first mode proportional, adaptive modal pushover analysis and multimodal pushover analysis. These methods are a static approach; the response spectrum is used as input instead of the whole accelerogram of the earthquake. Thus, only peak values will be obtained and not the whole time history of the displacements of the building.
The *force based* design procedure starts by proportioning the strength and stiffness for the structure in critical elements to calculate the periods. From there it is possible to calculate the seismic forces and analyse the structure. If the displacements are bigger than the maximum allowed it is necessary to start from the beginning, Máca and Oliveira (2011) (“Assessment and improvement of the structural performance of Buildings in Earthquakes” 2006). This method is not widely used because iterations are needed and it is more time consuming than displacement based methods.

The *displacement based* design approach starts from the target displacements. Then the analysis is performed and strength and stiffness are determined (as the end result of the design process) to achieve the design displacements. The method defines the capacity of a building relating the potential deformation (displacements) with its fundamental period of vibration at different limit states. Afterwards this relation is compared with a displacement response spectrum to assess the integrity of the

building. Figure 7 shows an example of the relation between expected displacements (straight line with circles) and capacity curve. In this example, for the periods between 0.9 and 3.15 second the building would collapse, see (Crowley et all 2004).

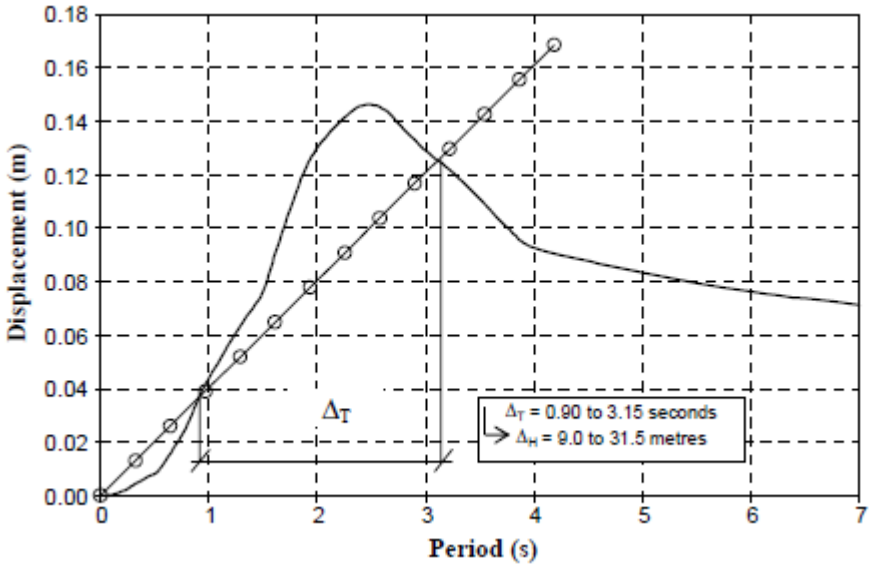

Figure 7 - Expected displacement against capacity curve.

Chapter 3

Description of the case study

Abstract

In this chapter the case study is fully described. The chapter starts with a geometrical description of the model and an explanation of how the adopted parameters were set up. Then the material properties are described from the modelling point of view. The chapter includes both the parameters to be assessed in subsequent chapters and those which will not be modified. The material behaviour is also explained. The last part of this chapter defines the load to be applied in the model. For static loads the different modal patterns that are going to be used in subsequent chapters are defined. For dynamic loads the accelerograms of the input in both North-South and East-West direction are given and described.

3.1 Geometrical description

The building chosen for this case study is representative of a typical building typology used from middle of the 19th century to the beginning of 20th century, with four storeys. The load bearing structural configuration of the building, which is semi-detached to the surrounding buildings, is constituted by two parallel gabble walls without openings and two main parallel façades. All walls are made of masonry and are considered to have the same characteristics. The building is considered to be isolated next, instead of semi-detached, as this is the way it was tested on the shaking table. The floors are made with timber joists and MDF panels. There are timber beams attached to the walls, connected with the floor system and to the masonry walls. These panels are taken into account in the parametric study to discuss the influence of rigid diaphragm floors on the seismic behaviour, (Mendes and P.B. Lourenço 2009)

The dimensions of the whole building in real scale are 9.45 X 12.45 meters in plan with an inter-storey height of 3.60 meters. Since the building has 4 storeys, the total height is 14.40 meters. The façades have 16 openings of 2.70 X 0.90 meters, which results in a percentage equal to 28% of openings. The walls have a thickness of 0.51 meters. The thickness of the MDF panels is 0.036 meters. The dimensions of the timber joists are 0.30 X 0.225 meters. In Figure 8 a general view of the building with the dimensions and the orientation of the façades can be seen.

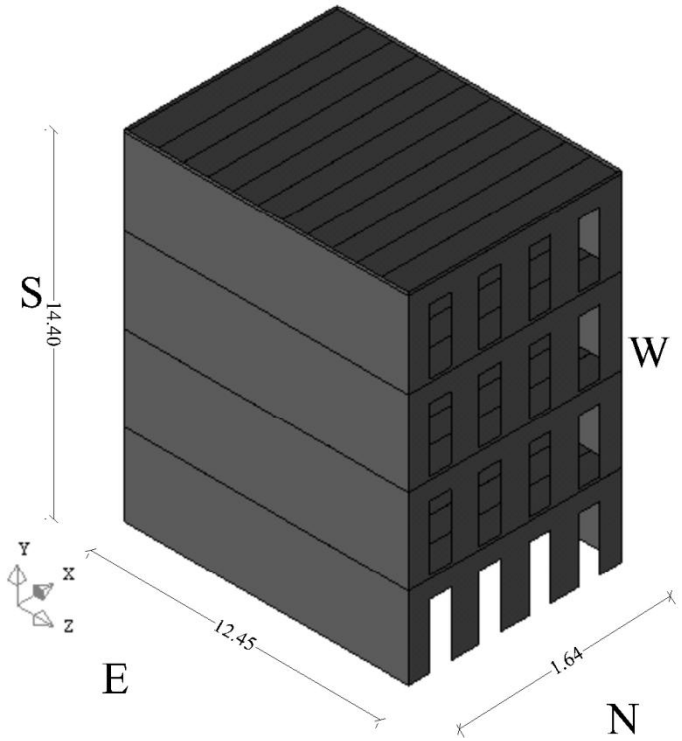

Figure 8 - General perspective of the case study building, units in meters.

3.2 Finite element model

The numerical code used for the finite element modelling is Diana V.9.4. Shell elements are used in the finite element modelling for the walls and MDF panels. For the timber joists modelling, beam elements are used. The shell element used is called CQ40S, which is an eight-node quadrilateral isoparametric curved shell element. This element is based in quadratic interpolation with Gauss integration over the area and Gauss or Simpson over the thickness. The adopted integration scheme has four integration points in the plan and five Simpson integration points in the thickness. Thus, each element has 20 integration points. The beam element used is called CL18B and it is a three-node, three-dimensional class-III beam element. The variables are the translations and the rotations in the nodes, in the three directions. The boundary conditions were assigned to the base of the building, which is totally fixed to the ground; both translational and rotational movement are restricted.

The calibration of the model was made previously by (Yang 2010).To calibrate the model a mock-up was prepared to reproduce the characteristics of the case study; geometrical, physical and dynamical. There was a size limitation due to the shaking table measures, so all the dimensions of the mock-up were reduced 1:3 from the real ones. The tests carried out at the 3D shaking table of the National Laboratory of Civil Engineering (LNEC), Lisbon, and can be seen at (Candeias et al. 2004). In this work, full scale values were used because the objective is not to compare the model with the experimental tests. Using a full scale model allows to avoid any size effect.

3.3 Material properties of the finite element model

3.3.1 MDF panels and timber joists

In order to assess the influence of rigid diaphragms in floor structure the stiffness of the MDF panels is modified to perform four different calculations, besides the reference one. The parameter changed to assess the stiffness is the modulus of elasticity, which is underlined next; the other parameters explained in this section (Poisson ratio and density) are not changed in the parametric study, and they are just italicized.

The *modulus of elasticity* is also known as the Young's modulus, and it is defined as the ratio of the uniaxial stress over the uniaxial strain in the range of stresses in which the Hooke's law governs. Thus, the floor structures have only linear behaviour. Another two properties of the timber joists and MDF panel need to be assigned: Poisson ratio and density. When a material is stretched or compressed it tends to shrink or expand. This is called the Poisson effect. *Poisson ratio* is the relation between these shrinkages or expansions and their related tensile or compression stresses. The *density* is the quantity of mass per volume of material. These two values, Poisson ratio and density, remain constant in the model; their influence is not evaluated in the parametric study. Though timber joists are not included in the parametric study their properties are given below, as well as the

properties of the MDF panels. The underlined property (Modulus of elasticity) is changed in the sensitivity analysis. The italicized ones (Poisson ratio and density) remain constant.

- Timber joists:
  - *Modulus of elasticity* equal to $12x10^3$ MPa
  - *Poisson ratio* equal to 0.3
  - *Density* equal to 580 kg/m^3
- MDF panels:
  - <u>*Modulus of elasticity*</u> equal to $0.14x10^3$ MPa
  - *Poisson ratio* equal to 0.3
  - *Density* equal to 760 kg/m^3

3.3.2 Masonry walls

The masonry is considered to have inelastic behaviour. The modulus of elasticity defines the elastic stiffness and its influence in the final results is assessed. The inelastic behaviour is mostly governed by the strength and the fracture energy. The influence of these two parameters is evaluated only in tension. Since the collapse in masonry is usually due to the lack of tensile strength the values of compression are not modified for the sensitivity analysis. Damping is also assessed to study the influence of the oscillations in the structure. All of the evaluated parameters are underlined, while the parameters which are not taken into account in the parametric study are just italicized.

<u>*Modulus of elasticity*</u>, *Poisson's ratio* and *density* were already explained in the definition of the properties of the floor structure. <u>*Tensile strength*</u> is the maximum stress that a material is able to withstand while being axially stretched.

The behaviour of the material is linearly dependent from zero to the point where the tensile strength is reached, which is equivalent to the crack point. After that, the softening starts and, in the case study, it has an exponential behaviour. At the beginning strains decrease slowly for a large variation of stresses. At the end of the curve the strains experiment a big variation for a small decrease of stresses. A graphic representation of this exponential behaviour is shown in Figure 9, Diana user's manual, Manie, J. 2010.

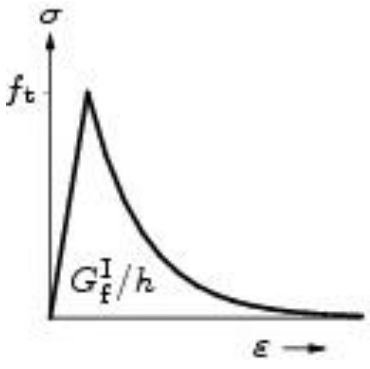

Figure 9 - Exponential behaviour.

<u>*Fracture energy in tension*</u> *(Gft)* is defined as the energy consumed to cause the total breakage of the material by tensile forces per unit area of the fracture plan. The fracture area is the projected area on a plane parallel to the crack direction, (Hillerborg 1985).

$$G_f = \frac{absorbed - fracture - energy}{fracture - area} \quad (1)$$

Compressive strength is the maximum capacity of materials to withstand the stresses while being axially compressed. *Fracture energy in compression (Gfc)* is defined as the energy consumed to cause the total breakage of the material by compressive forces per unit area of the fracture plan.

In the case study the compressive behaviour of the masonry is parabolic. The strains decrease as the stresses decreases following a parabolic equation. When the compressive strength is reached the softening behaviour of the masonry follows the same equation, but in this case the stresses decrease as the strains increase. A graphic representation of this parabolic behaviour is shown in Figure 10, Diana user's manual, Manie, J. 2010.

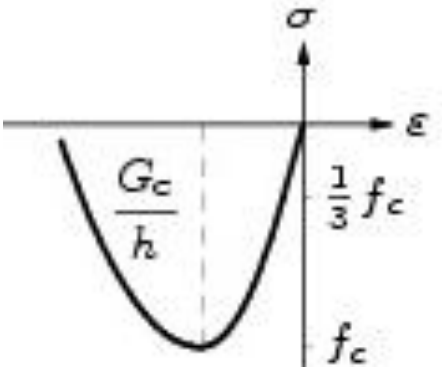

Figure 10 - Exponential behaviour.

Shear retention factor is the coefficient which modifies the shear strength after the crack point. Shear strength is the maximum stress the material is able to withstand when it is subjected to shear forces before failure. Shear force tends to cause the failure of the material in a plain parallel to the force. In the case study the shear retention factor is constant. Thus, the shear behaviour is linearly dependent. This value is not involved in the sensitivity analysis; its value is constant for every calculation. A graphic representation of this parabolic behaviour is shown in Figure 11, Diana user's manual, Manie, J. 2010.

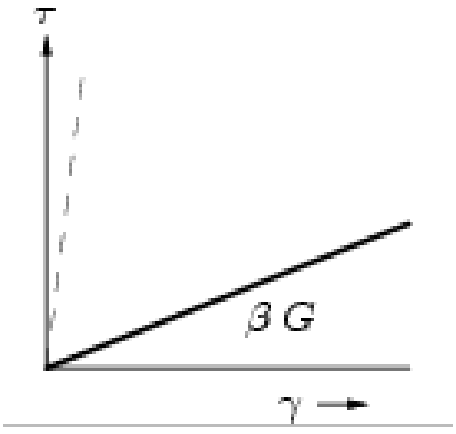

Figure 11 - Shear constant behaviour.

Damping reduces the amplitude of oscillations in the system. In other words, it is the mitigation of the vibration effects in a structured due to the dissipation of energy. Damping is linearly related to the velocity of the vibrations. For structures with many different mode shapes and a wide range of natural frequencies the most common and suitable type of damping is Rayleigh damping. Rayleigh damping is a linear combination of mass and stiffness of the initial elastic system. This damping varies with frequencies, following the formula given by the EQ 3, (Spears and Jensen 2009).

$$\zeta = \frac{\alpha}{2 \times \omega} + \frac{\beta \times \omega}{2} \quad (2)$$

Where;

ζ is the damping ratio for each natural frequency

α is the first Rayleigh damping coefficient, related with the mass

β is the second Rayleigh damping coefficient, related with the stiffness

ω is the natural frequency

However, it is easier and simpler to assume the Rayleigh damping in a way that all the frequencies are involved. The equation (4), which governs these matrix calculations, is shown below, (Chowdhury and Dasgupta 2007).

$$[C] = \alpha[M] + \beta[K] \quad (3)$$

Where;

$[C]$ is the damping matrix

α is the first Rayleigh damping coefficient, related with the mass

β is the second Rayleigh damping coefficient, related with the stiffness

$[M]$ is the mass matrix

$[K]$ is the stiffness matrix

Thus, the values that change in the sensitivity analysis to assess the influence of damping in the final results are α and β.

All the values regarding masonry are listed below as a summary. The values that are evaluated are underlined, while the other values are just italicized.

- Masonry:
  - *Modulus of elasticity* equal to 1x10^3 MPa
  - *Poison ratio* equal to 0.2
  - *Density equal* to 2150 kg/m^2
  - *Tensile strength* equal 0.1 MPa with exponential behaviour
  - *Fracture energy in tension* equal to 0.12 kPa/m
  - *Compressive strength* equal to 6 MPa with parabolic behaviour
  - *Fracture energy in compression* equal to 9.6 kPa/m
  - *Shear retention factor* 0.1
  - *Rayleigh damping values*; α =0.7611 and β =0.002618

3.4 Load cases of the model

For vertical forces only self-weight is taken into account, as the additional loads are not significant in this type of structures. These loads are constant and depend on the density of the elements. For horizontal forces of seismic origin there are several loading possibilities. They are divided between static loads (with different load patterns) and dynamic loads (in which the input is the earthquake accelerograms).

3.4.1 Static – Pushover analysis

The horizontal loads are applied in a static way, independently of time. Sequences of load steps are defined to perform the analyses incrementally. All the load patterns applied will take into account both E-W and N-S directions. The simplest load pattern is mass proportional, in which the self-weight of the structure is applied in a horizontal way. This is the load pattern applied in the model and used in the parametric analysis, since the first mode proportional load pattern is too conservative, as it can be concluded by comparing the results obtained using the pushover methods with those obtained with time history analysis. The comparison between the capacity curves for mass and first mode proportional with both displacement and force based load pattern distribution can be seen in the Figure 12 for the east-west direction and in the Figure 13 for the north-south direction.

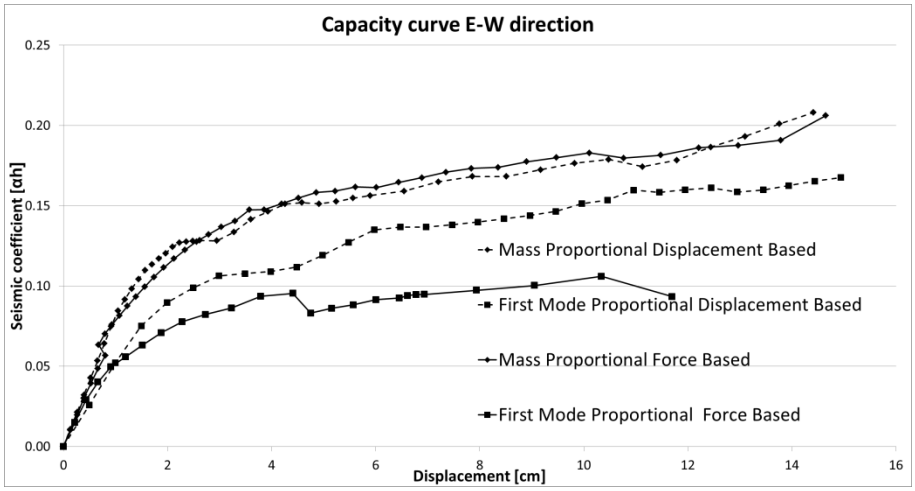

Figure 12 - Comparison capacity curves E-W direction.

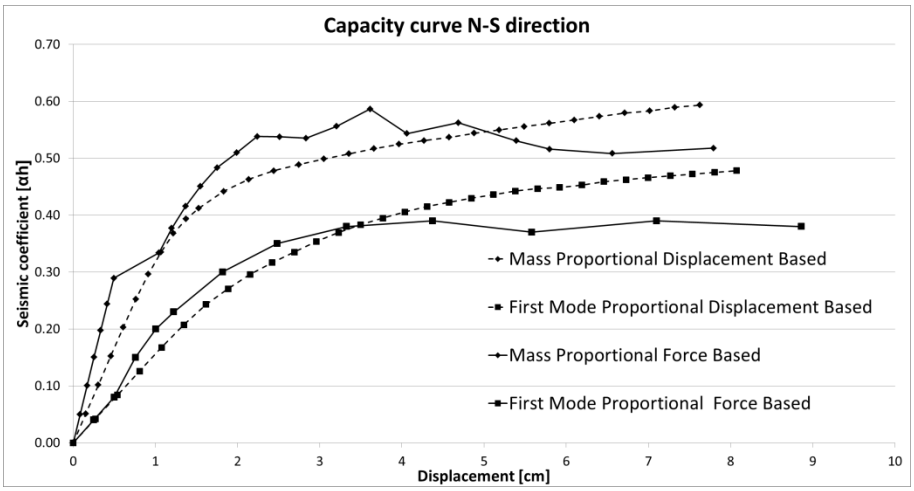

Figure 13 - Comparison capacity curves N-S direction.

In the first mode proportional load pattern the input is applied proportional to the first mode of response. These load patterns suffer from some drawbacks: (1) they do not take into account the effects of the progressive changes in the mode shapes because of structural yielding and damages. In order to remedy this disadvantage some researches have proposed multimodal procedures, see (Aydinoglu 2003) and (Antoniou and Pinho 2004). The damage progression has effects on the response of structures when the load levels are increased. In this kind of pushover analysis these effects are taken into account, updating the loading vector at each analysis step. The application of this incremental loading vector leads to better response predictions (without additional modelling or analysis effort) and its structural response estimations correspond to equilibrated structural stress states, (Antoniou and Pinho 2009); (2) they are restricted to a single-mode response, not considering the contribution of the higher modes. Even in small buildings of a few storeys and regular building configurations many modal shapes influence the final response of the structure. For simplification, in normal pushover analysis only fundamental vibration mode is considered in the calculations. To find a solution for this problem adaptive modal procedures have been proposed, see (Shakeri et al. 2012), (Chopra and Goel 2002) and (Shakeri et al. 2007) This improved method aims to make pushover analysis more accurate considering the contribution of higher modes to the response, in addition to the fundamental one. Thus, the contribution of multiple modes and the effects of their interactions are taken into account, (PAN and Ohsaki 2006)

3.4.2 Dynamic – Time history analysis

In the case study two different earthquakes, each with two horizontal ground motions are considered. The accelerograms corresponding to the first earthquake were generated based on the response spectrum given in (CEN 2003a)(CEN 2003b), type 1. The soil type chosen is type A, corresponding to region of Lisbon and the selected damping is 5%. The accelerograms are obtained from the Portuguese National Annex (LNEC 2009). The vertical ground motion is neglected because it was also not considered in the shaking table test. The horizontal accelerograms are in East-West direction and in North-South direction. The earthquake records have a full duration of 36 seconds. They are divided into 6000 time steps. The E-W direction accelerogram is shown in Figure 14. The numbers at the bottom represents the time step history. In the Y axis the acceleration is labelled in m/s^2. This earthquake is called 100% PGA in this work. A second calculation is made with a PGA increased three times, called 300% PGA, just scaling up the acceleration. This calculation is made to try to obtain the maximum shear base capacity of the structure.

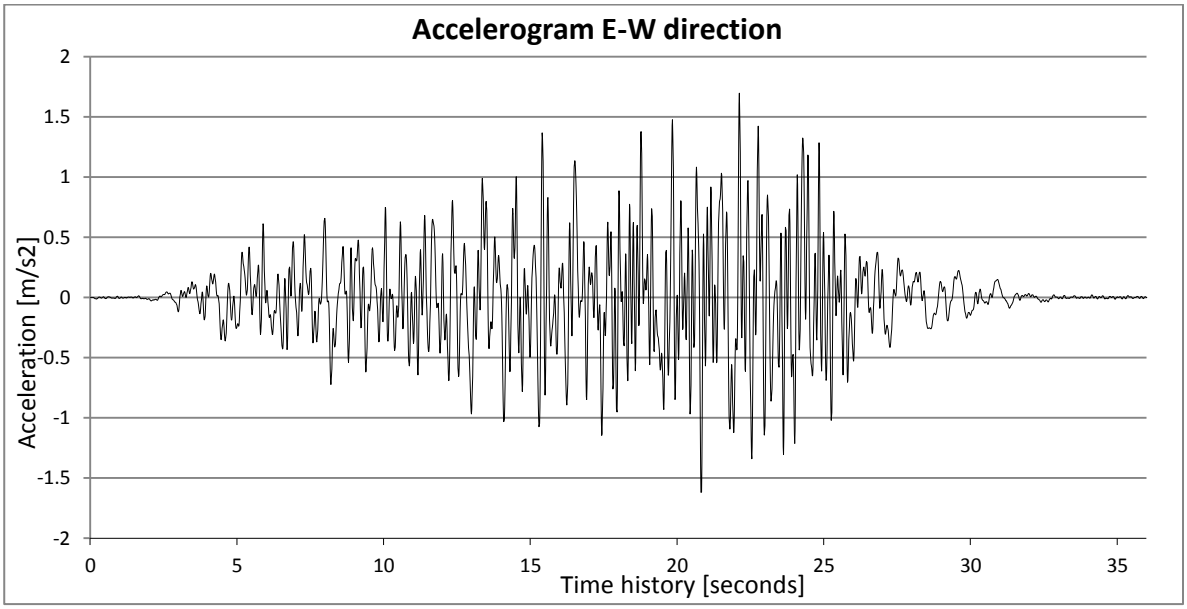

Figure 14 - Accelerogram in E-W direction.

The highest accelerations of the earthquake in E-W direction are between second 15 and 25 seconds. In the E-W direction the largest value is 1.7 m/s^2 and it takes place in the time step number 1849, which corresponds with the second 22.2.

N-S earthquake

The N-S direction accelerogram is shown in Figure 15. As well as for the earthquake in E-W direction, the highest accelerations of the earthquake in N-S direction are between second 15 and 25. In the N-S direction the largest value is 1.9 m/s^2 and it takes place in the step number 1333, which corresponds with the second 16.0.

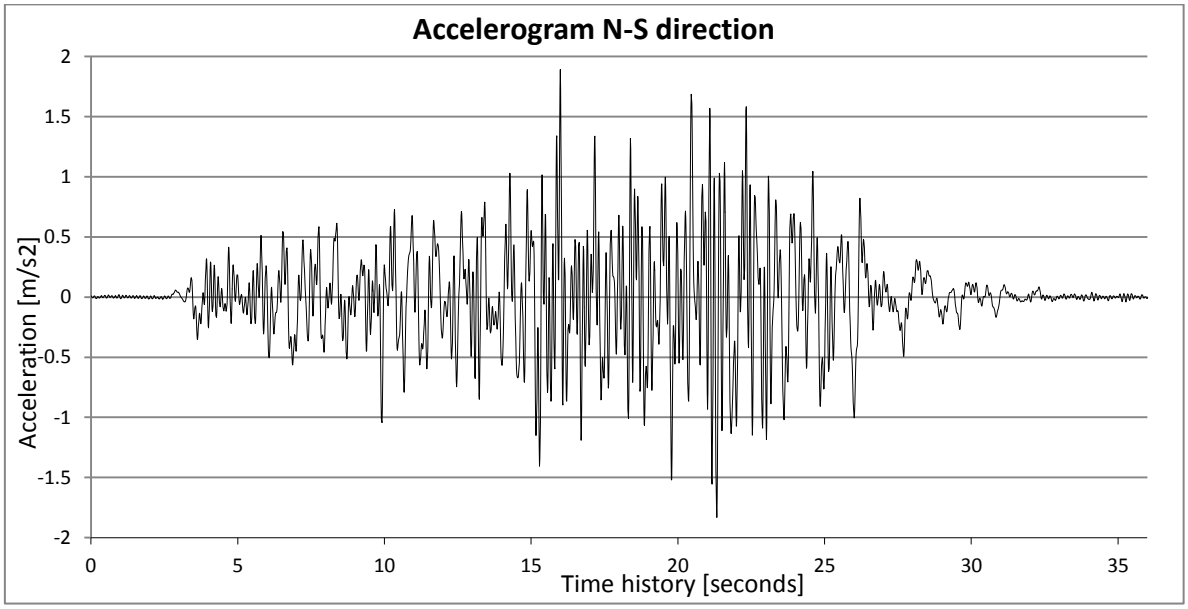

Figure 15 - Accelerogram in N-S direction.

3.5 Analysis procedure

For the pushover analyses the procedure the force applied in each step is equal to 2.5% of the self-weight of the structure. When the steps do not converge the load is modified to different values, never larger than 5% of the self-weight. The arc-length displacement control is used, combined with the spherical path method, being the control point at the top of the gabble walls for east-west direction and at the top of the façades for north-south direction. The iteration method used is Newton-Raphson regular with energy convergence criteria. The tolerance is established as 0.001.

For time history calculations the size of the time steps is 0.006 second. Since the duration of the earthquake is 36 seconds there are 6000 steps. However, in order to have shorter times of analysis, measurements are taken only in one step every two. The integration method is HHT, also called alpha method. Linear iteration method is used for this type of calculation as it fits better loading-unloading systems. The convergence criteria and tolerance are the same as in the pushover analyses.

Chapter 4

Reference model - Pushover analysis

Abstract

The response of the case study building to horizontal incremental static loads replicating the earthquake is discussed in this chapter. Directions east-west and north-south are considered and the results obtained in the analysis are discussed. The incremental analysis continues until collapse is found, the so-called pushover analysis. Thus, it is possible to distinguish and identify the macro blocks and failure mechanisms. This analysis is helpful to understand the global behaviour of the structure

As expected, different behaviour is found for each main building direction and the stiffness of the floor is not enough to replicate a box response, with rigid floors. The influence of this feature is especially noticeable for the north-south direction, due to the orientation of the timber joists in the east-west direction.

4.1 Introduction

The interpretation of results from a pushover analysis is based mostly in the capacity curves, which give the relation between the static loads applied in horizontal direction and a selected control displacement caused by these loads. Here, the seismic coefficient is used to quantify the horizontal load, which is defined as the ratio between the applied loads and the weight of the building.
For every step analysed several figures are shown, illustrating the deformed mesh, and the distribution of stresses and strains in the structure. These figures help to explain and understand the global structural behaviour.

4.2 E-W direction

The capacity curve for the east-west direction can be seen in the Figure 16 for the collapse mechanism indicated in Figure 17, and three different branches are observed. The first branch has almost linear properties. The displacement increases in a proportional way to the applied load and no damage is observed in the model in this first part. The first step in which figures are shown (Figure 18 and Figure 21) is immediately after this section and it is the step number 5. The second branch starts in this point, in which the ratio between displacement increments and applied loads is higher than in the previous branch i.e. the curve softens. It means that some damages are appearing in the structure, so it is able to bear smaller loads for the same displacements. In this branch the Figure 19 and Figure 21, corresponding to the step number 9, can be seen. The collapse of the structure is expected to occur around this step number 9. The last part starts after this step. In this last structural behaviour a small increment of load causes a big rise of displacements. The curve tends to have idealistic behaviour; almost horizontal. This part is not considered to be realistic; the actual building would be already collapsed. The figures corresponding to the last step, which is the number 19, are shown in Figure 17, Figure 20 and Figure 23.

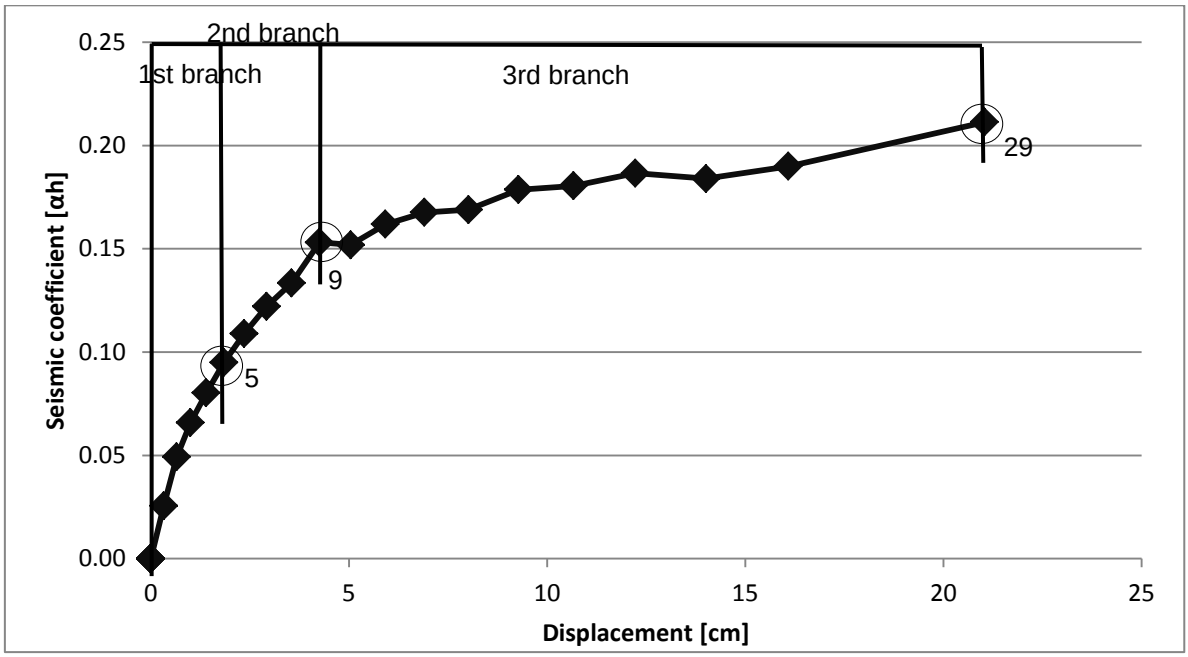

Figure 16 - Capacity curve in E-W direction.

4.2.1 Deformed mesh (displacements) E-W direction

The deformed mesh can be seen in Figure 17 for the step number 19, which is the last step of the analysis. For more detailed examination, the deformed meshes corresponding to the steps number 5 and 9 can be seen in Annex A. The magnification factor has different values for every step. For the step 5 the value is 100, for the step 9 it is 50 and for the step 19 the value is equal to 10. It means that the displacements are much higher in the last step than at the beginning, as expected. The deformation of the structure presents, undoubtedly, the consequence of applying horizontal loads in the direction perpendicular to the gabble walls (from east to west). All the building is leaning to the west direction, being the largest displacements at the top of the structure. The windows are being deformed, losing their rectangularity; the corners are opening or closing. It is in these corners that the concentration of strains and stresses is larger, as can be seen in the Figure 19 and Figure 22. The large deformation of the piers at the basement can also be observed. Two of the piers are being split; the strains in that point can be seen in Figure 20 (b). It is important to mention that the deformation of the gabble walls is larger than the deformation of the façades. The out-of-plane stiffness of the gabble walls is lower than the in-plane stiffness of the façades, so the middle point of the gabble walls is more deformed than the façades.

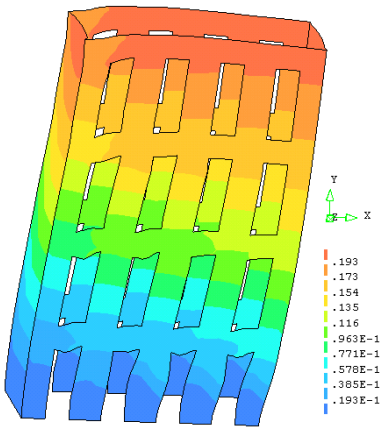

Figure 17 - Deformed mesh in the step number 19, units in meters.

4.2.2 Principal tensile strains (maximum) E-W direction

The images shown here give an idea of the crack pattern. Figure 18 and Figure 19corresponding to the steps 5 and 9 respectively, show the inner side of the north and east walls. For the other two walls, south and west, the outer sides are shown. For detailed results, see Annex A, where two different perspectives are shown for each step. For each perspective the interior and exterior side of the walls are shown. The objective of these images is to show the walls that are closer to the observer, because the ones in the back are less clear. In other words, for the S-W perspective only the south and west walls are more important, while for the N-E perspective the north and east walls are more important. This configuration is the same for every perspective shown in this work. A view of the different orientations and axes is shown in the Figure 8.

In the step number 5, which corresponds to the end of the almost linear behaviour, there are only larger strains in the corners of the windows, see Figure 18. Since the wall is bending slightly, the strains are larger in the outer side of the façades, when compared to the inner side. As mentioned before, the strains are rather low at this step.

Around the cracking point, which corresponds to the step number 9, the strains in the corners of the openings become wider and new damage in the gabble walls appear. The east and west walls are bending and a long line of large strains concentrate in the vertical direction, in the inner side of the walls, close to the edges. These strains appear here due to the stiffness of the edges as they constrain the walls. In the middle of the wall the material is not so constrained so it can deform more freely. New damages appear as well at the base of the piers, which indicate that the piers are overturning. As they are fixed to the ground, larger strains appear at that point. A graphic representation of this step can be seen in the Figure 19.

The ultimate strain state can be seen in Figure 20 and it corresponds to the step number 19. The strains in the corners are much larger than in the previous step. The line of strains along the height of the gabble walls are also larger and new damages appear in the outer side of the edges due to the bending of the walls. The strains at the base of the piers disappear because they concentre in the centre due to splitting, as already mentioned above. New damages appear along the base of the gabble walls. The tensile strains are rather large and the walls are starting to overturn. Given the very large displacement attained, the building would be possibly already collapse and the damage concentration is excessive, which is the reason why the red area is so extensive.

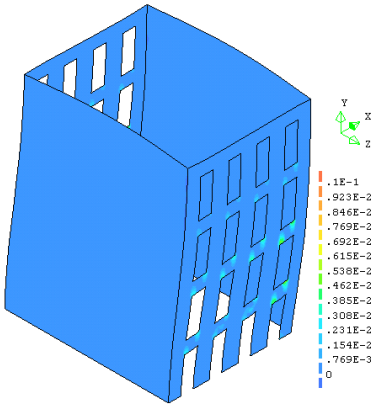

Figure 18 - North-east perspective of the tensile principal strain state in the step number 5.

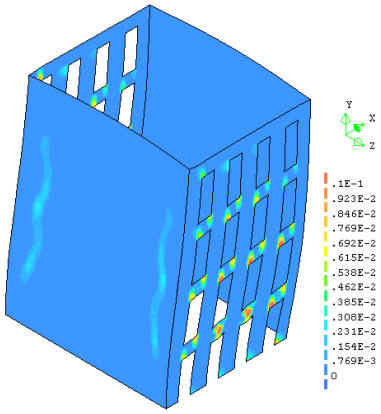

Figure 19 - North-east perspective of the tensile principal strain state in the step number 9.

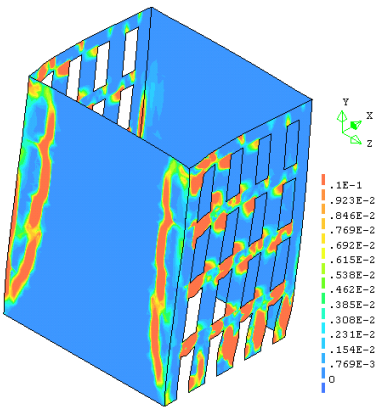

(a)

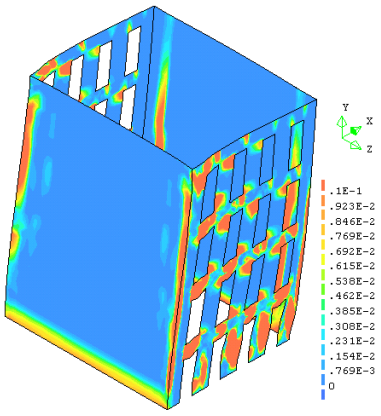

(b)

Figure 20 - North-east perspective of the tensile principal strain state in the step number 19, showing (a) the inner side and (b) the outer side of the walls.

4.2.3 Principal compressive stresses (minimum) E-W direction

In this section the minimum compressive stresses are shown for the steps selected in the capacity curve of Figure 16, see Annex A for more details.

The stress state for the almost linear initial behaviour can be seen in the Figure 21. It corresponds to the step number 5. Only the south-west perspective is shown in this section. In the gabble walls the stresses are larger at the bottom and in the west side. This is the expected behaviour since the horizontal loads are applied in this direction and the walls tend to overturn. These stresses are larger in the edges because the whole façade is loading the gabble wall towards west, while in the middle of the gabble wall only the wall itself provides loading. These stresses are opposite to the strains appeared in the step 19, see Figure 20, i.e. there are compressive stresses in one side and tensile strains in the opposite side. Other compressive stresses appear in the corners of the openings. They are showing the way that the horizontal load is driven to the ground by the structure, in a perpendicular line from the gabble wall to the ground. However, the concentration of stresses is larger in the corners of the openings and this effect is more visible in the subsequent steps.

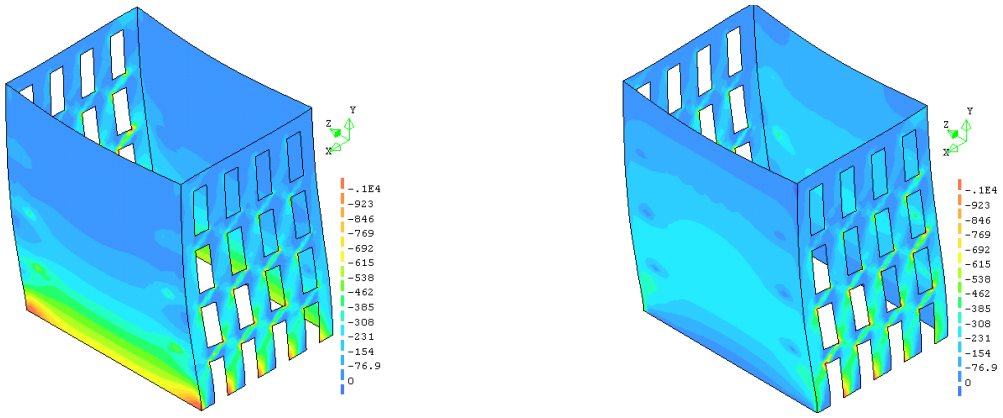

(a) (b)

Figure 21 – Principal compressive stress state in the step number 5, from the south-west perspective, showing the (a) outer side of the walls and the (b) inner side of them, units in kPa.

The stress state in the cracking point can be seen in the Figure 22, which corresponds to the step number 9. The south-west perspective is shown, like for the previous step. The outer side of the walls is shown in the left side while the inner side is shown in the right side. The stresses at the bottom of the gabble walls are larger than in the previous step, as expected. The thrust line that drives the horizontal loads to the ground is now more obvious than in the previous stress state. The loads in this step are so big that the timber floor beams are causing some punching in the walls. This effect can be seen in the Figure 22, where a dot-shape patch of stresses appear in the gabble walls. These

compressive stresses are larger in the proximity of the façades than in the middle of the gabble walls. The compressive stresses in the gabble walls are spread by the walls themselves, more especially in vertical direction, causing the long concentration of stresses close to the edge that can be seen in the Figure 23.

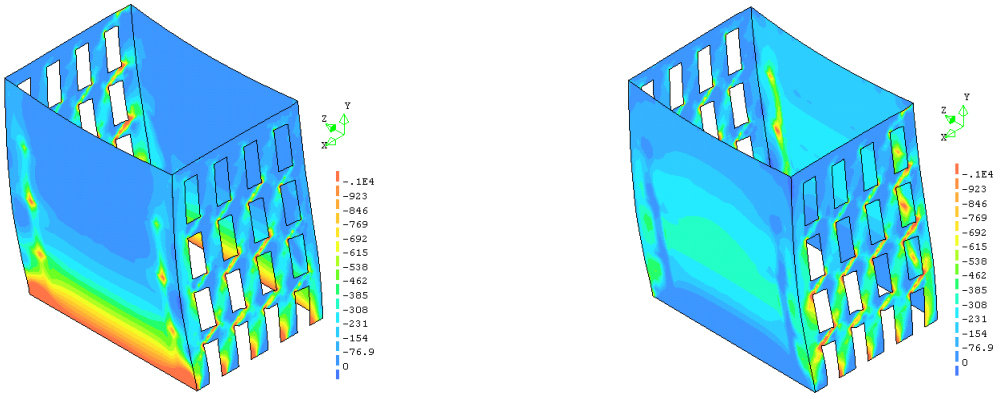

Figure 22 – Principal compressive stress state in the step number 9, from the south-west perspective, showing (a) the outer side of the walls and (b) the inner side of them, units in kPa.

For the ultimate state all the views are shown, to make the behaviour easier to understand. They correspond to the step number 19, and they can be seen in the Figure 23. The stresses at the bottom are much larger than in the previous steps and the diagonal stresses are more visible. It is also possible to notice the compressive diagonal stresses in the piers that cause their split. Also the punching stresses are larger than before and they affect every floor structure, not only to the first and second floor like in the step number 9. New stresses concentrations also appear and one example is the one in the interior part of the edges, due to the closing of the corner. The bending of the gabble walls is so large than new stresses appears at mid-height. They are reflected in the green patch visible in the Figure 23.

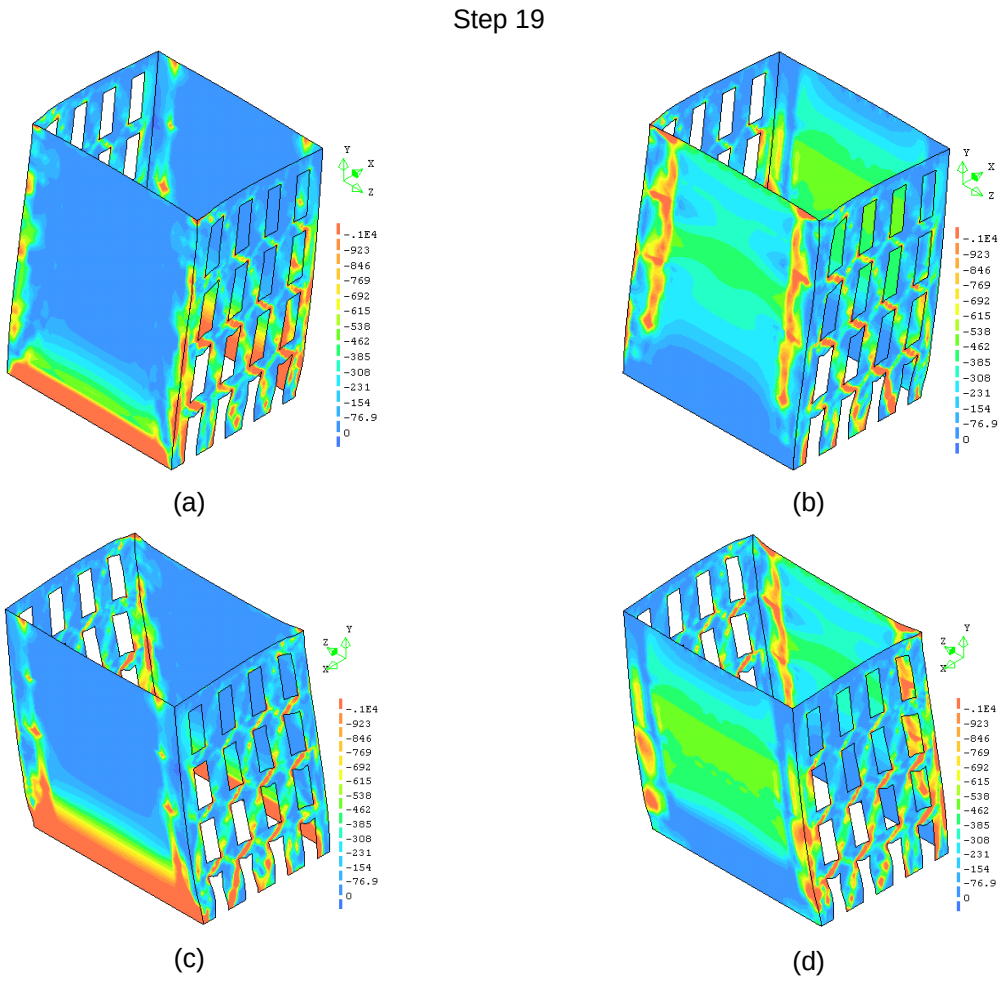

Figure 23 - Principal compressive stress state: (a) N-E view inside (b) N-E view outside (c) S-W view outside and (d) S-W view inside, units in kPa.

4.3 N-S direction

In the Figure 24 the capacity curve for the north-south direction can be seen. The curve has a similar shape to the one in the east-west direction. The first branch corresponds to the almost linear behaviour, the second one to the more extensive stress redistribution and definition of a failure mechanism, and the third branch is almost ideal-plastic.

In the first branch it is seen that the stiffness in the north-south direction is higher than in the east-west direction. Images are shown in the point where the almost linear behaviour finishes, which is the step number 26 (Figure 25). The seismic coefficient is much higher than for the east-west direction, and the displacements are smaller. The difference of stiffness is due to the gabble walls, which do not have any opening and their stiffness is higher than the global stiffness of the façades.

The jump point between the second and the third branch, which can be considered a collapse point, is more obvious and drastic than for east-west direction. Some images (Figure 25 (b), Figure 26 (b) and Figure 27 (b)) are taken in this point, step number 31, where a sudden decrease of loads occurs with a displacement increase. The last branch is almost horizontal and some pictures (Figure 25 (c), Figure 26 (c) and Figure 27 (c)) are shown in the last point, step number 37.

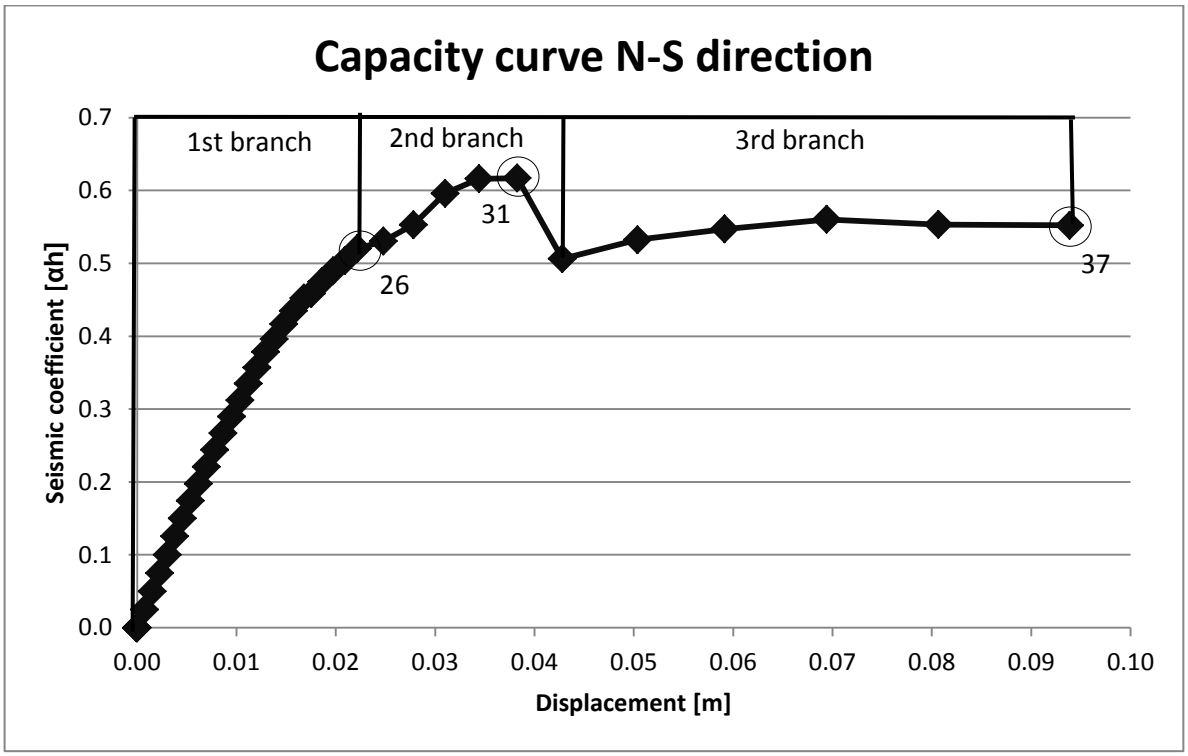

Figure 24 - Capacity curve in N-S direction.

4.3.1 Deformed mesh (displacements) N-S direction

In the Figure 25 the deformed mesh in the steps 26, 31 and 37 is shown. The magnification factors are different in every step. The value is equal to 100 in the step number 26, 50 in the step number 31 and 20 in the step number 37. These graphics are also shown in Annex A.

The behaviour of the structure is obvious. The whole building is leaning, tending to move to the north, since the load is applied in this direction. The discontinuous lines help to see this leaning. It is easy to notice that the façades' displacements are larger than those in the gabble walls. The dots lines mark those local displacements. This feature is in accordance with the stiffness of the walls, which is bigger for the gabble walls. However, it is mainly caused because the displacements of the façades are out-of-plane. It is also interesting to notice that, at the beginning, the most displaced points are not at the top of the structure, but in the third floor. In the next steps these maximum displacements move up to the top of the building, being there at the last step. The shear failure is visible in the steps number 31

and 37. The lower part of the wall remain stable but the upper part moves a lot. The bold line delimits these two areas.

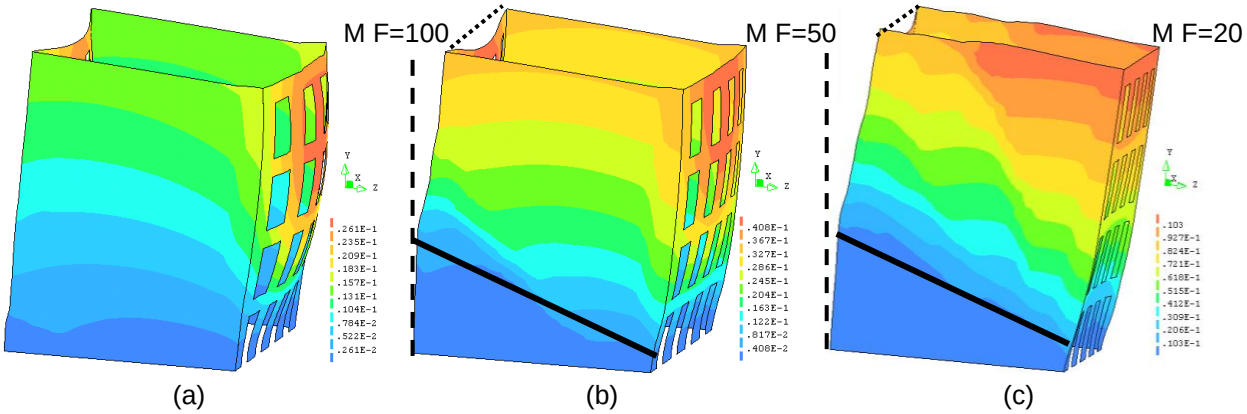

Figure 25 - Deformed mesh in the steps number 26 (a), 31 (b) and 37 (c), units in meters.

4.3.2 Principal tensile strains (maximum) N-S direction

Only one view is shown here for every step, namely the north-east view. These two walls are the closer to the observer, in which the inner side of the walls are visible. In the other two walls, south and west, their outer side is visible. A graphic view of the orientation of the building can be seen in Figure 8. The Figure 26 (a) corresponds to the end of the almost linear behaviour, step number 26, and small strains appear in some parts of the building. There is also a long vertical line of strains in the gabble walls close to the edges with the north façade. This occurs because the north façade is trying to overturn more than the gabble walls, so it is tending to detach from the building. Smaller strains appear in the corners of the north façade, due to the bulk seen previously in Figure 25 (a). There are also horizontal lines of strains in the gabble walls, which grow up in the next steps to become perpendicular and define a macro-block. Large strains appear also in the outer side of the edges between the gabble walls and the south façade. These strains are caused by the bending of the south façade, which is causing the closing of the corners between these two walls.

In the Figure 26 (b) and (c) the strain state for the steps number 31 and 37 can be seen respectively. In the step number 31, which corresponds to the cracking point, the strains are larger. They are especially large in the outer corner of the edges between the south façade and the gabble walls. A diagonal line of strains has grown and it is perfectly visible, caused by shear stresses. The building is being divided in three blocks; the north façade, the south façade plus the lower part of the gabble walls and the upper part of those walls. Like for the east-west direction, the last step corresponds to a large displacement and the building could be already collapse in a real test. The strain state in the step number 37 is the scaling up of the strains in the step number 31. The only difference is that now

there are more diagonal lines, but the one that caused the collapse would be the one that already appeared in the previous step.

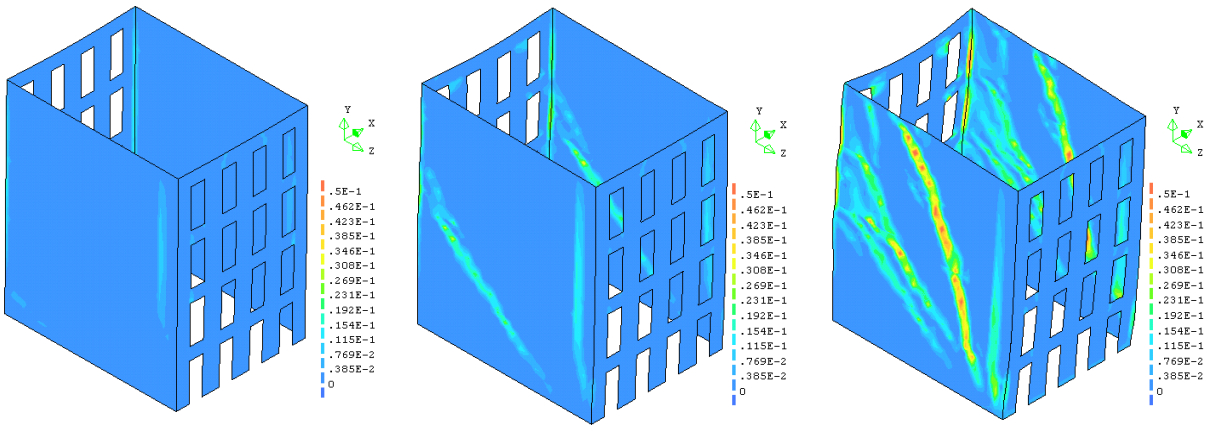

(a) (b) (c)

Figure 26 - Tensile principal strain state for the steps number (a) 26, (b) 31 and (c) 37.

4.3.3 Principal compressive stresses (minimum) N-S direction

As for the strain states, only one view is shown in this section, as the north-east perspective is enough for the general explanation of the structural behaviour. Annex A provides additional details. In the step number 26, corresponding to the end of the almost linear behaviour, it is possible to notice that the largest stresses are concentrated at the bottom of the structure, in the corners between the south façade and the gabble walls; see Figure 27 (a). From there the stresses are spread through the gabble walls adopting a sort of circular shape. There is a release of stresses in a vertical line close to the edge between the gabble walls and the south façade. This is in concordance with the strain state seen in the Figure 26 (a), where a long vertical line of cracking strains can be seen. A small concentration of stresses appears in the corners of some windows, but they are not very large for this step.

In the steps number 31 and 37 it is possible to observe the releases from the previous stress configuration due to the diagonal strains, see Figure 27 (b) and (c). There is only one for the step number 31 but for the step number 37 there are several diagonal lines of strains, according with the strain states shown in the Figure 26 (b) and (c). The stress concentrations in the corners of the windows are larger. A new patch of stresses appears in the step number 31, corresponding to the cracking point. These stresses grow in the step number 37, which corresponds to the ultimate step, and they are especially visible in the lateral piers of the south façade, caused by the bending of the façade.

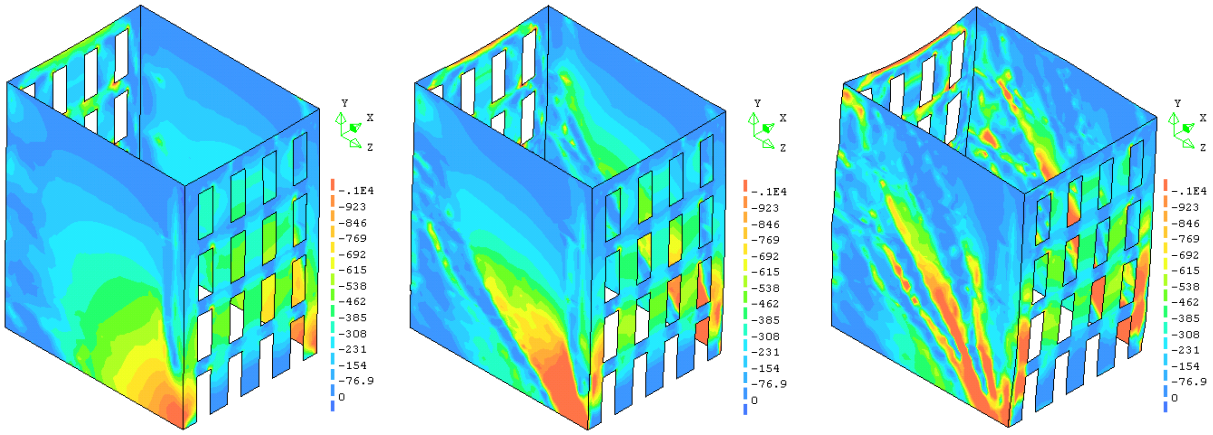

(a) (b) (c)

Figure 27 - Compressive principal stress states for the steps number (a) 26, (b) 31 and (c) 37, units in kPa.

4.4 Conclusion

The response of the building in the west-east direction differs significantly from the response in the north-south direction. This is an expected behaviour, since the global stiffness is very different for each direction, due to the openings in the façades and by the beams of the floor structures. The stiffness of the floor structures is not large enough to provide a fully rigid diaphragm action.

This analysis is helpful to distinguish the macro blocks and the failure mechanisms, and how damage appears when the load is increased. The analysis also allows identifying the weaker parts of the building, in order to improve its capacity. The analysis can also be helpful to understand the behaviour of the building, and how it responds to uniaxial loads. Finally, it gives an approximation of the cracking loads and ultimate loads that the structure is able to bear.

It is noted that this analysis neglects the effect of real earthquakes in the structure. The input is applied in only one direction and only in one sign (without load reversal), without considering dynamic effect, meaning that in order to obtain the response of the building to real earthquake further analyses are recommended, such as time history analysis.

Chapter 5

Reference model - Time history analysis

Abstract:

The response of the structure to an earthquake is discussed in this chapter. In the analysis of the in-plane and out-of-plane behaviour several parameters were used, namely; displacements, accelerations, base shear forces and principal strains. The analysis takes into account the direction of the results and the walls under consideration, because the behaviour of gabble walls and façades is rather different.

The building is subject to the type 1 earthquake of Lisbon (soil A), being the damage concentrated in the façades. Although the loads are not large enough to cause the collapse of the building, the damage can be appreciated and it is a good starting point to understand the non-linear response of structure to dynamic loads. The influence of the floor stiffness and the different global stiffness of walls and façades can also be evaluated. The buildings is subsequently subjected to an earthquake three times larger than the first earthquake to observe the differences obtained with a much larger input, close to full structural collapse.

5.1 Introduction

In this chapter the time history results are shown and discussed. The amount of data to describe the response of the building to a dynamic analysis is larger than for a static analysis. The results are based on time history series, such as acceleration, displacements, etc, and the images presented next for example for a deformed mesh show the response of the building at a given time.

In addition, the envelopes of the control displacement against the seismic coefficient (i.e. the sum of all reactions at the base of the building) are also shown. They give a good approximation of the capacity of the structure. These graphs can be compared with the capacity curves of pushover analyses, even if they are rather different. The principal tensile strains obtained from the envelope of tensile strains are a good indicator of the damage and they are shown as well. Note that these envelopes do not correspond to a given time.

The accelerograms used as input for this analysis are chosen considering the Lisbon seismic area, at 100% PGA and at 300% PGA, as explained in Section 3.4.2

5.2 Lisbon area earthquake – 100% PGA

In this section the results for the earthquake in Lisbon seismic area are analysed and discussed. The PGA used is the original one obtained for this earthquake. The loads are thus lower than the ones expected to cause the collapse of the building.

5.2.1 Acceleration history response

The acceleration is measured at the top of the walls, in their middle point. The time history response for the gable wall is shown in Figure 28; (a) for direction X and (b) for direction Z. For both directions the maximum acceleration has a similar value, about 6 m/s^2. However, the response is different, depending on whether the acceleration is measured in-plane or out-of-plane. The in-plane stiffness is bigger than the out-of-plane stiffness and the average acceleration in X direction is bigger than in Z direction.

The time history response for the façade is shown in Figure 29; (a) for direction X and (b) for direction Z. The maximum value has a very different value; about 3.5 m/s^2 for X direction and more than 10 m/s^2 for the Z direction. As for the gabble wall the behaviour is different for each direction, but in this case the difference is bigger, due to the openings and the orientation of the timber floor joints.

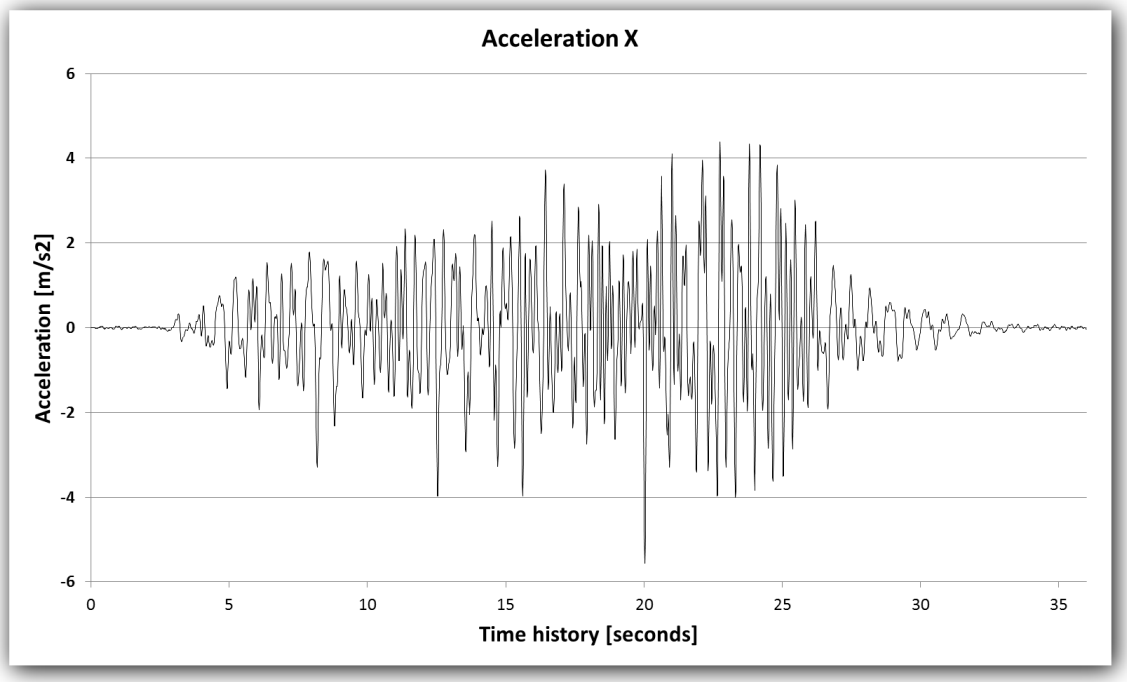

(a)

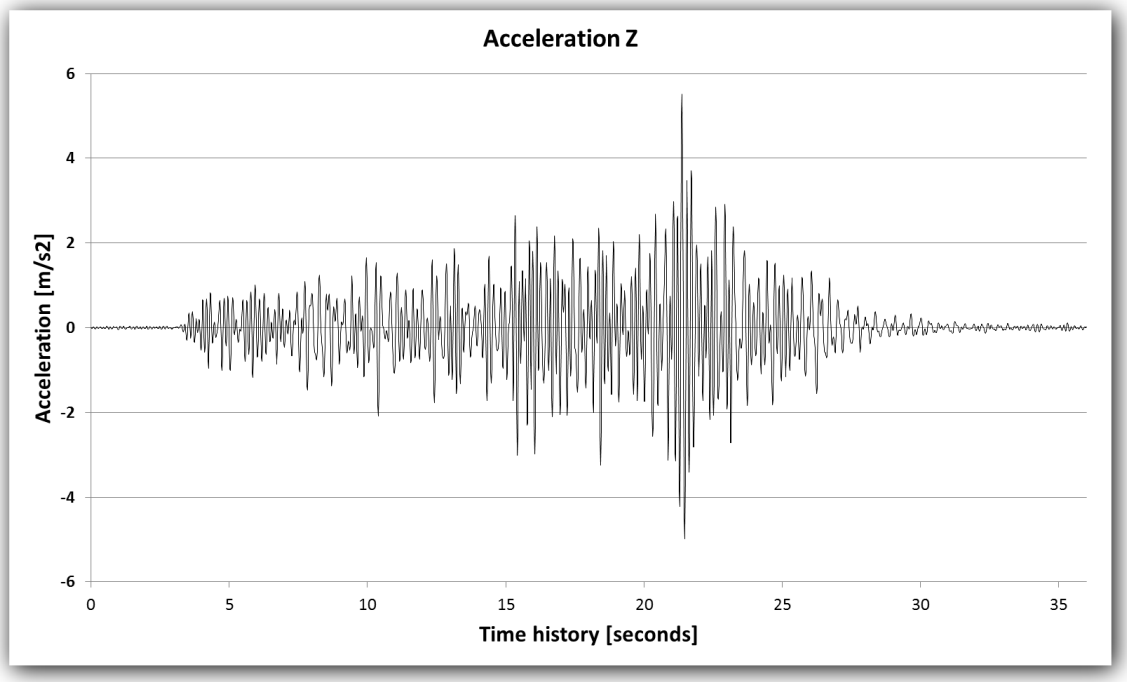

(b)

Figure 28 - Acceleration history response in the axis (a) X and (b) Z for the gabble wall.

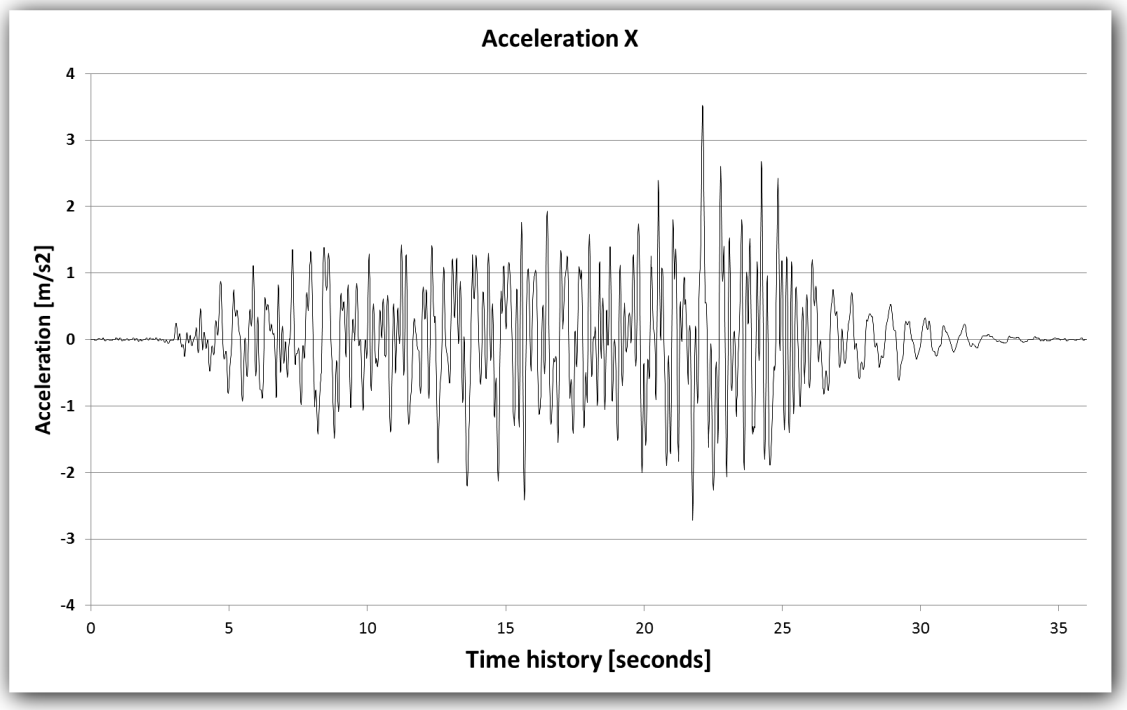

(a)

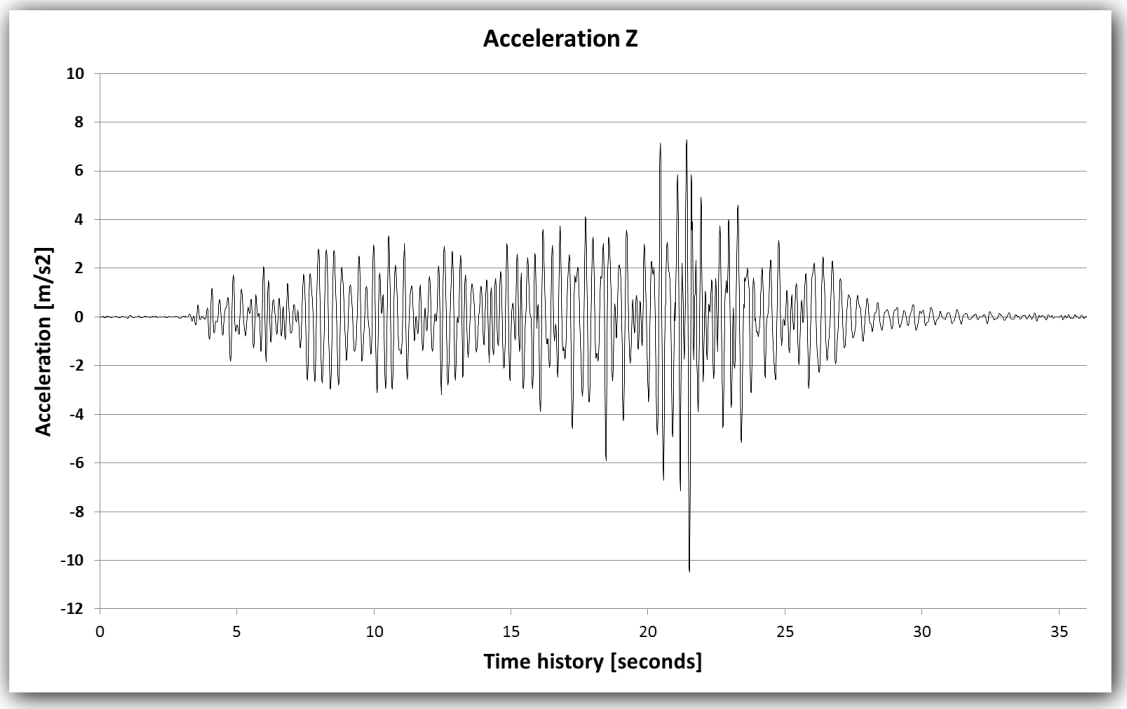

(b)

Figure 29 - Acceleration history response in the axis (a) X and (b) Z for the façade.

5.2.2 Displacements and drifts

The displacements are measured in the façades and in the gabble walls. For each graph two vertical alignments are given; one in the middle of the wall and another at 25% distance from the corner. The displacements given are divided in global translational displacements and local displacements. The global displacements are perpendicular to the wall in the undeformed configuration. They are the sum of translational displacements and displacements due to the bending of the wall. The local displacements are the ones occurred in the wall itself, due to its bending. A graphic explanation of these displacements can be seen in Figure 30. The drifts are the relation between displacements wall and the height of the point where these displacements occur. Note that the displacements (global or local) do not correspond to the same time step and they can be either positive or negative.

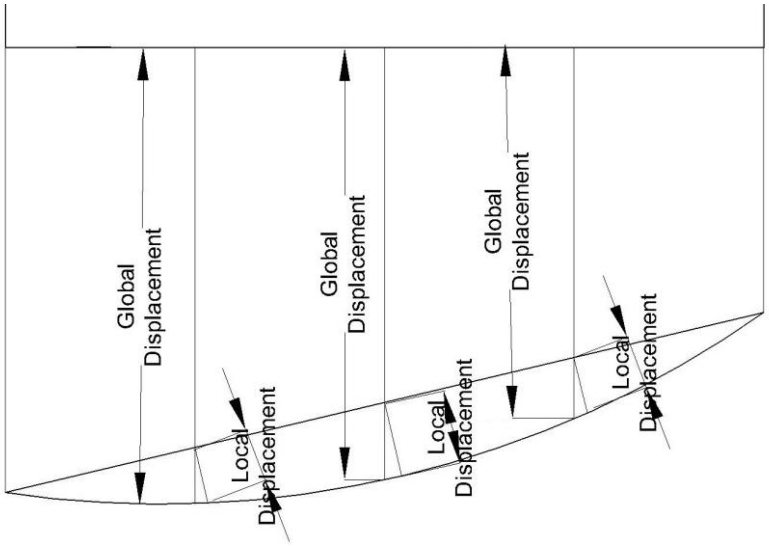

Figure 30 - Graphic explanation of global and local displacements.

Gabble walls

The perpendicular displacements can be seen in the Figure 31 and Figure 32. In these walls only 4 points were measured, one for each floor. The Figure 31 corresponds to the east wall displacements, while the Figure 32 corresponds to the west wall. The middle alignment moves more than the alignment at 25%, which is the expected behaviour because the wall is able to move more freely in the middle section. These displacements are bigger in the third and fourth floors. It means that the wall moves more and bends more in the upper floors of the structure. This occurs because the bottom of the structure is constrained to the ground. The difference of the response between east and west walls is small; the values are very similar. However, in the second and fourth floors the difference between global and local displacements is bigger in the west wall, while in the third floor is smaller.

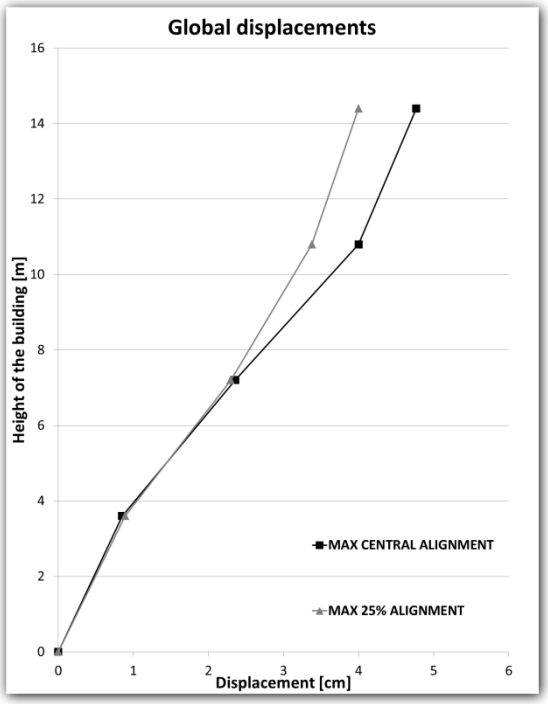

(a)

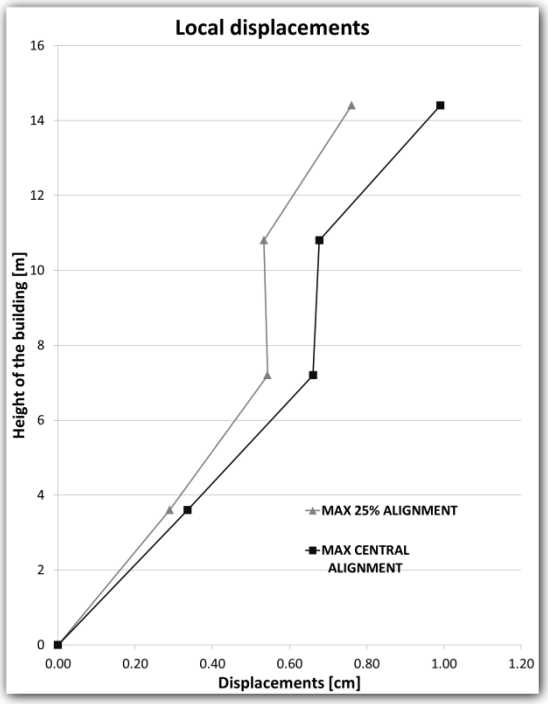

(b)

Figure 31 – Out-of-plane (a) global and (b) local displacements for the east gabble wall.

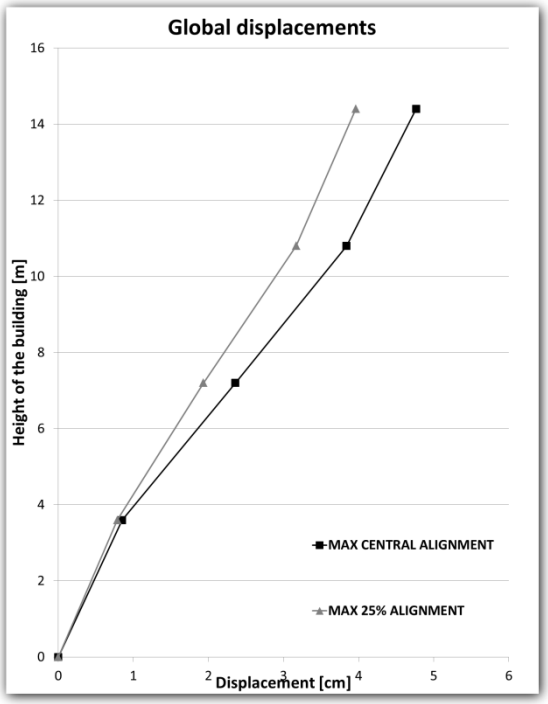

(a)

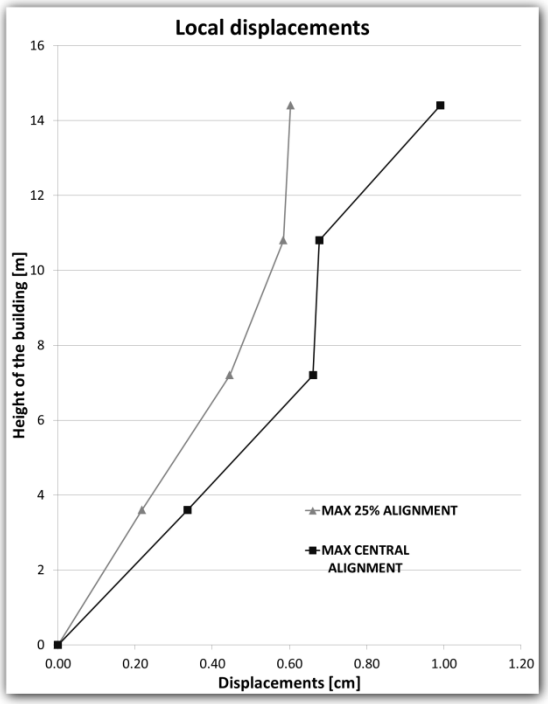

(b)

Figure 32 – Out-of-plane (a) global and (b) local displacements for the west gabble wall.

The in-plane drifts are in the Figure 33, (a) for east wall and (b) for west wall. The drifts are rather small meaning that damage is indeed limited, but they are larger in the upper floors. This happens because in the upper floors the wall is not as constrain as in the lower part. However, the third floor drifts is larger than the fourth one. The difference between middle and 25% alignment is bigger at the base of the structure. The bottom of the wall is more constraint than the base, so the wall here tends to bend instead of drifting. As for the out-of-plane displacements the alignment at 25% of the edges moves less than the middle alignment. The constraint comes from the edge with the other wall, which limits the drift of the alignment.

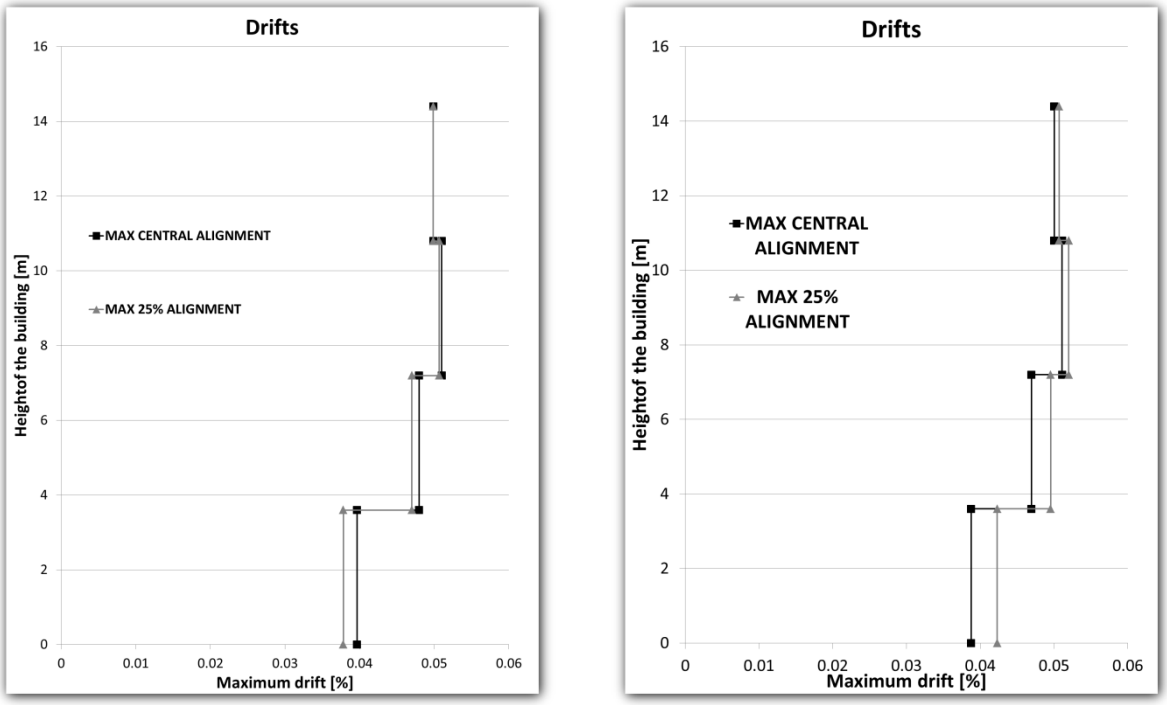

(a) (b)

Figure 33 - In-plane drifts for the (a) east and (b) west gabble walls.

Façades

The displacements in the façades can be seen in the Figure 34, Figure 35 and Figure 36. The graphs are the similar to the ones for the gabble walls. The difference is that in these graphs there are 12 measured points instead of 4. More points are measured in the façades because they are considered to be more important and they are also weaker. Thus, it is necessary to have a more detailed analysis of these walls. Firstly, perpendicular displacements can be seen in the Figure 34 for global displacements and Figure 35 for the local ones. As for the gabble walls the middle alignment moves

more than the 25% alignment. A big different of displacements can be seen in the middle alignment at the top of the wall because the pier in the last two floors moves significantly, as can be seen in the strains envelope in the Figure 39. For the façades the global and the local displacements are very similar. It happens because the gabble walls are very stiff, so the displacements are almost all due to bending. This effect is especially visible in the last floor, where the pier has a large displacement at the top.

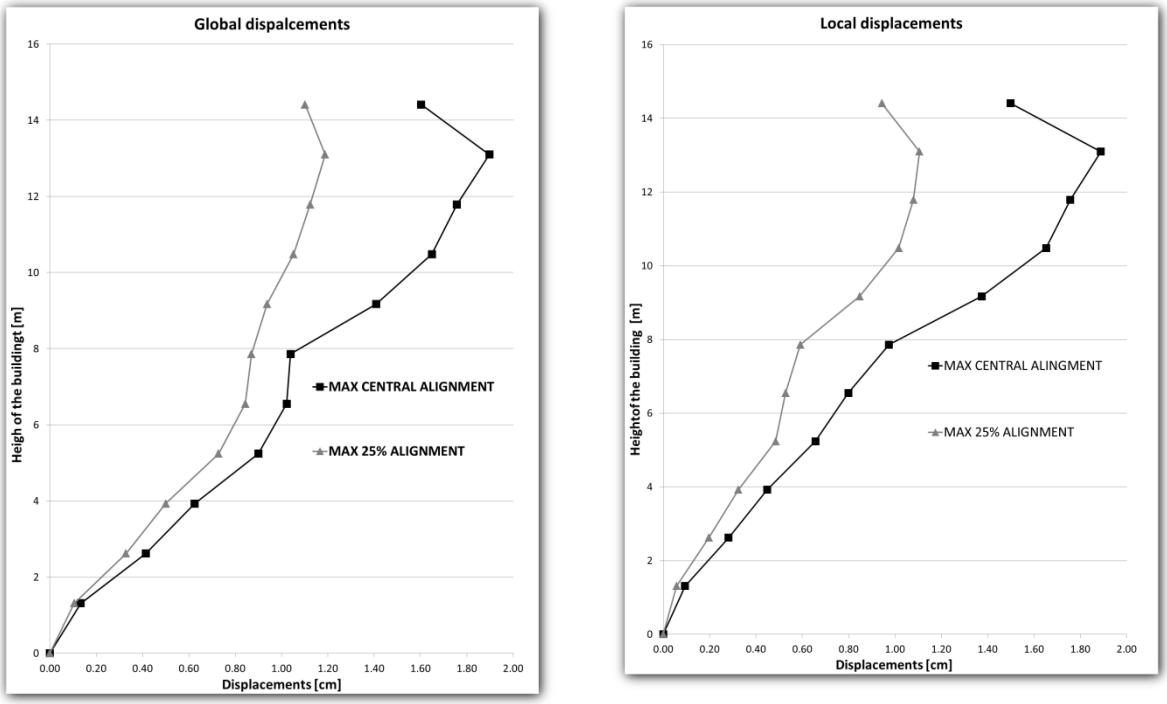

(a) (b)

Figure 34 – Out-of-plane (a) global and (b) local displacements for the south façade.

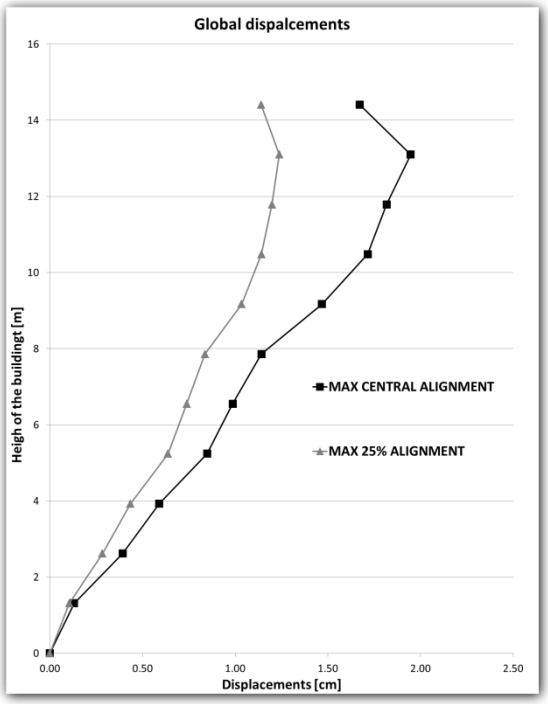

(a)

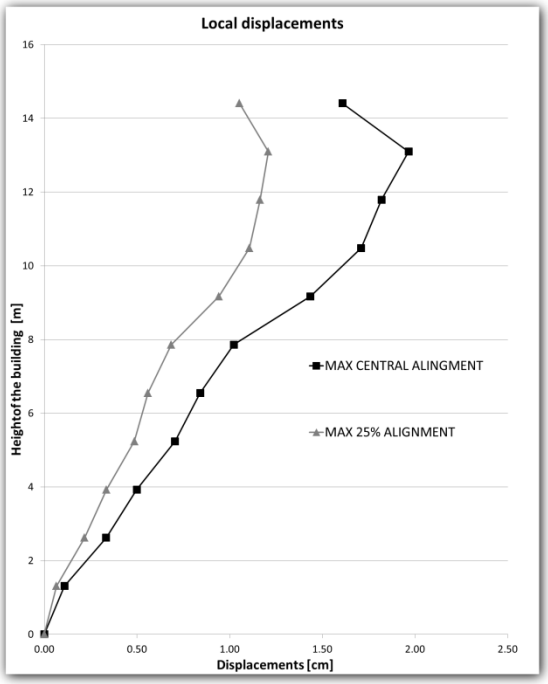

(b)

Figure 35 – Out-of-plane (a) global and (b) local displacements for the north façade.

The drifts are given in the Figure 36, for the south façade (a) and for the north façade (b). In this case drifts are already more important (reaching about 0.3%) and they are very similar both façades. This is because the gabble walls do not bend as much as the façades do, so they do not let the façades drift very freely. As for the gabble walls, the drifts increase as the height of the building increases. In the last floors the walls are able to bend more than at the bottom of the structure. Here, the walls are bending instead of drifting and, in the last floor; the drifts are smaller than in the third floor.

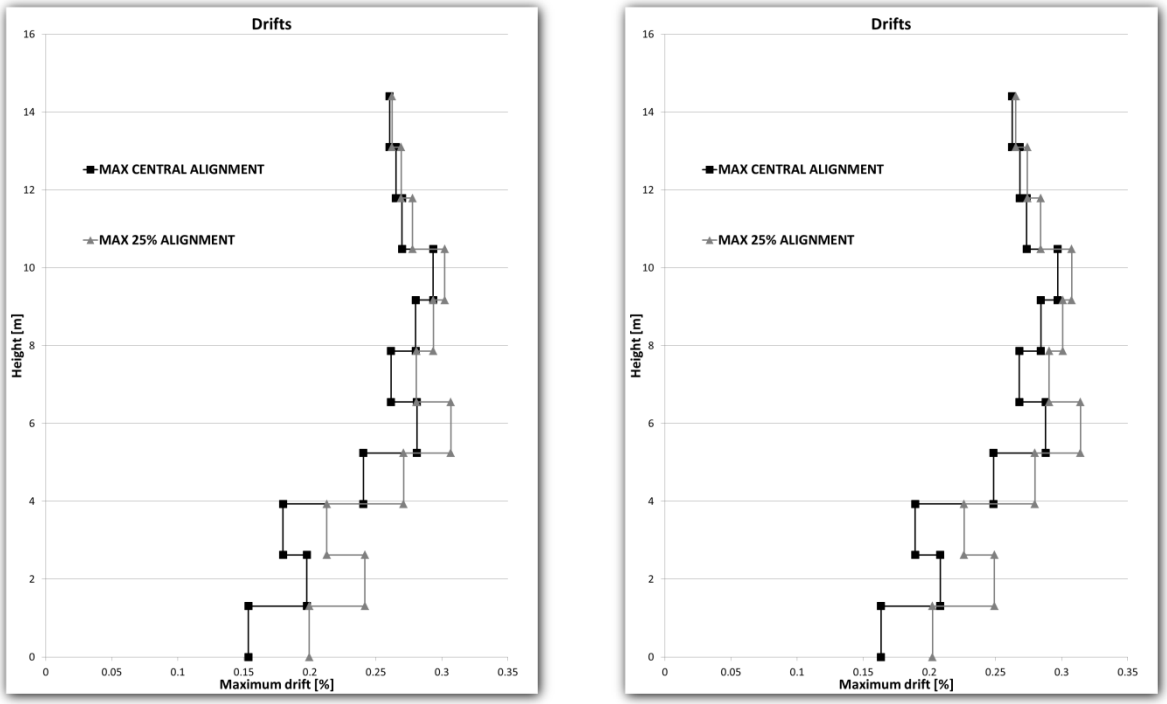

(a) (b)

Figure 36 - In-plane drifts for the (a) south and (b) north façades.

5.2.3 Envelopes

The envelopes of the seismic coefficient against the displacement at the top in the middle of the gabble walls are shown in this section. These graphs can be considered as a measure of the global response and of the behaviour of the building.

The graphs for the gabble wall are shown in the Figure 37; (a) for the X direction and (b) in the Z direction. The shape of the envelope in the X direction is more irregular than in the Z direction because the displacements are out of plane and mode sensitive to a pulse. The response of the building is, thus, very different depending on the direction and magnitude of the load. However, the maximum positive and minimum negative values of seismic coefficient and displacement are similar,

as expected. In the Z direction the shape is more regular because the displacements are in-plane, so the input does not have as much effect as for X direction. The displacements are smaller in the direction Z than in the direction X. This is because the in-plane stiffness is larger than the out-of-plane stiffness. The seismic coefficient is bigger in the direction Z than in the direction X because global stiffness of the structure is larger in this direction.

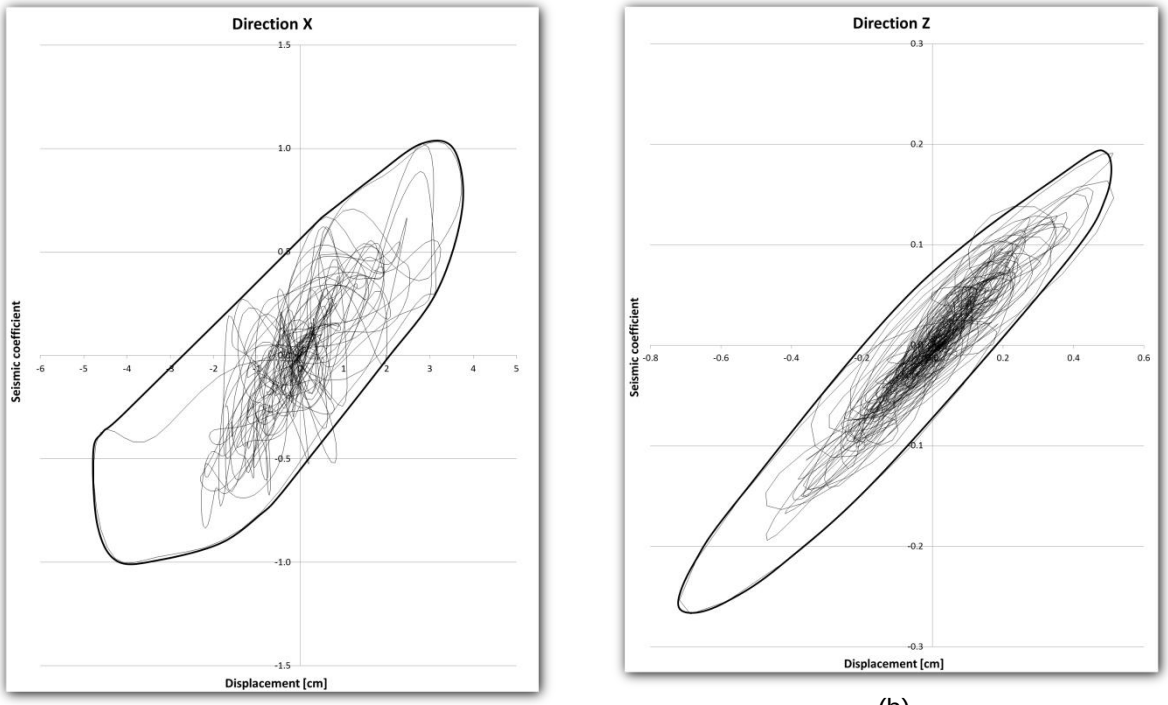

(a) (b)

Figure 37 - Envelope displacement-seismic coefficient in (a) axis X and (b) axis Z for the gabble wall.

The envelopes for the façade are shown in the Figure 38; (a) in the X direction and (b) in the Z direction. The response in the X direction provides a smooth envelop due to in-plane stiffness of the façades, than together with the floor structures make the movements equal in both gabble walls and façades for the X direction. In the Z direction the response is different. The wall is very flexible because of the openings, so the building is moving in a different way than the gabble wall for the same direction. In addition the floor beams are not in this direction, so they do not help to transfer the movements between gabble walls and façades. As consequence, the displacements in the Z direction are much higher for the façades than for the gabble walls, even with the same seismic coefficient.

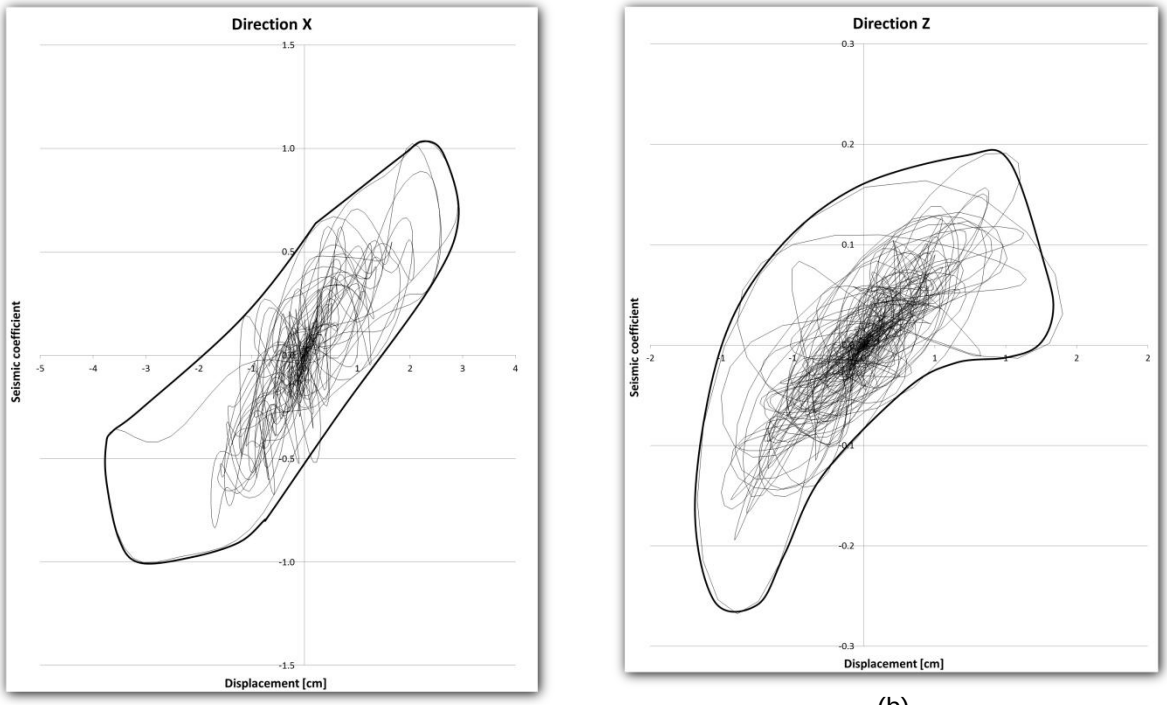

(a) (b)

Figure 38 - Envelope displacement-seismic coefficient in (a) axis X and (b) axis Z for the façade.

5.2.4 Principal tensile strains

The envelope of the tensile strains is shown in Figure 39. This can be considered an approximation of the crack pattern of the building. The north-east perspective is shown; the inner side of the walls (a) and the outer side of the walls (b). The damage is concentrated in the lintels of the windows, especially in the first and second floors, due to the low level of damage obtained for this accelerogram. Large strains are also visible at the basement of the piers, due to in-plane bending. A long vertical line of strains is also observable in the inner side of the gabble walls, due to their out-of-plane bending. It is important to notice the strains at the top of the middle pier. These strains are larger in the external side of the walls and indicate that the pier might detach from the façade and fall down for a larger input. This crack pattern is in accordance with the damages seen in the mock-up described in (Yang 2010).

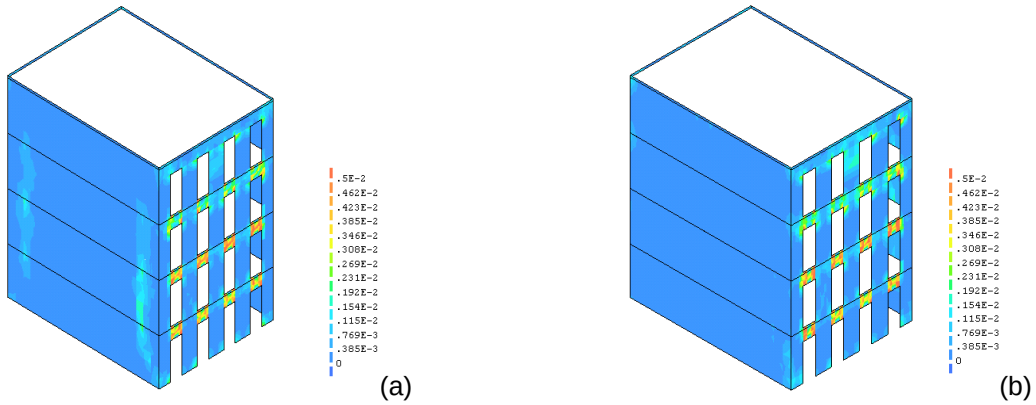

Figure 39 - North-east view of the tensile principal strains envelope showing (a) the inner side and (b) the outer side of the walls.

5.3 Magnified earthquake – 300% PGA

In this section the results for the magnified earthquake in Lisbon seismic area are analysed and discussed. The PGA used for the calculations in this section is augmented 3 times, resulting in the so-called 300% PGA earthquake.

5.3.1 Acceleration history response

The results are presented in the same way as in the previous earthquake; they were measured in the middle alignment of the walls, at the top. The time history response for the gable wall is shown in Figure 40; (a) for direction X and (b) for direction Z. The time history response for the façade is shown in Figure 41; (a) for direction X and (b) for direction Z

For this earthquake the acceleration response history is more regular; it has several peaks with quite similar value, indicating that the capacity of the walls in terms of base shear has been reached. This is valid for both gabble walls and façades. As expected, the peak values are higher than for the 100% PGA earthquake, even if a direct relation between input and results is not to be expected due to the dynamic and non-linear effects. The values for the accelerations are about the double for a three times stronger earthquake.

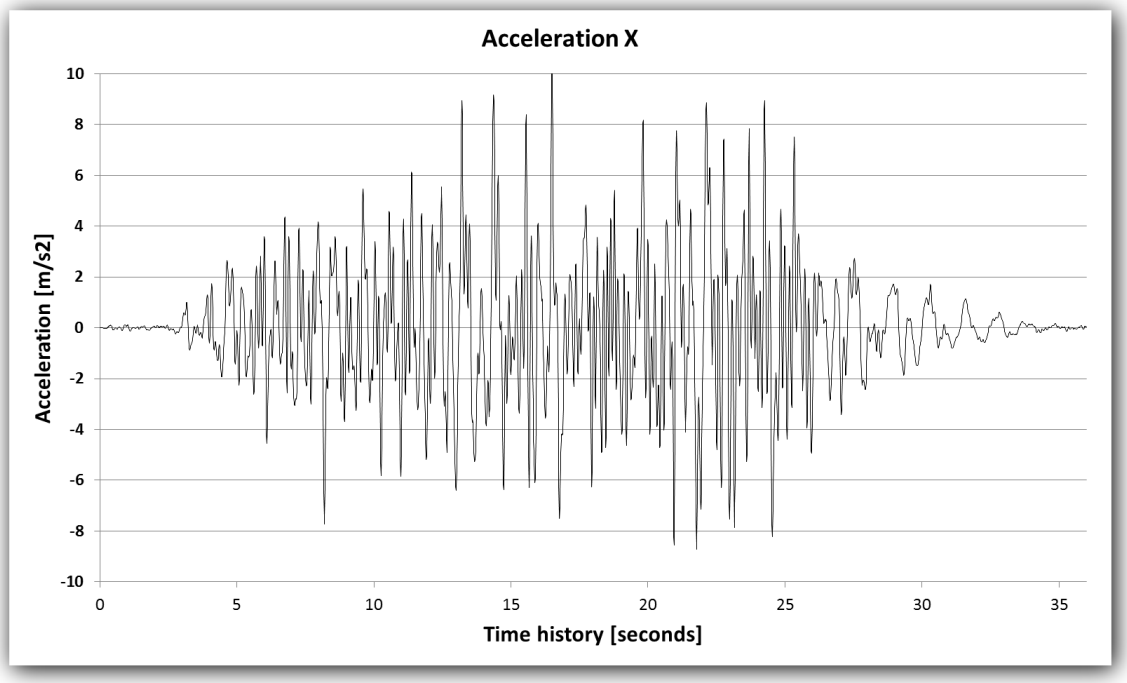

(a)

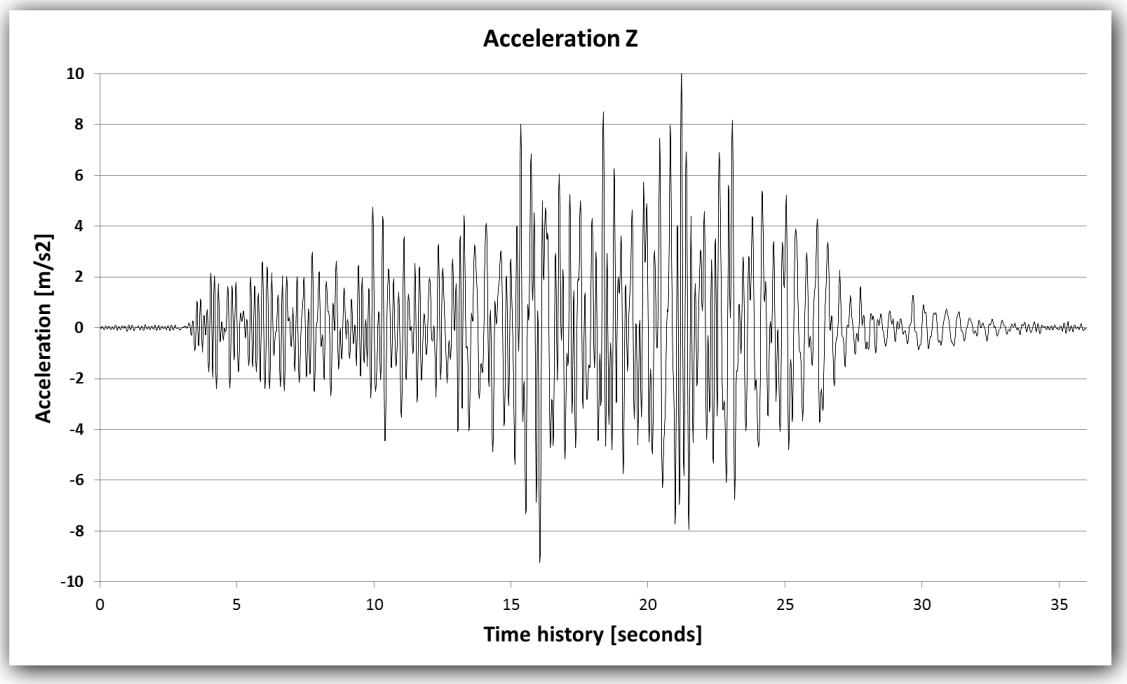

(b)

Figure 40 - Acceleration history response in the axis (a) X and (b) Z for the gabble wall.

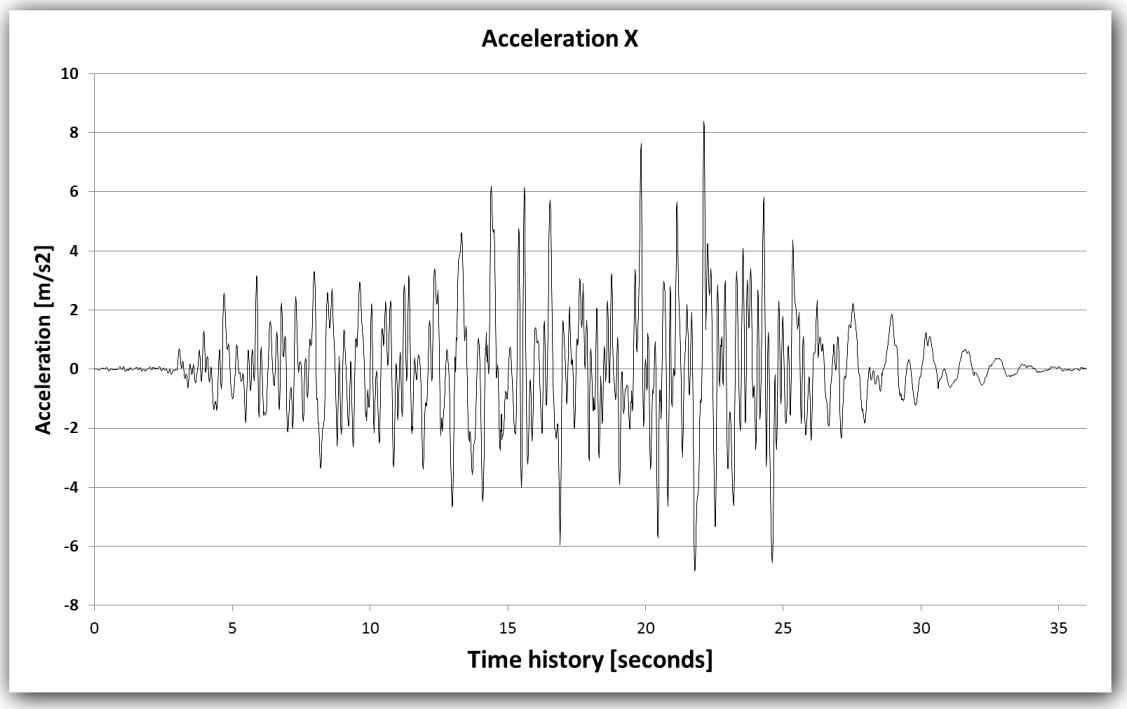

(a)

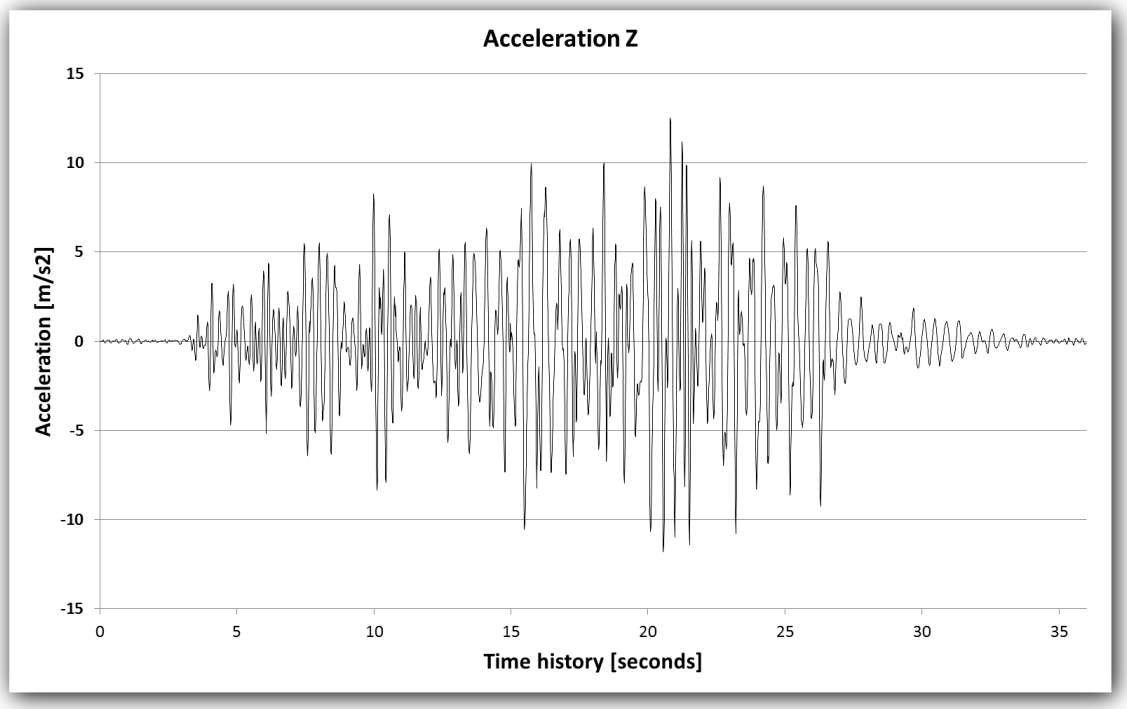

(b)

Figure 41 - Acceleration history response in the axis (a) X and (b) Z for the façade.

5.3.2 Displacements and drifts

The presentation of the results is the same as in the previous earthquake. For an explanation of displacements and drifts, see 5.2.2.

Gabble walls

The perpendicular displacements in the east gabble wall can be seen in the Figure 42. It is interesting to notice that for this earthquake the local displacements represent a small percentage of the global displacement of the wall (around 10%), while for the 100% PGA earthquake it was about 20 %. This is because the global movement of the building is larger, but the bending capacity of the walls is not increased. However, a common feature is the fact that the middle alignment moves more than the 25% alignment. It makes sense for both 100% and 300% PGA because the wall is less constrained in the middle than close to the corners. The results for the west gabble wall can be seen in the Figure 43.

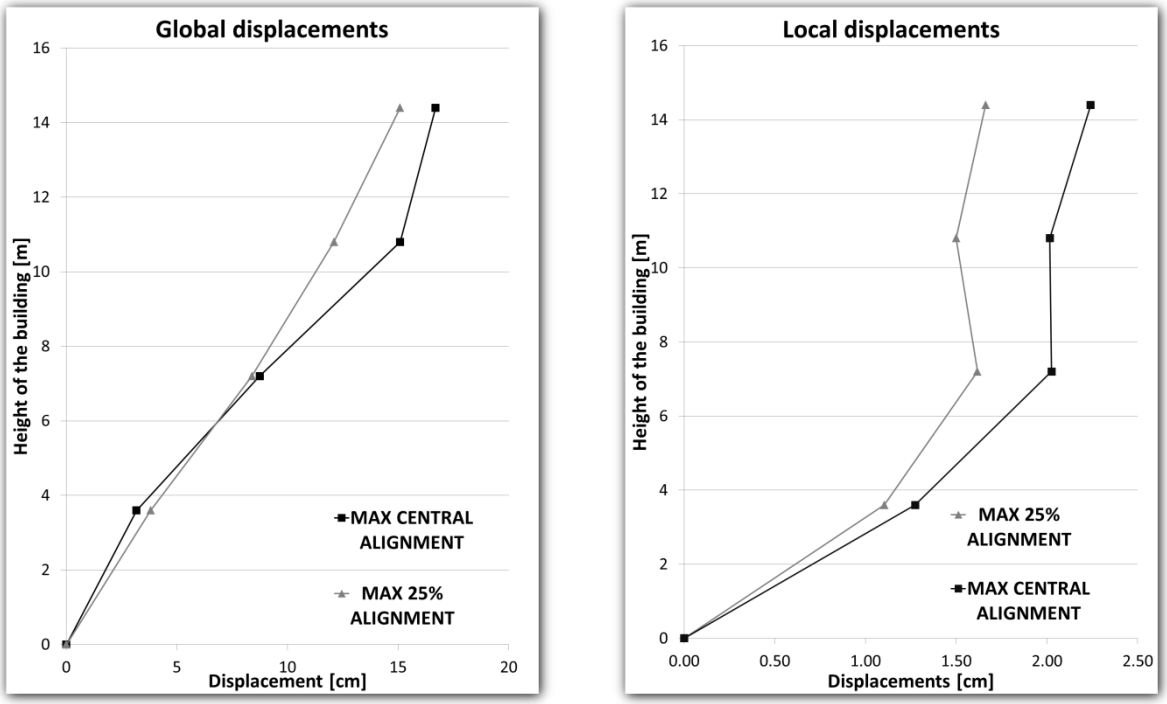

(a) (b)

Figure 42 – Out-of-plane (a) global and (b) local displacements for the east gabble wall.

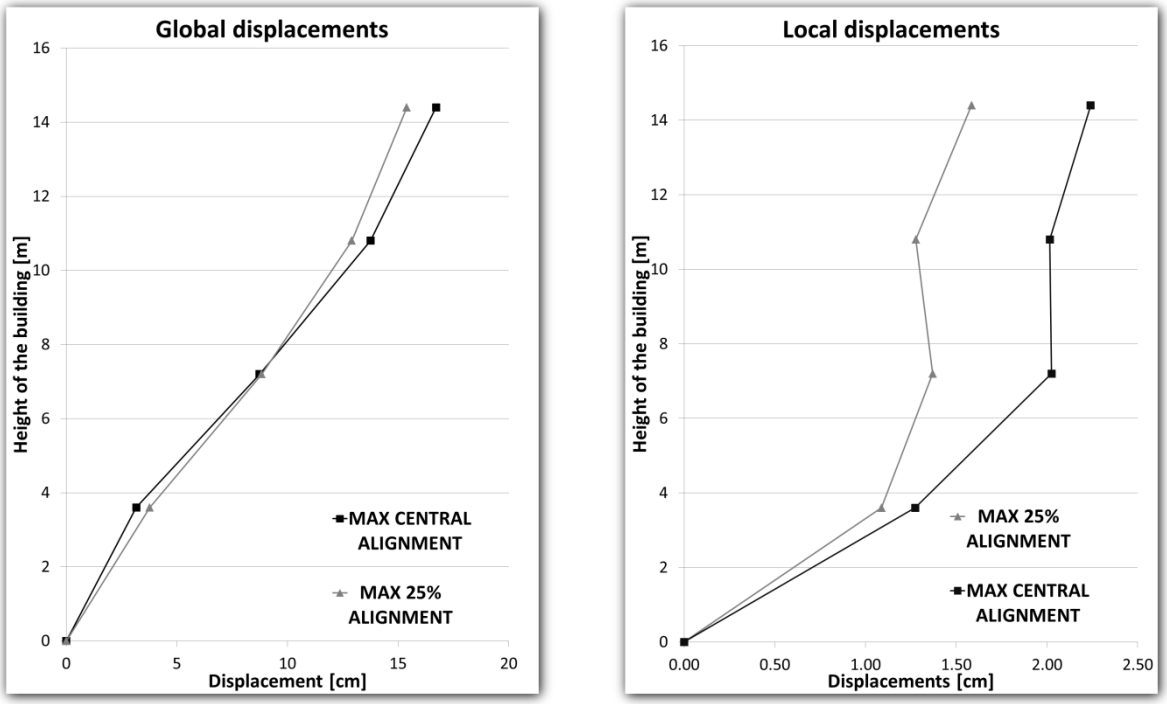

(a) (b)

Figure 43 – Out-of-plane (a) global and (b) local displacements for the west gabble wall.

The in-plane drifts are in the Figure 44, (a) for east and (b) for west gabble walls. As expected, the drifts are much larger for this calculation (about 10-15 times larger) than for the 100% PGA earthquake. It means that the building is moving much more, so more damages can be appreciated. Collapse might be occurring soon. In this calculation the maximum values of drifts take place in the second floor instead of in the last floors as before. The in-plane collapse is most likely to happen in the lintels of the second floor. The differences between 25% alignment and central alignments are larger than for the previous analysis because the wall is being split in several parts.

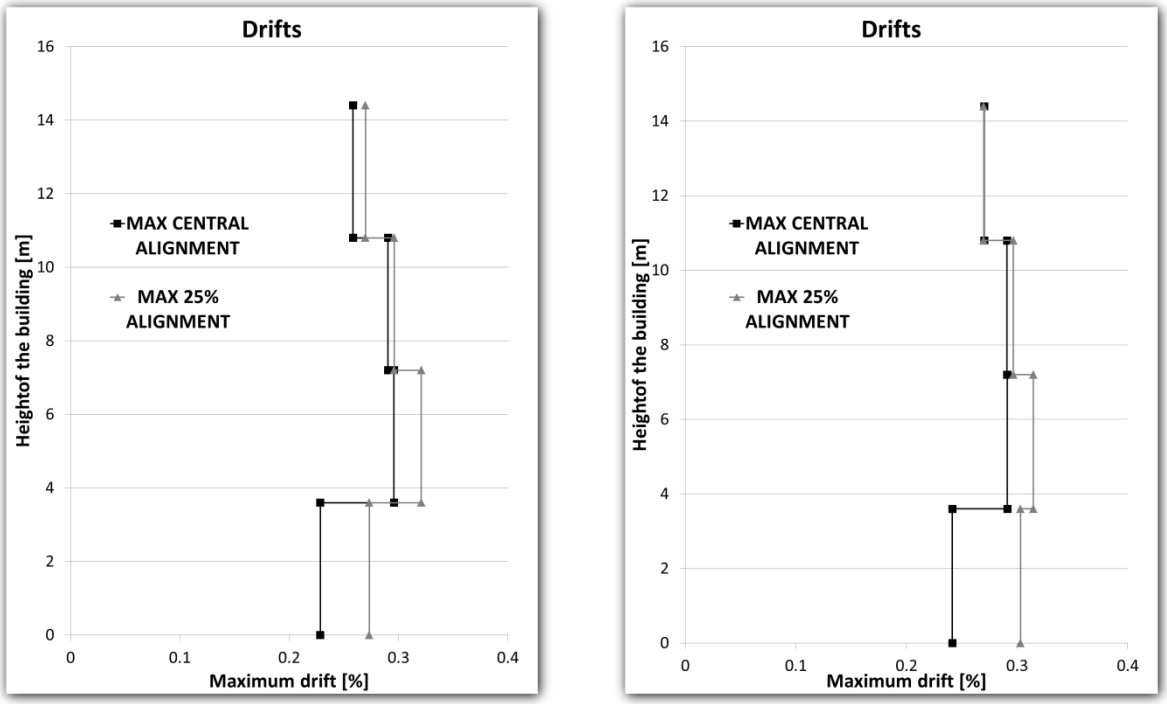

(a) (b)

Figure 44 - In-plane drifts for the (a) east and (b) west gabble walls.

Façades

The results shown are the same than for the previous analysis in the gabble walls. The perpendicular displacements are shown in the Figure 45 for the south façade and in the Figure 46 for the north façade.

As expected, the displacements are larger than for the 100% PGA earthquake, as for the gabble walls. However, in these walls the local and global displacements are very similar. This is due to their flexibility; the major part of the displacements is caused by the bending of the walls. In this case the difference between central and 25% alignments are smaller than for the previous analysis. The damage of the building is much higher and it makes the whole building to move, and not only the central alignment of the walls (the weakest parts).

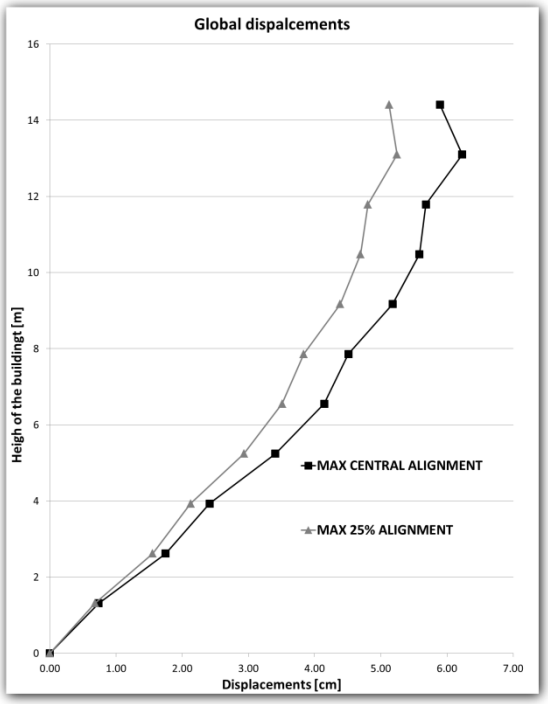

(a)

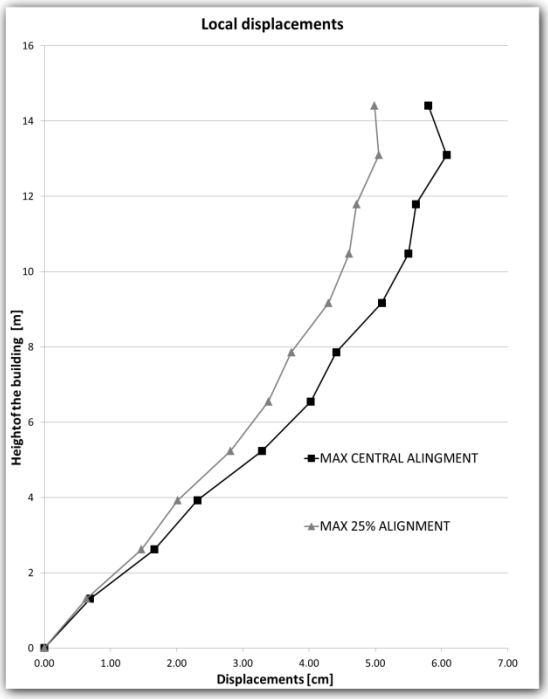

(b)

Figure 45 – Out-of-plane (a) global and (b) local displacements for the south façade.

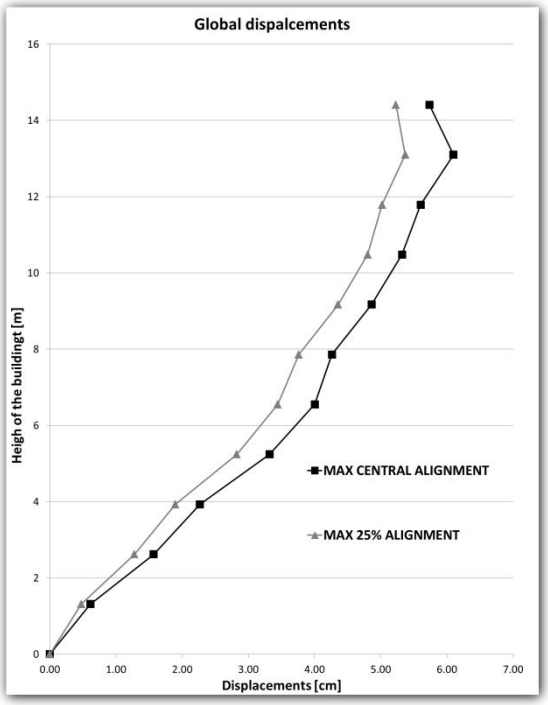

(a)

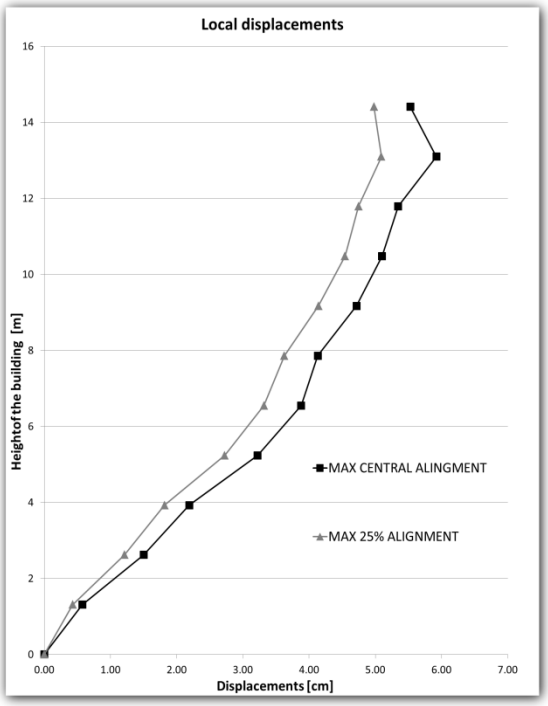

(b)

Figure 46 – Out-of-plane (a) global and (b) local displacements for the north façade.

The in-plane drifts are in the Figure 47, (a) for the south façade and (b) for the north façade. As for the gabble walls the drifts are larger than for the previous calculation, reaching values about 1.0%. However, the configuration is pretty similar, increasing slightly as the height of the building increases; the increment of PGA in the input does not modify the way the building responds to it, only the values of this response.

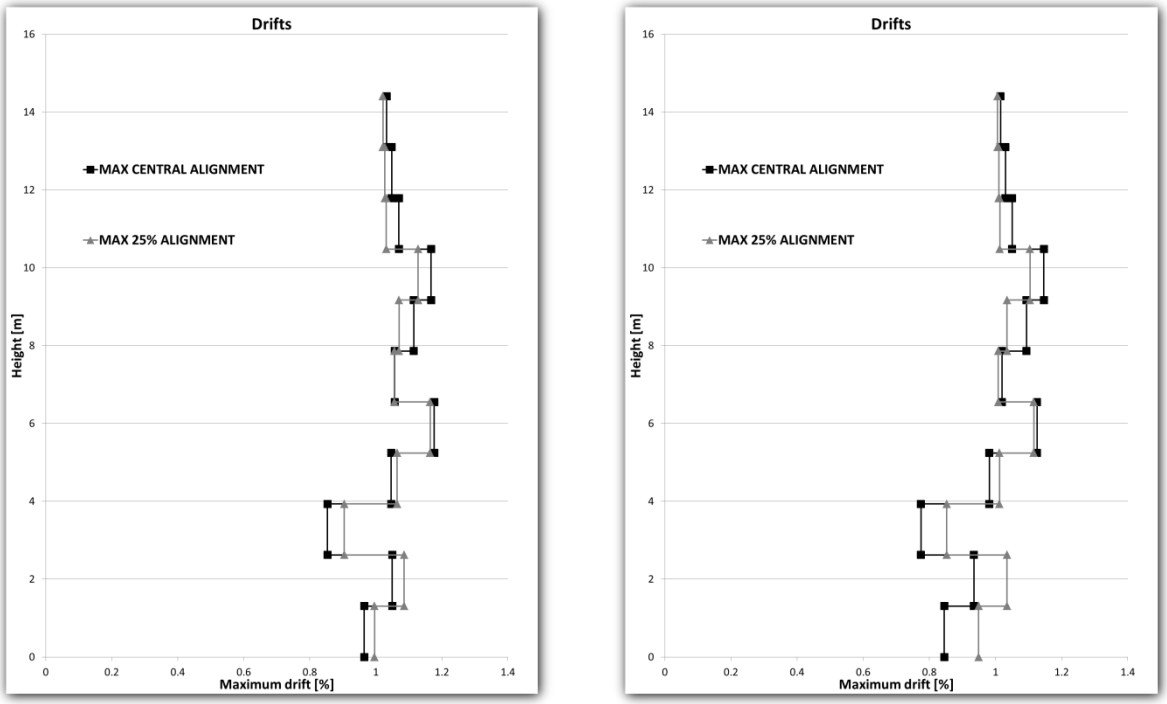

(a) (b)

Figure 47 - In-plane drifts for the (a) south and (b) north façades.

5.3.3 Envelopes

The graphs shown here have the same configuration as for the 100% PGA earthquake. The graphs for the gabble walls can be seen in the Figure 48; (a) in the X direction and (b) in the Z direction. For the façades the graphs can be seen in the Figure 49. As expected, both displacements and seismic coefficient are larger. For this earthquake the shape of the envelopes is not as regular as for the 100% PGA earthquake. The building demand is higher and its response is more irregular. In addition, local collapses can be expected. However, as before, the response is very dependent on the directions of the load as well as the direction in which the measures are taken. The critical points of the envelopes are highlighted with a bold circle. Point A corresponds to the step number 1798, B to 1810, C to 1646, D to 1632, E to 1328 and F to 1354. Since the behaviour patterns are similar for several of those points, with two different mechanisms, only the response in the points C and F are shown here. All the other results can be seen in the Annex B.

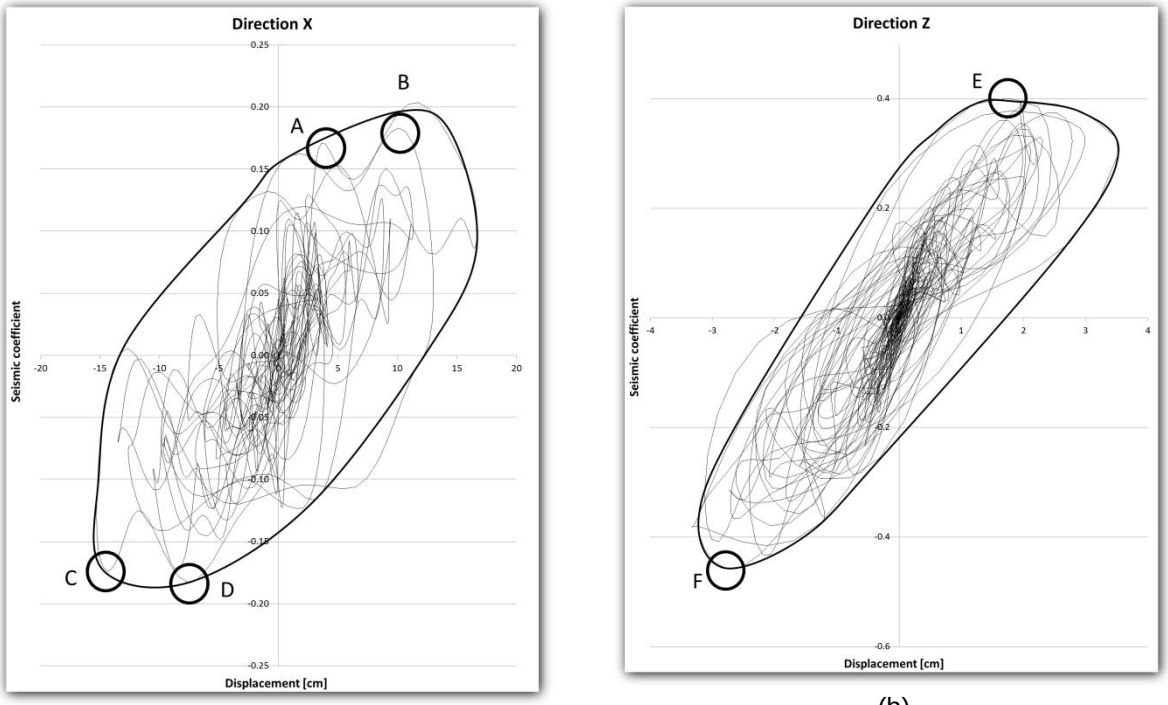

(a) (b)

Figure 48 - Envelope displacement-seismic coefficient in (a) axis X and (b) axis Z for the gabble wall.

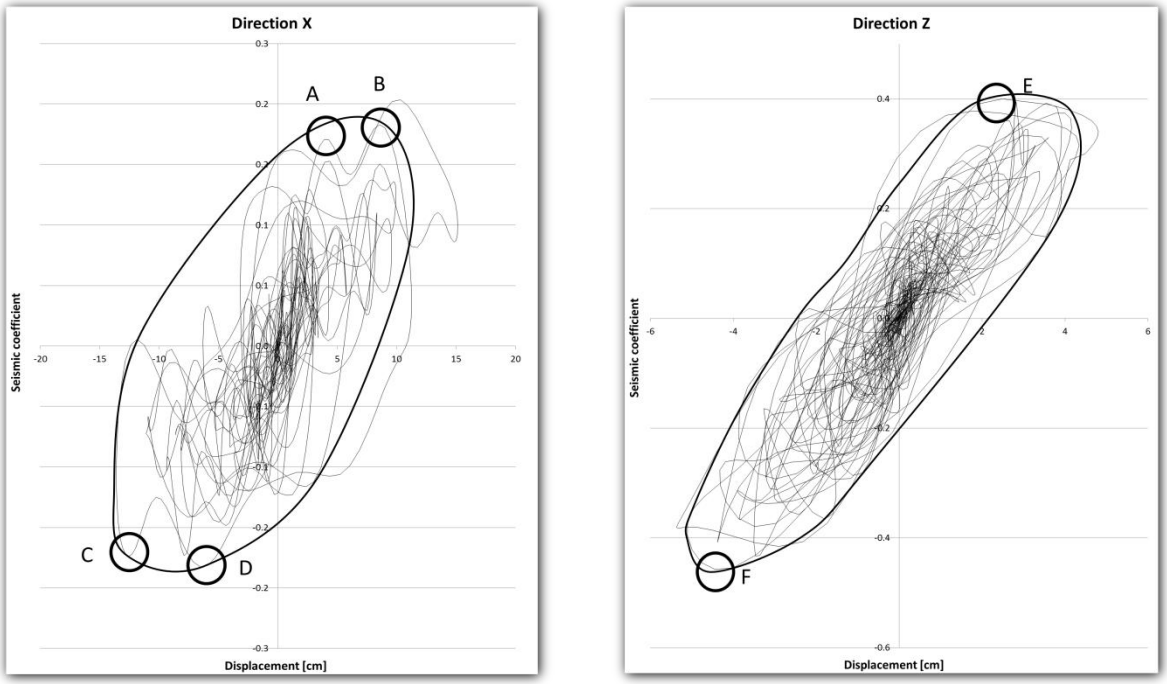

(a) (b)

Figure 49 - Envelope displacement-seismic coefficient in (a) axis X and (b) axis Z for the façades.

The deformed meshes are shown in the Figure 50, while some examples of the strains states and of the stresses states can be seen in the Figure 51 and Figure 52 respectively. The scale factor for all the images is the same, 150. All the other images at these loading stages can be seen in the Annex B. The point C, which corresponds to the step number 1646, is the global mechanism of the building. It is important to mention that in the point A the mechanism is the same. For the points D and E the mechanism is very similar, the difference is that the most displaced walls are the gabble ones instead of the façades. All the building is leaning and the maximum displacements are at the top of the façades. It is the most dangerous response of the building, since the façades are the weakest parts of the structure. This effect can be seen in the tensile strain concentrations in the lintels of the openings, which is quite large. The compressive stresses are concentrated at the base of the gabble walls, due to shear action.

In the point F, which corresponds to the step number 1354, one of the most common local mechanisms that occur in the structure is shown. The same response can be observed in the point B, but without the bulging of the gabble walls; that is the reason why this point B is not shown. The out-of-plane displacements of the façades are very large, and they cause a significant damage concentration in a small part of the façades, in the central pier at the last floor. This effect is causing a lot of strains concentrations around the bulge of the façade. This is, most probably, the mechanism that caused the collapse of the pier in the mock-up tested in (Yang 2010).

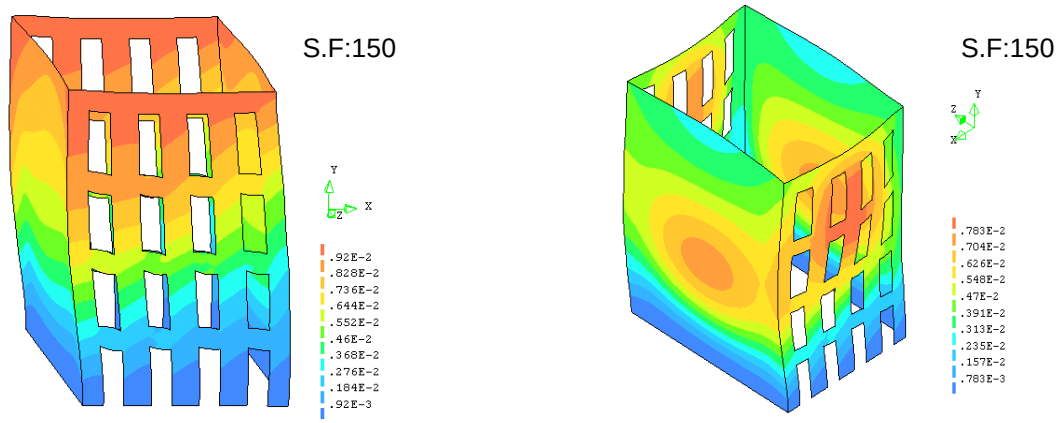

Figure 50 - Deformed meshes in the critical points, (a) for the point C and (b) for the point F.

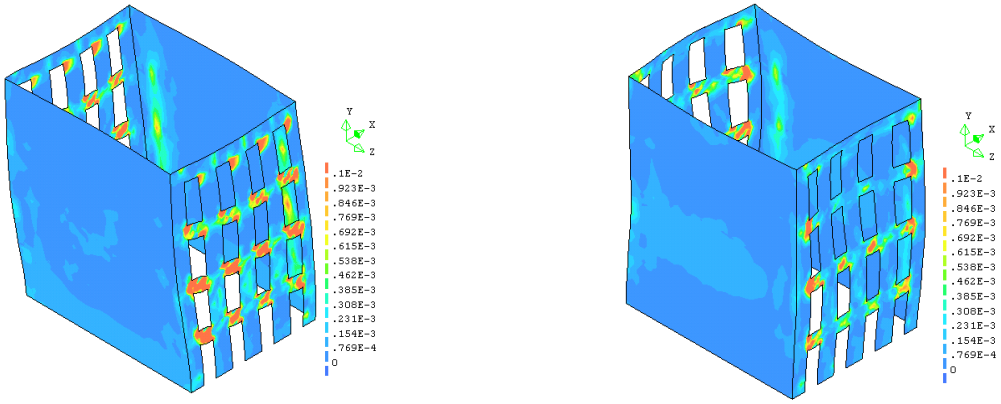

(a) (b)

Figure 51 – Strain states in the critical points, showing the north-east perspective, (a) for the point C and (b) for the point F.

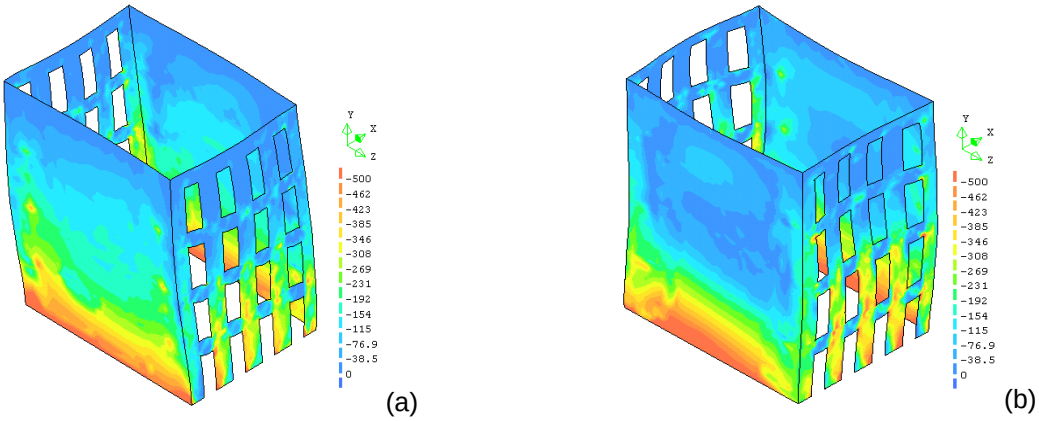

(a) (b)

Figure 52 – Stress states in the critical points, showing the north-east perspective, (a) for the point C and (b) for the point F.

5.3.4 Principal tensile strains

The envelope of the strains is shown in Figure 53. The strains have a similar contour to the 100% PGA earthquake; the difference is the intensity and the concentration of the strains, which are larger in this analysis. The strains are concentrated in the lintels, showing the typical X shape due to in-plane damage. However, small damages can be seen at the base of the piers, due to their rotation, and in the gabble wall, due to the punching of the joists. It is interesting to notice the concentration of strains at the top of the piers. Like for 100% PGA earthquake, the crack pattern is in accordance with the damages seen in the mock-up described in (Yang 2010).

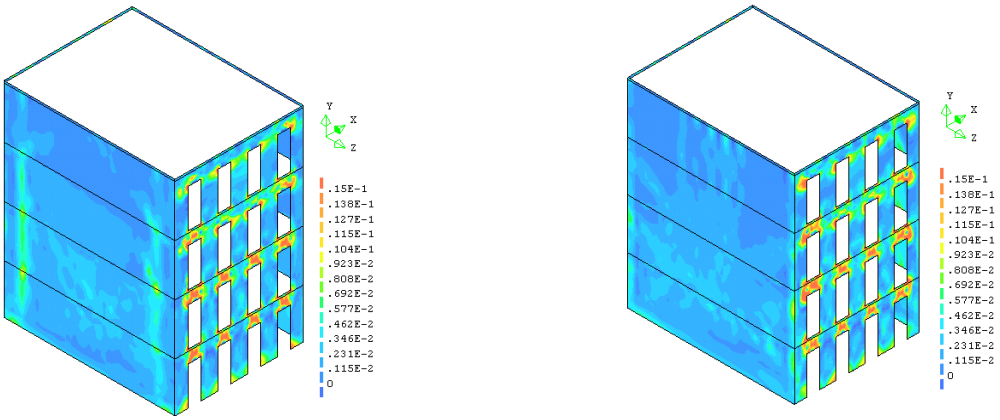

(a) (b)

Figure 53 - North-east view of the tensile principal strains envelope showing (a) the inner side and (b) the outer side of the walls.

5.4 Conclusion

The results show that the most important factor that influences the response of the structure is the direction in which the loads are being applied and in which the quantities are evaluated: in-plane or out-of-plane. This means that the stiffness of the floors is not enough to transfer the loads and forces between the different walls and thus the building does not have full box behaviour, with rigid diaphragms, but as 4 walls joined in the corners and partly connected with the floors.

The building is safe for the earthquake of Lisbon. Thus the damage shown is moderate and no clear macro block or failure mechanism can be recognised at this load level. The strains and the envelopes match reasonably well with the damages observed in the pushover analyses of the previous chapter. The relation between seismic base coefficient and maximum horizontal displacement is also similar.

The 300% PGA earthquake allows determining the most probable collapse mechanism, which is due to the failure of the lintels, as can be seen in the envelopes of tensile strains. Moreover, the analysis shows also some local mechanisms, like the bending of the gabble walls or the bulging stresses in the façades. Most probably the PGA could be still augmented, since the seismic coefficients reached are slightly lower than the ones obtained with the pushover analyses, and the displacements are still reasonably moderate. This analysis provides a clear idea of the response of the structure and the expected failure mode.

Chapter 6

Sensitivity analysis

Abstract

In this chapter a parametric study is developed, aimed to assess a range of values for relevant analysis parameters and to discuss the influence of these parameters in the final behaviour of the structure. The goal of the sensitivity analysis is to validate the influence of the parameter selection in the building performance. Thanks to the range of parameters used it is possible to discuss the reliability of the numerical analysis results and the needs for more advanced material or structural characterization in this type of buildings.

6.1 Introduction

The usage of advanced non-linear structural analysis tools requires experienced analysts and the doubt arises on the quality of data adopted in the simulations, particularly on existing buildings, in which scatter is large and material / structural characterization is difficult and expensive. Parametric studies are useful to define the range of expected results and to know how parameter variation influences the final response and safety of the structure.

The parameters that were assumed able to change here are: stiffness of the floor panels and stiffness, damping ratio, tensile strength and fracture energy tensile of the masonry. These changes of material properties are assessed in both static and dynamic analysis. The sensitivity analysis takes into account both east-west and north-south directions for the static analysis. For dynamic analysis both 100% and 300% PGA earthquake are analysed and discussed. However, since 100% PGA earthquake analysis only indices moderate non-linear behaviour its results is included only in the Annex C and the 300% PGA earthquake results are discussed in the main body.

6.2 Non-linear static analysis – Pushover method

6.2.1 Stiffness of the MDF panels

The objective of these calculations is to evaluate the influence of rigid diaphragms in the final behaviour of the structure. The safety of this typology of buildings with box behaviour can also be assessed thanks to this sensitivity analysis. The first result is obtained reducing the Young's modulus of the MDF panels 10 times. It is basically if there were connections with the floor structures, meaning that the structure is constituted just by the four walls. Afterwards, three calculations are done increasing the Young's modulus 10 times for each calculation, aiming at a basically rigid floor. The obtained values are thus 0.1xE, 10xE, 100xE and 1000xE, being E Young's modulus in the reference model.

The capacity curves for each analysis together with the reference model are shown in the Figure 54 for the direction east-west. The responses are similar in shape with a significant variation in seismic coefficient, between 0.23 and 0.15. The most relevant changes in the response are discussed next.

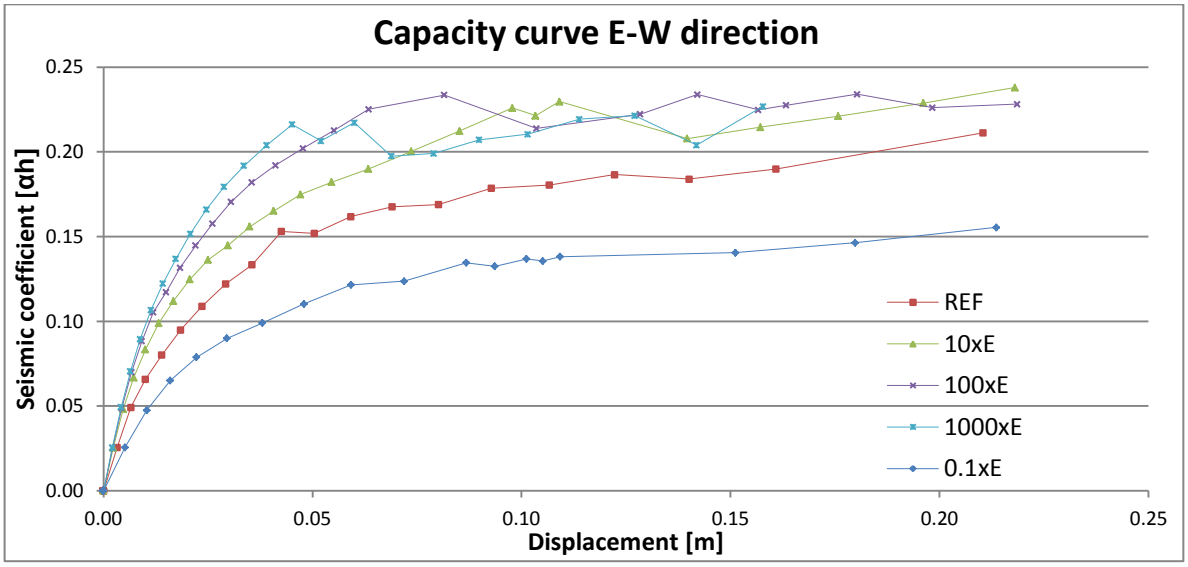

Figure 54 - Capacity curves for east-west direction.

A comparison between the deformed meshes in the ultimate step for each analysis can be seen in Figure 55. The scale factor differs for each of them. When the stiffness of the floor is very low there is no transference of loads between the walls, meaning that the walls subjected to out-of plane load move more than the ones subjected to in-plane loads. This effect can be easily identified in the Figure 55 (b). When the stiffness is increased the structure works as a whole, each wall has a similar displacement. For example, for 1000xE (e) the walls have almost the same displacement in each floor. Furthermore, this effect increases the split of the piers at the base because the global in-plane stiffness of the façades is low. The values of displacements at peak load are slightly smaller for the larger stiffness calculations.

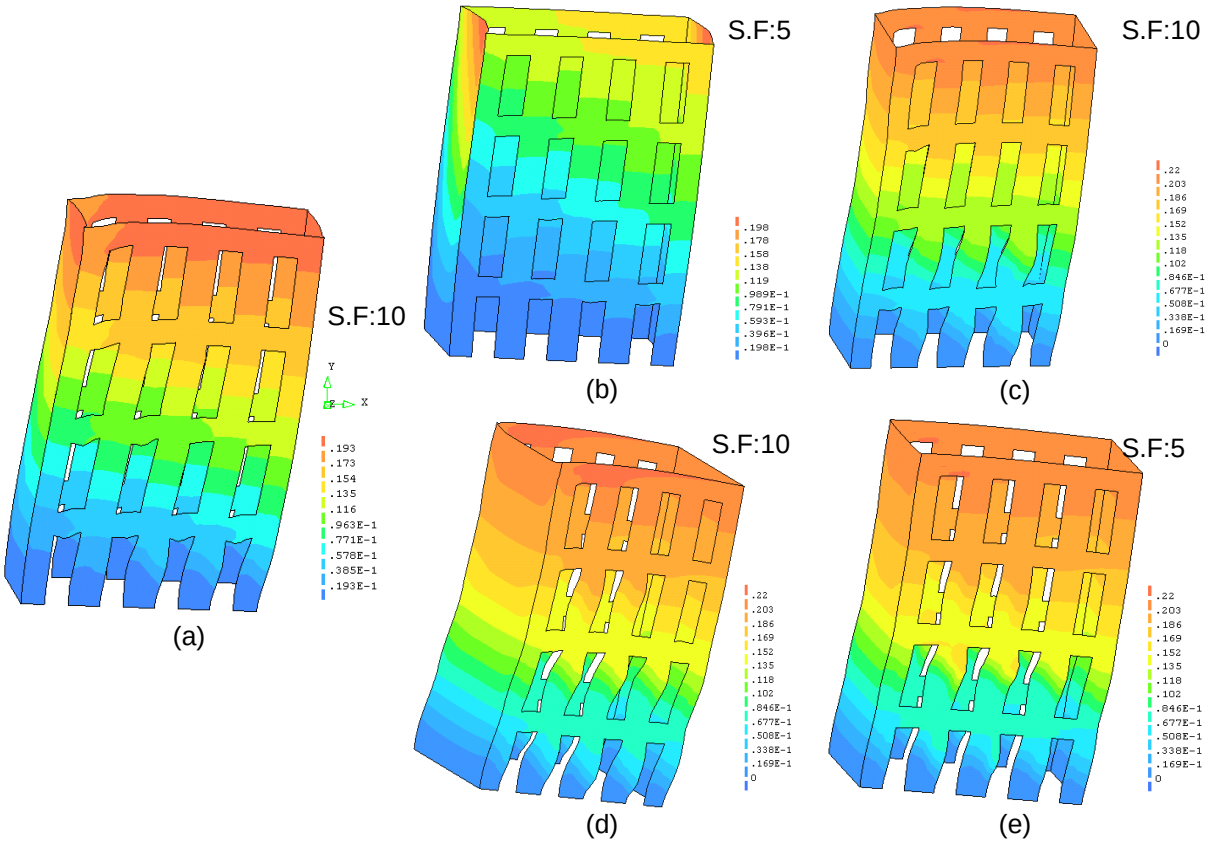

Figure 55 - Deformed meshes in the ultimate step for (a) reference mode, (b) 0.1xE, (c) 10xE, (d) 100xE and (e) 1000xE, units in meters.

The comparison of strain states is showed in Figure 56. When the stiffness is decreased the detachment of the gabble walls from the façades is more visible, with the long vertical lines of large cracks. Also the strains in the lintels are bigger, confirming that the building becomes weaker in this direction because of the change in the deformation mode and lack of flanges for the façades. Having a much bigger value of stiffness does not significantly improve the capacity of the building, when compared to the reference response. It is also noted that the peak values of strains become larger when the stiffness is increased, as deformation tends to localize more extensively. In the figures below only the southwest perspective is shown, with the inner side of the walls. For full details about the results, see Annex A.

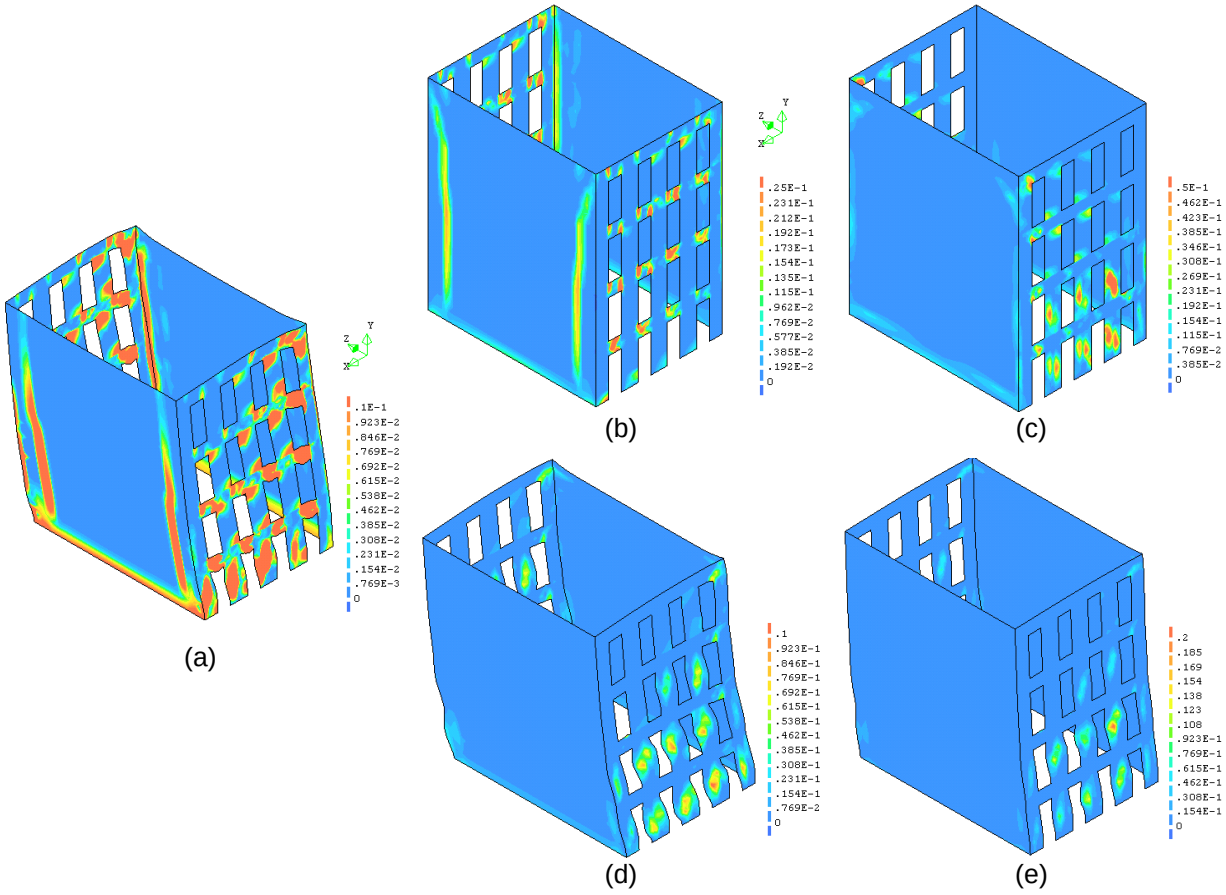

Figure 56 - South-west perspective showing the inner side of the walls at the ultimate tensile principal strain state for (a) reference, (b) 0.1xE, (c) 10xE, (d) 100xE and (e) 1000xE.

In the case of stress states both inner and outer side of the walls are necessary to understand the behaviour of the building and the possible presence of out of plane bending. The south-west perspective for the ultimate step in each calculation can be seen in the Figure 57. The peak values of compressive stresses are more or less the same for each calculation. However, as the stiffness of the floor structures is increased, the compressive stresses in the gabble walls are larger. When the stiffness is equal to 1000xE (e) there is a line of very high stress concentrations in the outer side of the gabble wall that does not appear in the reference model. Basically, the building is more stressed when the stiffness is higher. However, these stresses are not larger than the stresses at the bottom of the gabble so it means that if the gabble is able to bear the stresses at the bottom it will withstand the new stresses at middle height as well. More figures are shown in Annex A.

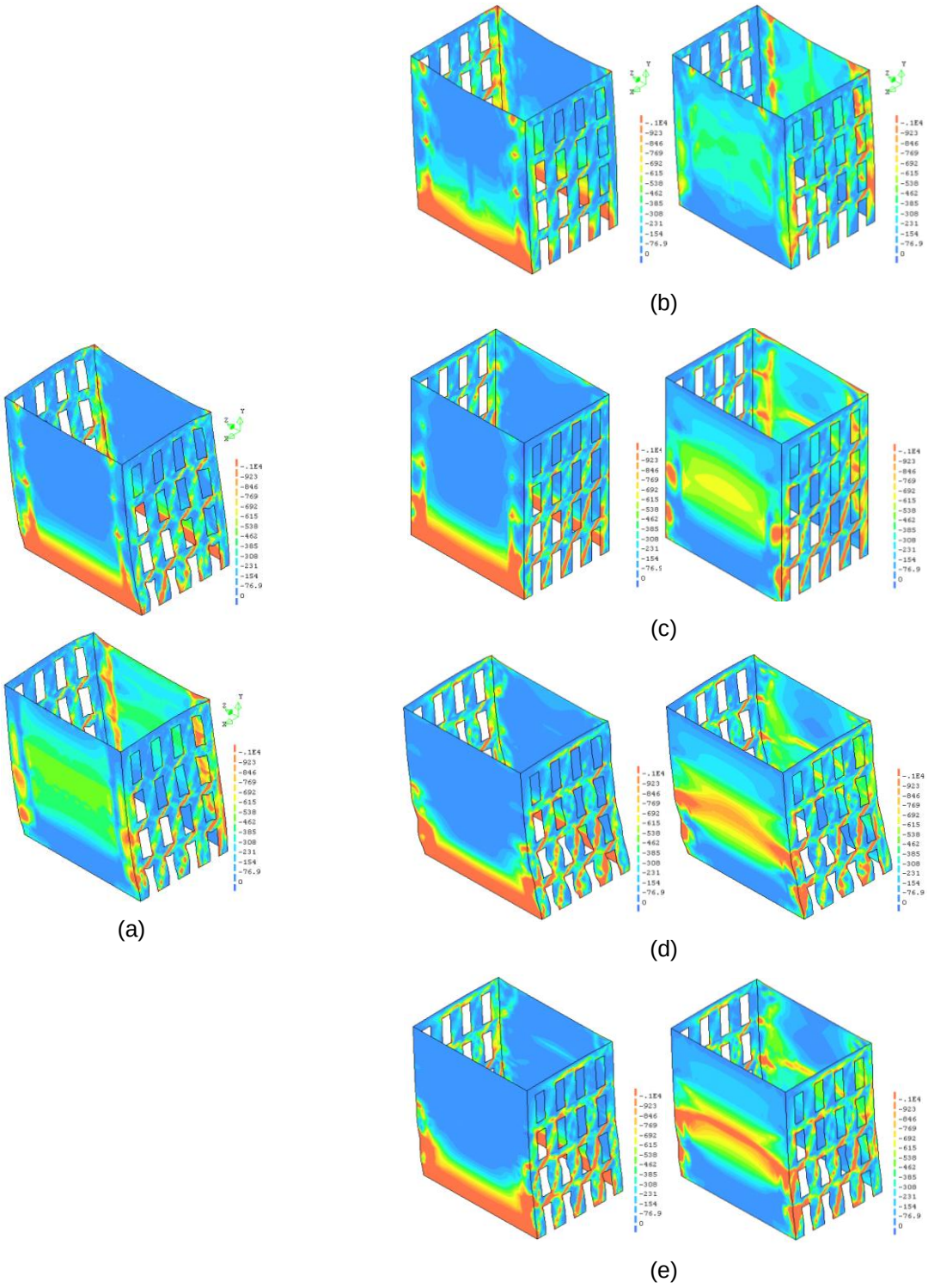

Figure 57 - South-west perspective showing the compressive principal stress state, firstly the outer and then the inner side of the wall, for (a) reference, (b) 0.1xE, (c) 10xE, (d) 100xE and (e) 1000xE, units in kPa.

The capacity curves in the direction north-south can be seen in Figure 58, with a significant variation in seismic coefficient, between 0.65 and 0.42, and changes in behaviour are more obvious. The deformed meshes in the ultimate state for every calculation can be seen in Figure 59, being the scale factors different among the calculations. For the reference model the stiffness of the floors is not enough to transfer all the loads from the gabble walls to the façades, with the largest displacements being located in the south façade. In addition, the gabble walls show an important deformation due to the shear stresses. When the stiffness is reduced to 0.1xE (b), the floors are not able to transfer any forces among the walls. The shear stresses disappear from the gabble wall and all the displacements are concentrated in the façades. As the stiffness of the floors is augmented the structure starts to work as a rigid block, and the difference of displacements between the south façade and the gabble walls tends to disappear. Furthermore, the floors are so stiff than the loads are transferred to the north façade. The consequence of this behaviour is that the displacements are bigger in the north façade than in the south one. When the stiffness of the floor structures is very low the out-of-plane displacements of the south façade can cause its local collapse. On the contrary, when the floors are stiff the building works as whole, leaning in all its height. This avoids large shear stresses and out-of-plane displacements.

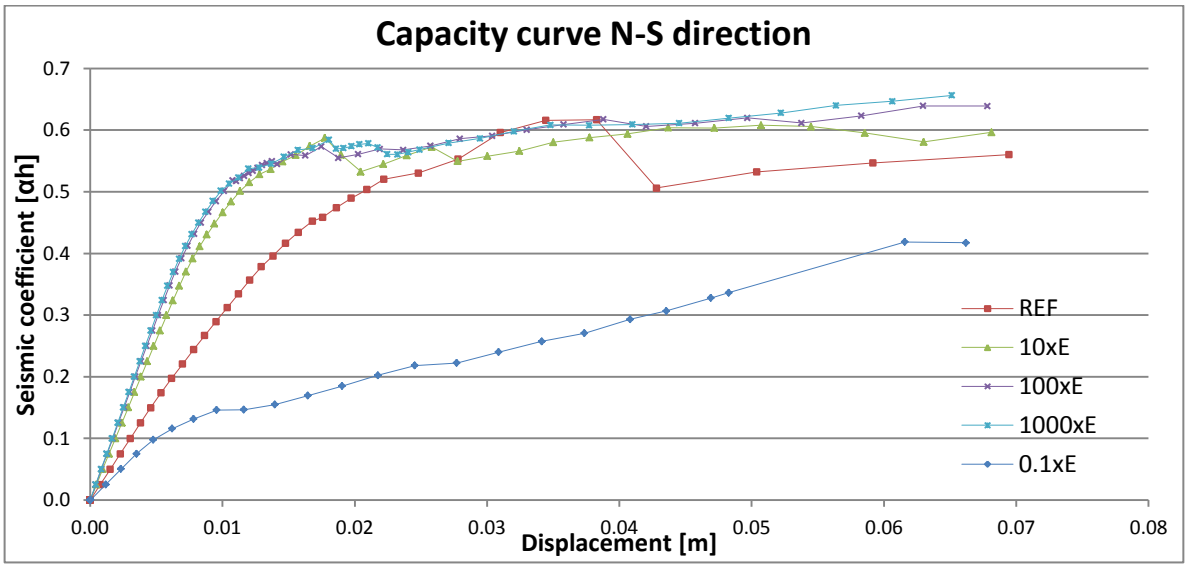

Figure 58 - Capacity curves for north-south direction.

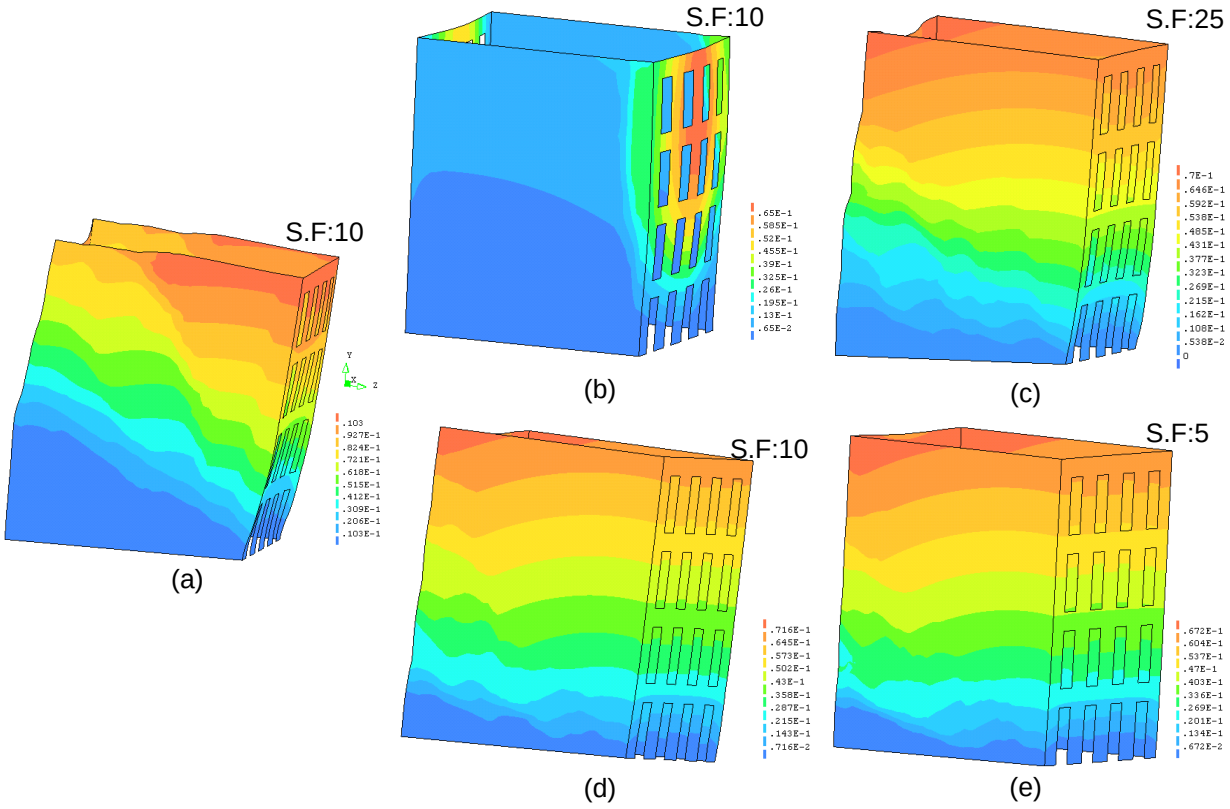

Figure 59 - Deformed meshes in the ultimate step for (a) reference mode, (b) 0.1xE, (c) 10xE, (d) 100xE and (e) 1000xE, units in meters.

The tensile strain states in the ultimate step are shown in Figure 60. The figures show again the perspective southwest, and the outer side of the walls close to the observer and the inner side of the walls far to the observer. The behaviour differs for the reference model and for those in which the stiffness is smaller (b) or very large (e). The strains that define the macro-block are in a different place, ranging between out-of-plane rotation of the façades, shear failure of the gabble walls and rocking of the gable walls. There is another minor difference: the collapse of the upper part of lintels in the south façade is more likely as the stiffness is increased, due to the combined effect of the restraining effect of the floors and the uplift of the rocking building. When the stiffness of the floors is decreased, the north façade is detaching from the building, because the floors do not transfer the loads between the walls, so the out-of-plane displacement of the façade (Figure 59 b) is too big to be supported by the corner joints. The failure is due to rotation of the façades with large tensile stress in the backing gabble walls. Small strains are also visible in the façade, due to its horizontal bending. For a more detailed examination see Annex A.

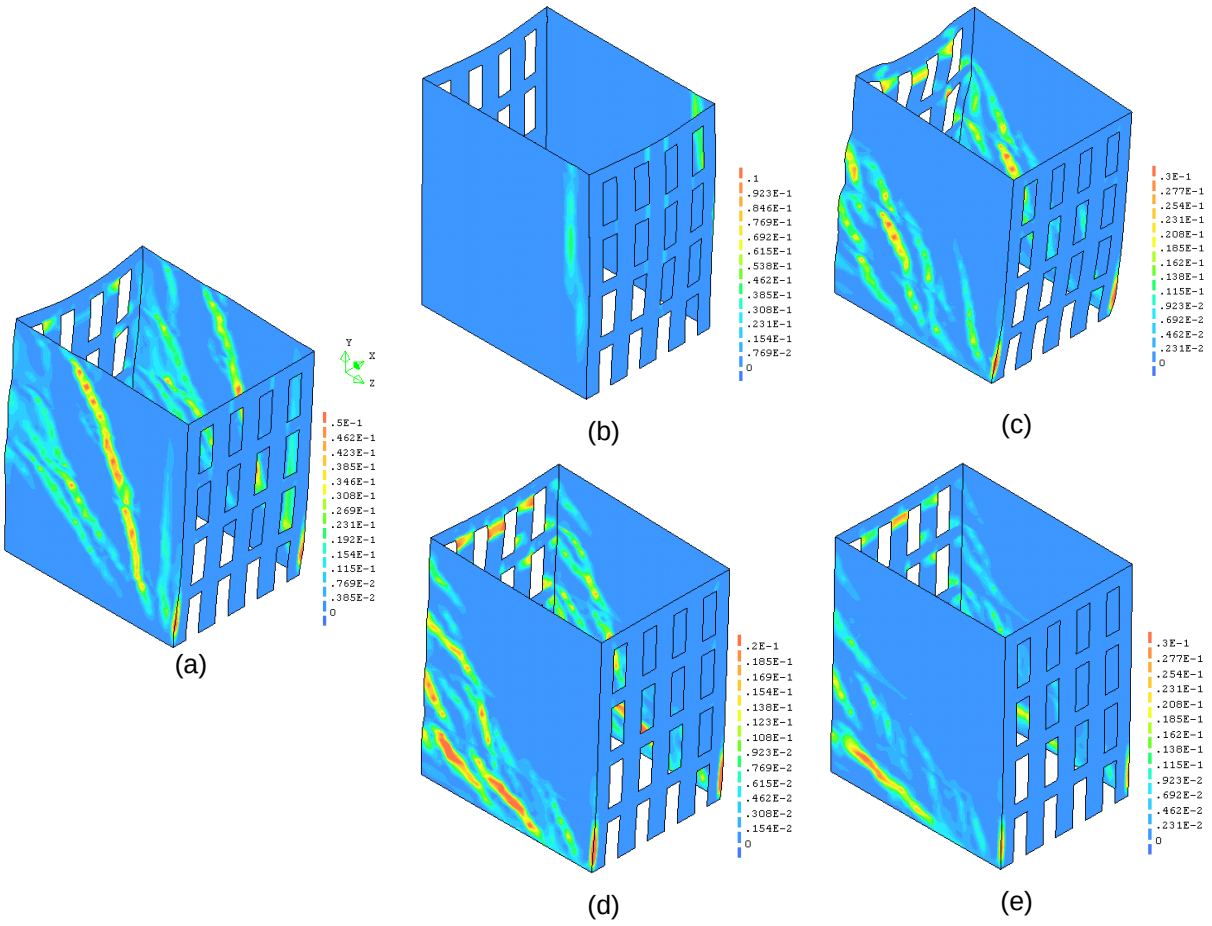

Figure 60 – North-east perspective showing the outer side of the walls at the tensile principal strain state for (a) reference, (b) 0.1xE, (c) 10xE, (d) 100xE and (e) 1000xE.

The compressive stress states in the ultimate steps are shown in the Figure 61. The north-east façade is shown, which is enough to understand the behaviour of the building. Similarly to the tensile strains, the compressive stress state is different for the different calculations. When the stiffness is increased the lintels in the last floor show slight differences as before but the most important change is the distribution of the lines of stresses. When the stiffness is decreased (b) the stress pattern changes a lot too. According to the strain state showed in Figure 60 (b) a release of stresses due to a presence of strains can be seen in the gabble walls, close to the corners of the façades. The north façade is working independently of the rest of the building, as indicated below. For a more carefully examination of the stress states, see Annex A.

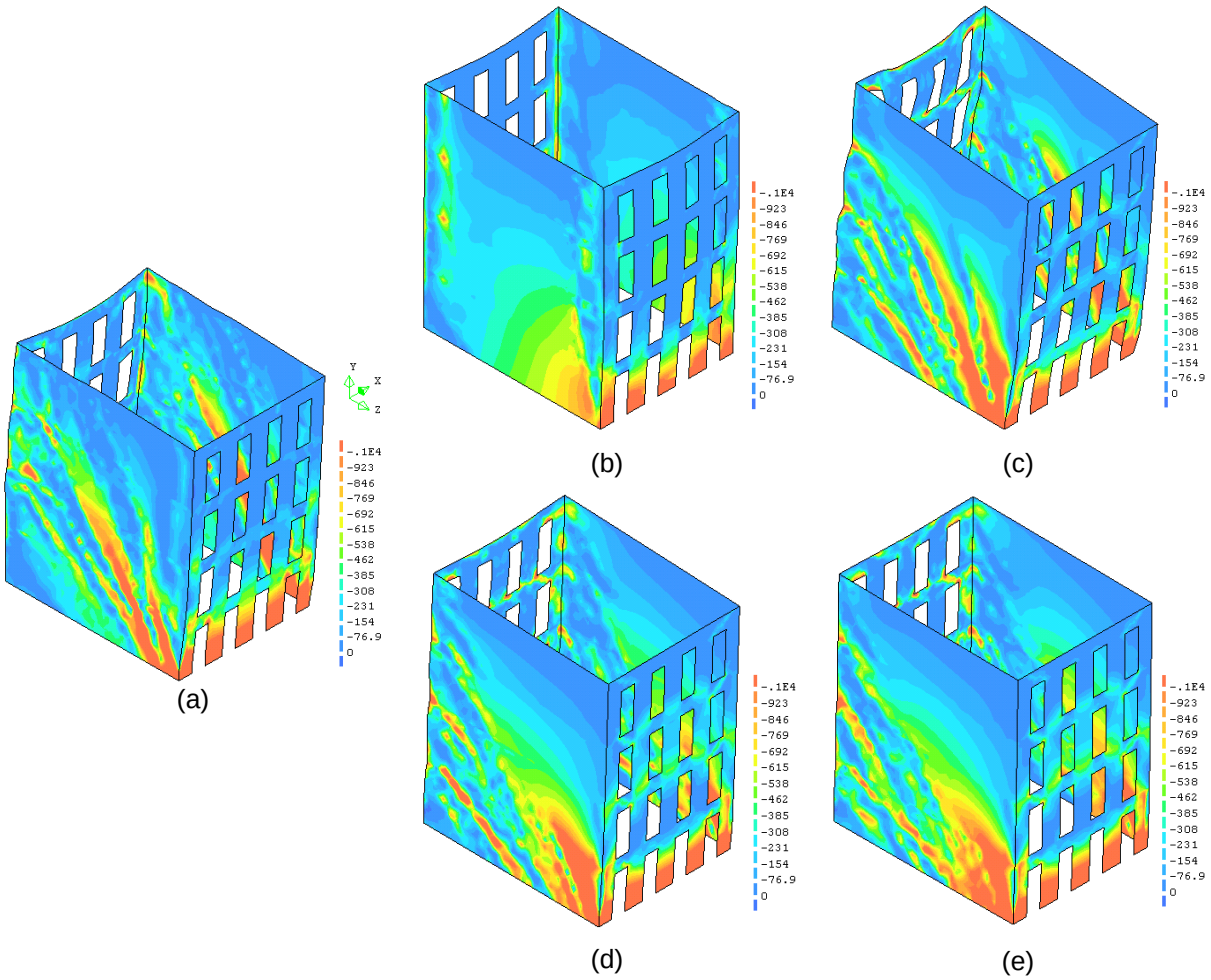

Figure 61 – North-east perspective showing the compressive principal stress state in the outer side of the wall, for (a) reference, (b) 0.1xE, (c) 10xE, (d) 100xE and (e) 1000xE, units in kPa.

6.2.2 Stiffness of the masonry walls.

The value to be modified in this section is the Young's modulus of the masonry, with the aim to evaluate the influence of the stiffness of the masonry in the final behaviour. Two different analyses are shown here; with half stiffness (0.5xE) and with double stiffness (2xE). The capacity curves for east-west direction are shown in the Figure 62, with a variation in the seismic coefficient between 0.23 and 0.17.

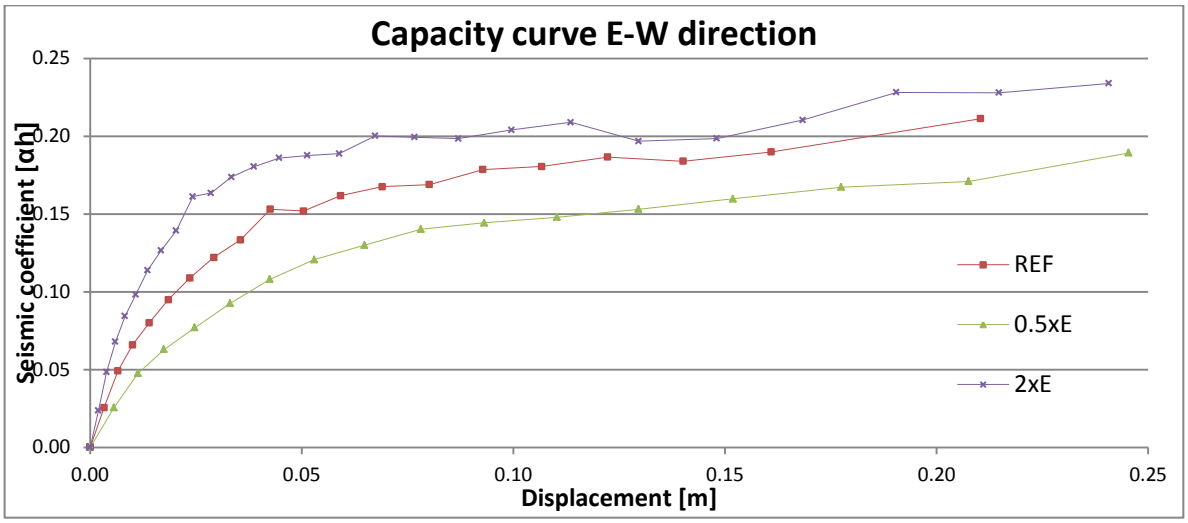

Figure 62 - Capacity curves for east-west direction.

The deformed shapes can be seen in Figure 63. The difference of masonry stiffness in the given range does not affect the displacements. The distribution and the maximum values of displacements are very similar for each calculation. In this case the scale factors are the same for all of them.

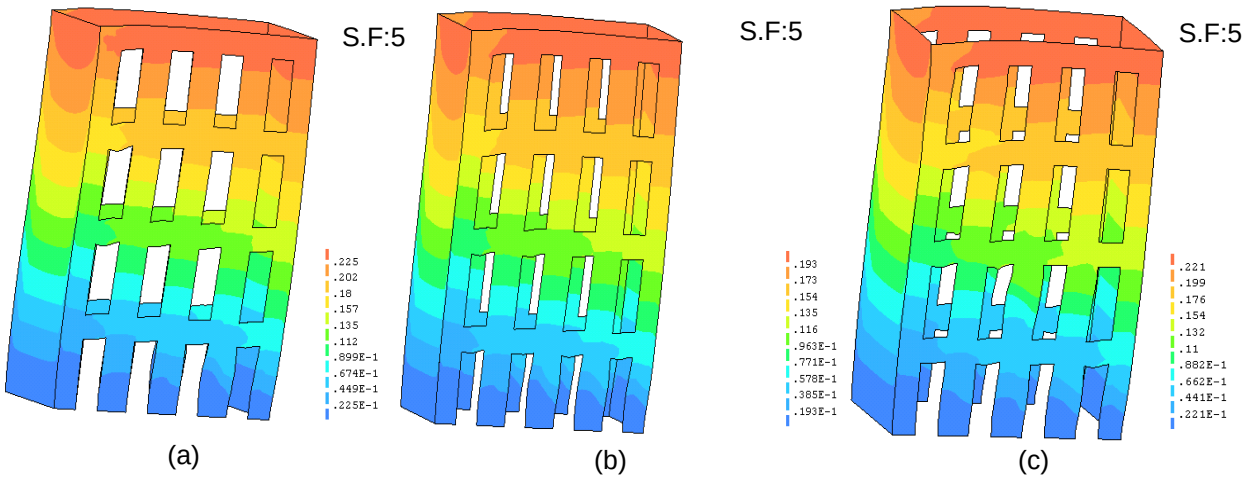

Figure 63 - Deformed shapes in the ultimate steps for (a) 0.5xE, (b) reference and (c) 2xE, units in meters.

The tensile strain states at the ultimate step can be seen in the Figure 64. Only the southwest perspective is shown, which is enough to understand the response of the structure. As for deformation, the influence of the stiffness of masonry is very slight. The behaviour of the building is

basically the same. Only the distribution of the strains is a bit different but the peak values remain in the same range. For more detailed examination see Annex A.

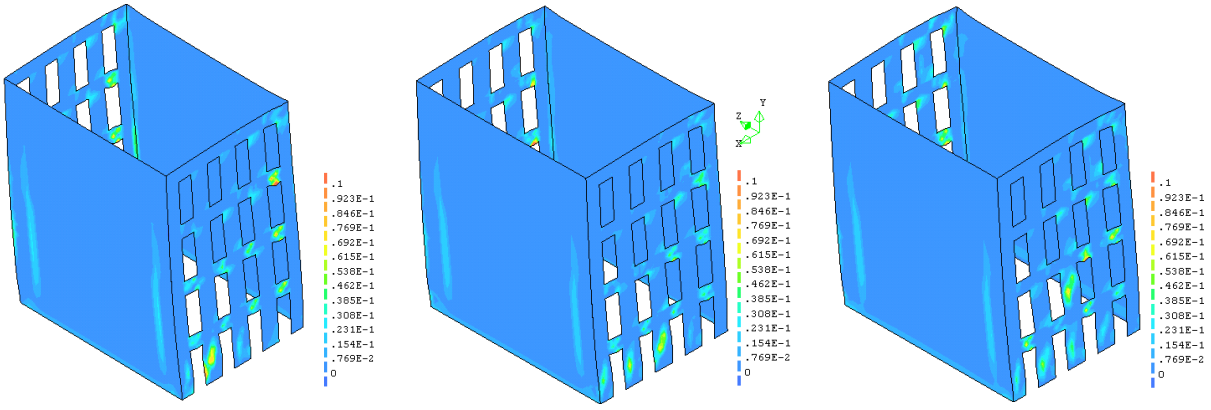

(a) (b) (c)

Figure 64 – Tensile principal strain states in the ultimate steps for (a) 0.5xE, (b) reference and (c) 2xE.

The compressive stress states in the ultimate steps are shown in the Figure 65. The perspective southwest is shown. First the inner side of these walls and the outer side of north and east walls and, afterwards, the other way around. As before, the behaviour is similar for each calculation and the building responds in the same way. However, the stiffer the masonry is the larger stresses it has to bear. Thus, for the 0.5xE calculation the peak value is 500 kPa, for the reference is 600 kPa and for 2xE is 800 kPa. These data were obtained directly from the postprocessor and it is not easy to observe them in the graphs. Still, the patch of stresses becomes bigger when the stiffness is increased. There are more figures available in the Annex A, for further details.

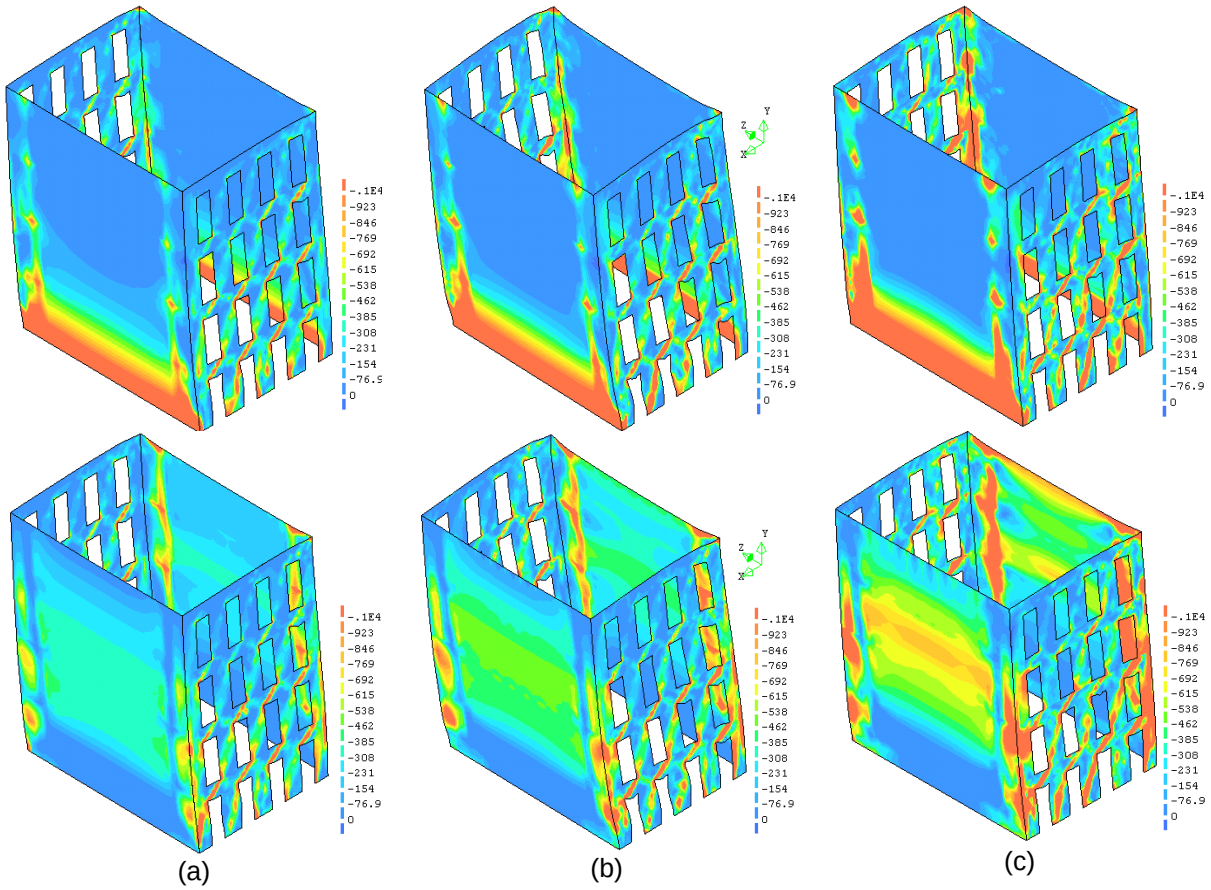

Figure 65 – Compressive principal stress states in the ultimate steps for (a) 0.5xE, (b) reference and (c) 2xE, units in kPa.

The curves for north-south direction can be seen in the Figure 66, with a variation in the seismic coefficient between 0.63 and 0.48.

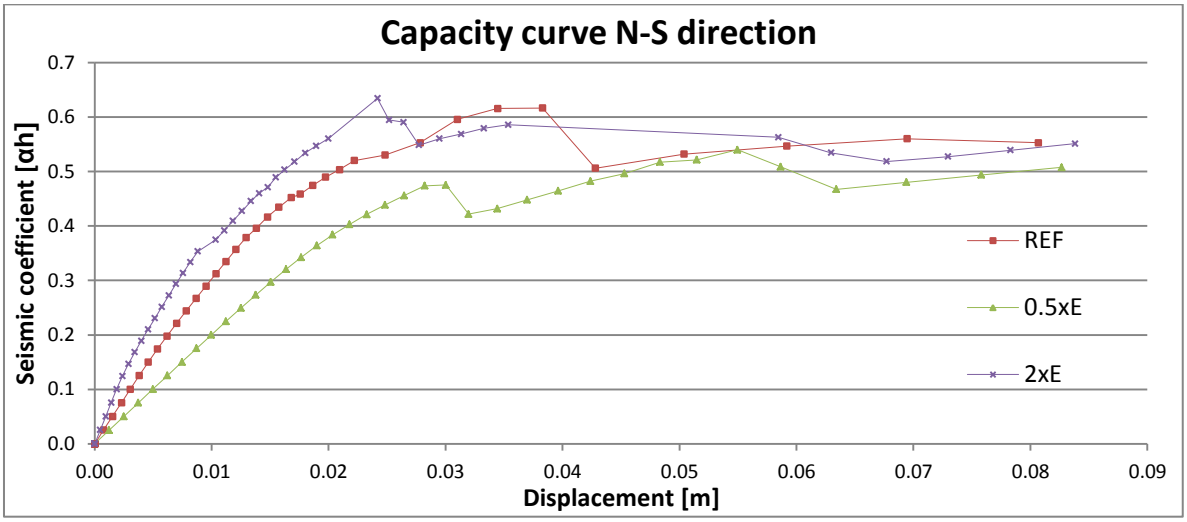

Figure 66 - Capacity curves for north-south direction.

The deformed meshes can be seen in Figure 67. The peak displacements are similar for the different calculations. However, the response is slightly different. As the stiffness of the walls is increased the shear stress becomes larger. When the stiffness is 0.5xE (a) the shear deformation concentrates on the lower part of the model. On the contrary, when the stiffness is 2xE (c) the deformation moves to an upper part. This effect can be seen in the Figure 68 and Figure 69, which correspond to strain and stress states.

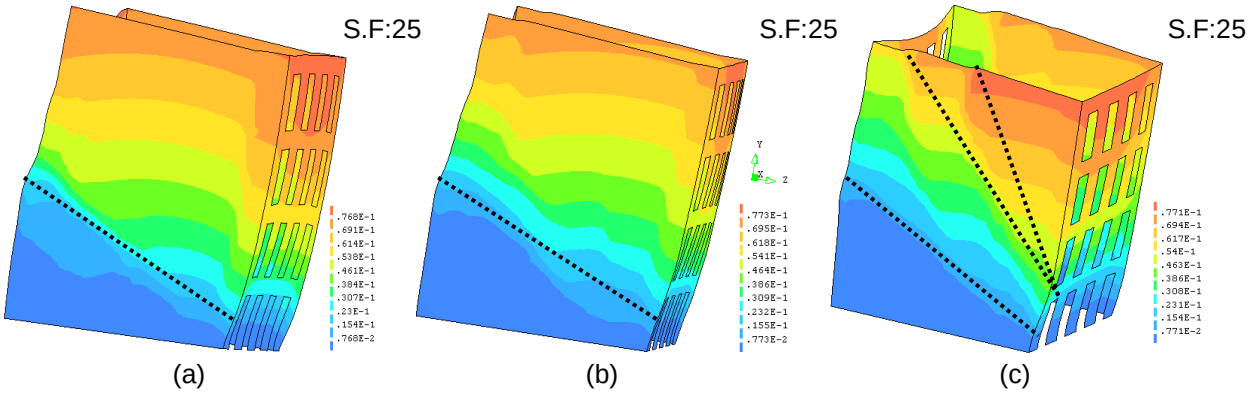

Figure 67 – Deformed meshes in the ultimate steps for (a) 0.5xE, (b) reference and (c) 2xE, units in meters.

The tensile strains states in the ultimate steps are shown in the Figure 68 for (a) 0.1xE, (b) reference and (c) 10xE. The perspectives shown are the northeast. The response of the building is similar for the different calculations. The lines of strains delimit the possible macro blocks in which the building can be divided at failure. As the stiffness of the masonry increases the structure becomes more independent of the floors and the gabble walls work more as isolated walls, providing higher strains. Therefore, an increase of stiffness does not necessarily provide a positive improvement of the capacity of the building. For a more detailed examination see Annex A.

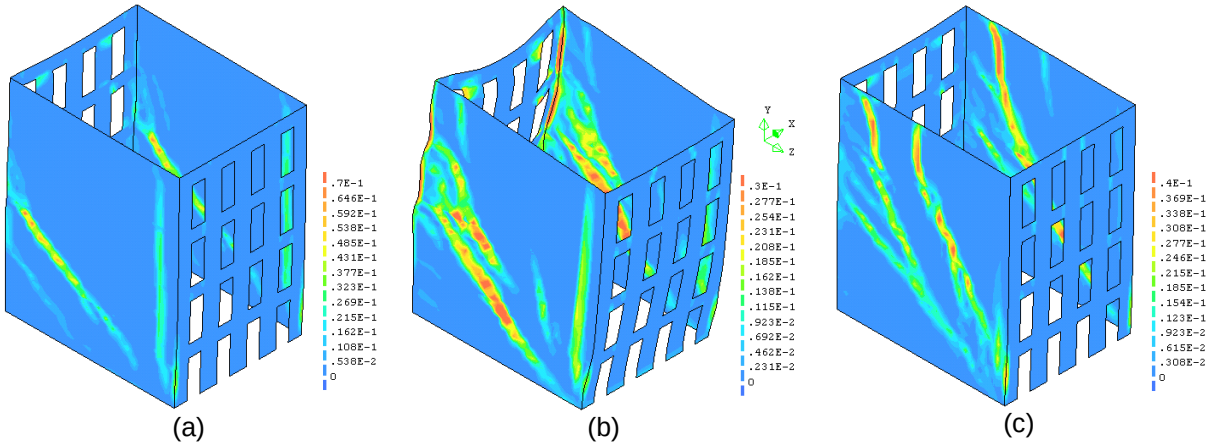

Figure 68 – Tensile principal strains states in the ultimate steps for (a) 0.5xE, (b) reference and (c) 2xE.

he compressive stress states in the ultimate step can be seen in Figure 69. In this case the perspectives shown are again the northeast. In accordance with the strains states showed before, the stresses increase when the stiffness of the walls is increased. More figures can be seen in Annex A.

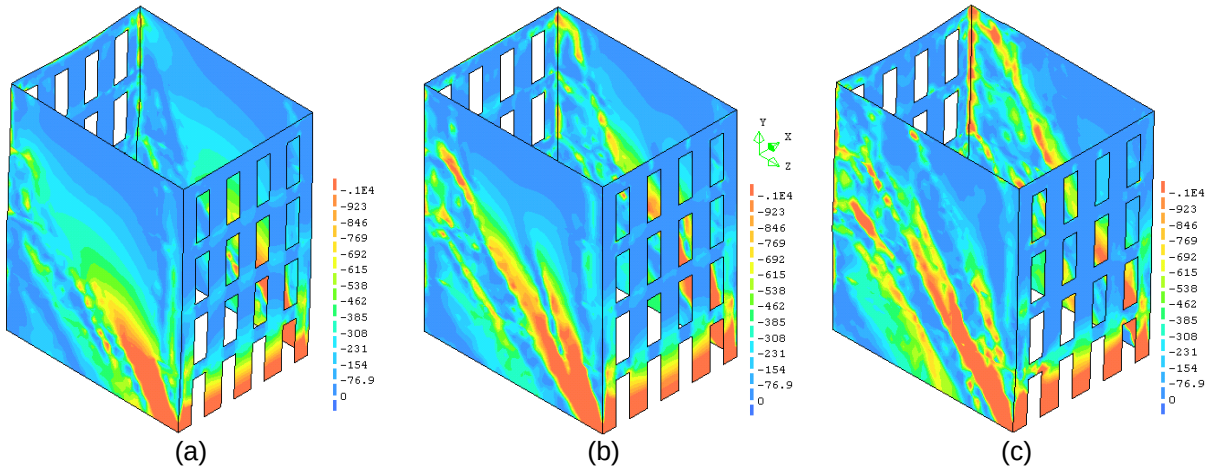

Figure 69 – Compressive principal stress states in the ultimate steps for (a) 0.5xE, (b) reference and (c) 2xE, units in kPa.

6.2.3 Tensile strength

The results for two different calculations on tensile strength are shown next, one for double tensile strength (2xFt) and another one with half strength (0.5xFt). The curves for east-west direction can be seen in the Figure 70, with a small variation in the seismic coefficient and a similar shape.

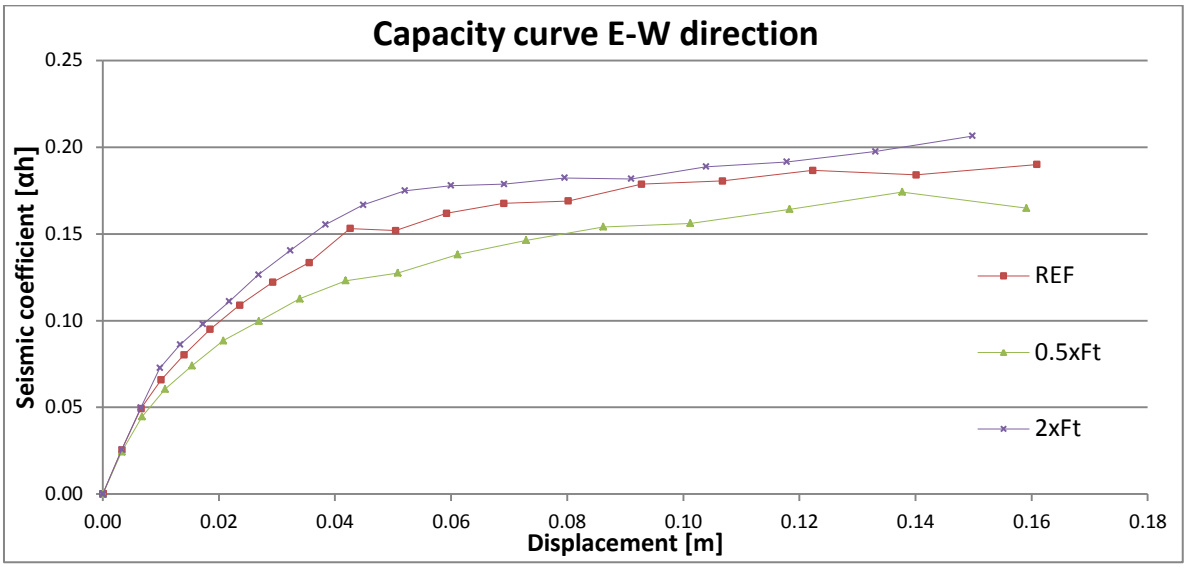

Figure 70 - Capacity curves for east-west direction.

The deformed meshes can be seen in Figure 71. The tensile strength has very little influence in the response of the structure in this direction. The distribution of displacements is very similar among the calculations and also the peak values are almost the same. The scale factor is the same for each calculation.

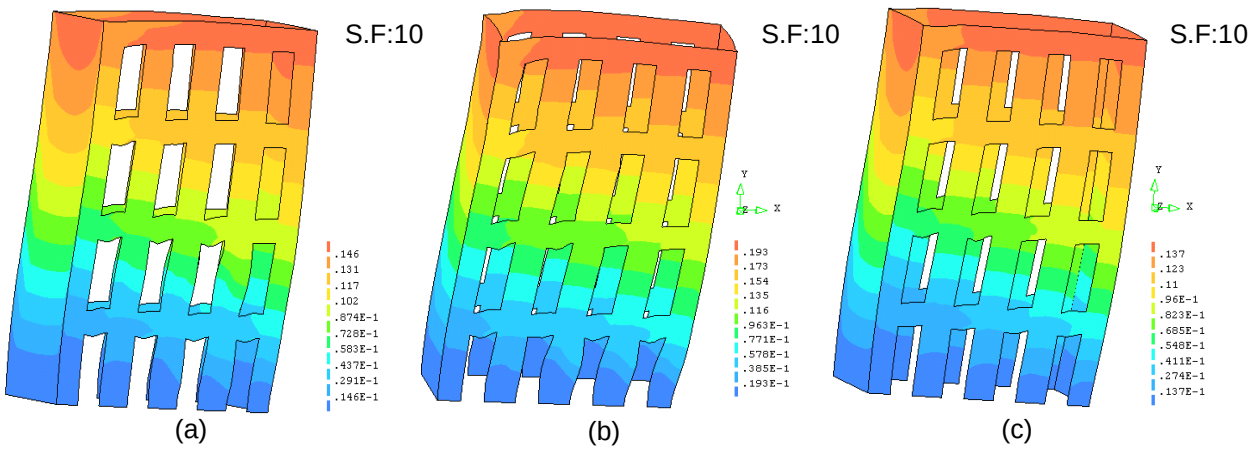

Figure 71 – Deformed meshes in the ultimate steps for (a) 0.5xFt, (b) reference and (c) 2xFt, units in meters.

The tensile strain states for the ultimate step can be seen in Figure 72. The perspective shown is the southwest and the response of the structure is very similar for all cases. The peak values are more or less the same but the strains distribution is slightly different. For 0.5xFt (a) there is a concentration of strains in the pier of the second floor, which moves to the first floor for the reference (b). For 2xFt (c) there is no any concentration in the piers, they are only in the lintels. The vertical line of strain concentration is common to all calculations. This is due to the detachment of the gabble walls and in the corners of the walls. See Annex A for more details.

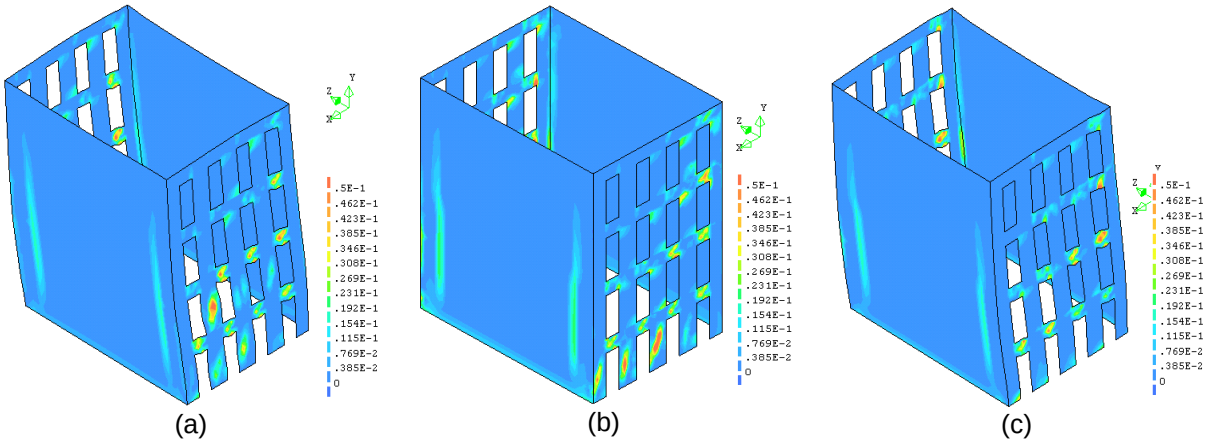

Figure 72 – Tensile principal strain states in the ultimate steps for (a) 0.5xE, (b) reference and (c) 2xFt.

The stress states are shown in Figure 73. As for deformed meshes and strains the behaviour of the building almost does not vary when the tensile strength is modified. The perspective shown is the southwest, first the outer and then the inner side of these walls. For more details, see Annex A.

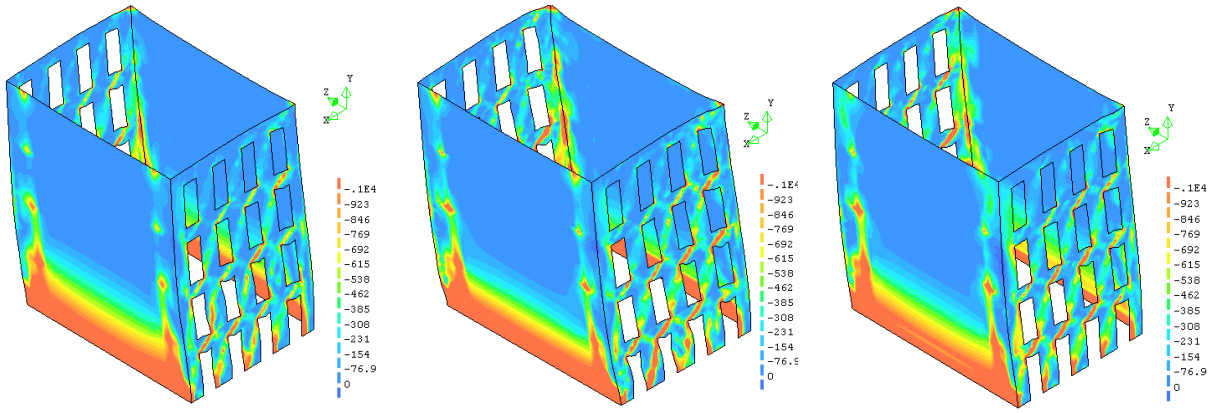

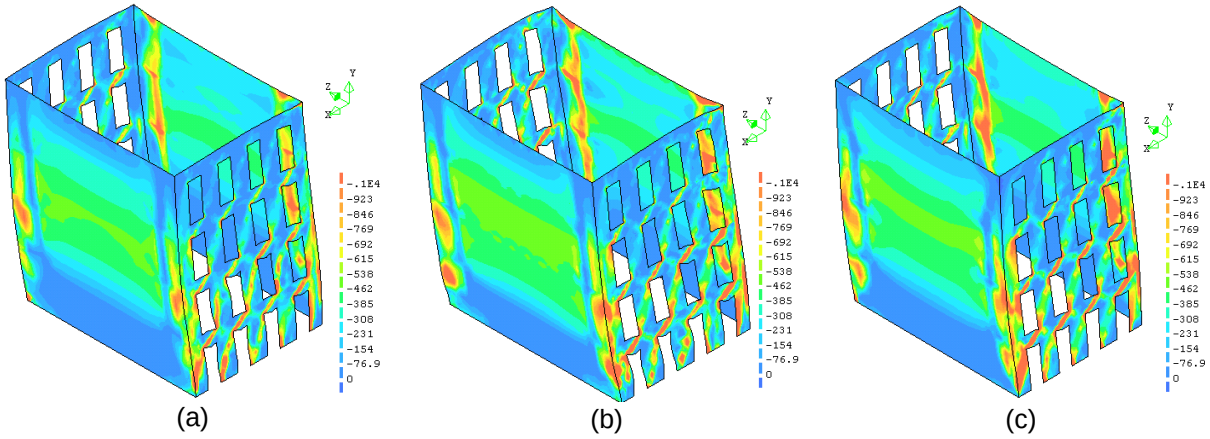

Figure 73 – Compressive principal stress states in the ultimate steps for (a) 0.5xE, (b) reference and (c) 2xE, units in kPa.

The graph for north-south direction is shown in Figure 74, with a variation in the seismic coefficient between 0.66 and 0.43.

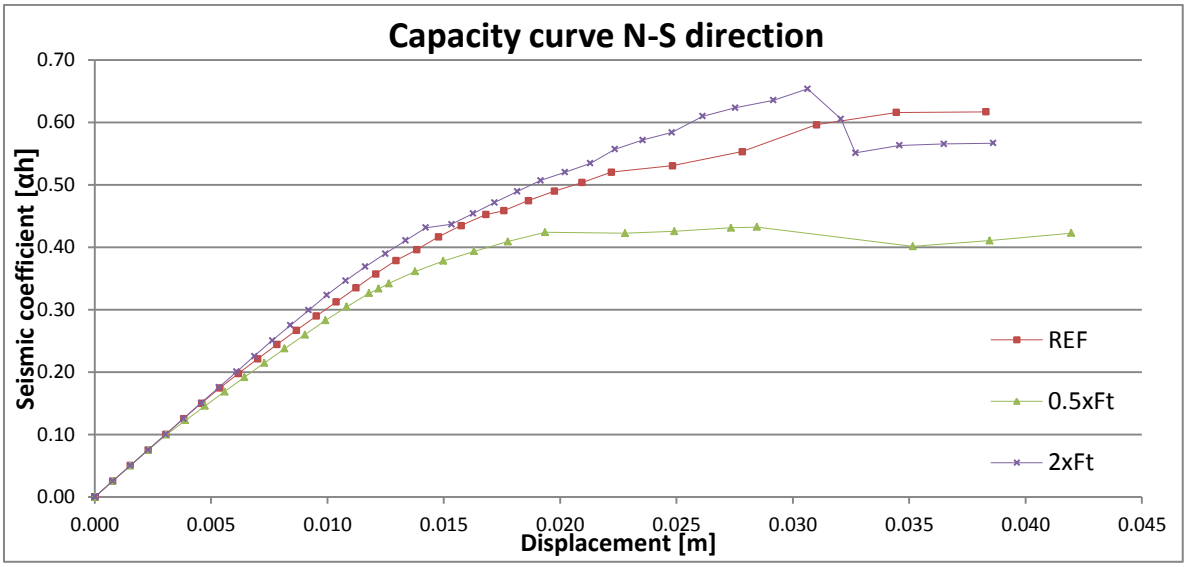

Figure 74 - Capacity curves for north-south direction.

The deformed meshes for the direction north-south can be seen in Figure 75. For this direction the influence of the tensile strength of the masonry is large. When the strength is very low (a) there is a clear shear failure in the gabble walls, see Figure 74 (a). The perpendicular displacements in the façade are concentrated in the north one. It means that there is low transferring of loads within the walls. However, when the strength is augmented to 2xFt (c) the shear stress in the gabble is very regular and the second shear failure of the façade with overturning is eliminated.

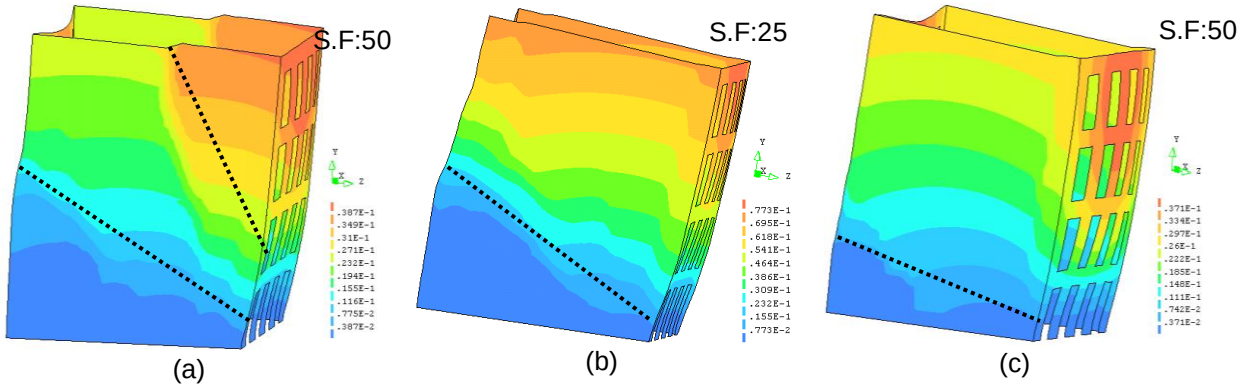

Figure 75 – Deformed meshes in the ultimate steps for (a) 0.5xFt, (b) reference and (c) 2xFt, units in meters.

The tensile strain states at the ultimate step are shown in the Figure 76. The response of the structure is very dependent on the tensile strength. When the strength has a value of 0.5xFt (a) the shear stresses are concentrated in a vertical line, in accordance with the deformed mesh showed above. In the reference model (b) there are several of inclined lines of strains, plus more strains on the corners of the building. When the strength is 2xE (c) the concentration of strains occurs mostly at the bottom of the model. Some new strains appear in the façade because it is bending more than before, but their values are not very high. More figures are available in Annex A.

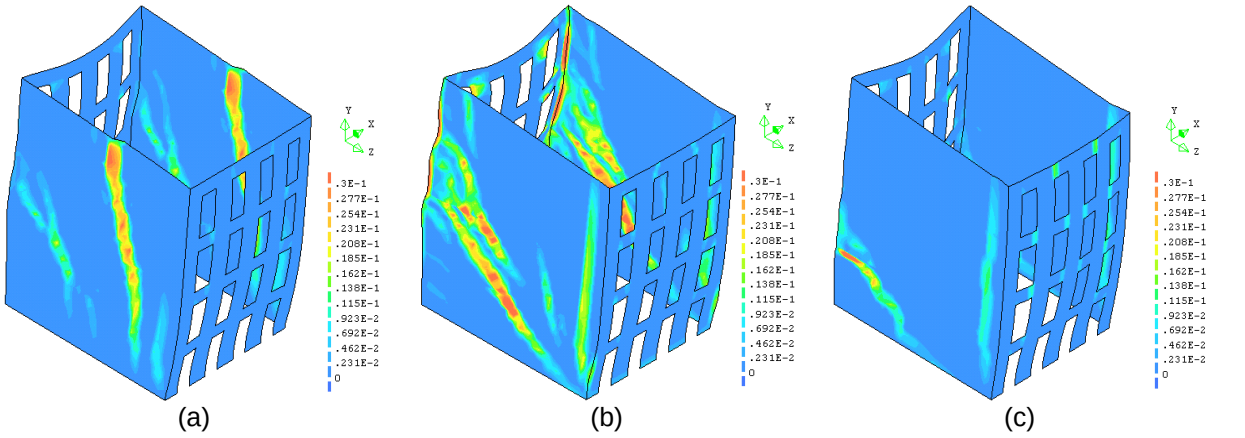

Figure 76 – Tensile principal strain states in the ultimate steps for (a) 0.5xFt, (b) reference and (c) 2xFt.

The compressive stress states are shown in Figure 77. They reflect well the strains concentration from the previous figures. It is possible to distinguish the struts aligned with the strains discussed in the gabble walls. One large strut for 0.5xFt (a), several inclined struts for the reference (b) and one less inclined strut and closer to the base for 2xFt (c). There are more figures in Annex A.

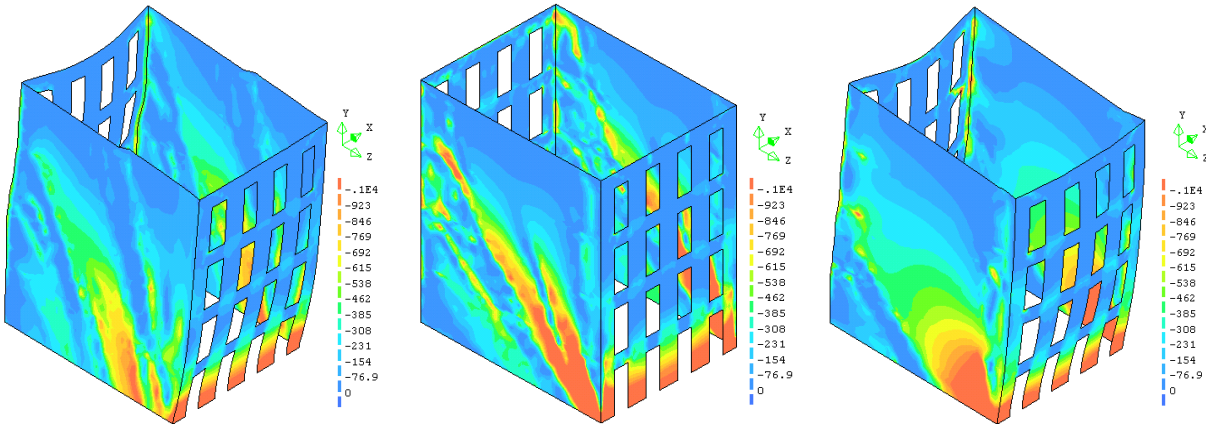

Figure 77 – Compressive principal stress states in the ultimate steps for (a) 0.5xFt, (b) reference and (c) 2xFt, units in kPa.

6.2.4 Fracture energy tensile

As for the previous calculations, two different calculations were performed with half (0.5xGft) and double (2xGft) the reference fracture energy. The curves for the east-west direction can be seen in the Figure 78, again with rather small variation.

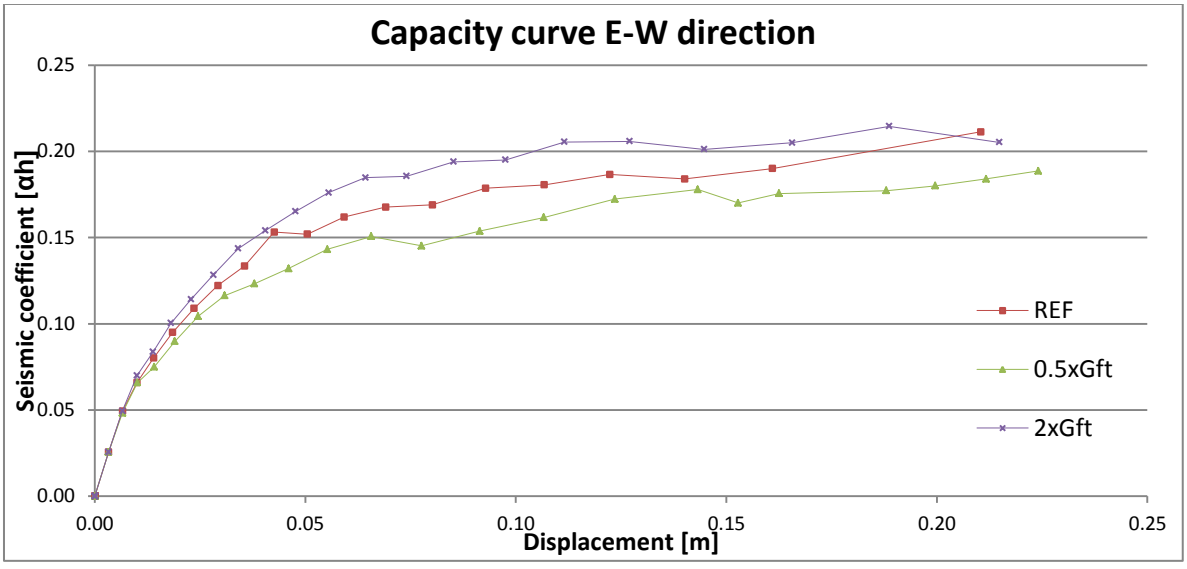

Figure 78 - Capacity curves for east-west direction.

The deformed meshes in the ultimate steps can be seen in Figure 79. As for the previous calculation, the material properties of the masonry do not have a significant influence in the response of the

structure in the east-west direction. The distribution of displacements and the peak values are very similar among the different calculations. For a more detailed observation, see Annex A.

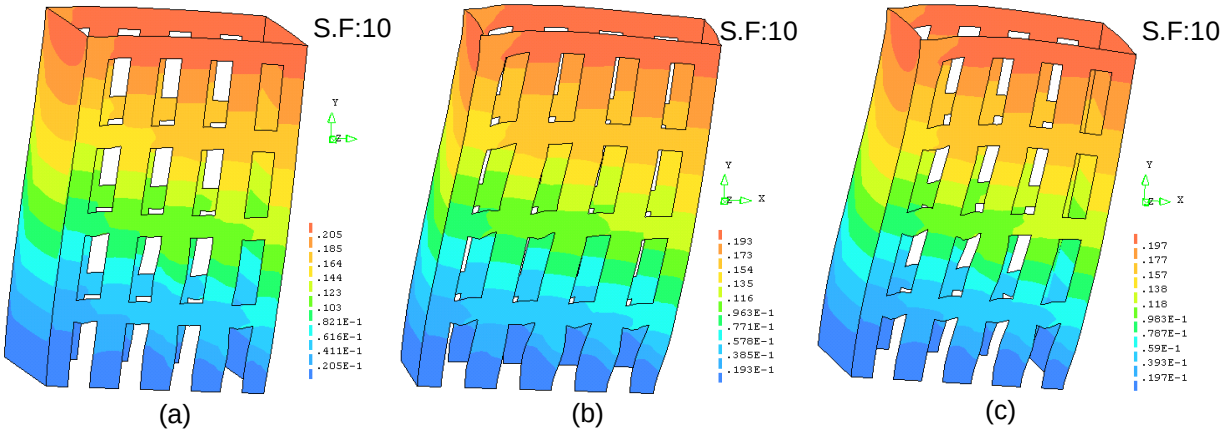

Figure 79 – Deformed meshes in the ultimate steps for (a) 0.5xGft, (b) reference and (c) 2xGft, units in meters.

The tensile strain states in the ultimate steps can be seen in Figure 80. The strain damage is concentrated in the façades. The variation of tensile fracture energy only affects the distribution of strains. As the fracture energy tensile is increased the strain concentration moves from the piers to the lintels. For more detailed figures see.

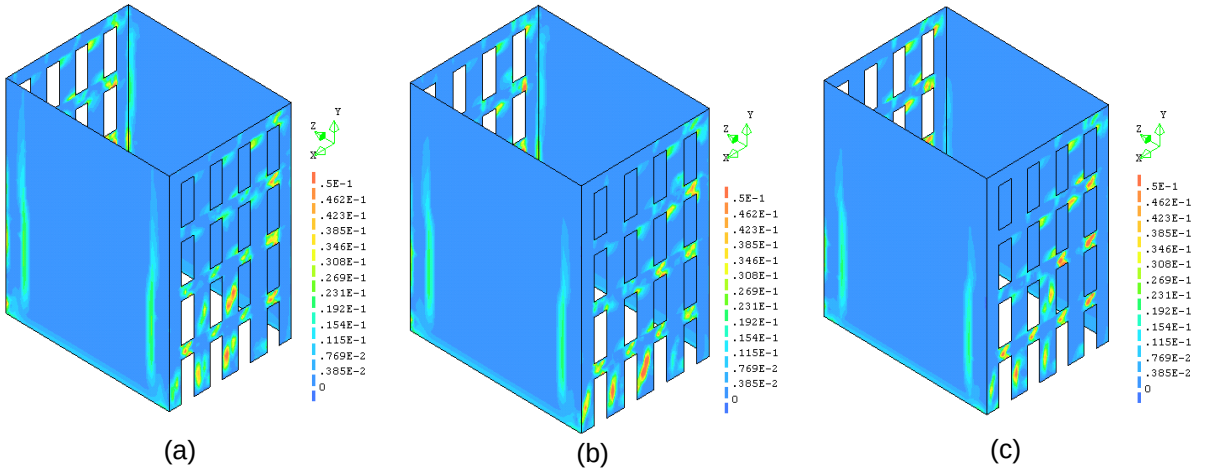

Figure 80 – Tensile principal strain states in the ultimate steps for (a) 0.5xGft, (b) reference and (c) 2xGft.

The compressive stress states can be seen in Figure 81. The distribution and peak values of stresses are almost the same for all calculations. The fracture energy tensile has very little influence in the east-west direction. More figures can be seen in the Annex A.

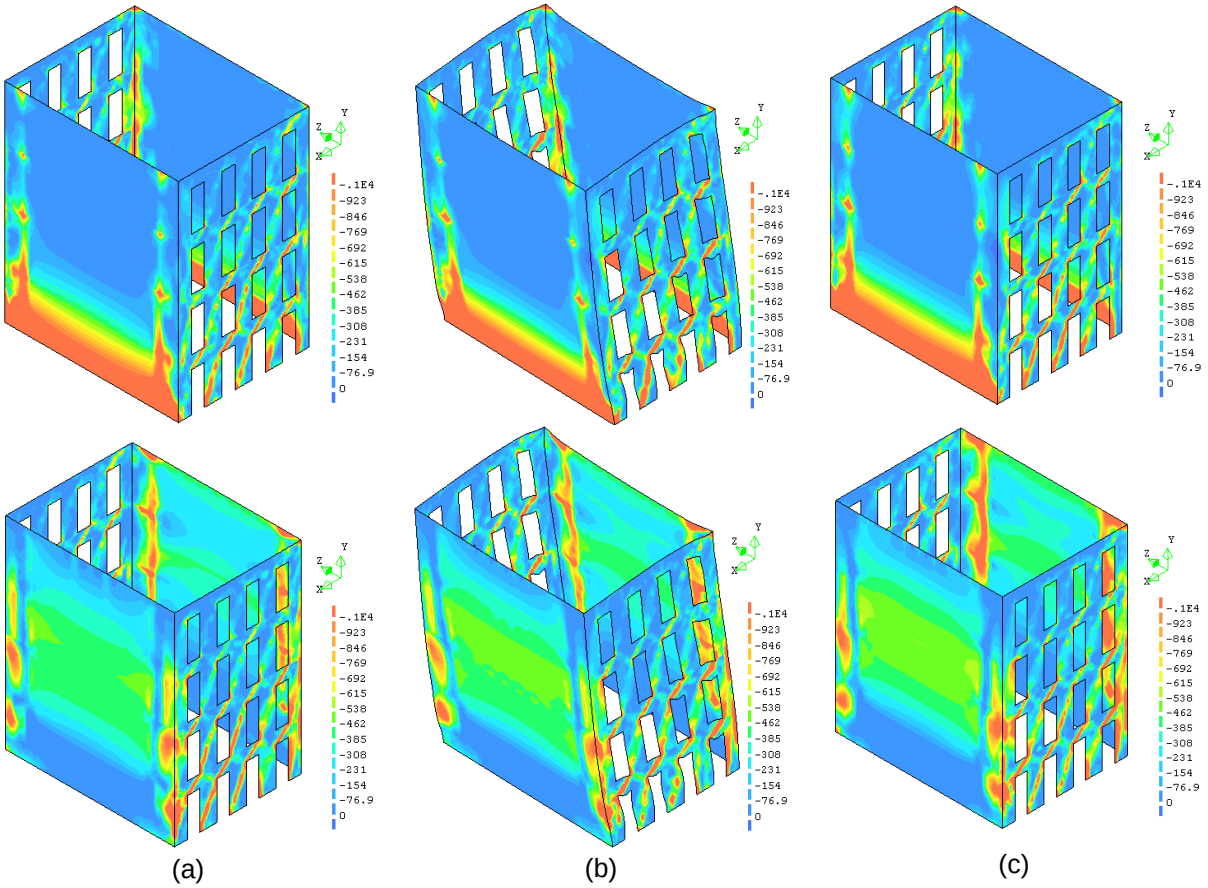

Figure 81 – Compressive principal stress states in the ultimate steps for (a) 0.5xGft, (b) reference and (c) 2xGft, units in kPa.

The curves for north-south direction are shown in the Figure 82, with a variation in the seismic coefficient between 0.62 and 0.52. Again, the changes are larger than for the east-west direction.

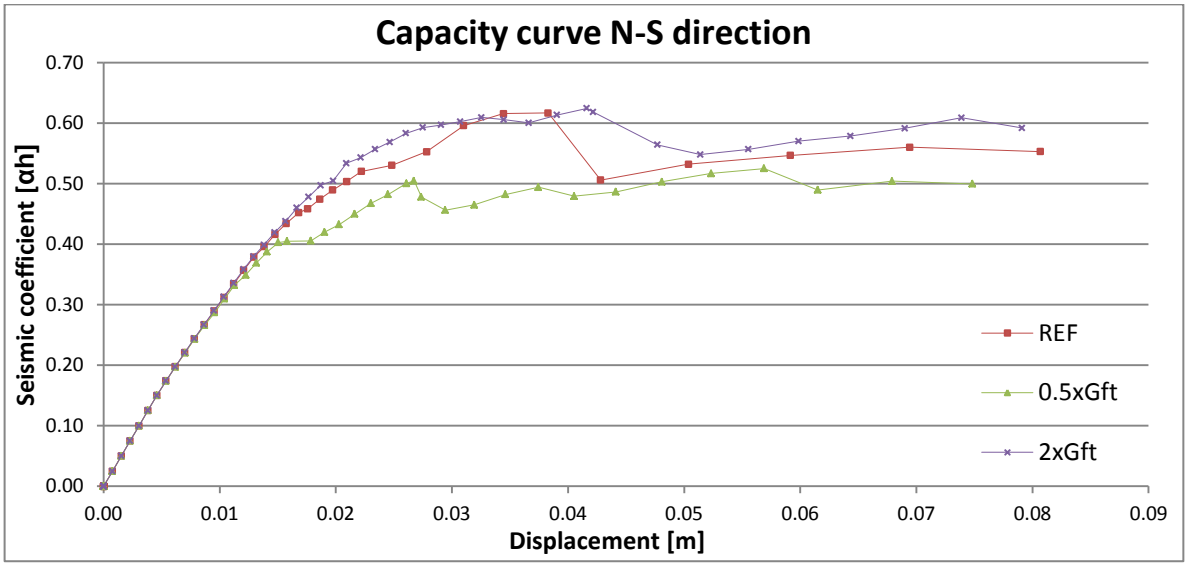

Figure 82 - Capacity curves for north-south direction.

The deformed meshes in the ultimate steps can be seen in the Figure 83. The variations of fracture energy tensile have a bigger influence in the response for north-south direction than for the east-west one. However, this influence is lower than for other material properties. As the fracture energy is decreased the capacity is also decreased. For 0.5xGft (a) the larger deformation is concentrated in the north façade, while for the 2xFt (c) the larger deformation is in the south façade.

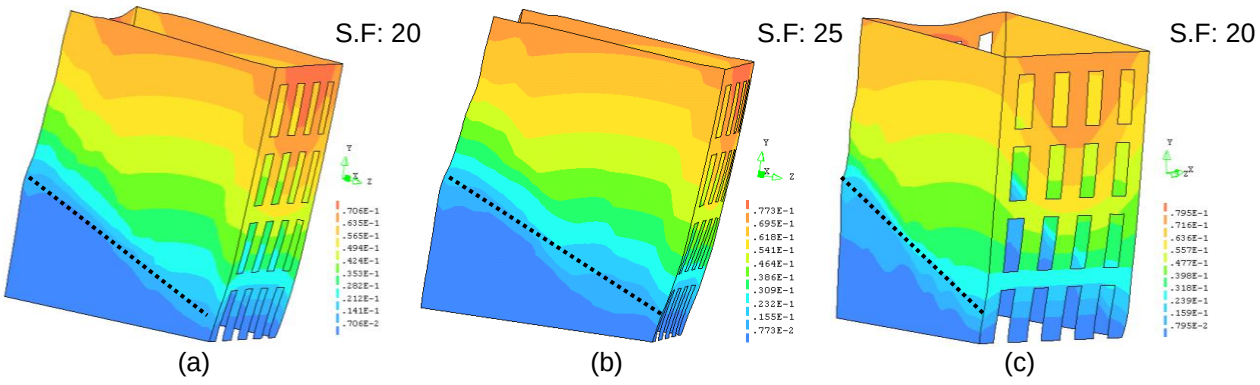

Figure 83 – Deformed meshes in the ultimate steps for (a) 0.5xGft, (b) reference and (c) 2xGft, units in meters.

The tensile strain states can be seen in the Figure 84. In this case the influence of the fracture energy is not very high. The distribution of strains and the peak values are similar among the different calculations. More figures can be seen in the Annex A.

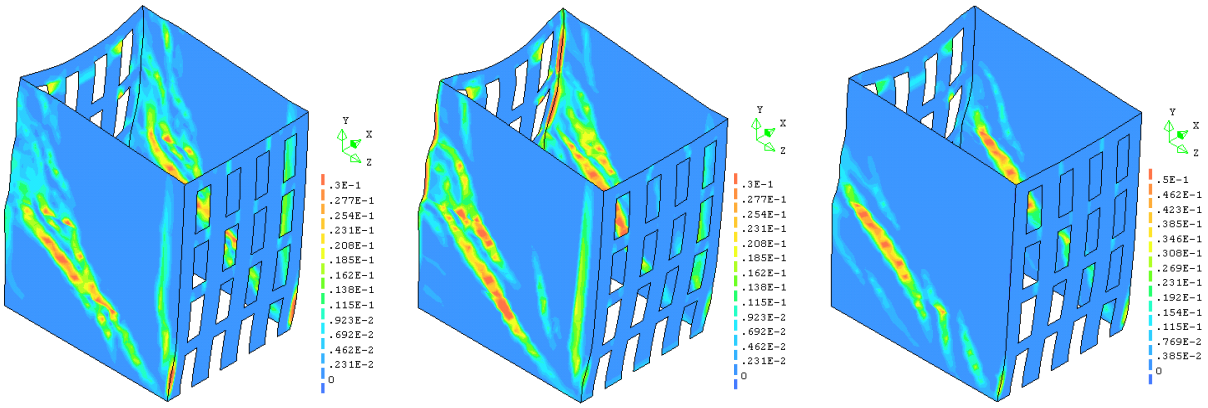

Figure 84 – Tensile principal strain states in the ultimate steps for (a) 0.5xGft, (b) reference and (c) 2xGft.

The compressive stress states can be seen in Figure 85. They confirm that the influence of fracture energy tensile in the global response is not very important. The stress states reflect the strain states seen before. For a more detailed examination see Annex A.

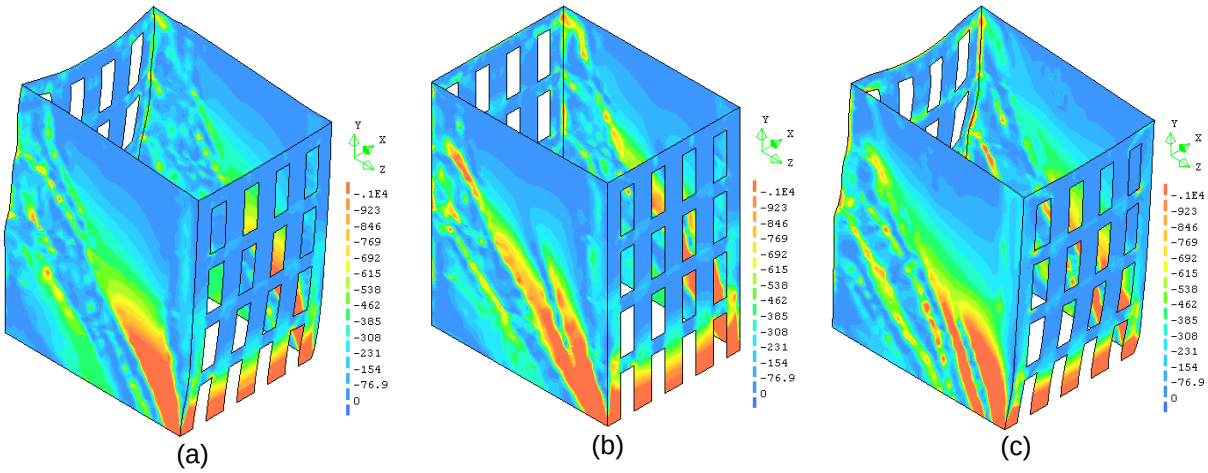

Figure 85 – Compressive principal stress states in the ultimate steps for (a) 0.5xE, (b) reference and (c) 2xE, units in kPa.

6.2.5 Conclusion

A common feature among all comparisons done in this chapter is the fact that the response in north-south direction is much more influenced by the material properties than in east-west direction. In the east-west direction the global behaviour of the structure is based on the response of the façades. These walls have a lot of openings, and the geometry has more influence in the performance of the building than the moderate change in the material properties. On the contrary, in the north-south direction the gabble walls have much more to do in the response than the façades. Since those gabble walls do not have any opening the material properties have more influence in the response than their geometrical configuration, as the failure modes and stress distribution change.

The stiffness of the MDF panels has an important influence in the global behaviour of the building. This effect is especially noticeable when the stiffness is very low (0.1xE) or very high (1000xE). When the stiffness of the floors is very low there are no rigid diaphragm, and the building is not working as a whole. On the contrary, when the stiffness is high the loads are transferred between the walls and the structure has box behaviour. The stiffness of the floor structures influences the response in both east-west and north-south directions. Nevertheless, the north-south direction is more influenced than the east-west one.

The material properties of the masonry do not have almost any influence in the behaviour in the east-west direction, as said before. But the influence in the north-south direction can be important, changing the shear stress behaviour and the failure mechanisms. This effect is especially noticeable when the stiffness of the floors is modified.

It is interesting to notice that a stiffer configuration of the building does not necessarily mean that the structure is safer. There are more factors to take into account due to the effect of the floors.

Change on capacity for non-linear static analysis (in comparison to reference analysis). Capacity is calculated as the maximum value or the value at a displacement of 0.20 and 0.065 m for E-W and N-S direction, respectively

Parameter	Range	Min. (%)	Max. (%)	Max. Diff. (%)
Floor stiffness	0.1-1000	75	115	25
Masonry stiffness	0.5-2.0	77	110	23
Tensile strength	0.5-2.0	89	106	11
Fracture energy	0.5-2.0	89	111	11

Parameter	Range	Min. (%)	Max. (%)	Max. Diff. (%)
Floor stiffness	0.1-1000	76	118	24
Masonry stiffness	0.5-2.0	91	104	9
Tensile strength	0.5-2.0	78	150	22
Fracture energy	0.5-2.0	96	106	6

Min = F_min/ F_ref * 100; Max = F_max/ F_ref * 100; Max. Diff. = Maximum (1-Min; Max-1)*100

6.3 Non-linear dynamic analysis – Time history – 300% PGA earthquake

The parameters to be assessed in time history analysis are the same than for pushover analyses (stiffness of the floor structures and stiffness, tensile strength and tensile fracture energy of the masonry) and also the damping ratio. In this section the 300% PGA earthquake is compared with the reference.

6.3.1 Stiffness of the MDF panels

The same range than for static analysis of Young's modulus are assessed. The obtained values are 0.1xE, 10xE, 100xE and 100xE; being E the reference Young's modulus. The graphs used to compare the calculations are the envelopes of displacements versus seismic coefficient. The displacements are measured in the middle of the gabble walls at the top. The seismic coefficient is defined as the sum of base reactions divided by the total weight of the building.

In the Figure 86 and Figure 87 the comparison between the reference and (a) 0.1xE, (b) 10xE and (c) 1000xE in the X direction can be seen for the gabble wall and (d) 0.1xE, (e) 10xE and (f) 1000xE for the façade. The envelope of 100xE is not shown because the response is very similar to the calculation 1000xE; it can be seen in the Annex D with all the other envelopes. Every graph has the same scale, for sake of simplicity in the comparison.

When the stiffness of the floors is decreased the response of the building to out-of-plane displacements becomes rather large and the building is most likely collapsing in this direction. Thus, it is possible to observe that in the X direction for the gabble wall (Figure 86 (a)) and in the Z direction for the façade (Figure 87 (d)) the displacements are out of range. However the response to in-plane displacements is very similar to the response of the reference model. It makes sense, since the stiffness of the floor structures almost does not affect the in-plane behaviour of the masonry.

On the contrary, when the stiffness of the floor structures is increased the building behaves more as a box than for the reference model. In the case of 10xE (b) the difference is very slight and only a small decrease of displacements can be appreciated. However, when the stiffness is increased 100 and

1000 times the response is more concentrated than for the other analyses. The decrease of displacements is very significant for a very similar seismic coefficient. However, this decrease of displacements does not mean necessarily an improvement of the capacity of the building. The structure is not able to dissipate as much energy as for the reference values, and when a building is hit by an earthquake, usually the more energy the structure is able to dissipate the better. Thus it is not possible to say if the building is safer or weaker, even though the box behaviour is attained.

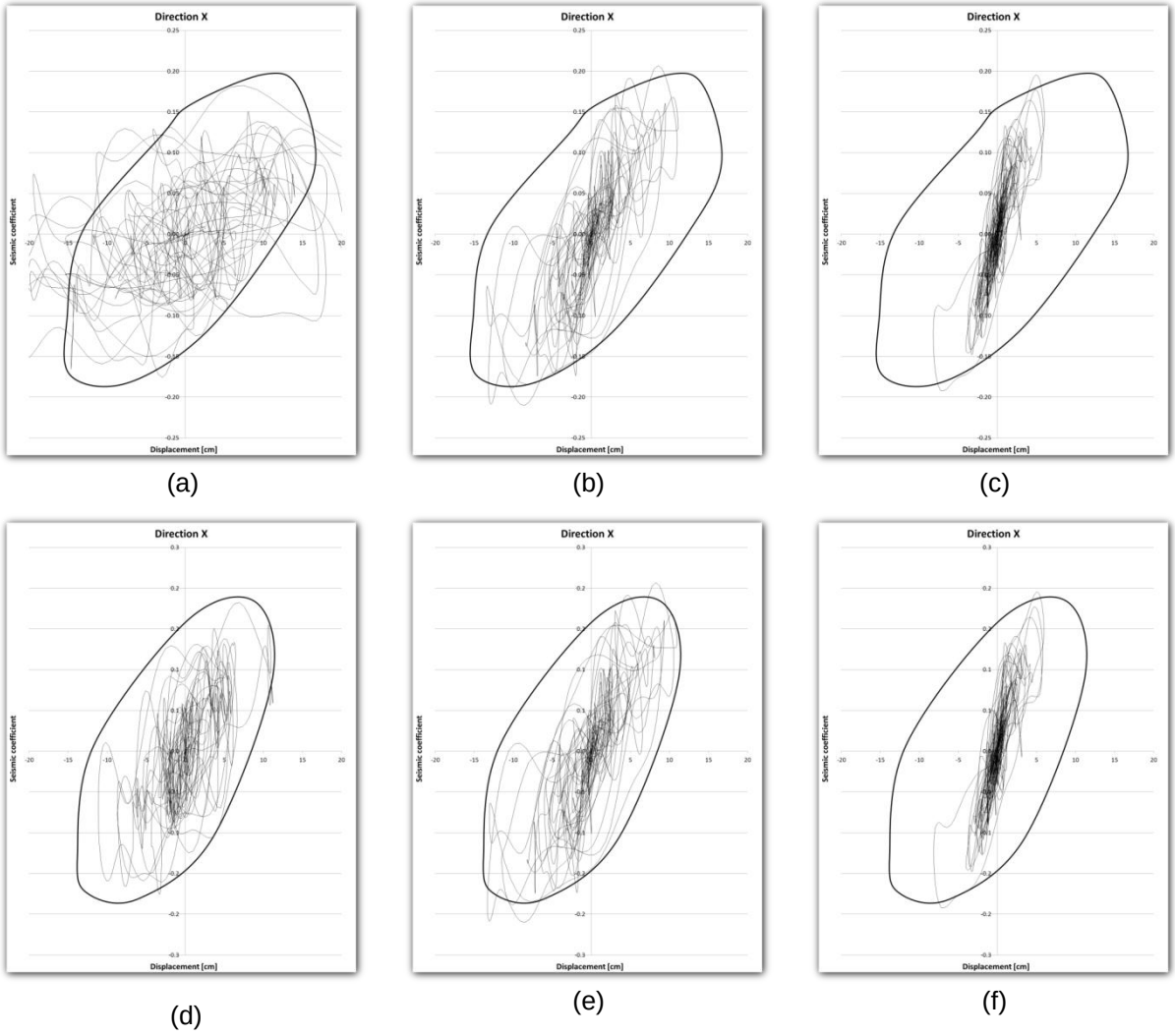

Figure 86 - Envelopes comparing the reference model with (a) 0.1xE, (b) 10xE and (c) 1000xE for the gabble wall and (d) 0.1xE, (e) 10xE and (f) 1000xE for the façade in the X direction.

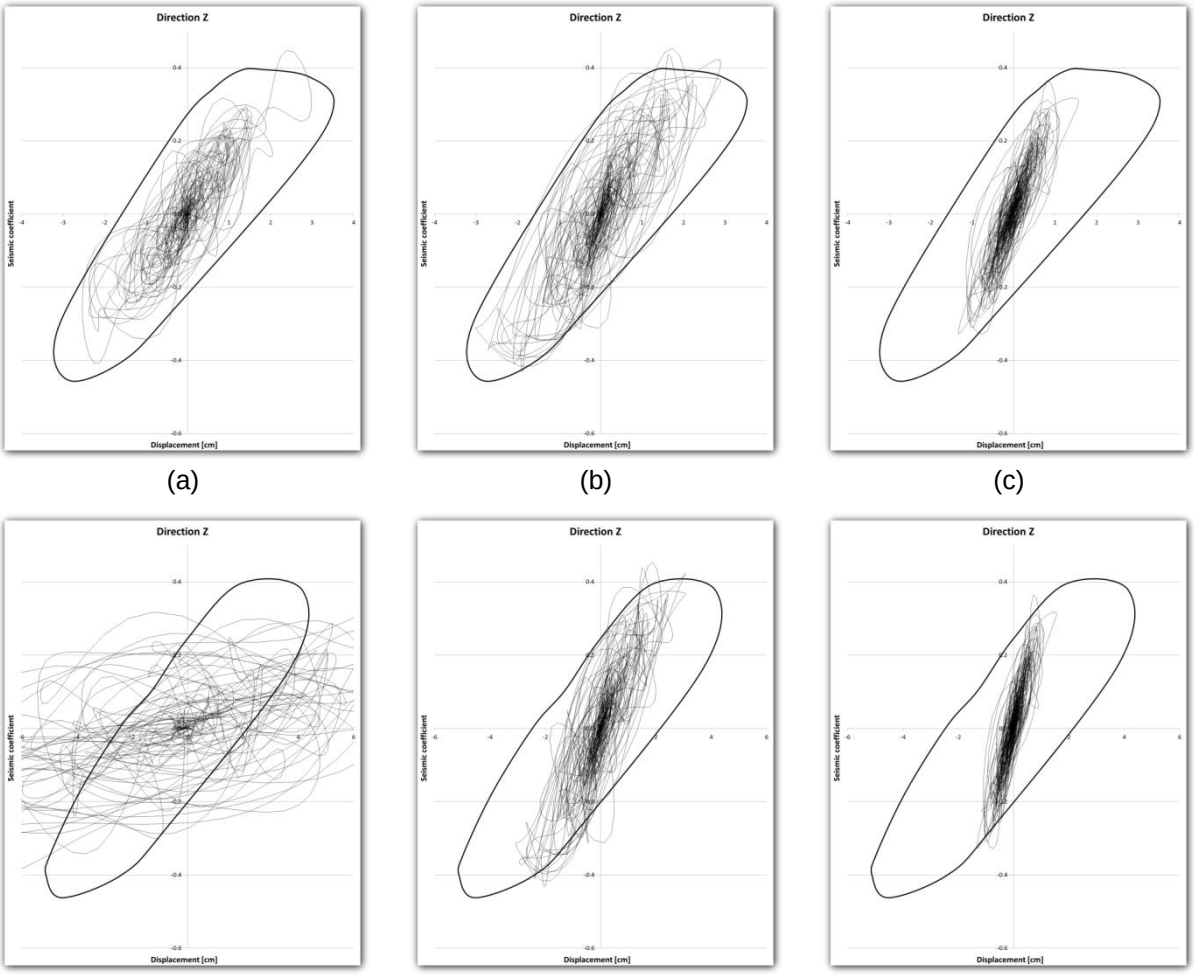

(a) (b) (c)

(d) (e) (f)

Figure 87 - Envelopes comparing the reference model with (a) 0.1xE, (b) 10xE and (c) 1000xE for the gabble wall and (d) 0.1xE, (e) 10xE and (f) 1000xE for the façade in the Z direction.

6.3.2 Stiffness of masonry

As for static analysis, two different calculations were performed to assess the influence of the masonry stiffness in the response. The Young's modulus was decrease to the half and increased to the double, obtaining thus the calculations 0.5xE and 2xE. The characteristics of the graphs are the same than for the previous comparison. Also the scale remains the same for the two different calculations to make it easier to compare. In Figure 88 the graphs of the envelopes in the X direction are shown for the façade. The envelopes for the gabble wall can be seen in the Annex D, as they are very similar and only the ones in the weaker wall (the façades) are shown.

When the stiffness of the masonry is decreased to the half the response of the building loses its original shape. Although some peak values are out of range, which could represent a collapse of the building, the major part of the values remains inside the shape of the reference model. However, there

is an important decrease of seismic coefficient. To summarize, the building seems to be strongly affected by the frequency change. Although this behaviour could be expected, such a large influence of the stiffness of the masonry in the final response is a surprising and conflicting with the pushover analyses.

On the contrary, when the stiffness of the masonry is doubled the response is a bit more concentrated and the displacements are smaller. However, the seismic coefficient is larger. The structure is stiffer than before, and it is not able to dissipate as much as energy as the reference model. Again this effect cannot be interpreted either as a positive or negative result, and more needs to be done in the definition of collapse for this type of analyses.

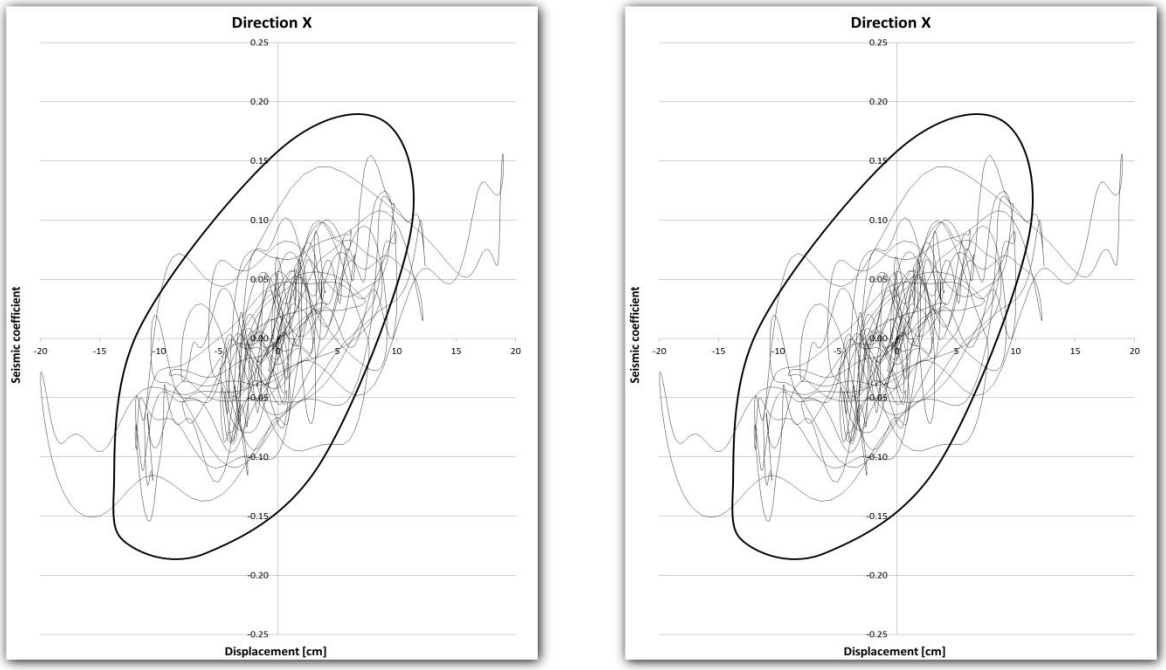

(a) (b)

Figure 88 - Envelopes comparing the reference model with 0.5xE (a) and 2xE (b) in direction X in the façade.

The comparison of the envelopes for the Z direction is shown in the Figure 89 for the façade. The envelopes for the gabble wall can be seen in the Annex D. In this direction the changes are more drastic. When the stiffness is decreased there is a big increase of displacements, which go out of the graph. Most probably these displacements are too big for be accommodated by the building and it might collapse. When the stiffness is doubled the reduction of the displacements is very significant, especially the in-plane displacements (Figure 89 b). In this case there are not curves going out of the

concentration of curves. This is because the stiffness of the façades in this direction is not as dependant of the masonry properties as in the other direction.

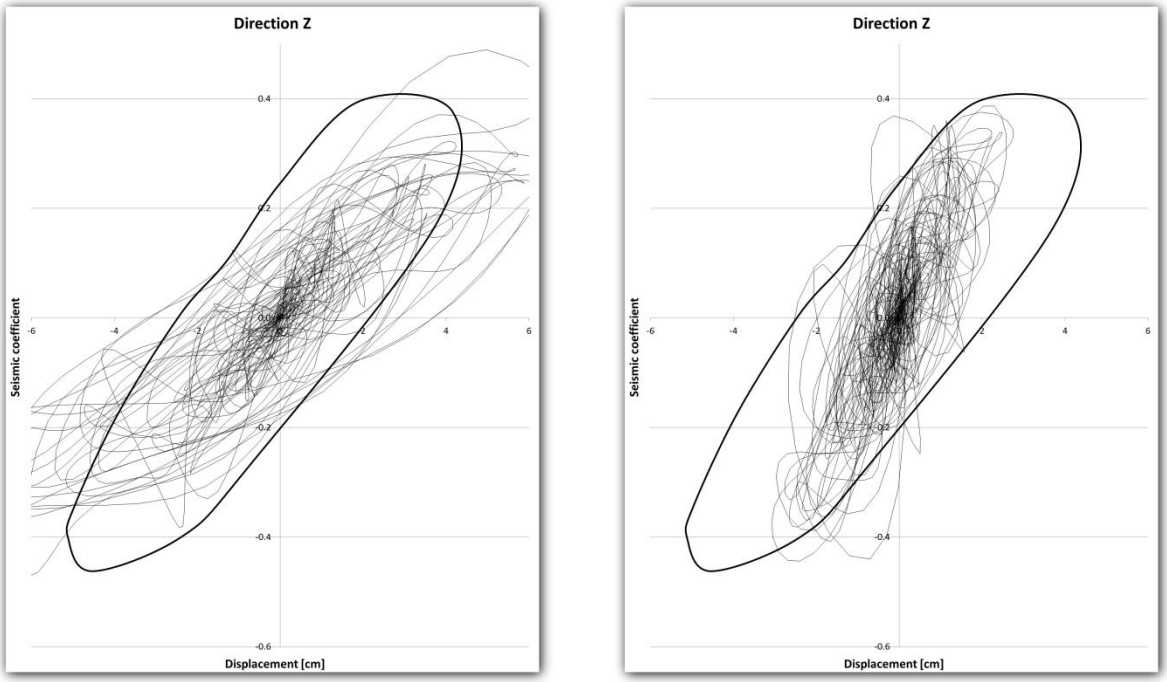

(a) (b)

Figure 89 - Envelopes comparing the reference model with 0.5xE (a) and 2xE (b) in direction Z in the façade.

6.3.3 Damping ratio.

The configuration of the graphs is the same as in the previous examples. Two different calculations are performed and compared with the reference model. Firstly, the damping parameters are changed to obtain the half (0.5xDamping) of the reference damping ratio and the double one (2xDamping). The envelopes for the Z direction can be seen in the Figure 90 for the façade. The other envelopes can be seen in Annex D.

When the damping ratio is reduced to the half, both the seismic coefficient and the displacements are larger than for the reference mode, as expected. The amount of energy dissipated by the damping of the structure is lower and larger displacements are found. On the contrary, when the damping ratio is doubled more energy is dissipated so that the displacements and seismic coefficient are smaller. The difference of displacements and seismic coefficients are large enough to affirm that the damping has some influence in the response of the building, even if moderate for the large variation of damping ratio assumed (from 2.5% to 10%).

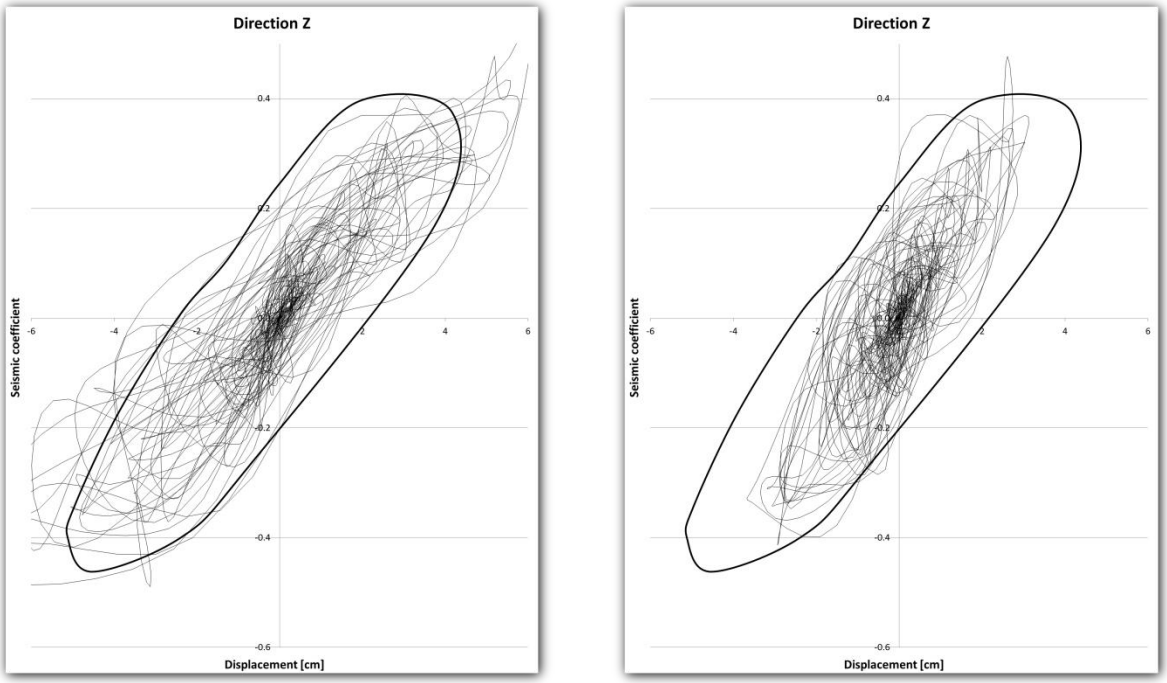

(a) (b)

Figure 90 - Envelopes comparing the reference model with 0.5xDamping (a) and 2xDamping (b) in direction Z in the façade.

6.3.4 Tensile strength

Two different calculation results are performed adopting half strength (0.5xFt) and double strength (2xFt) of the reference model. The comparison of the envelopes for the reference model and the two new analyses can be seen in Figure 91. Only the response in the Z direction of the façade is shown, because this is the weakest part. All the other responses can be seen in Annex D. However, the variation of the response is similar for the different graphs obtained. When the strength is lower (a) the displacements increase a lot, going out of the range, as well as the seismic coefficient. Possibly, collapse of the building would occur. On the contrary, when the tensile strength is increased (b) both seismic coefficient and displacements are much smaller than for the reference model. It can be asserted that the building is safer and the response is far away from the ultimate collapse.

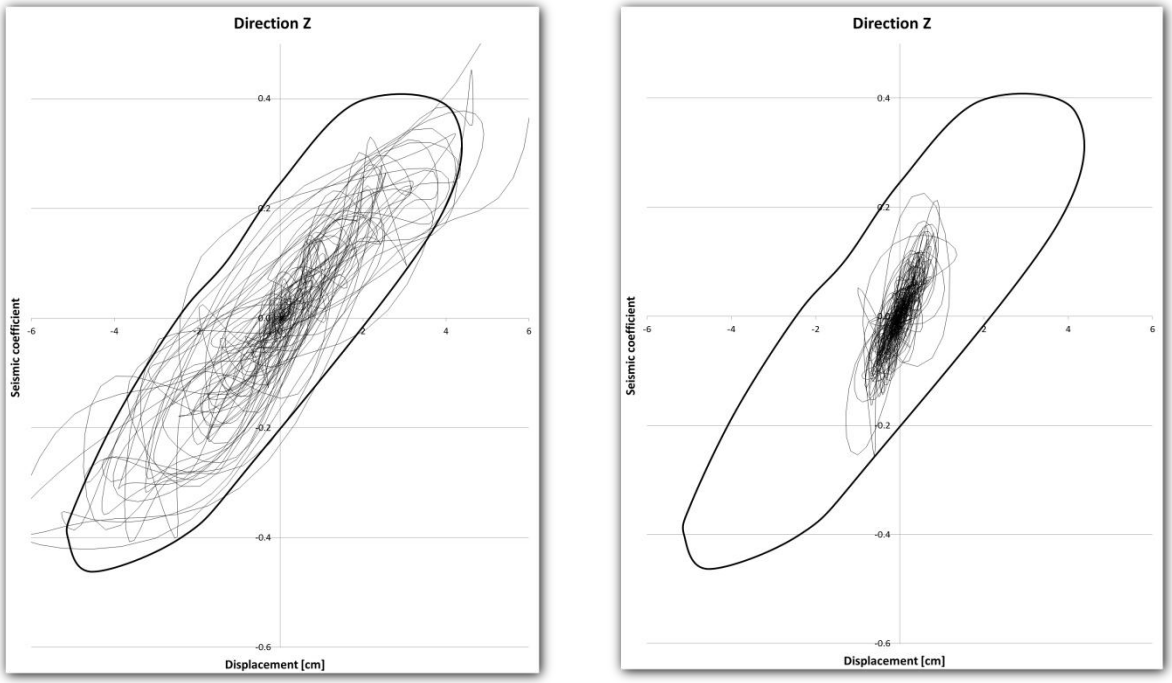

(a) (b)

Figure 91 - Envelopes comparing the reference model with 0.5xFt (a) and 2xFt (b) in direction Z in the façade.

6.3.5 Fracture energy tensile.

Two different results are shown, being one for half value of the tensile fracture energy (0,5xGft) and another one for double value (2xGft). The characteristics of the graphs are the same than for the previous results. The envelopes for the 0.5xGft calculation in the Z direction for the façade can be seen in Figure 92. Like for tensile strength, only these graphs are shown because they are measured in the weakest part of the building, and all the other graphs can be seen in the Annex D. The variation of fracture energy tensile within the prescribed range does not affect to the response of the building significantly; both shape and peak values are very similar to the ones obtained in the reference model.

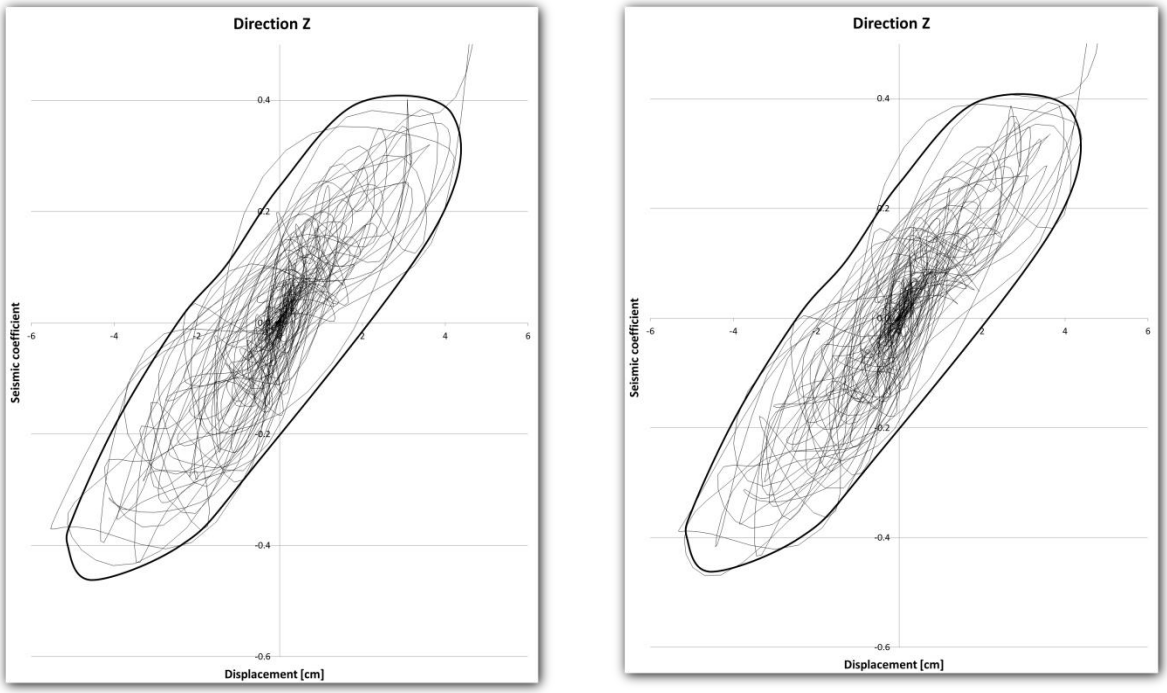

(a) (b)

Figure 92 - Envelopes comparing the reference model with 0.5xGft (a) and 2xGft (b) in direction Z in the façade.

6.3.6 Conclusion

Like for static analysis the direction in which the measures are taken has a large influence in the results. However, since the model is subjected to input in the two directions, this comparison is more reliable.

The stiffness of the floor structures has a very big influence in the response of the building. The lower the stiffness is the weaker the building becomes. However, this direct relation cannot be asserted when the stiffness is increased. More carefully and detailed examination should be carried out to assess the integrity of the structure, evaluating the strain states, deformation and other parameters, aiming to define a clear indication of collapse.

Some of the masonry properties considered in this sensitivity analysis have a large influence in the response, namely tensile strength and stiffness. This conclusion is different from the one obtained for static analysis. Damping has also some influence on the response, even if the range f values considered here is rather large (2.5 to 10%). The tensile fracture energy range considered is not large enough to obtain an difference in the results and further calculations need to be done, with a wider range (possibly from 0.2 to 5 times the reference value).

Change on response for non-linear dynamic analysis (in comparison to reference analysis). Base shear and maximum displacement are calculated as the maximum value of the envelope.

		Base Shear			Maximum displacement		
Parameter	Range	Min. (%)	Max. (%)	Max. Diff. (%)	Min. (%)	Max. (%)	Max. Diff. (%)
Floor stiffness	0.1-1000	75	108	25	25	200	100
Masonry stiffness	0.5-2.0	80	127	27	50	175	75
Damping ratio	0.5-2.0	88	111	12	60	160	60
Tensile strength	0.5-2.0	55	125	45	20	140	80
Fracture energy	0.5-2.0	100	100	0	100	100	0

Chapter 7

Conclusion and future works

One of the main conclusions of this work is that this particular building, and possibly most historical masonry buildings, is very sensitive to the direction in which the load is applied, especially because its geometrical configuration (one wall with openings, another without them). Thus, the direction of the applied load is a very important factor to take into account when analysing structures using static methods. The time history analysis method is possibly more precise and provides a better representation of dynamic effects but the results obtained are extensive and there are problems to process and analyse them, namely with respect to the definition of collapse. This drawback, together with the fact that pushover analysis is able to give enough information about several important characteristics of the structure such as seismic capacity, maximum displacements, macro blocks or failure mechanisms, makes pushover analysis the most used method for advanced seismic studies of existing structures. Pushover analysis is also a simple and quick method to apply, while time history analysis is time consuming and computing demanding.

When the results from pushover analysis with mass proportional loading are contrasted with those obtained by time history procedure, the correlation seems mostly adequate in terms of maximum capacity, displacements and failure modes. However, since the processing of results obtained from time history analysis is so complex, it is not easy to discuss the comparison between pushover and time history analysis. Moreover, the sensitivity provides rather different conclusions, meaning that the use of pushover methods require a careful consideration.

Among the different parameters assessed in the thesis, the factor that has the strongest influence in the final response of the building is the stiffness of the floor structures, as expected. This parameter is able to change the behaviour of the structure, from box-behaviour to only four walls weakly joined. The other parameters can have an important influence in the maximum values reached by the structure, but they change less the way the building responds to the earthquake. The material parameters of masonry considered in the sensitivity analysis are the elasticity modulus, the tensile strength, the tensile fracture energy and the damping (only for time history analysis).For the pushover analysis, the most relevant material properties influencing the response are XXX. For the time history analysis, the most relevant material properties influencing the response are the Young’s modulus of masonry and its tensile strength. .

Some improvements that can be carried out in future works, regarding the analysis of the case study, can be to take into account more parameters in the sensitivity analysis (namely the influence of compressive strength parameters, the influence of vertical acceleration in time history analysis and the use of more advanced pushover methods , such as adaptive or multimodal) or to increase the range of the values of the parameters already discussed in this thesis (namely for the tensile fracture energy). There is the possibility to use another earthquake to assess the structure instead of a typical

earthquake from Lisbon, namely by considering real earthquake records. A final suggestion is to apply this sensitivity analysis to other complex historical structures, with more nonlinearities and irregular geometrical configuration. Only by doing this, it is possible to increase the reliability of using advanced numerical methods and to clarify the users in which parameters they need to focus the obtaining of reliable data or they need to carry out a sensitivity analysis.

8 Bibliography

Antoniou, S., and R. Pinho. 2009. “Displacement-based adaptive pushover.” *European Congress on Computational Methods in Applied Sciences and Engineering* 1st Intern: 22-24.

“Assessment and improvement of the structural performance of Buildings in Earthquakes.” 2006. *New Zealand society for earthquake engineering*.

Antoniou S, Pinho R. 2004 “Development and verification of a displacement-based adaptive pushover procedure. ” *J Earthquake Eng*.;8(5):643–61.

Aydinoglu MN. 2003 “An incremental response spectrum analysis procedure based on inelastic spectral displacements for multi-mode seismic performance evaluation.” *Bull Earthquake Eng*.;1:3–36.

Bommer J.J., Acevedo A.B., 2004 “The use of real earthquake accelerograms as input to dynamic analysis. ” Journal of Earthquake Engineering 8 (Special Issue 1), 43-91.

Brignola, A., S. Podestà, and S. Pampanin. 2008. “In-plane stiffness of wooden floor.” In Proceedings of the New Zealand Society for Earthquake Engineering Conference. Canterbury, New Zealand: University of Canterbury.

Candeias, P., A. C. Costa, and E. Coelho. 2004. “Shaking table tests of 1:3 reduced scale models of four unreinforced masonry buildings.” In Proceedings of the *13th World Conference on Earthquake Engineering*. Vancouver, Canada: University of Vancouver.

CEN. 2003a. “EuroCode 8: design of structures for earthquake resistance.” *European Committee for Standardization* 1: General.

———. 2003b. “Eurocode 8: Design of structures for earthquake resistance.” *European Committee for Standardization* 3: Strengt(July): 1-72.

Chopra, Anil K., and Rakesh K. Goel. 2002. “A modal pushover analysis procedure for estimating seismic demands for buildings.” *Earthquake Engineering & Structural Dynamics* 31(3): 561-582.

Chowdhury, I., and S. P. Dasgupta. 2007. “Computation of Rayleigh Damping Coefficients for Large Systems.” *Olin-NASA research group*.

Construir Portugal (2012) available at http://www.construlink.com/Homepage/2010_construirportugal.com/?accao=submenu2&id=29 on 16/04/2012

Crowley, H., R. Pinho, and J. J. Bommer. 2004. “A Probabilistic Displacement-based Vulnerability Assessment Procedure for Earthquake Loss Estimation.” *Bulletin of earthquake engineering - Kluwer academic publisher*: 173-219.

Davey, N., 1961- “A History of Building Materials”. *Phoenix House*, London.

Diana V.9.4, A computer program for Finite Element Analysis.

Digital Tectonic Activity Map (2012) available at http://denali.gsfc.nasa.gov on 02/05/2012

Hillerborg, A. 1985. “Influence of beam size on concrete fracture energy determined according to a draft RILEM recommendation.” *Lund Institute of Technology* Division of Technology.

Jianguo, N., Q. Kai, and X. Yan. 2006. “Push-Over Analysis of the Seismic Behavior of a Concrete-Filled Rectangular Tubular Frame Structure.” *Tsinghua Science & Technology* 11(1): 124-130.

Krawinkler, Helmut, and G.D.P.K. Seneviratna. 1998. “Pros and cons of a pushover analysis of seismic performance evaluation.” *Engineering Structures* 20(4-6): 452-464.

LNEC. 2009. “Norma Portuguesa - Eurocódigo 8.” *Instituto Portugues da Qualidade*.

Lourenço, P. B., N. Mendes, et al. 2011. “Analysis of Masonry Structures Without Box Behavior.” *International Journal of Architectural Heritage* 5(4-5): 369-382.

Lourenço, P. B., P. Franchetti, et al. 2011. “Course Structural analysis of historical masonry structure.”

Lutman, M. 2011. “Stone masonry construction.” *Slovenian National Building and Civil Engineering Institute*: 1-5.

Manie, J. 2010. “DIANA User’s Manual.” Release 9.4, *TNO DIANA BV.*

Mendes, N., P. B. Lourenço, and A. Campos-Costa. 2010. “Seismic Vulnerability Assessment of Ancient Masonry Building: An Experimental Method.” *Advanced Materials Research* 133-134: 635-640.

Mendes, N., and P.B. Lourenço. 2009. “Seismic Assessment of Masonry ‘Gaioleiro’ Buildings in Lisbon, Portugal.” *Journal of Earthquake Engineering* 14(1): 80-101.

Musgrove, J. and Fletcher, B., 1987 - “Sir Banister Fletcher's: A History of Architecture”. *Butterworths*, London.

Oliveira D., (2012) course “Seismic behaviour and structural dynamic”, material of *SAHC master*.

PAN, P., and M. Ohsaki. 2006. “Nonlinear multimodal pushover analysis method for spatial structures.” *International Association for Shell and Spatial Structures* IASS-APCS: 1-8.

Paquette, J., and M. Bruneau. 2000. “Pseudo-dynamic testing of unreinforced masonry buildings with flexible diaphragm.” In Proceedings of the *12th World Conference on Earthquake Engineering*. Auckland, New Zealand: University of Auckland.

Ramos, Luis F, and Paulo B Lourenço. 2004. “Modeling and vulnerability of historical city centers in seismic areas: a case study in Lisbon.” *Engineering Structures* 26(9): 1295-1310.

Roca, P, González, J.L., Oñate, E., and Lourenço, P.B. 1998. “Experimental and numerical issues in the modelling of the mechanical behaviour of masonry.” *CIMNE, Barcelona* Structural: 57-91.

Shakeri, Kazem, Karim Tarbali, and Mohtasham Mohebbi. 2012. “An adaptive modal pushover procedure for asymmetric-plan buildings.” *Engineering Structures* 36: 160-172.

Shakeri K, Shayanfar MA, Moghadam AS. 2007 “An efficient method for optimum combination of modes required for pushover analysis.” In: *Proceedings of the ninth Canadian conference on earthquake engineering*;.

Spears, R. E., and S. R. Jensen. 2009. “Approach for Selection of Rayleigh Damping Parameters Used for Time History Analysis.” *Volume 8: Seismic Engineering*: 17-24.

Tomaževic, M., M. Lutman, and P. Weiss. 1996. “Seismic upgrading of old brick–masonry houses: tying of walls with steel ties.” Earthquake Spectra Journal 12(3): 599–622.

Yang, G. 2010. “Dynamic analyses of a masonry building tested in a shaking table.” *SAHC Master*: 1-114.

Yi, T. 2004. “Experimental investigation and numerical simulation of an unreinforced masonry structure with flexible diaphragms.” *Georgia Institute of Technology*, Doctoral Thesis. Atlanta, GA.

ANNEXES – TABLE OF CONTENTS

1 ANNEX A – GRAPHICS FROM PUSHOVER ANALYSIS

1.1 Reference model

1.1.1 E-W direction

Deformed mesh

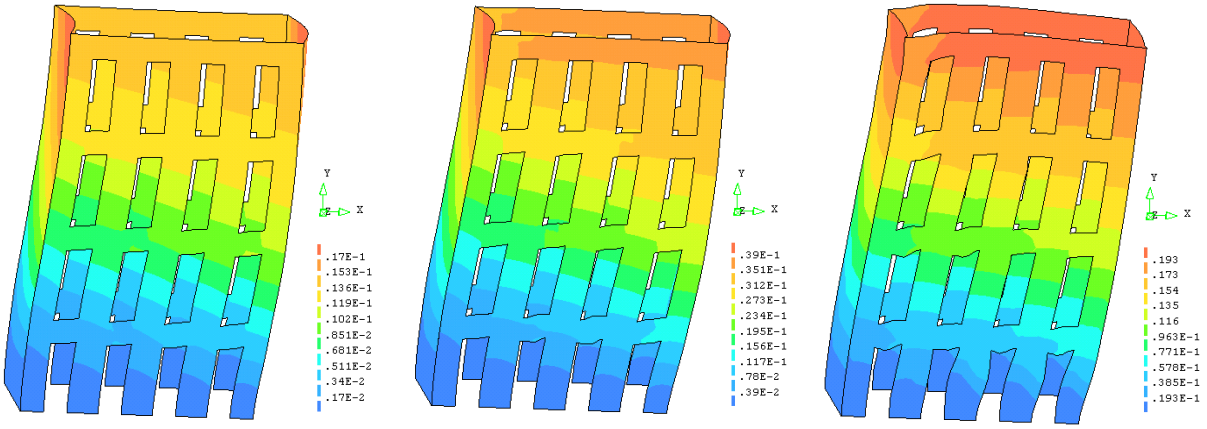

(a) (b) (c)

Figure 1 – deformed mesh for the steps number (a) 5, (b) 9 and (c) 19, units in meters.

Strain states

Step 5

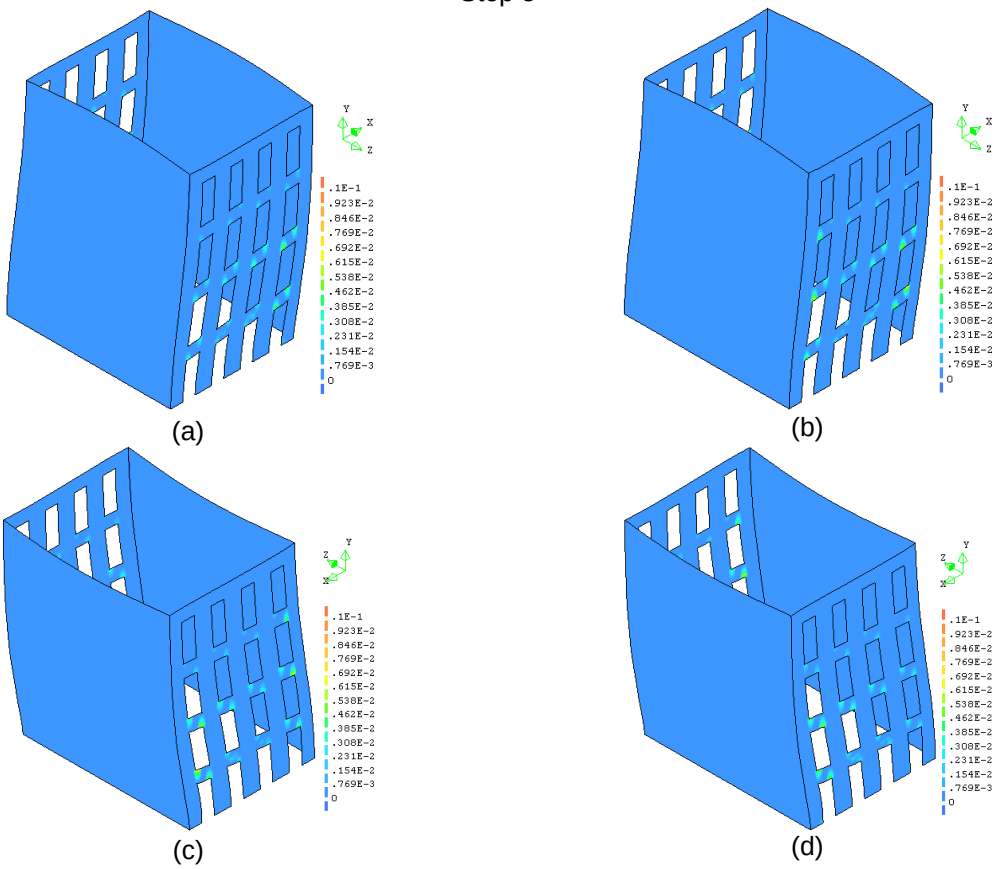

(a) (b) (c) (d)

Figure 2 - (a) N-E view inside (b) N-E view outside (c) S-W view outside and (d) S-W view inside.

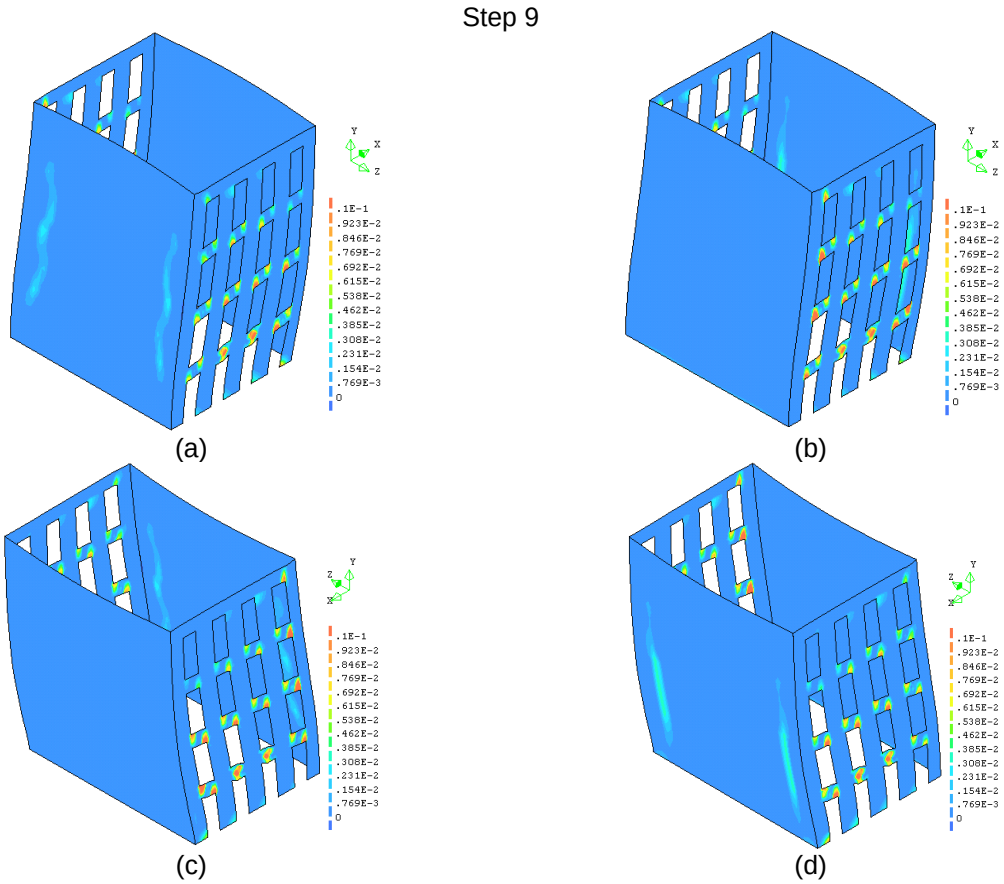

Figure 3 - (a) N-E view inside (b) N-E view outside (c) S-W view outside and (d) S-W view inside.

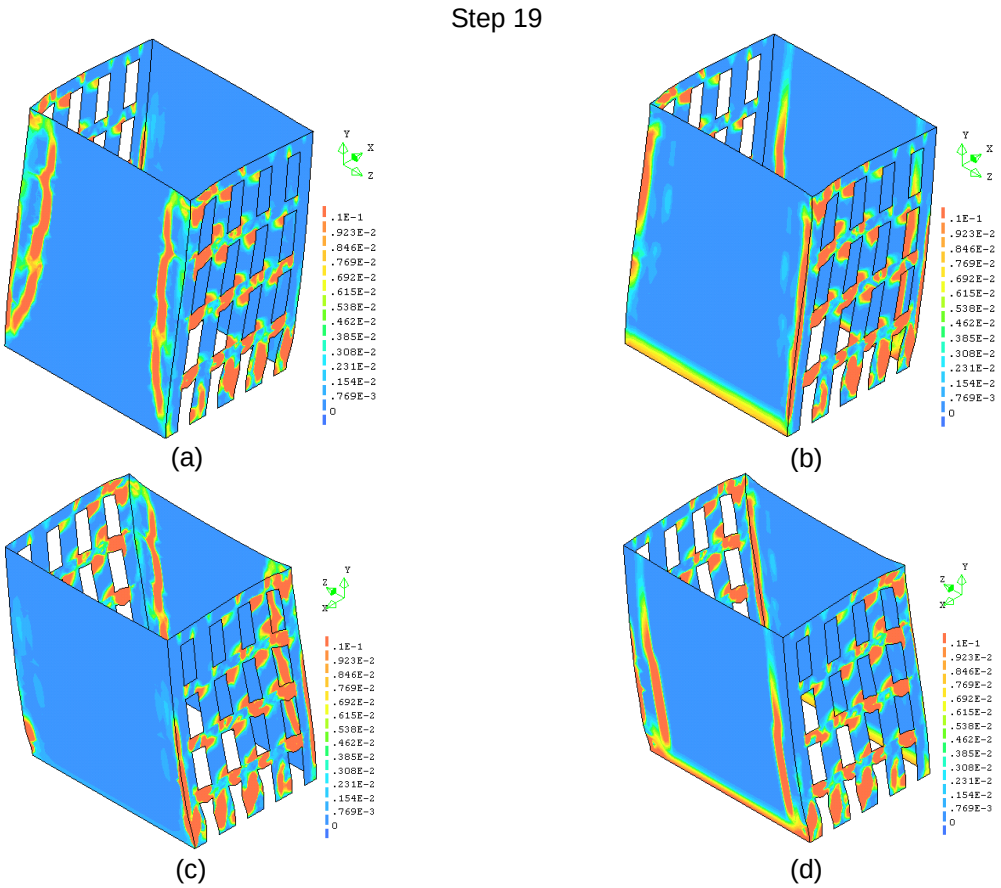

Figure 4 - (a) N-E view inside (b) N-E view outside (c) S-W view outside and (d) S-W view inside.

Stress states

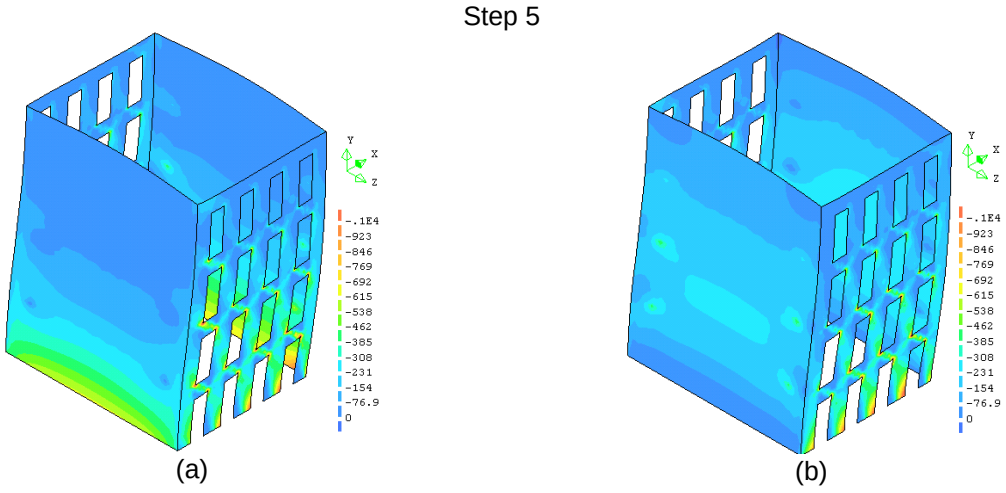

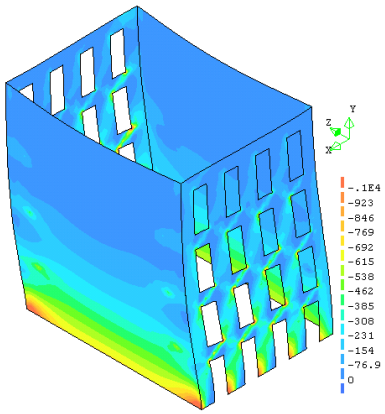

(c)

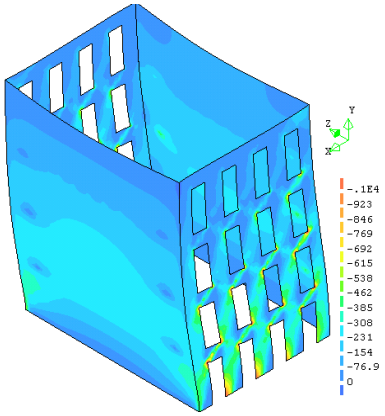

(d)

Figure 5 - (a) N-E view inside (b) N-E view outside (c) S-W view outside and (d) S-W view inside, units in kPa.

Step 9

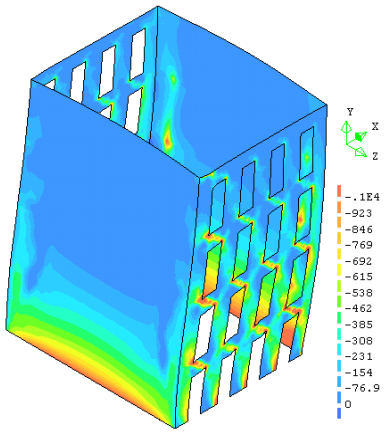

(a)

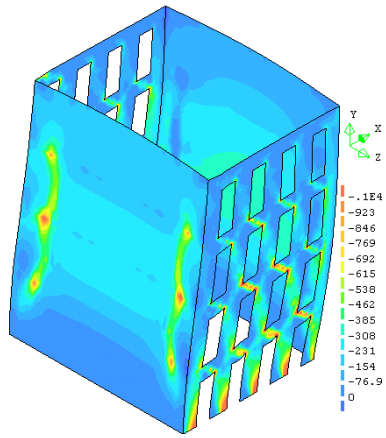

(b)

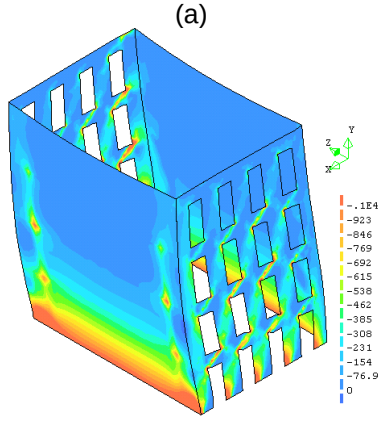

(c)

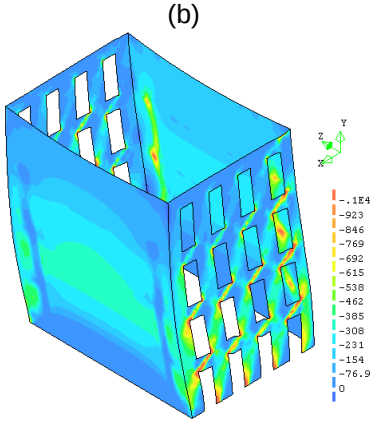

(d)

Figure 6 - (a) N-E view inside (b) N-E view outside (c) S-W view outside and (d) S-W view inside, units in kPa.

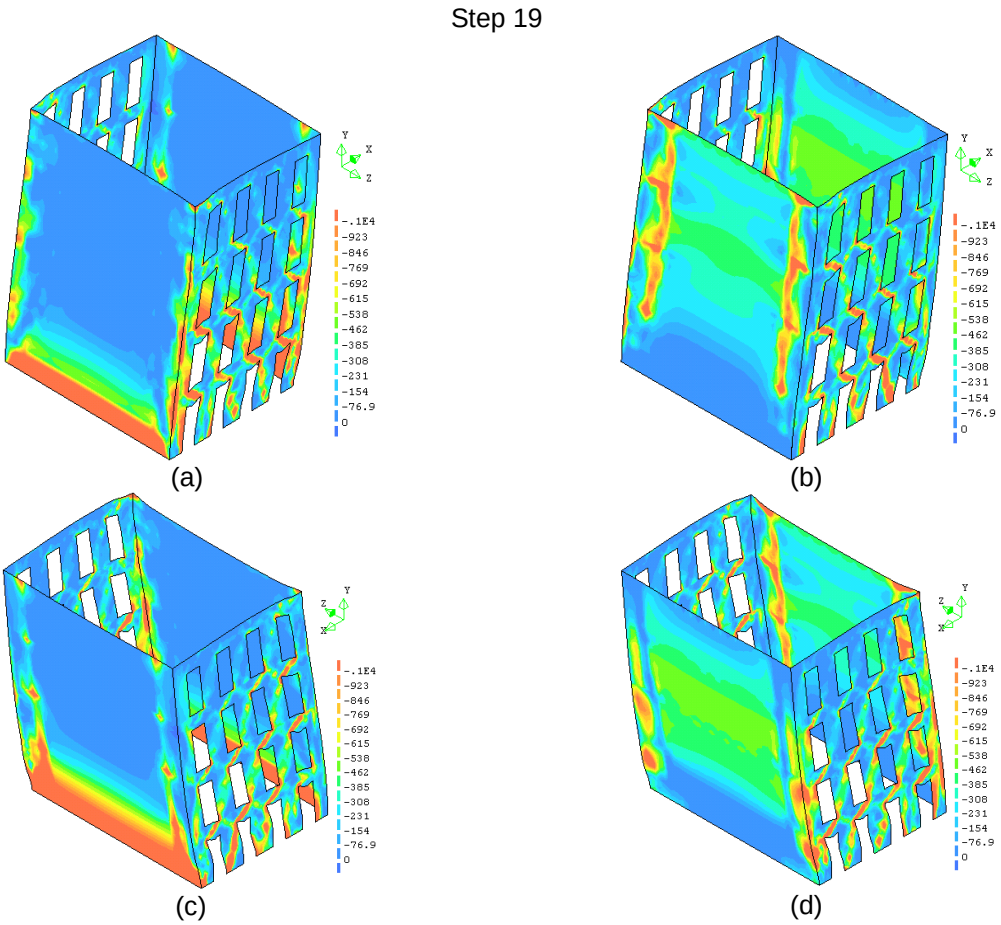

Figure 7 - (a) N-E view inside (b) N-E view outside (c) S-W view outside and (d) S-W view inside, units in kPa.

1.1.2 N-S direction.

Deformed mesh

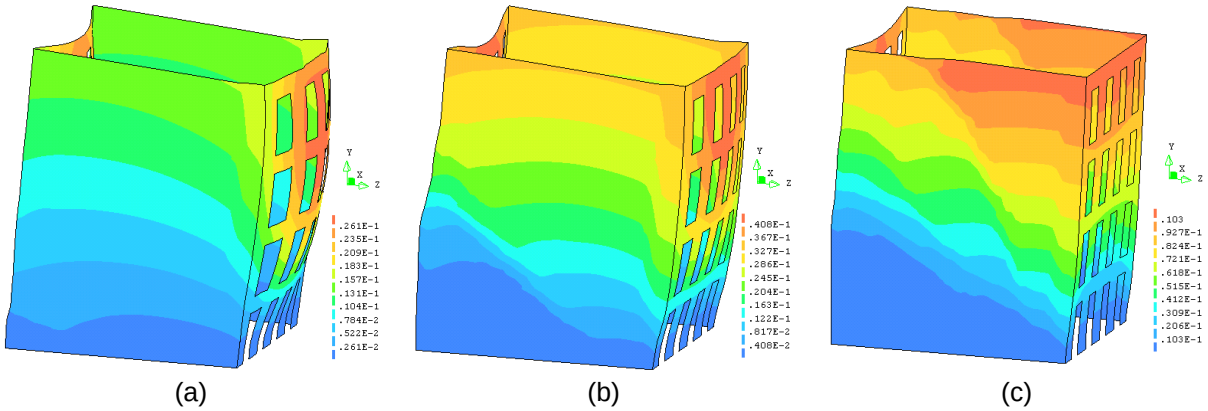

Figure 8 – deformed mesh for the steps number (a) 31, (b) 9 and (c) 37, units in meters.

Strain states

Step 26

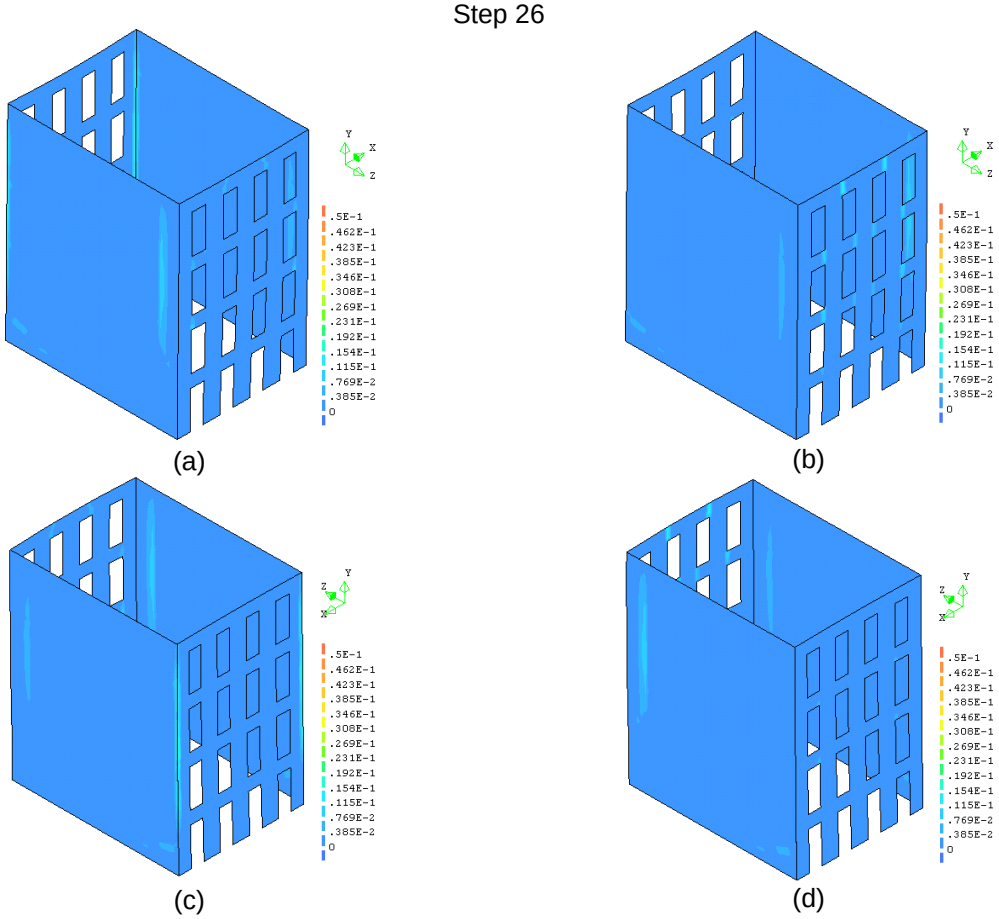

(a) (b)

(c) (d)

Figure 9 - (a) N-E view inside (b) N-E view outside (c) S-W view outside and (d) S-W view inside.

Step 31

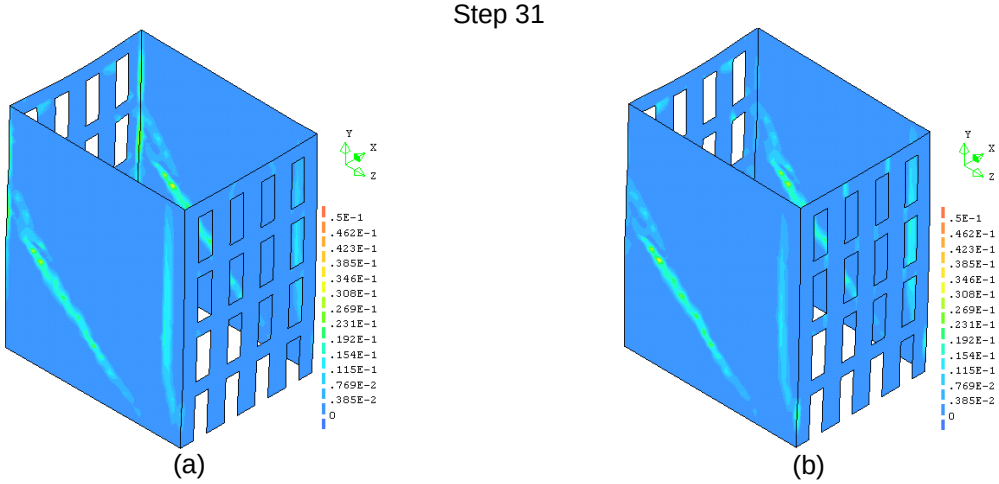

(a) (b)

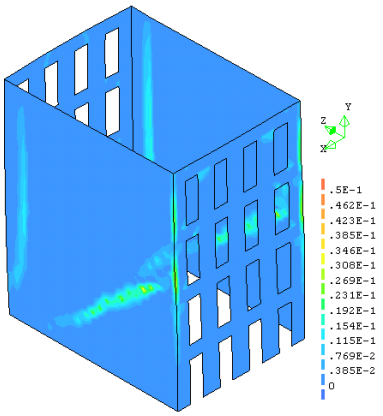

(c)

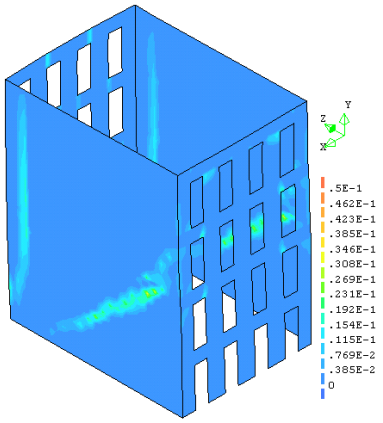

(d)

Figure 10 - (a) N-E view inside (b) N-E view outside (c) S-W view outside and (d) S-W view inside.

Step 37

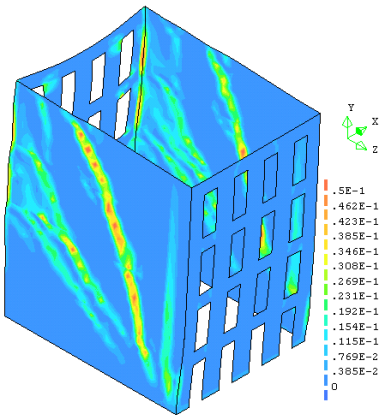

(a)

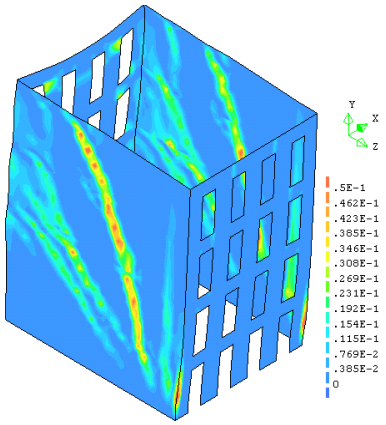

(b)

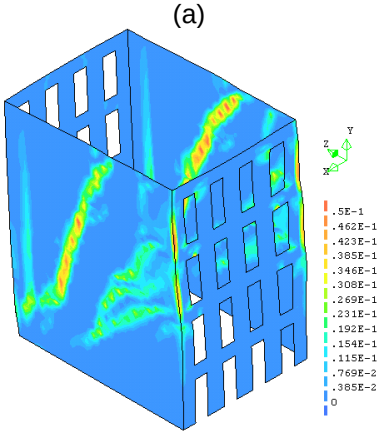

(c)

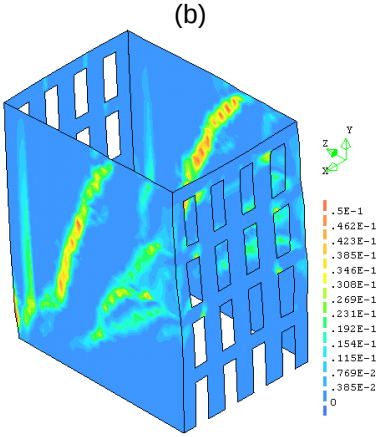

(d)

Figure 11 - (a) N-E view inside (b) N-E view outside (c) S-W view outside and (d) S-W view inside.

Stress states

Step 26

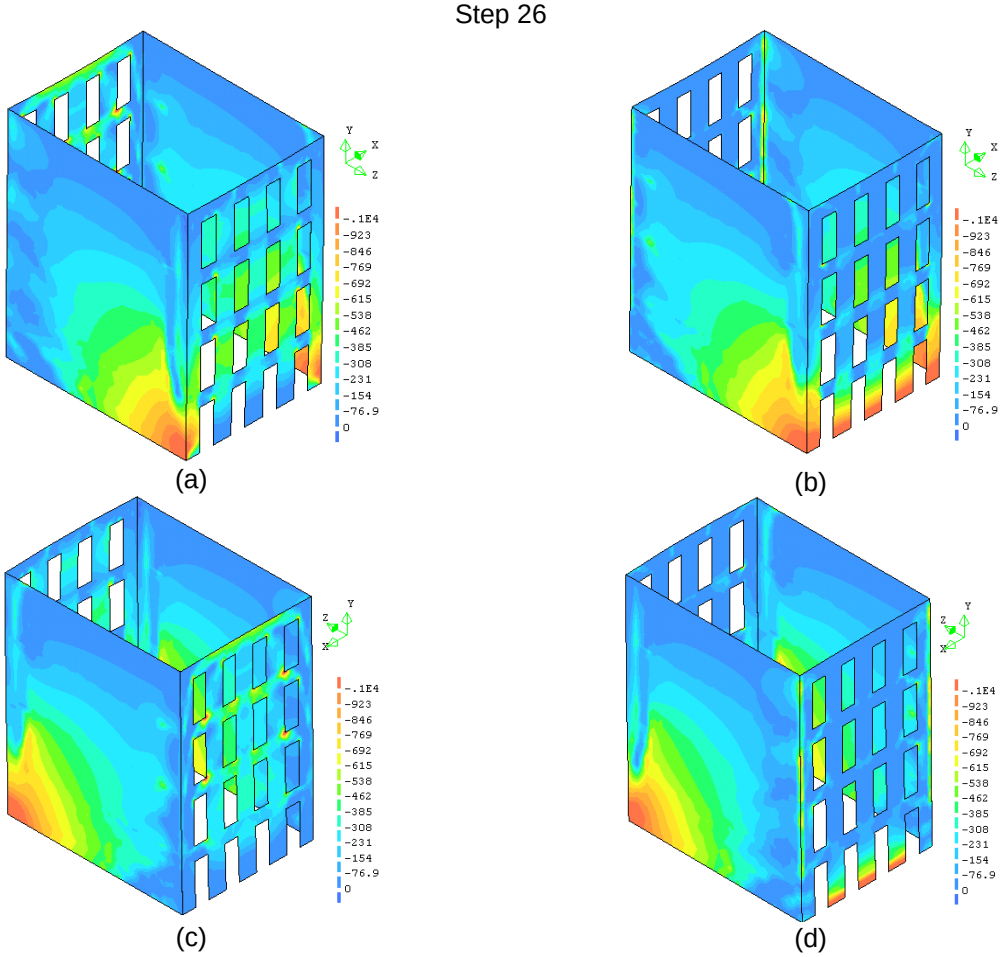

(a) (b)

(c) (d)

Figure 12 - (a) N-E view inside (b) N-E view outside (c) S-W view outside and (d) S-W view inside, units in kPa.

Step 31

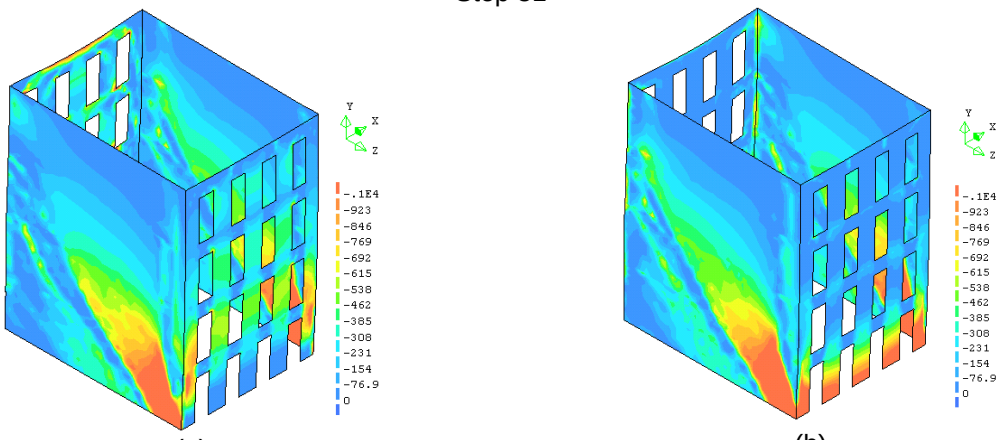

(a) (b)

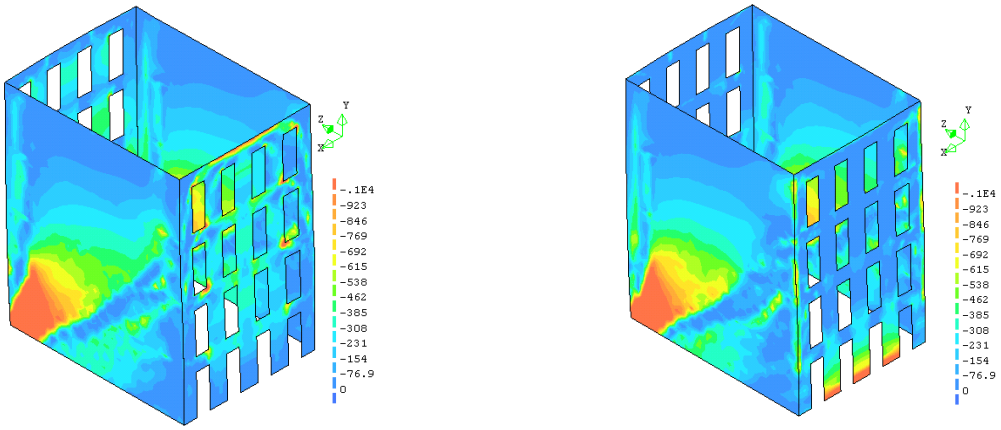

(c) (d)

Figure 13 - (a) N-E view inside (b) N-E view outside (c) S-W view outside and (d) S-W view inside, units in kPa.

Step 37

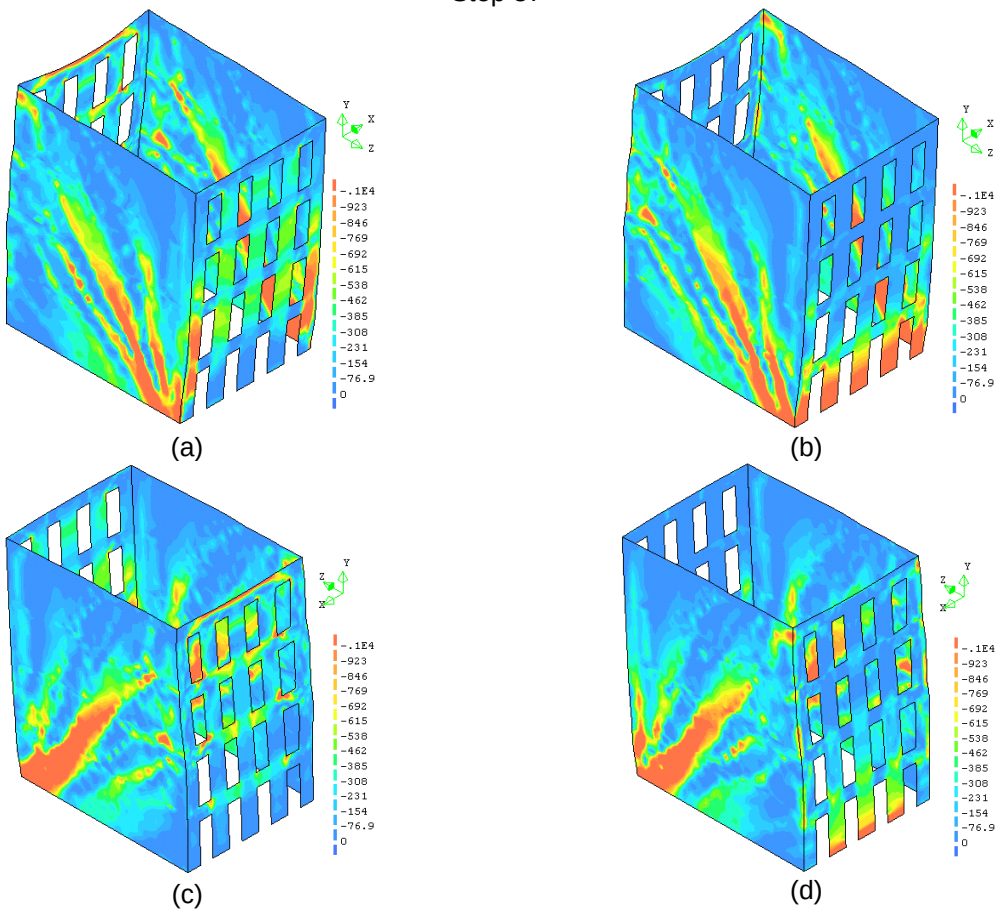

(a) (b)

(c) (d)

Figure 14 - (a) N-E view inside (b) N-E view outside (c) S-W view outside and (d) S-W view inside, units in kPa.

1.2 Stiffness of the MDF panels

1.2.1 0.1xE In E-W direction, step 27

Deformed mesh

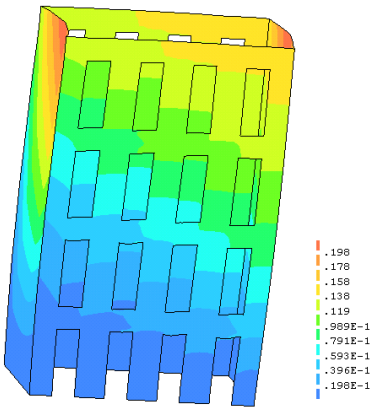

Figure 15 – deformed mesh, units in meters.

Strain states

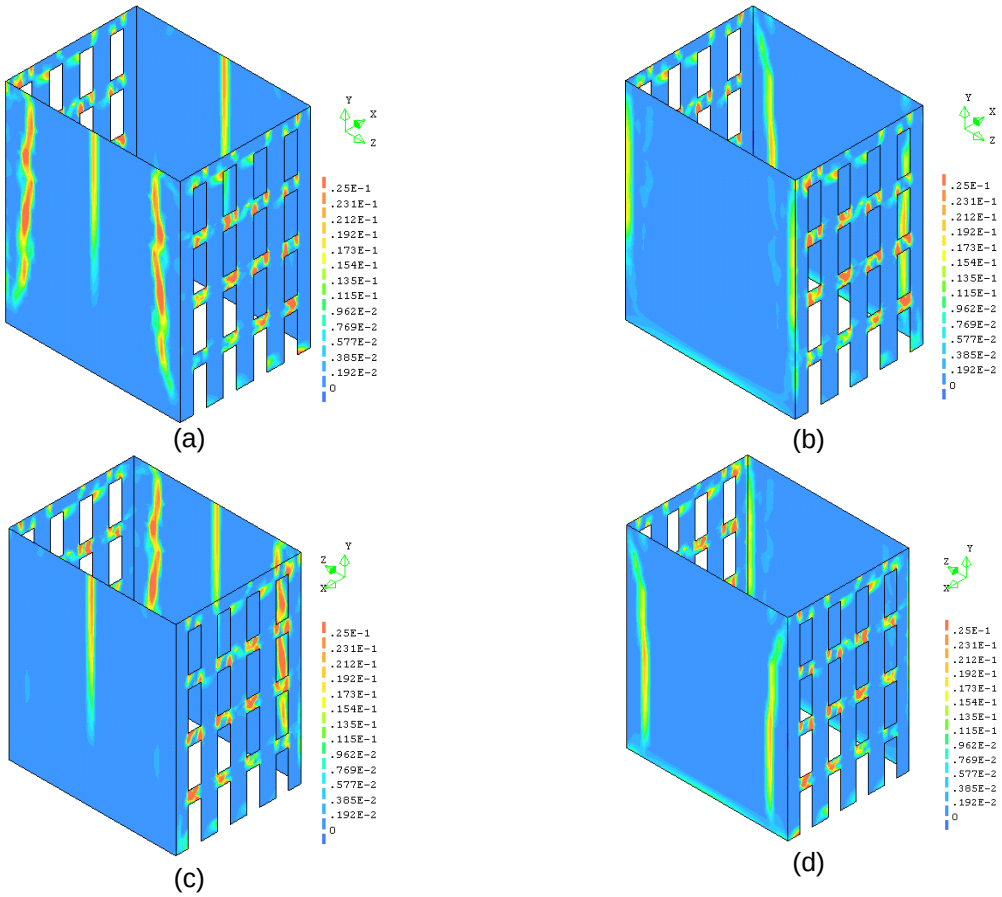

Figure 16 - (a) N-E view inside (b) N-E view outside (c) S-W view outside and (d) S-W view inside.

Stress states

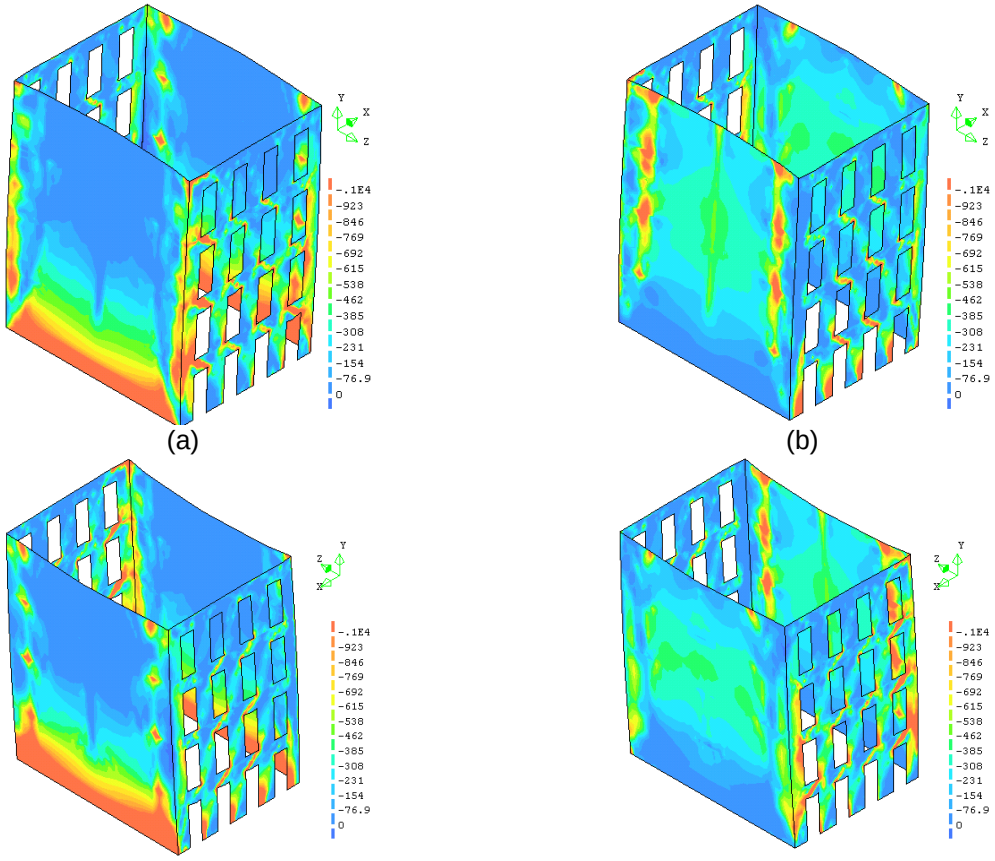

Figure 17 - (a) N-E view inside (b) N-E view outside (c) S-W view outside and (d) S-W view inside, units in kPa.

1.2.2 0.1xE In N-S direction, step 34

Deformed mesh

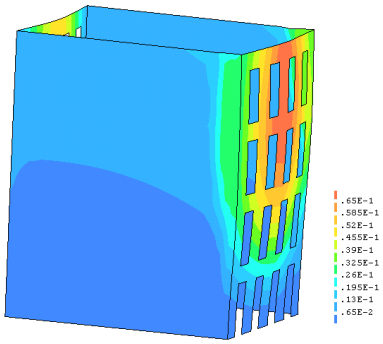

Figure 18 – deformed mesh, units in meters.

Strain states

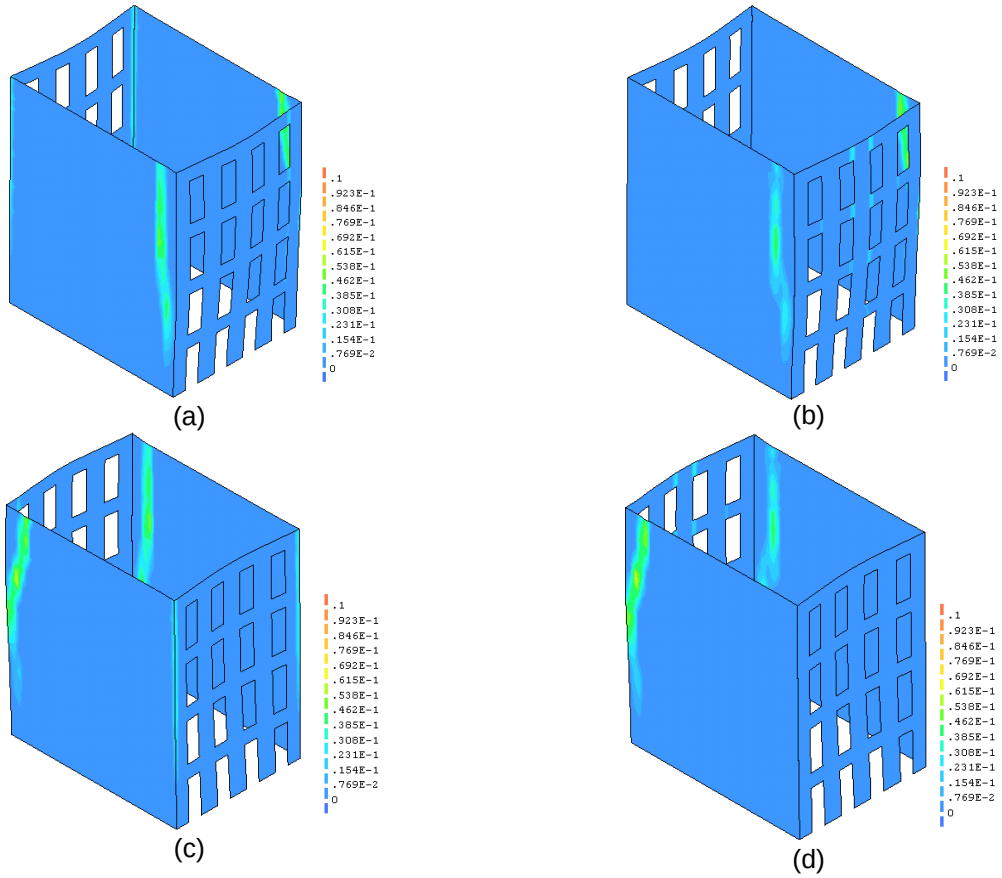

Figure 19 - (a) N-E view inside (b) N-E view outside (c) S-W view outside and (d) S-W view inside.

Stress states

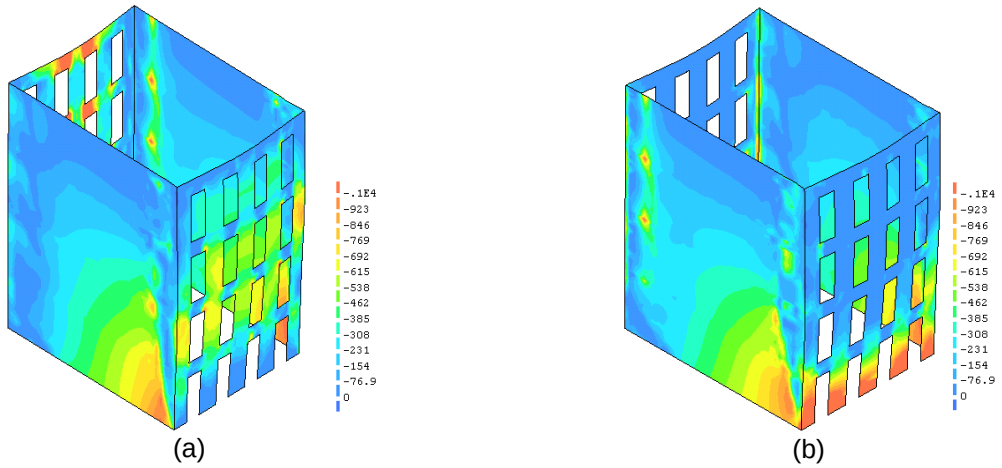

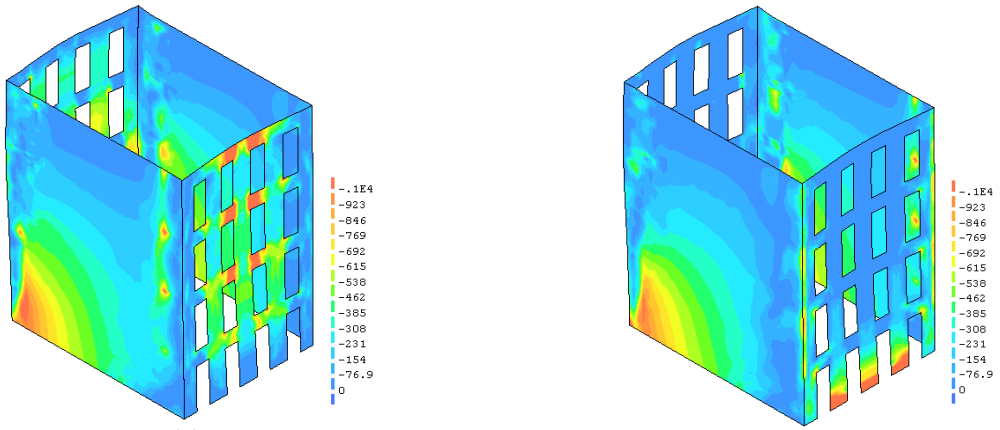

(c) (d)

Figure 20 - (a) N-E view inside (b) N-E view outside (c) S-W view outside and (d) S-W view inside, units in kPa.

1.2.3 10xE In E-W direction, step 34

Deformed mesh

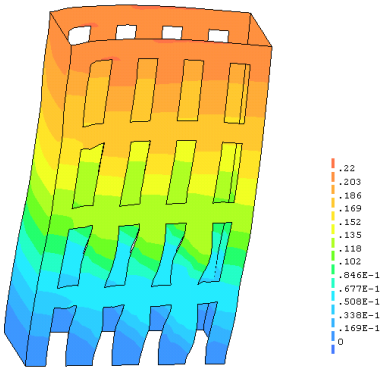

Figure 21 – deformed mesh, units in meters.

Strain states

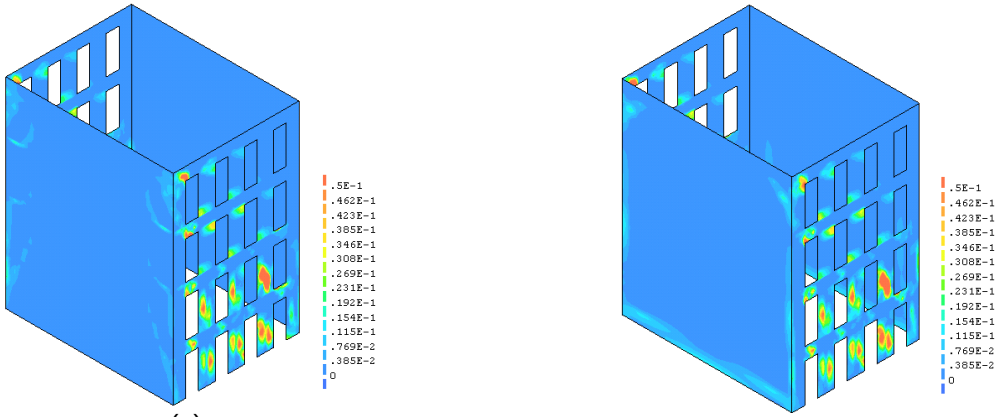

(a) (b)

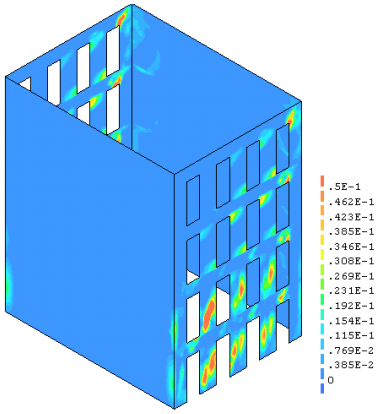

(c)

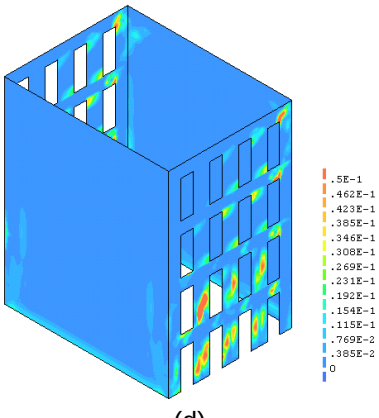

(d)

Figure 22 - (a) N-E view inside (b) N-E view outside (c) S-W view outside and (d) S-W view inside.

Stress states

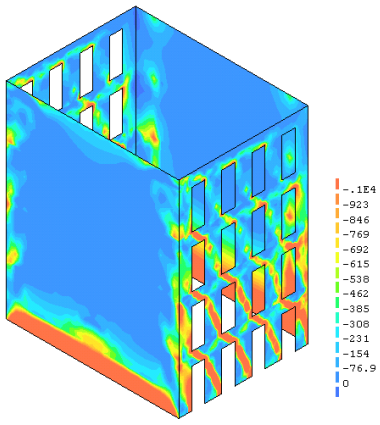

(a)

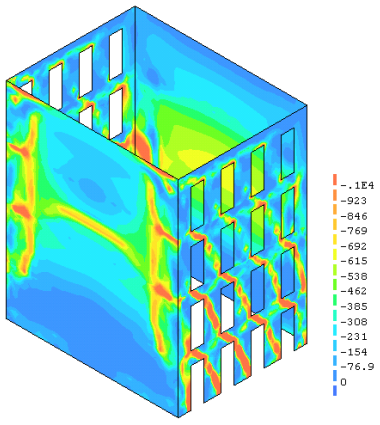

(b)

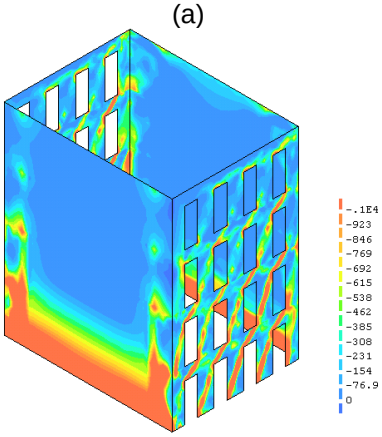

(c)

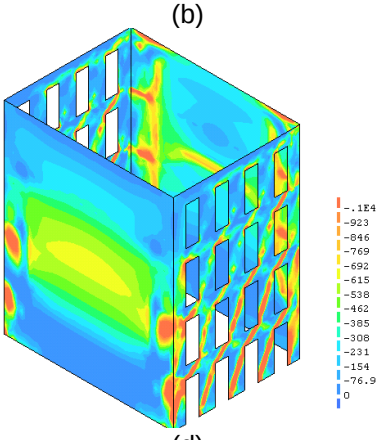

(d)

Figure 23 - (a) N-E view inside (b) N-E view outside (c) S-W view outside and (d) S-W view inside, units in kPa.

1.2.4 10xE In N-S direction, step 57

Deformed mesh

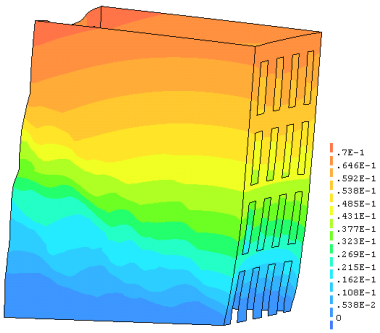

Figure 24 – deformed mesh, units in meters.

Strain states

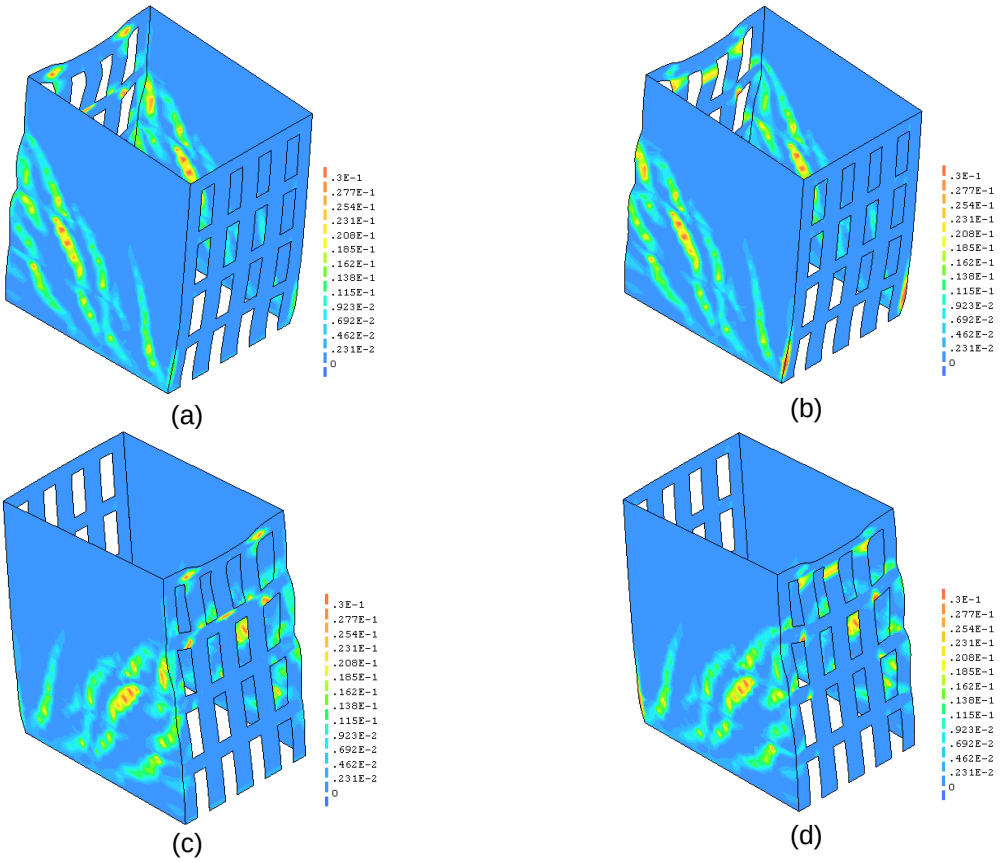

Figure 25 - (a) N-E view inside (b) N-E view outside (c) S-W view outside and (d) S-W view inside.

Stress states

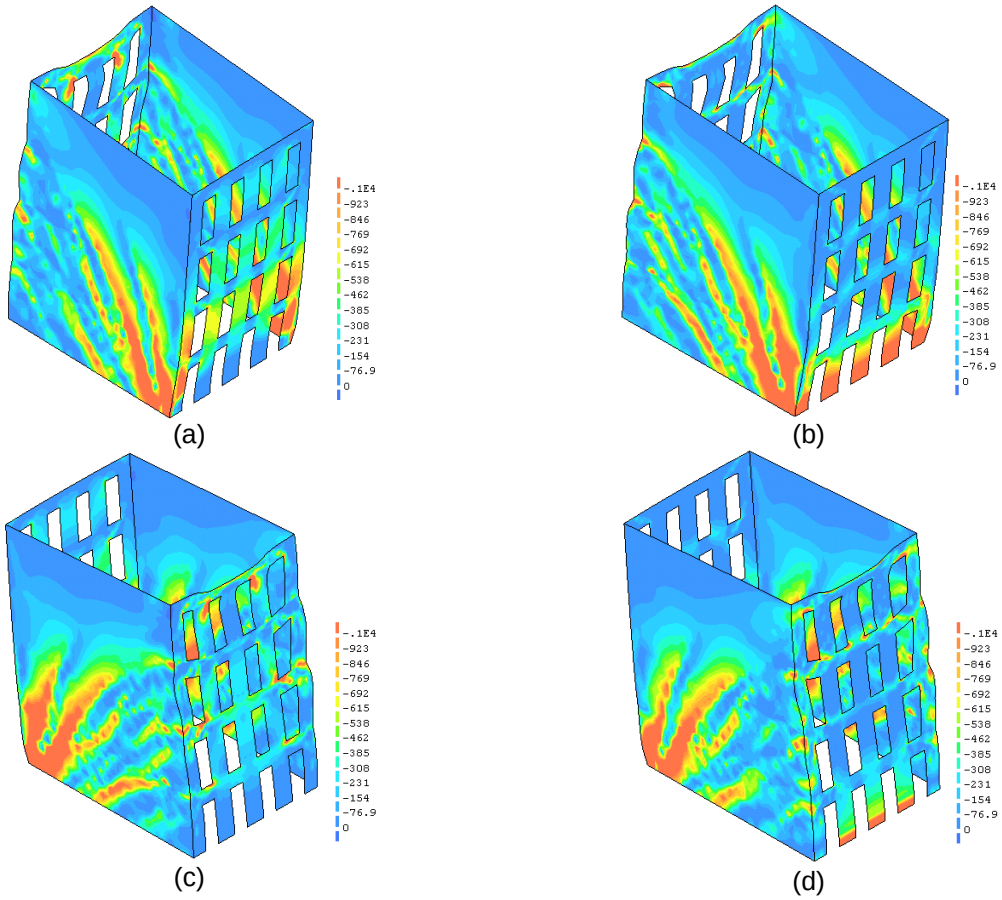

Figure 26 - (a) N-E view inside (b) N-E view outside (c) S-W view outside and (d) S-W view inside, units in kPa.

1.2.5 100xE In E-W direction, step 34

Deformed mesh

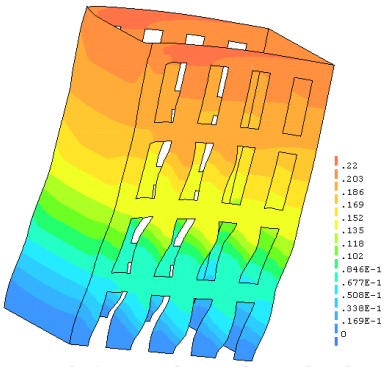

Figure 27 – deformed mesh, units in meters.

Strain states

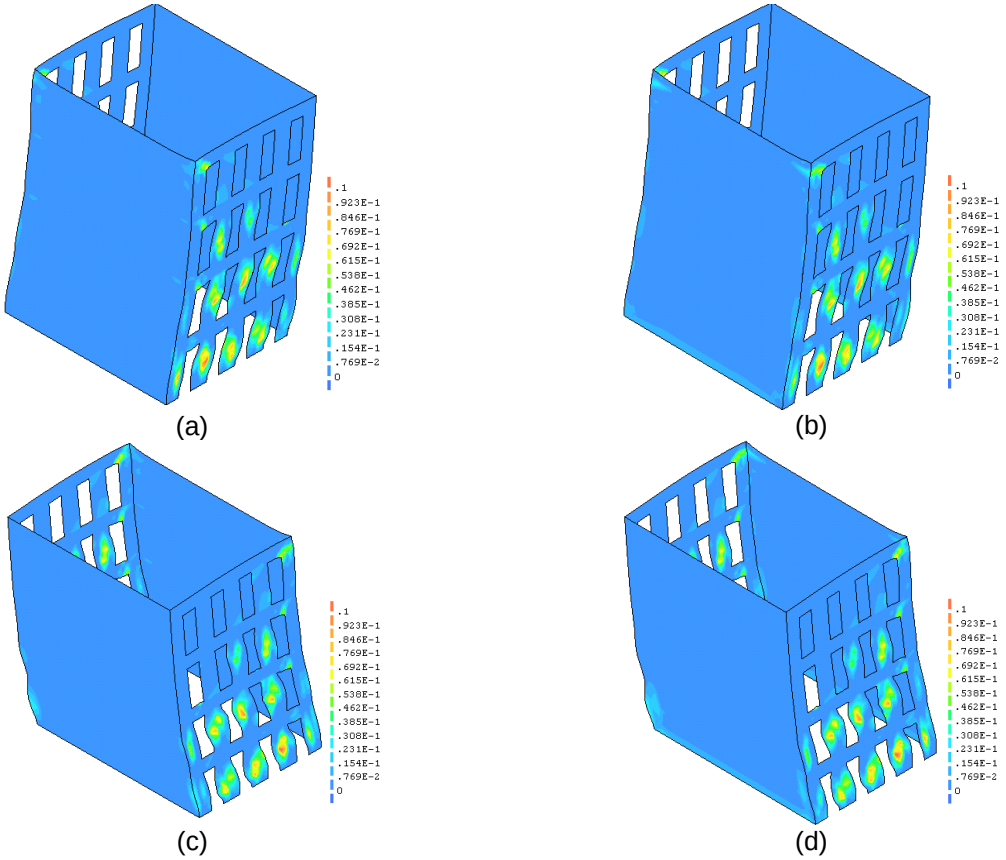

Figure 28 - (a) N-E view inside (b) N-E view outside (c) S-W view outside and (d) S-W view inside.

Stress states

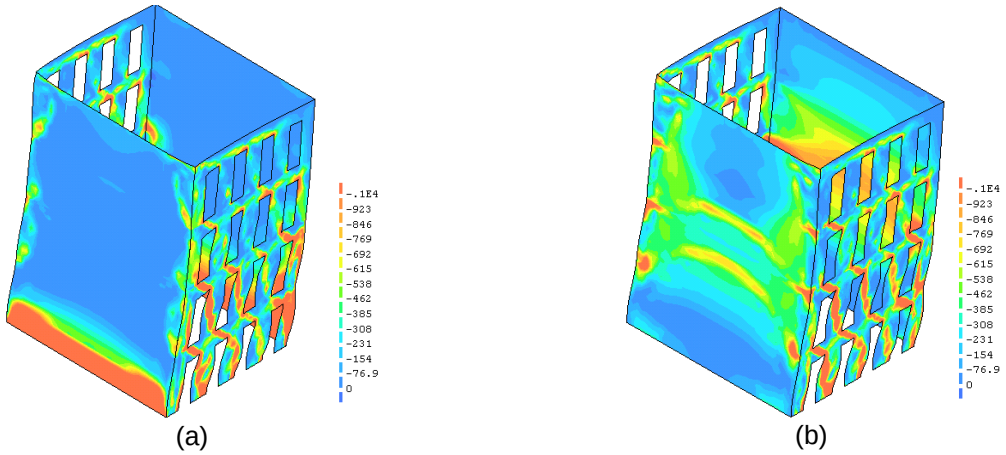

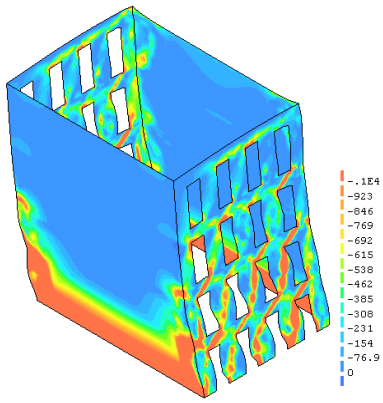

(c)

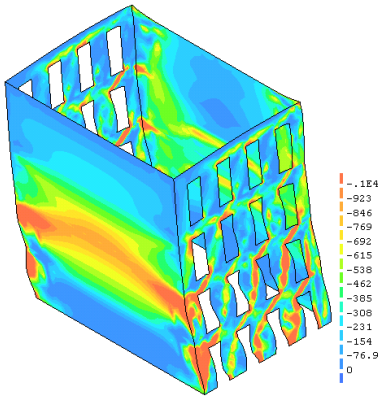

(d)

Figure 29 - (a) N-E view inside (b) N-E view outside (c) S-W view outside and (d) S-W view inside, units in kPa.

1.2.6 100xE In N-S direction, step 63

Deformed mesh

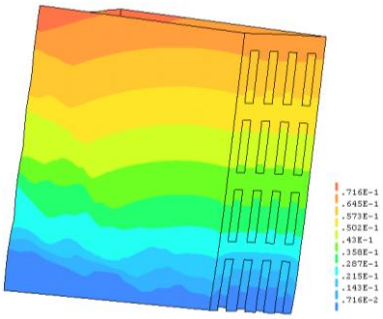

Figure 30 – deformed mesh, units in meters.

Strain states

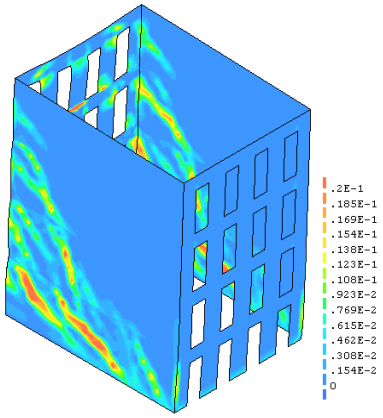

(a)

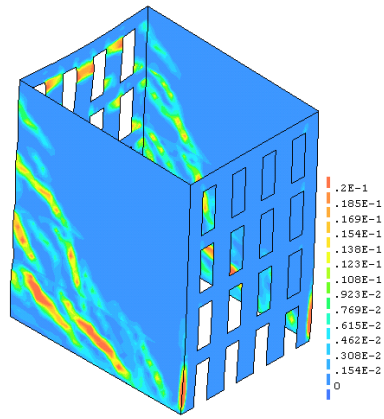

(b)

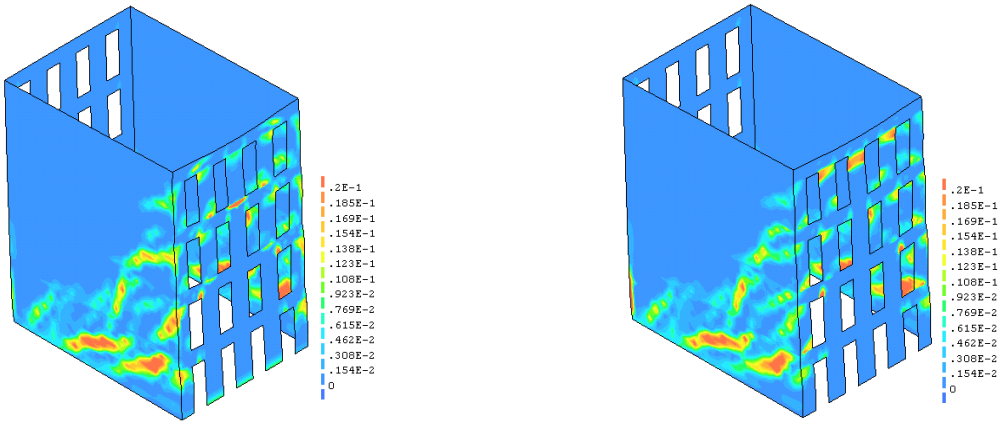

(c) (d)

Figure 31 - (a) N-E view inside (b) N-E view outside (c) S-W view outside and (d) S-W view inside.

Stress states

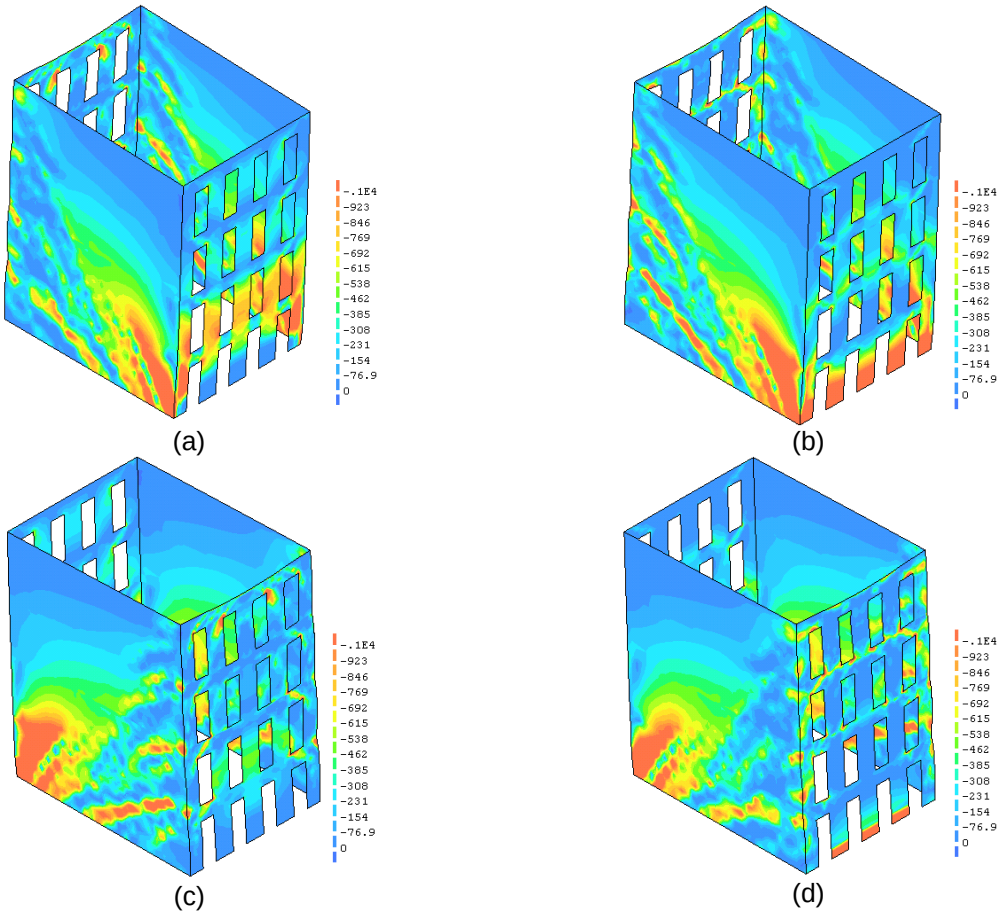

(a) (b)

(c) (d)

Figure 32 - (a) N-E view inside (b) N-E view outside (c) S-W view outside and (d) S-W view inside, units in kPa.

1.2.7 1000xE In E-W direction, step 34

Deformed mesh

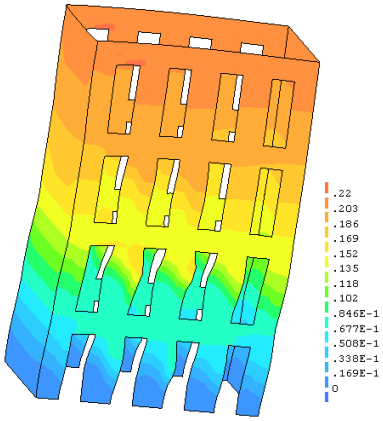

Figure 33 – deformed mesh, units in meters.

Strain states

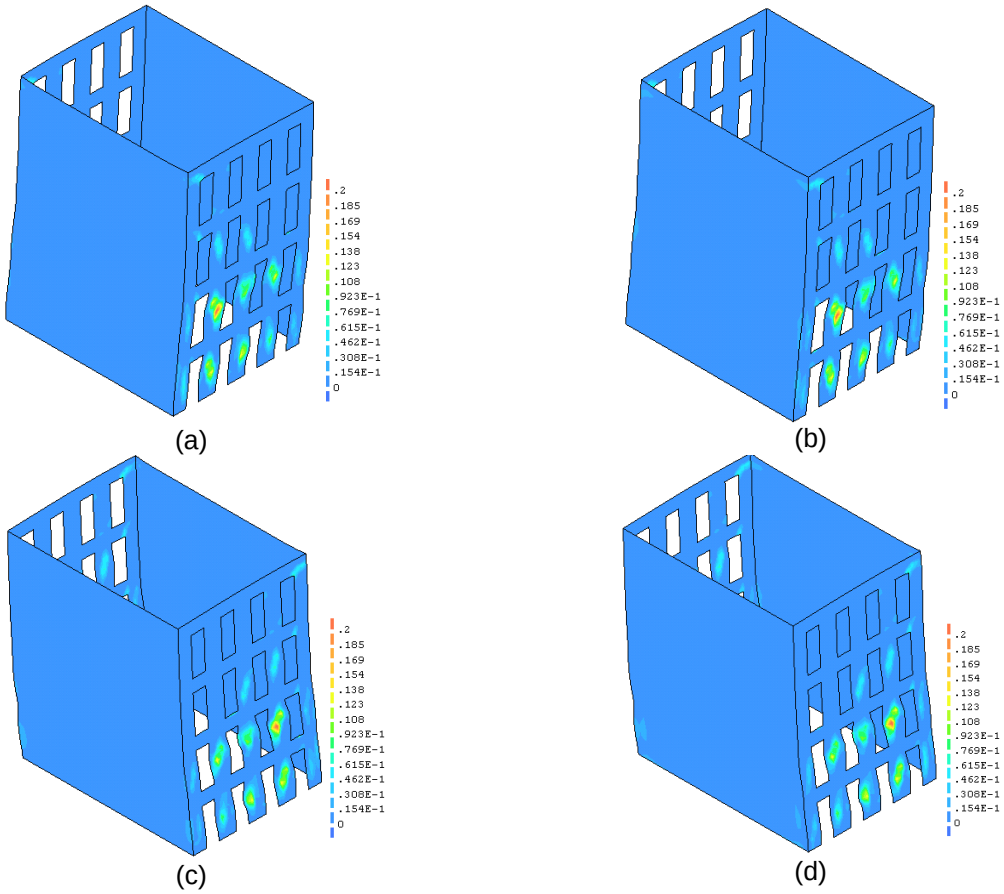

Figure 34 - (a) N-E view inside (b) N-E view outside (c) S-W view outside and (d) S-W view inside.

Stress states

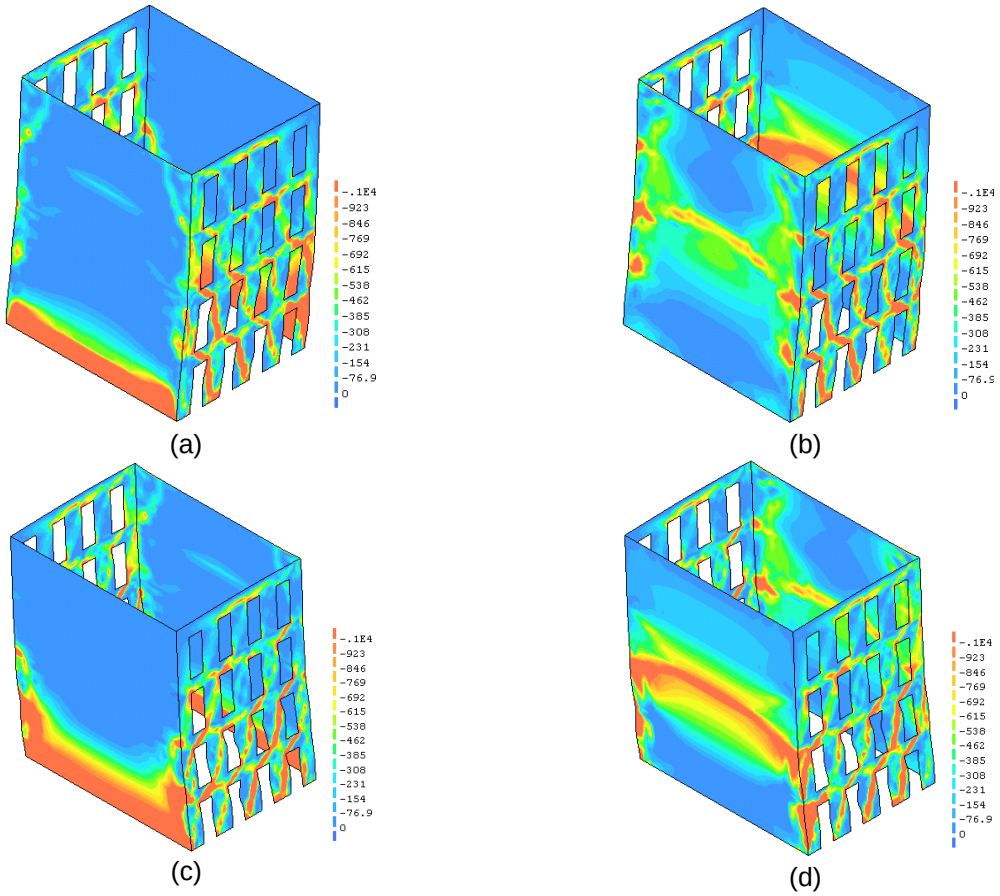

Figure 35 - (a) N-E view inside (b) N-E view outside (c) S-W view outside and (d) S-W view inside, units in kPa.

1.2.8 1000xE In N-S direction, step 63

Deformed mesh

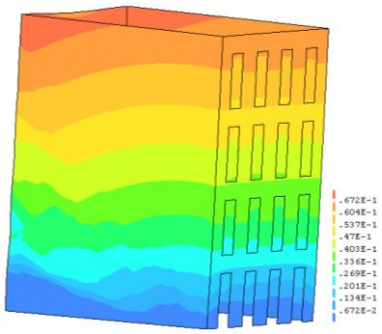

Figure 36 – deformed mesh, units in meters.

Strain states

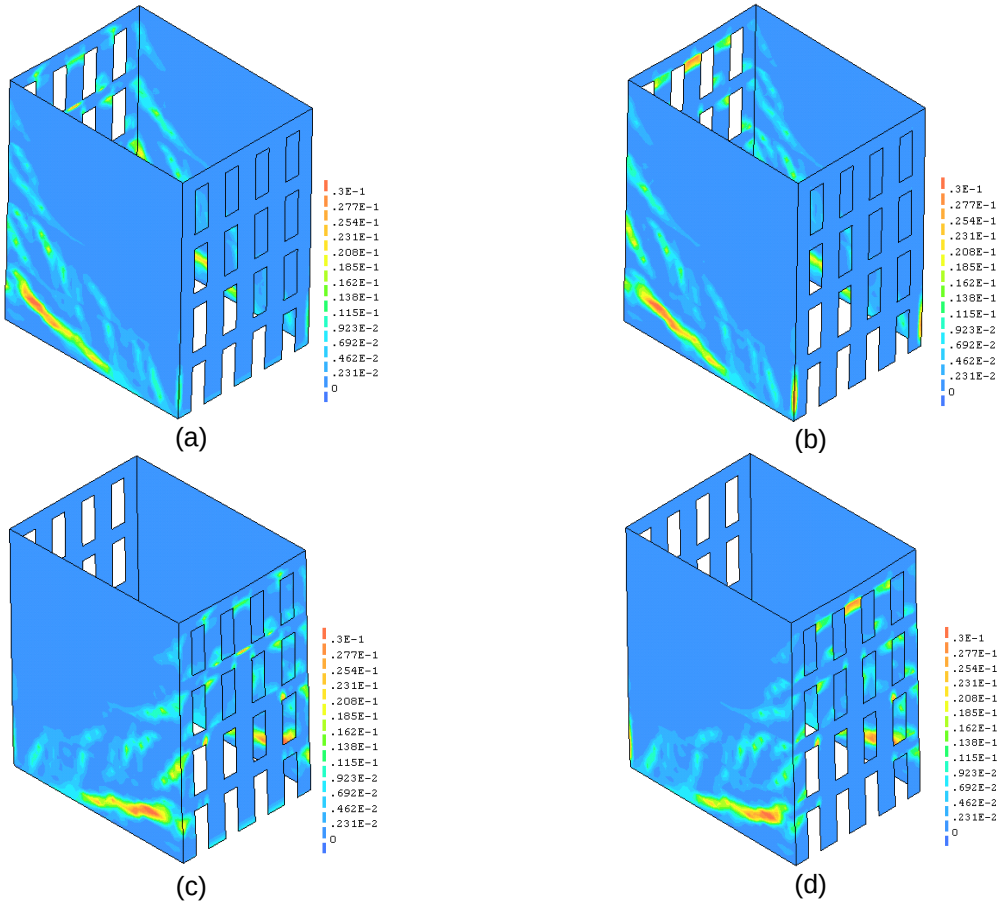

Figure 37 - (a) N-E view inside (b) N-E view outside (c) S-W view outside and (d) S-W view inside.

Stress states

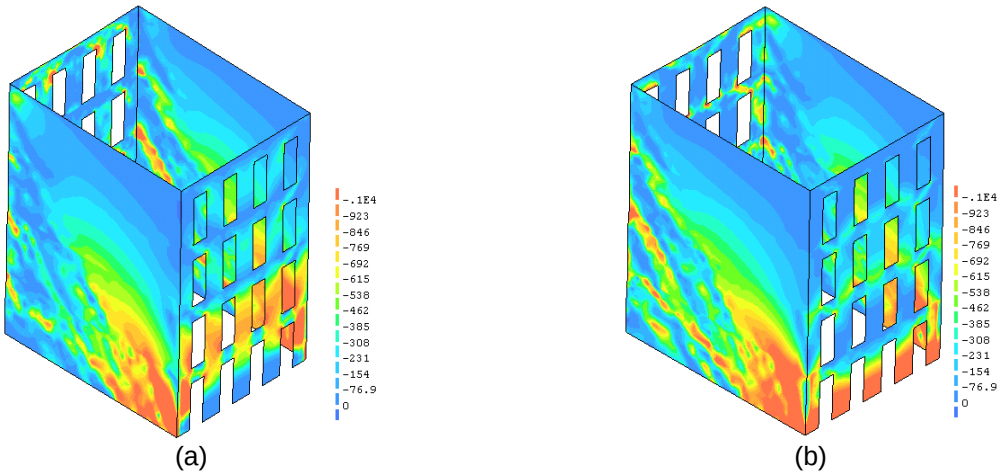

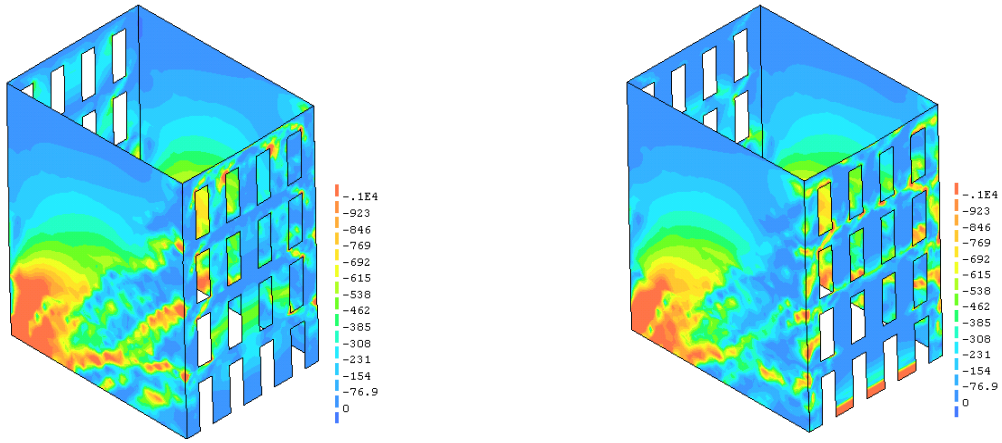

(c) (d)

Figure 38 - (a) N-E view inside (b) N-E view outside (c) S-W view outside and (d) S-W view inside, units in kPa.

1.3 Stiffness of the masonry

1.3.1 0.5xE In E-W direction, step 26

Deformed mesh

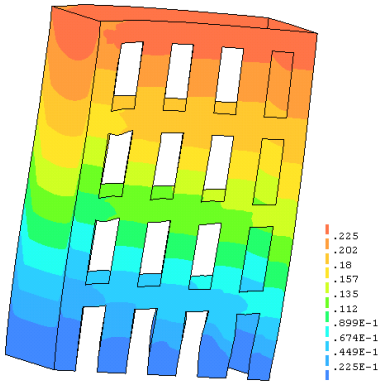

Figure 39 – deformed mesh, units in meters.

Strain states

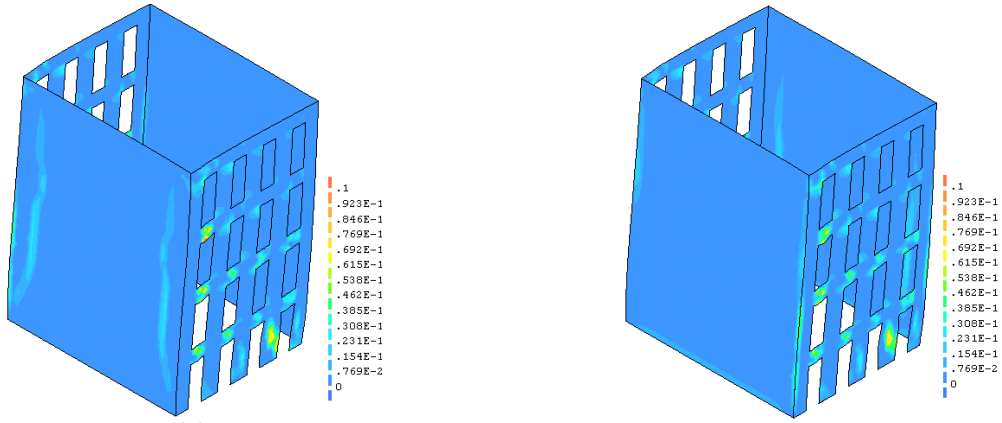

(a) (b)

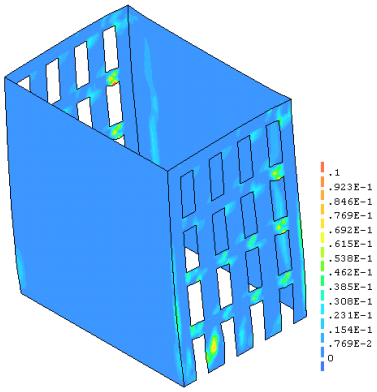

(c)

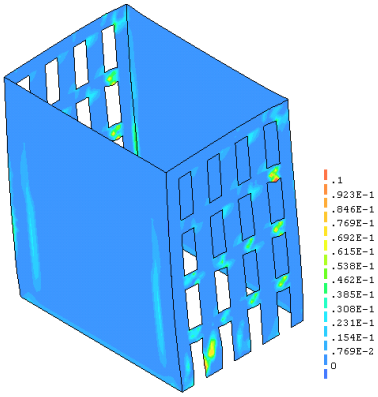

(d)

Figure 40 - (a) N-E view inside (b) N-E view outside (c) S-W view outside and (d) S-W view inside.

Stress states

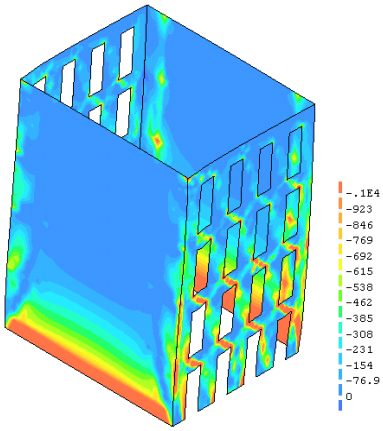

(a)

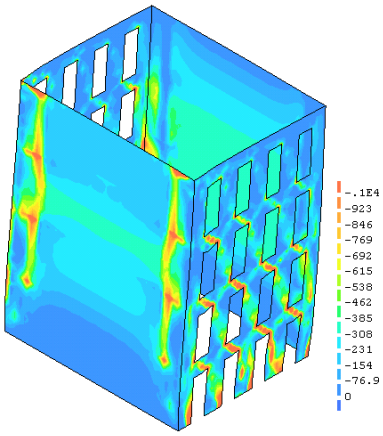

(b)

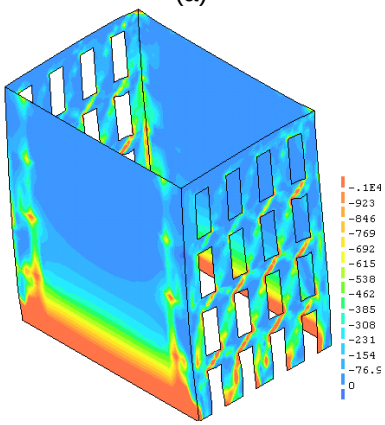

(c)

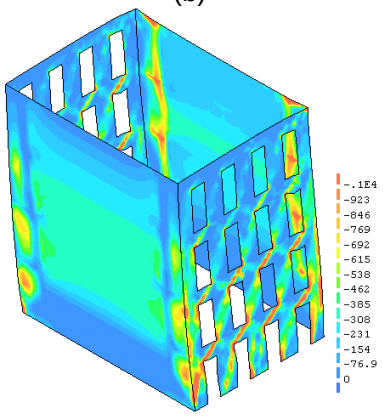

(d)

Figure 41 - (a) N-E view inside (b) N-E view outside (c) S-W view outside and (d) S-W view inside, units in kPa.

1.3.2 0.5xE In N-S direction, step 46

Deformed mesh

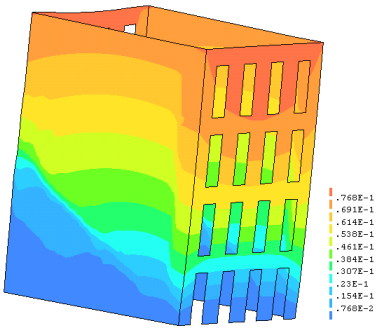

Figure 42 – deformed mesh, units in meters.

Strain states

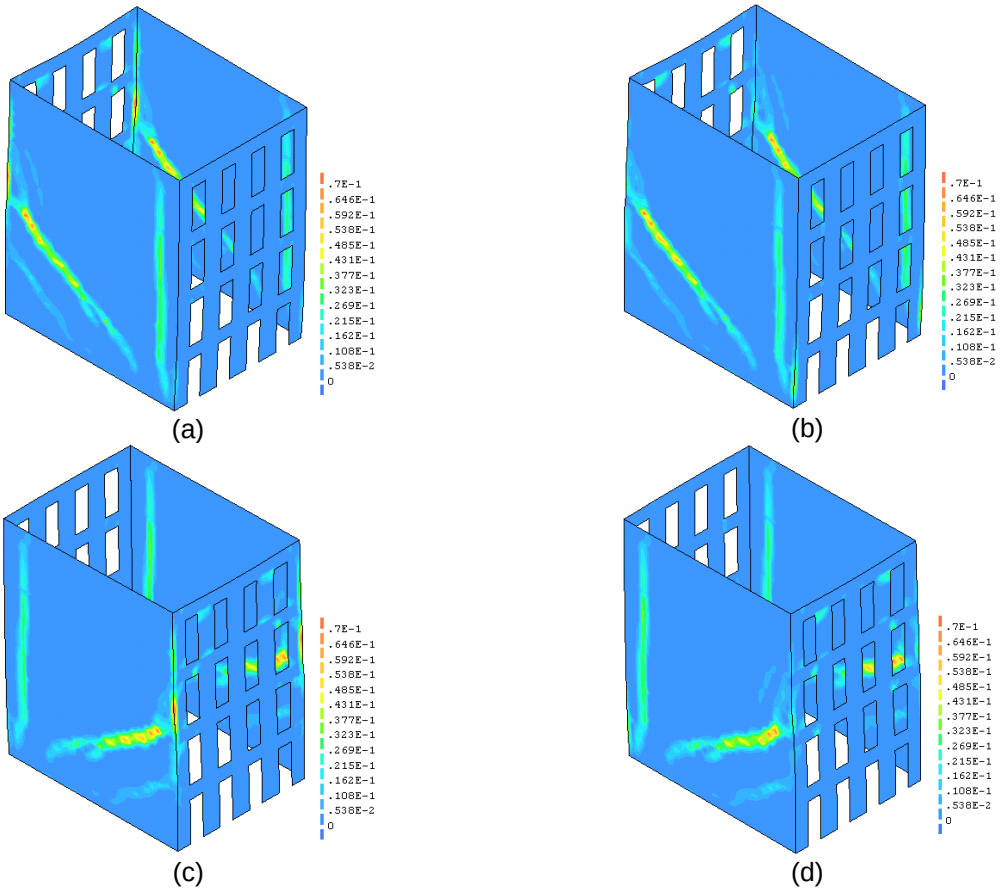

Figure 43 - (a) N-E view inside (b) N-E view outside (c) S-W view outside and (d) S-W view inside.

Stress states

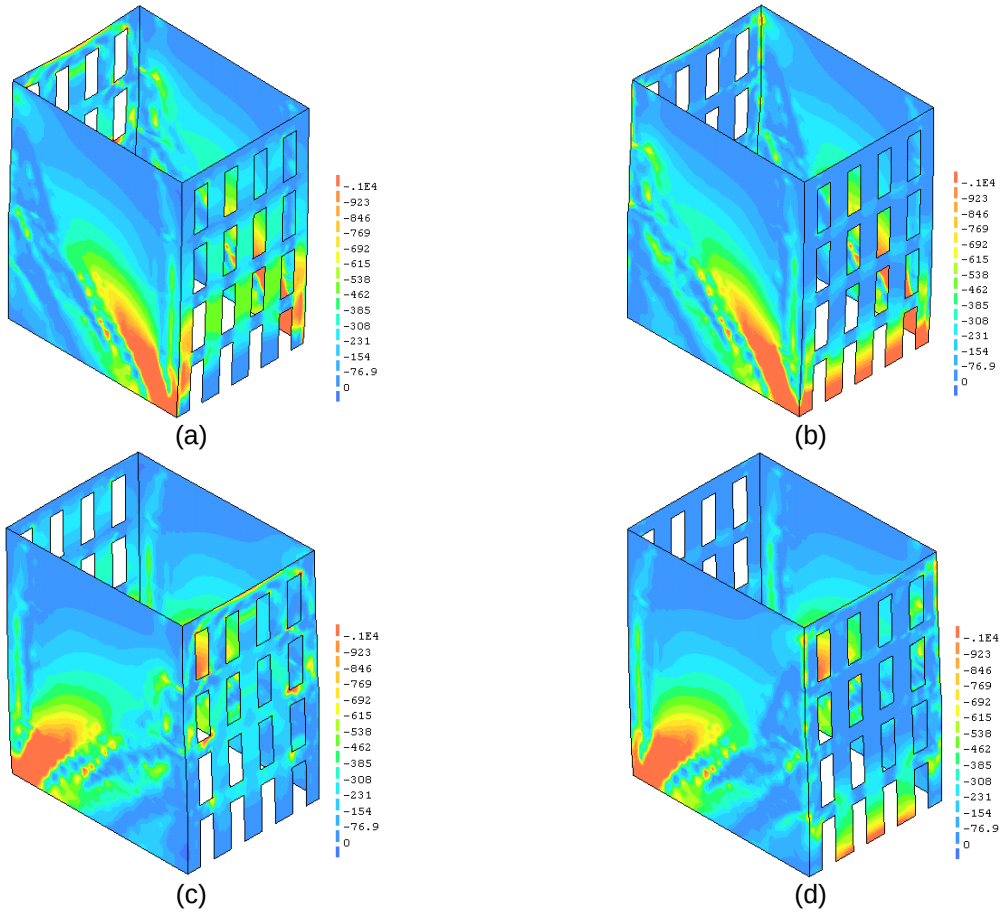

Figure 44 - (a) N-E view inside (b) N-E view outside (c) S-W view outside and (d) S-W view inside, units in kPa.

1.3.3 2xE In E-W direction, step 36

Deformed mesh

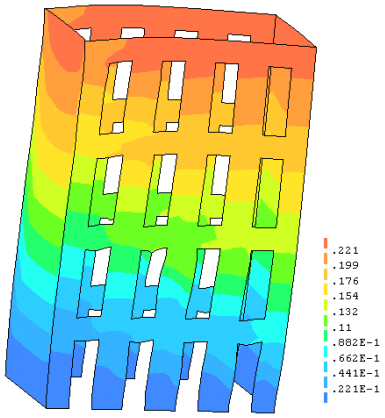

Figure 45 – deformed mesh, units in meters.

Strain states

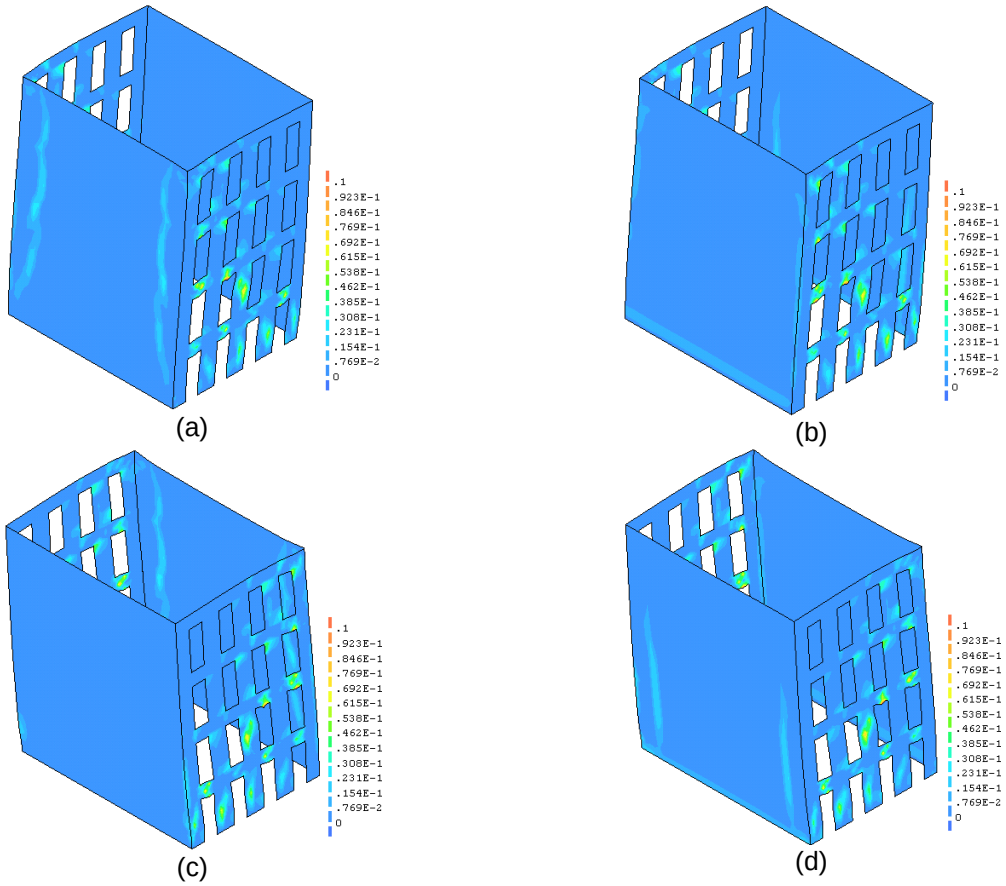

Figure 46 - (a) N-E view inside (b) N-E view outside (c) S-W view outside and (d) S-W view inside.

Stress states

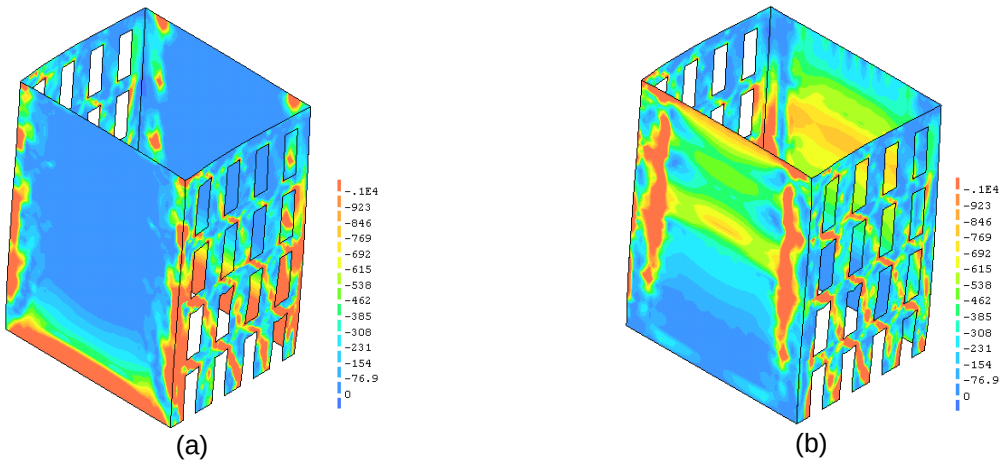

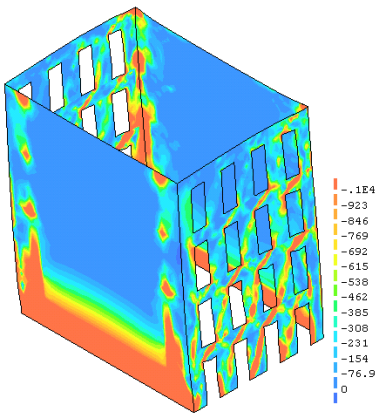

(c)

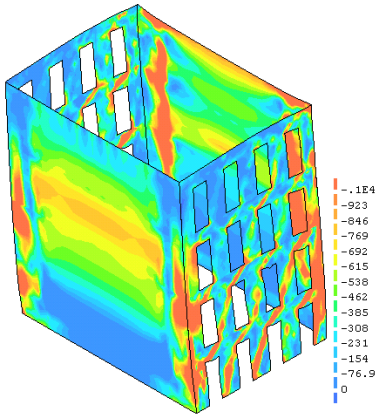

(d)

Figure 47 - (a) N-E view inside (b) N-E view outside (c) S-W view outside and (d) S-W view inside, units in kPa.

1.3.4 2xE In N-S direction, step 53

Deformed mesh

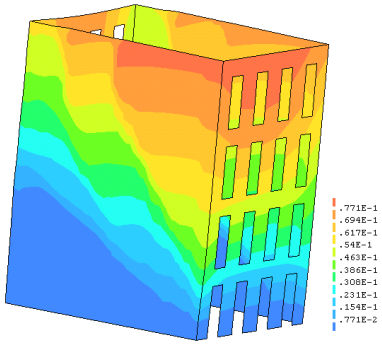

Figure 48 – deformed mesh, units in meters.

Strain states

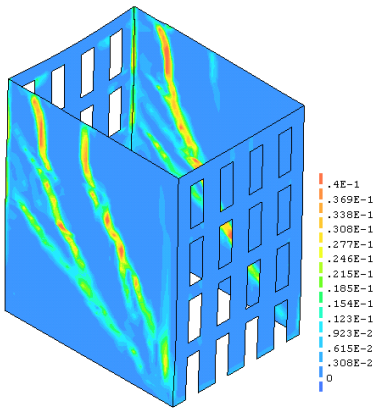

(a)

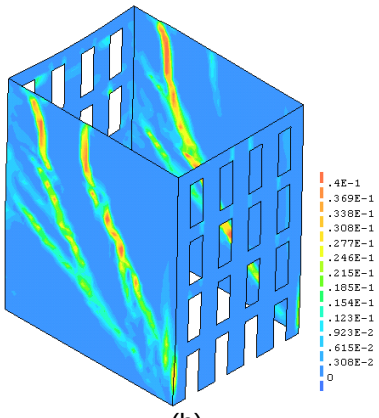

(b)

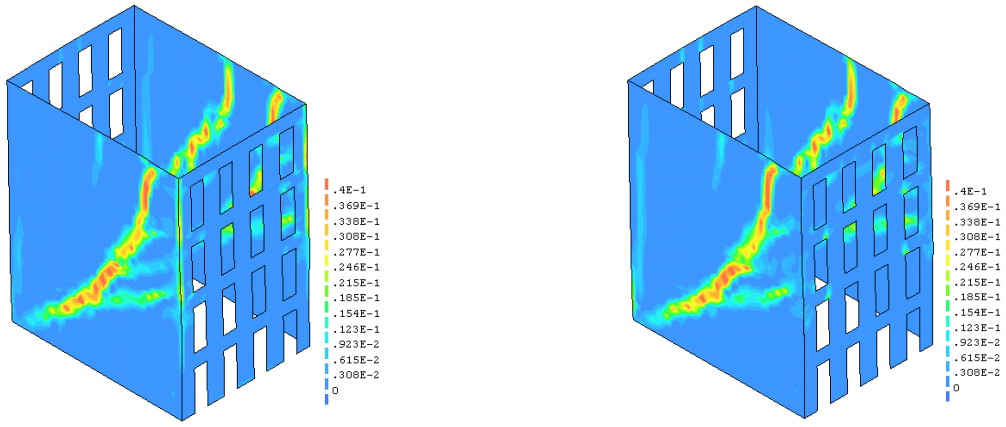

(c) (d)

Figure 49 - (a) N-E view inside (b) N-E view outside (c) S-W view outside and (d) S-W view inside.

Stress states

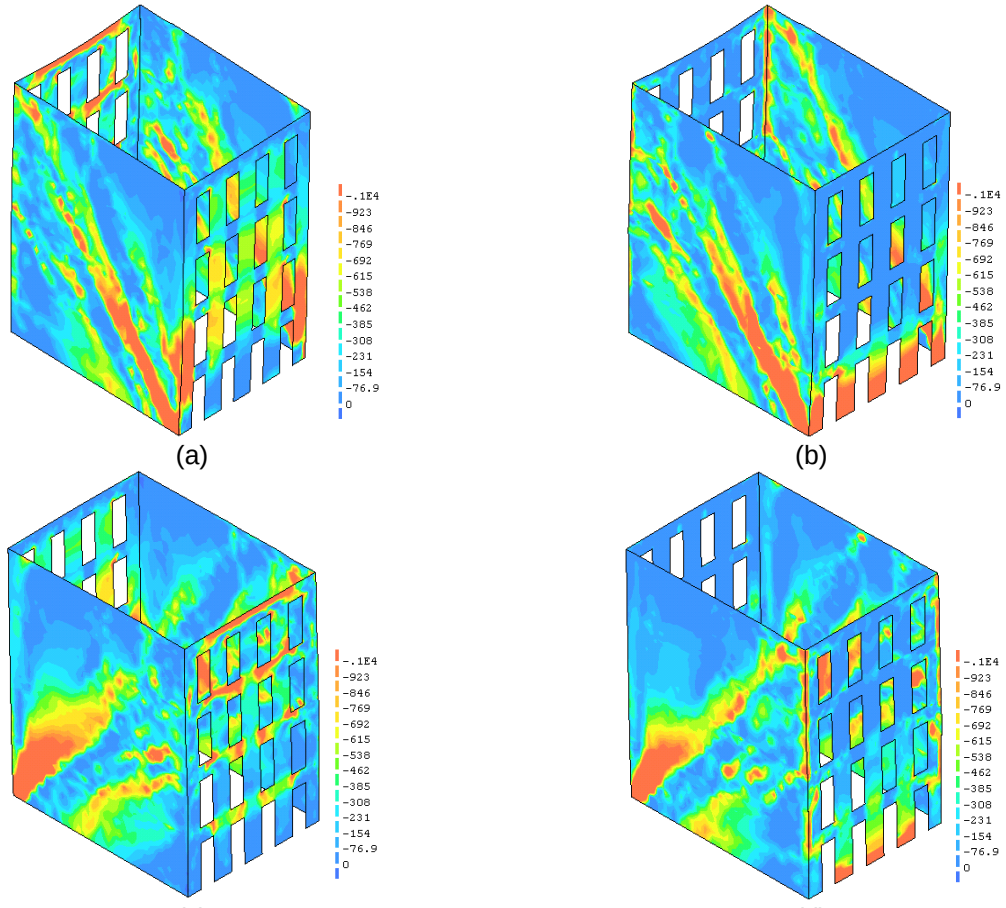

(a) (b)

(c) (d)

Figure 50 - (a) N-E view inside (b) N-E view outside (c) S-W view outside and (d) S-W view inside, units in kPa.

1.4 Tensile strength

1.4.1 0.5xFt in E-W direction, step 26

Deformed mesh

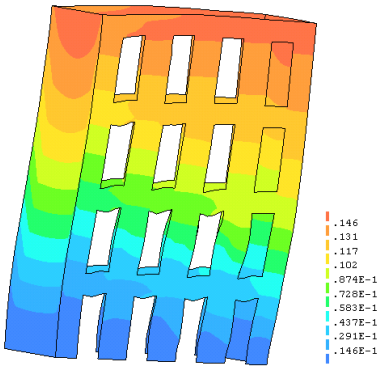

Figure 51 – deformed mesh, units in meters.

Strain states

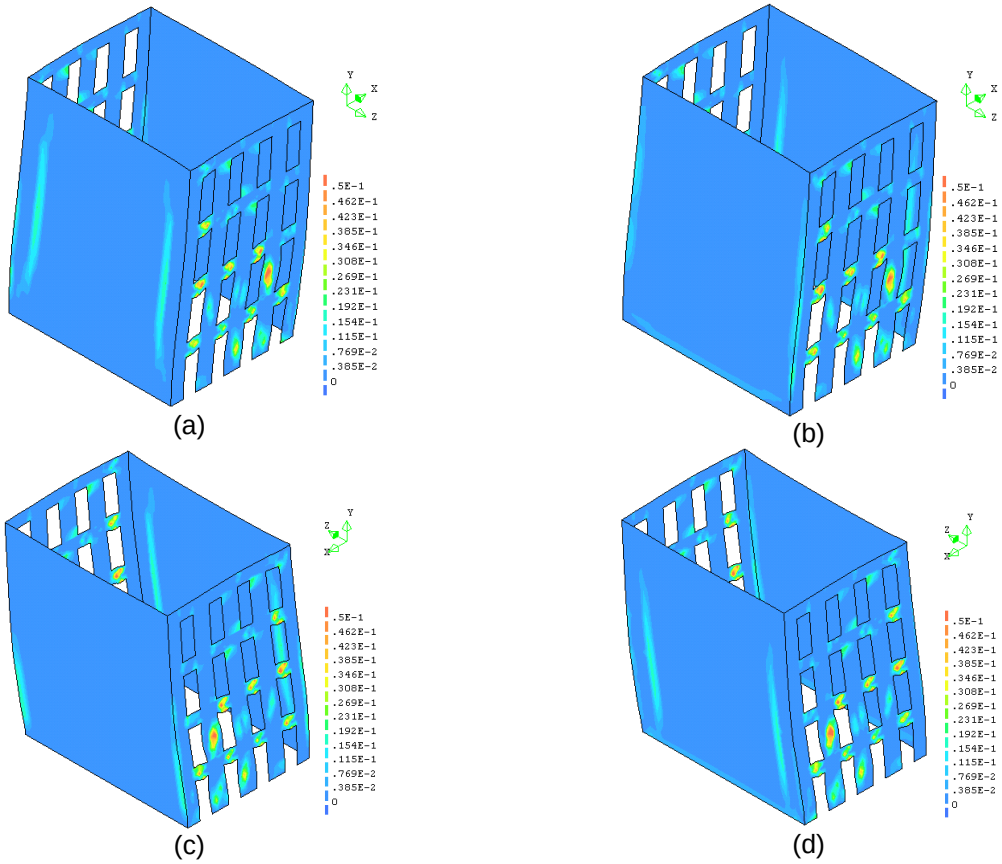

Figure 52 - (a) N-E view inside (b) N-E view outside (c) S-W view outside and (d) S-W view inside.

Stress states

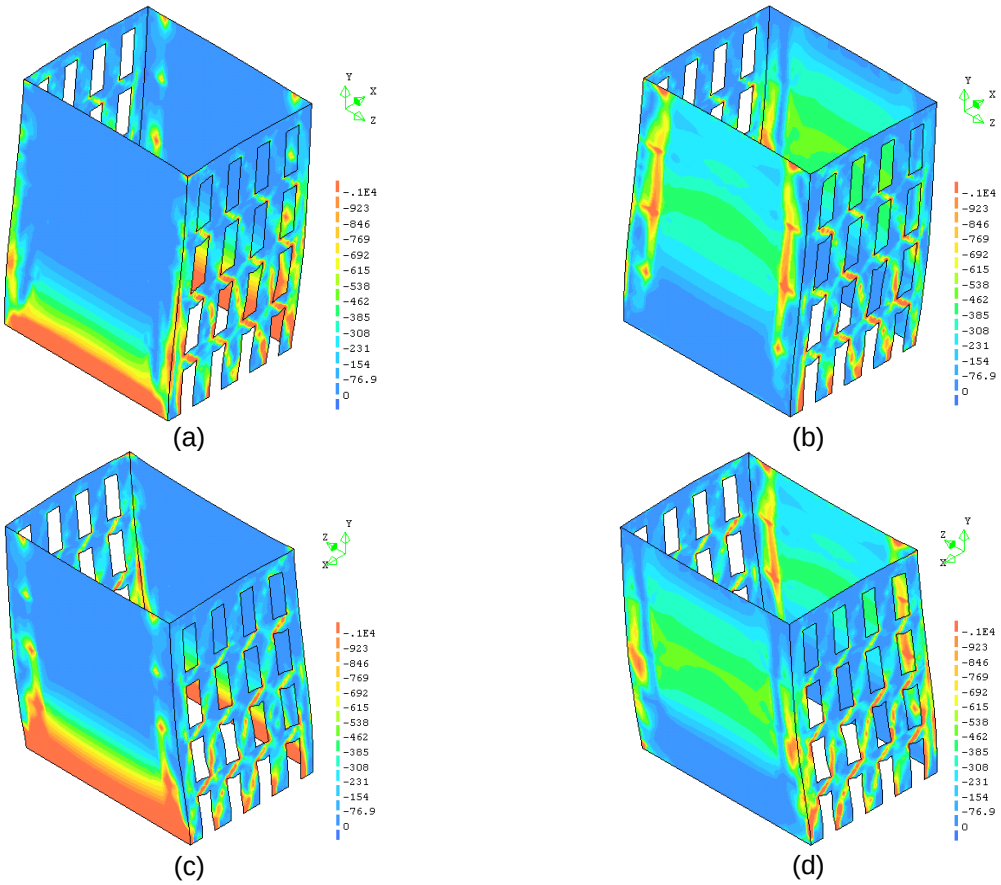

Figure 53 - (a) N-E view inside (b) N-E view outside (c) S-W view outside and (d) S-W view inside, units in kPa.

1.4.2 0.5xFt in N-S direction, step 26

Deformed mesh

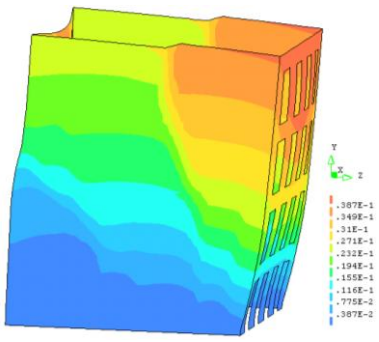

Figure 54 – deformed mesh, units in meters.

Strain states

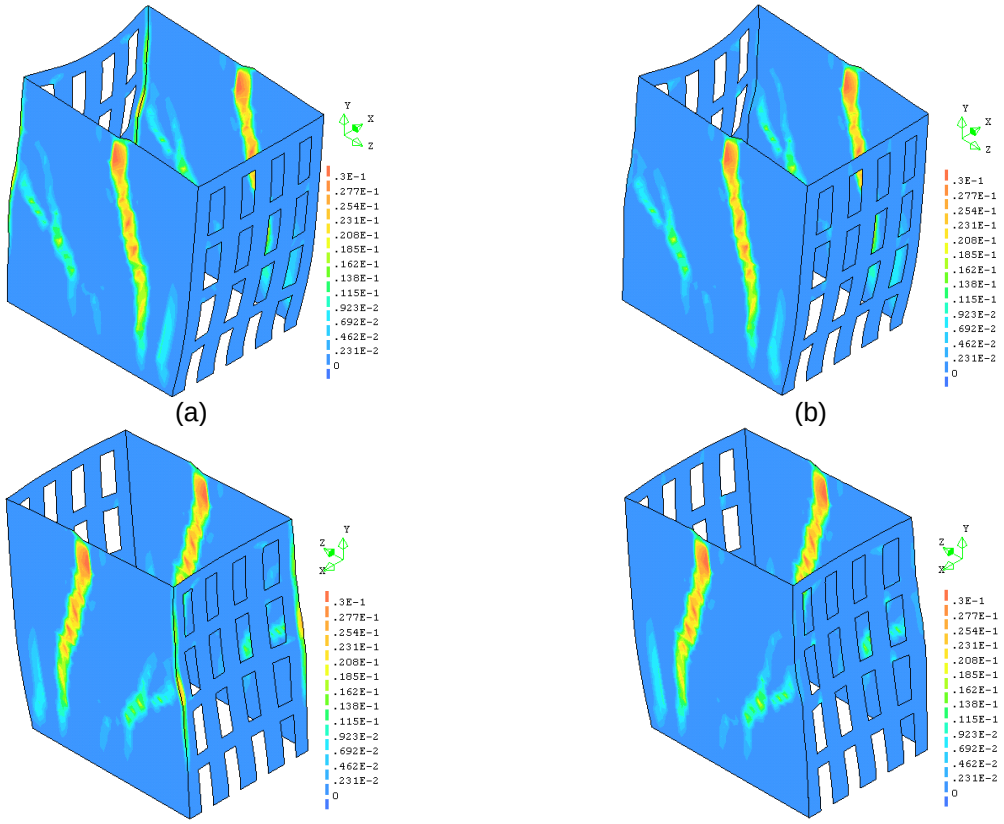

(a) (b)

(c) (d)

Figure 55 - (a) N-E view inside (b) N-E view outside (c) S-W view outside and (d) S-W view inside.

Stress states

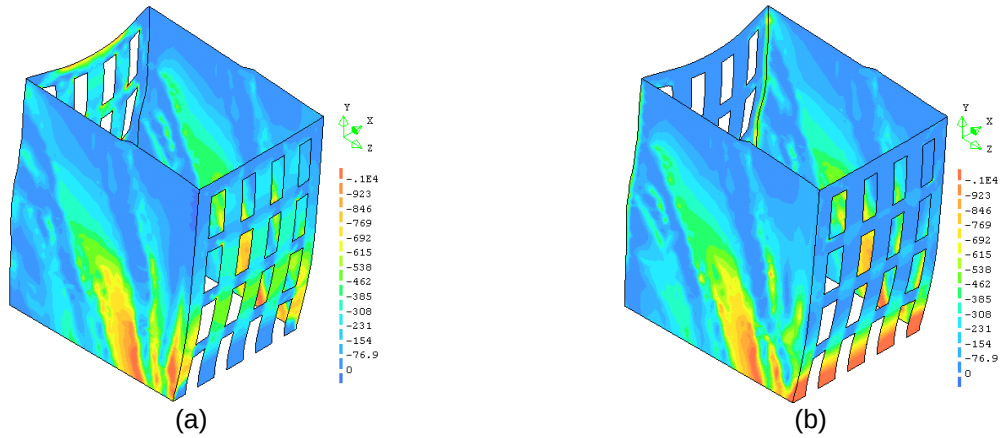

(a) (b)

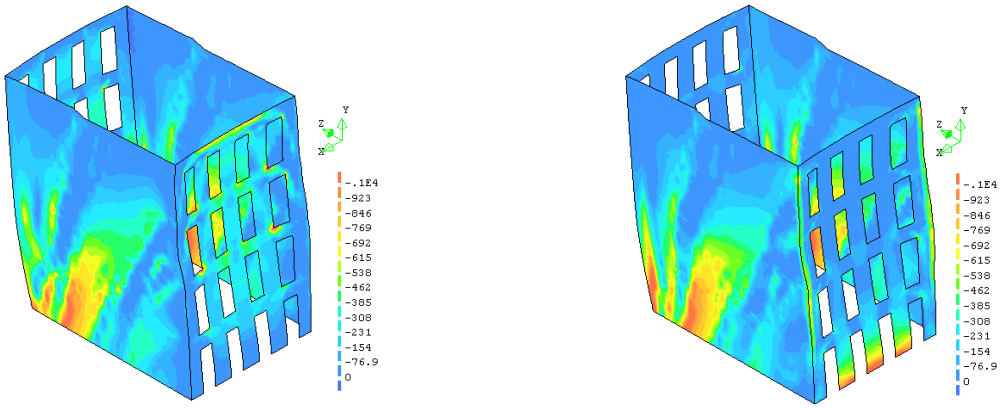

(c) (d)

Figure 56 - (a) N-E view inside (b) N-E view outside (c) S-W view outside and (d) S-W view inside, units in kPa.

1.4.3 2xFt in E-W direction, step 29

Deformed mesh

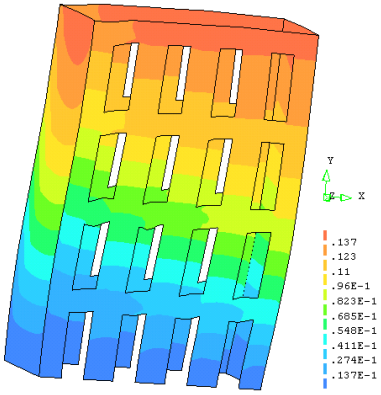

Figure 57 – deformed mesh, units in meters.

Strain states

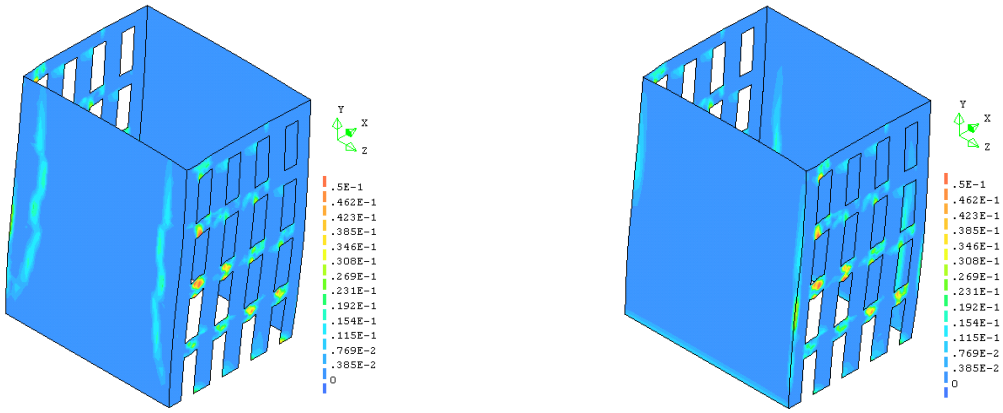

(a) (b)

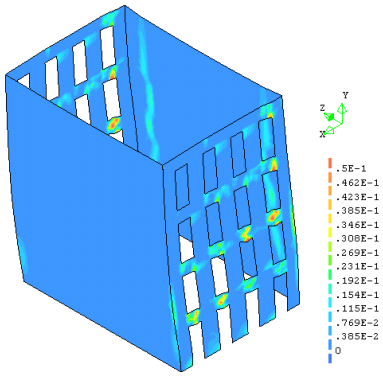

(c)

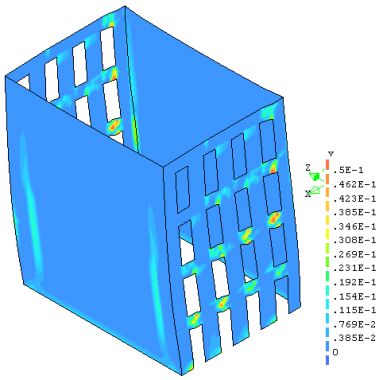

(d)

Figure 58 - (a) N-E view inside (b) N-E view outside (c) S-W view outside and (d) S-W view inside.

Stress states

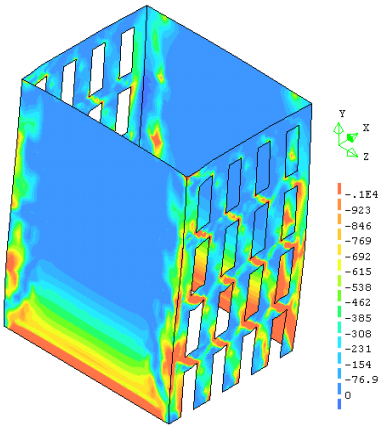

(a)

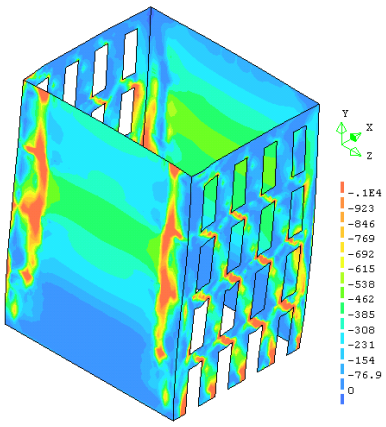

(b)

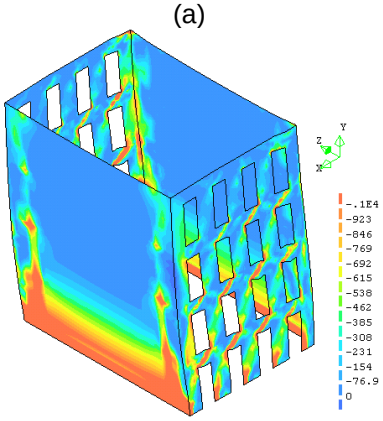

(c)

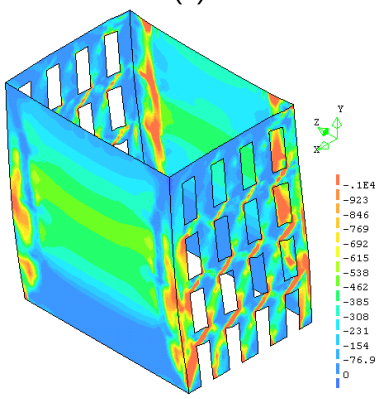

(d)

Figure 59 - (a) N-E view inside (b) N-E view outside (c) S-W view outside and (d) S-W view inside, units in kPa.

1.4.4 2xFt in N-S direction, step 47

Deformed mesh

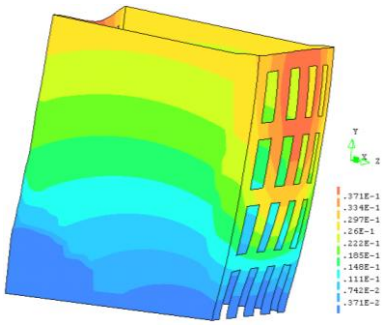

Figure 60 – deformed mesh, units in meters.

Strain states

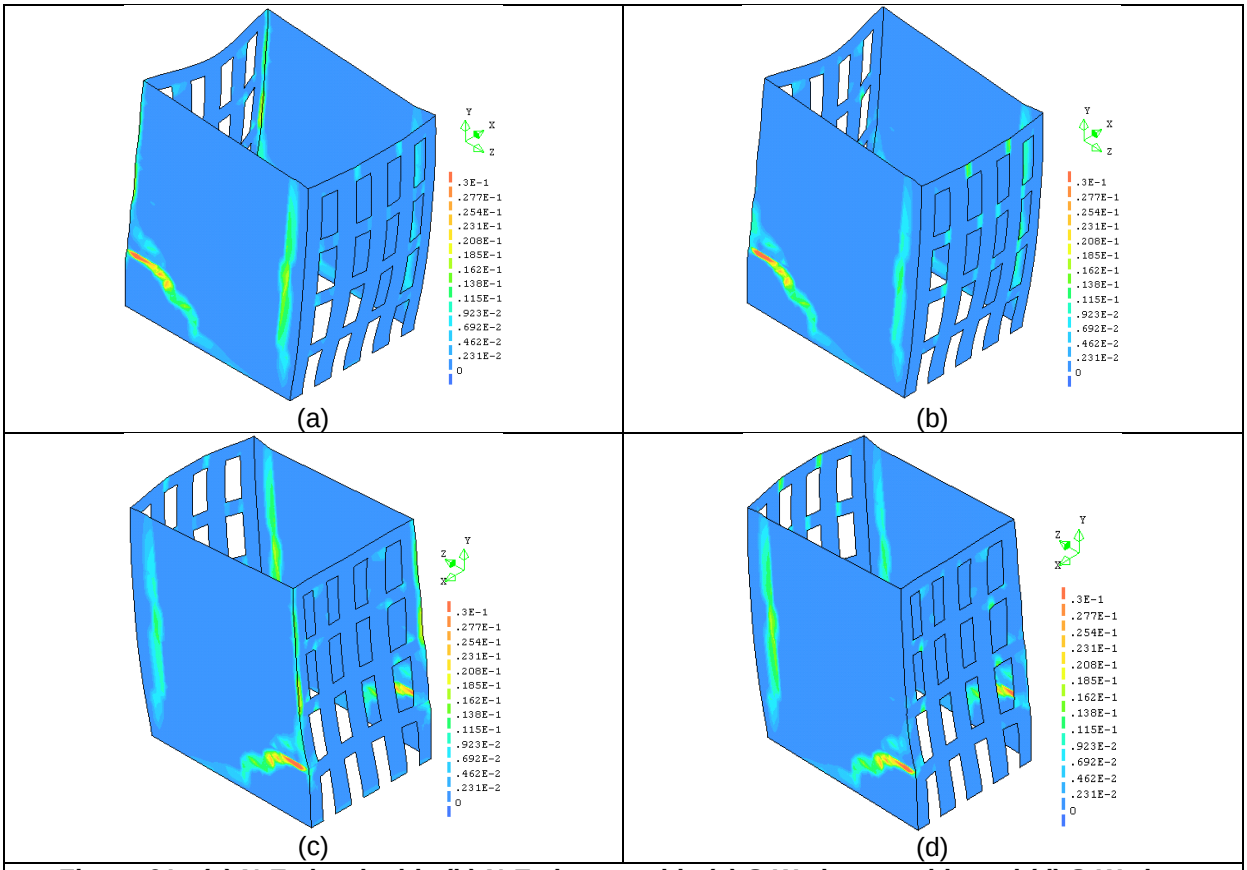

Figure 61 - (a) N-E view inside (b) N-E view outside (c) S-W view outside and (d) S-W view inside

Stress states

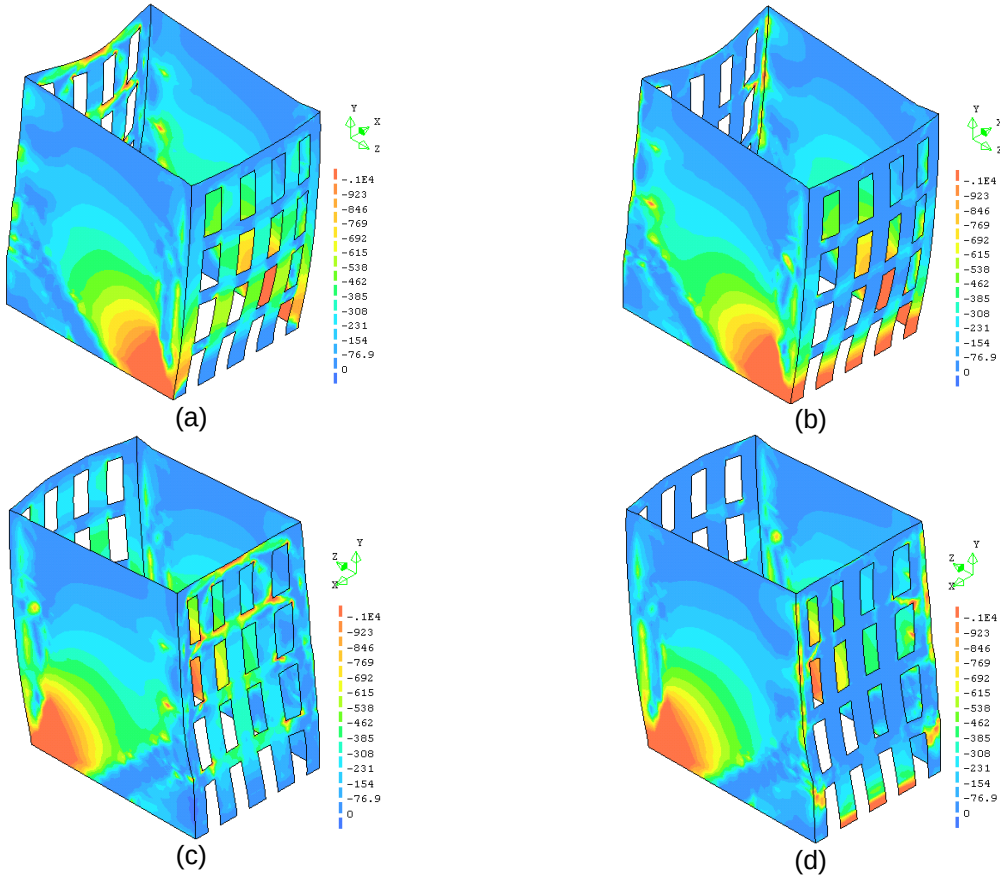

Figure 62 - (a) N-E view inside (b) N-E view outside (c) S-W view outside and (d) S-W view inside, units in kPa.

1.5 Fracture energy tensile

0.5xGft in E-W direction, step 26

Deformed mesh

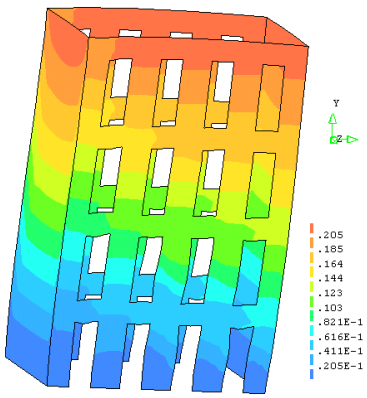

Figure 63 – deformed mesh, units in meters.

Strain states

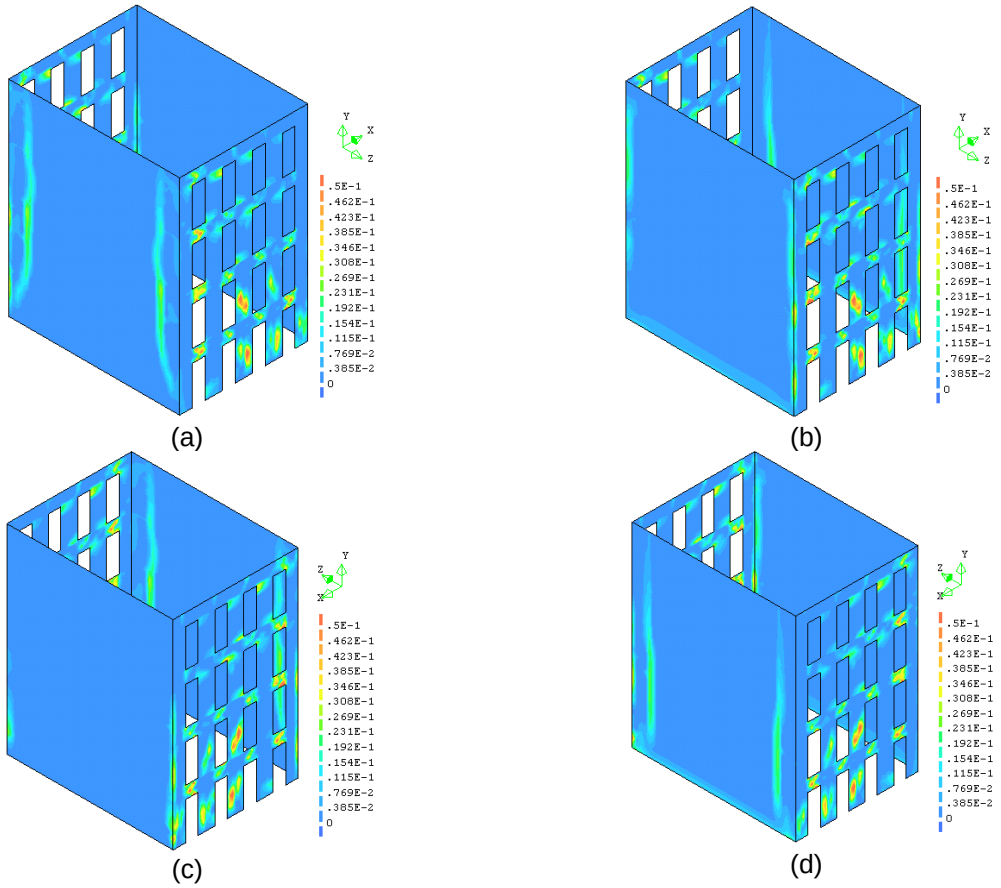

Figure 64 - (a) N-E view inside (b) N-E view outside (c) S-W view outside and (d) S-W view inside.

Stress states

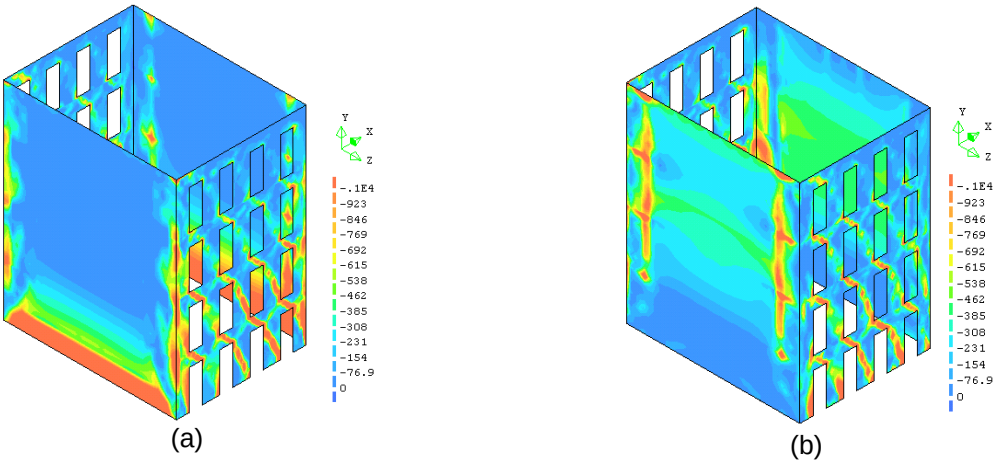

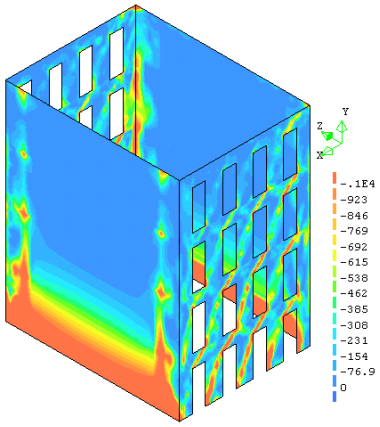

(c)

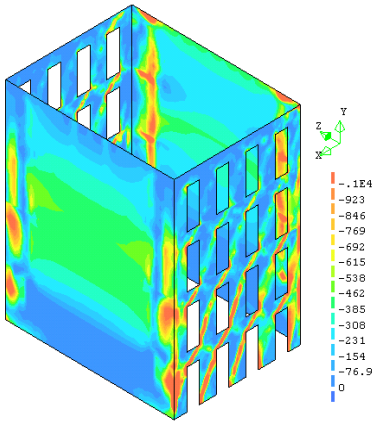

(d)

Figure 65 - (a) N-E view inside (b) N-E view outside (c) S-W view outside and (d) S-W view inside, units in kPa.

0.5xGft in N-S direction, step 38

Deformed mesh

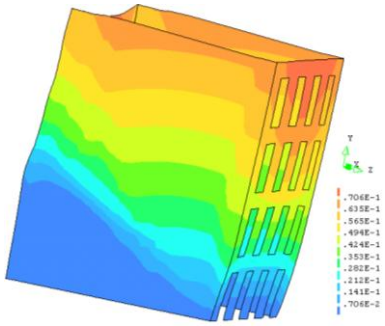

Figure 66 – deformed mesh, units in meters.

Strain states

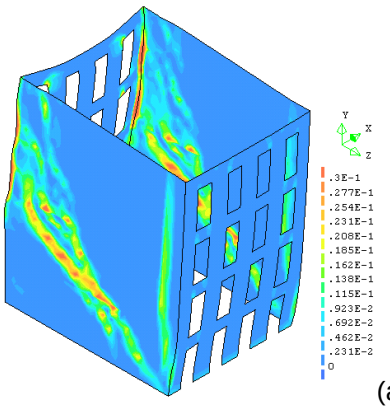

(a)

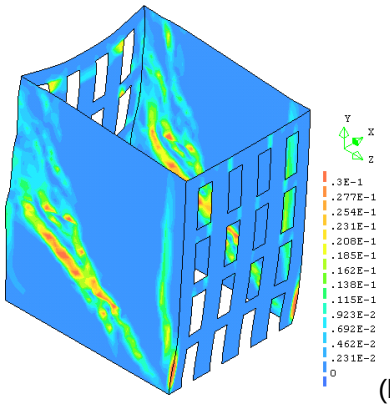

(b)

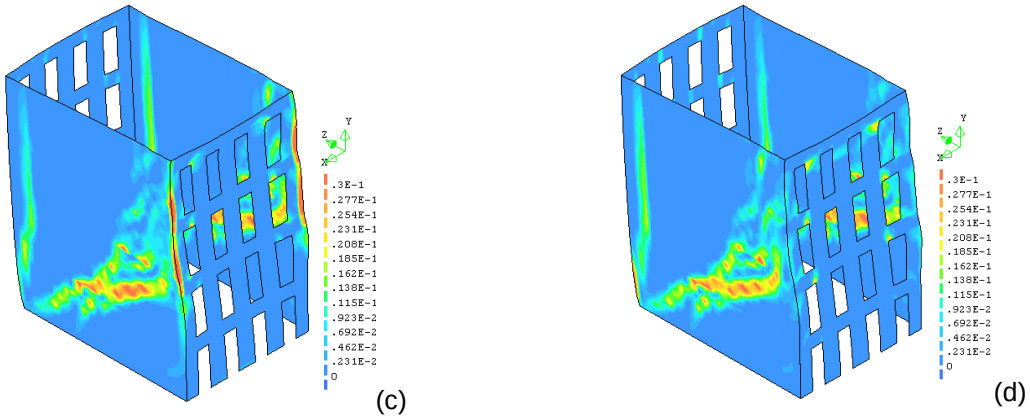

(c) (d)

Figure 67 - (a) N-E view inside (b) N-E view outside (c) S-W view outside and (d) S-W view inside.

Stress states

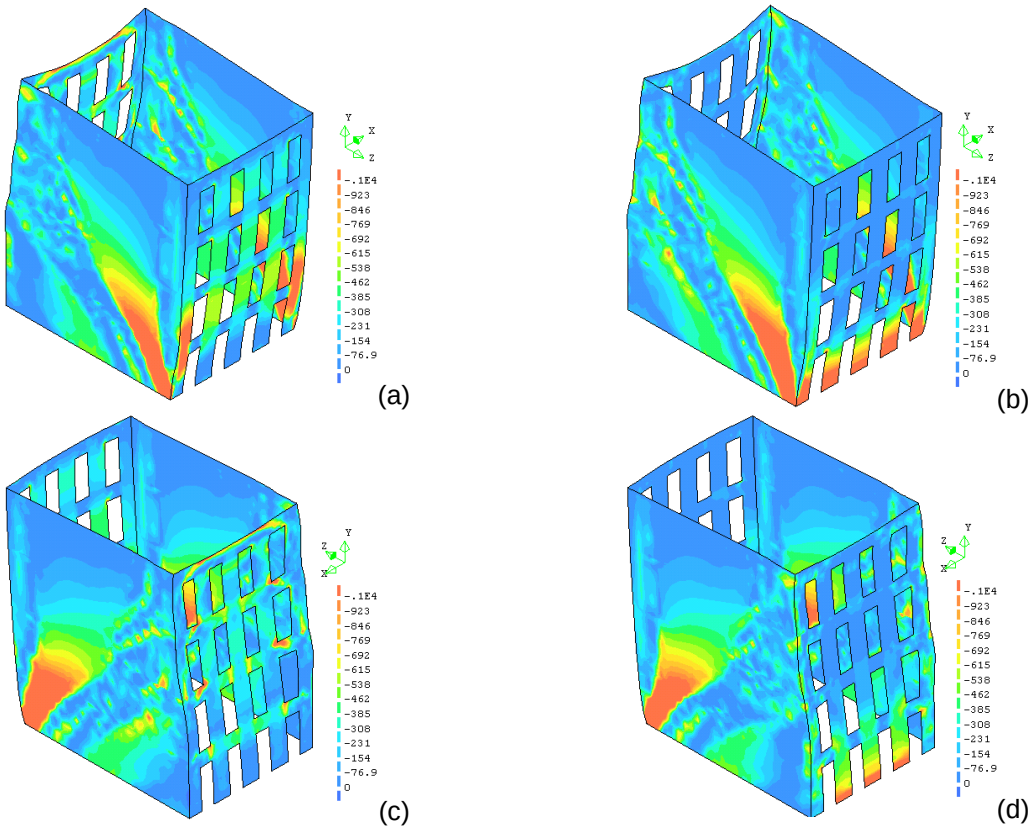

(a) (b)

(c) (d)

Figure 68 - (a) N-E view inside (b) N-E view outside (c) S-W view outside and (d) S-W view inside, units in kPa.

2xGft in E-W direction step 29

Deformed mesh

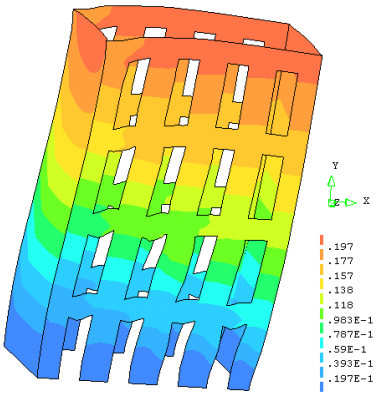

Figure 69 – deformed mesh, units in meters.

Strain states

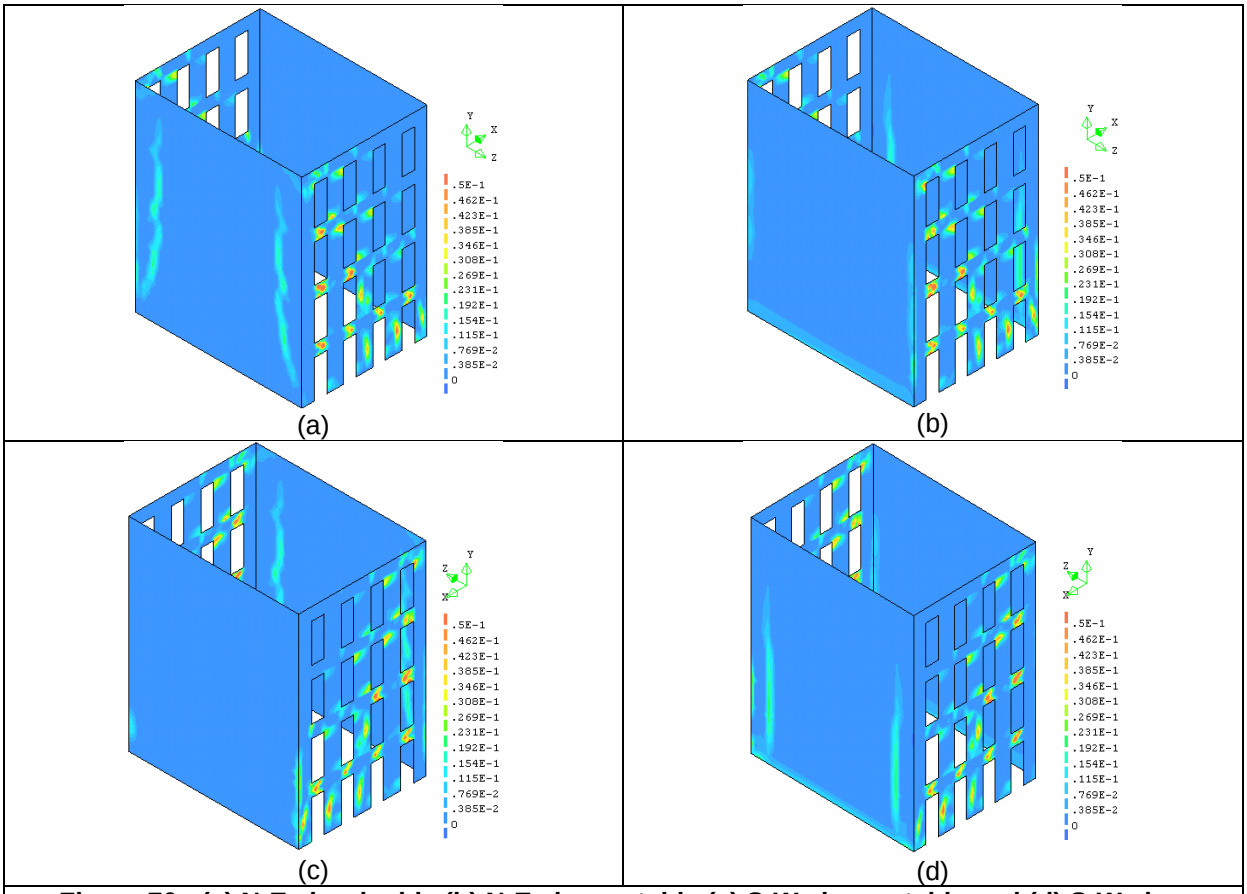

Figure 70 - (a) N-E view inside (b) N-E view outside (c) S-W view outside and (d) S-W view inside.

Stress states

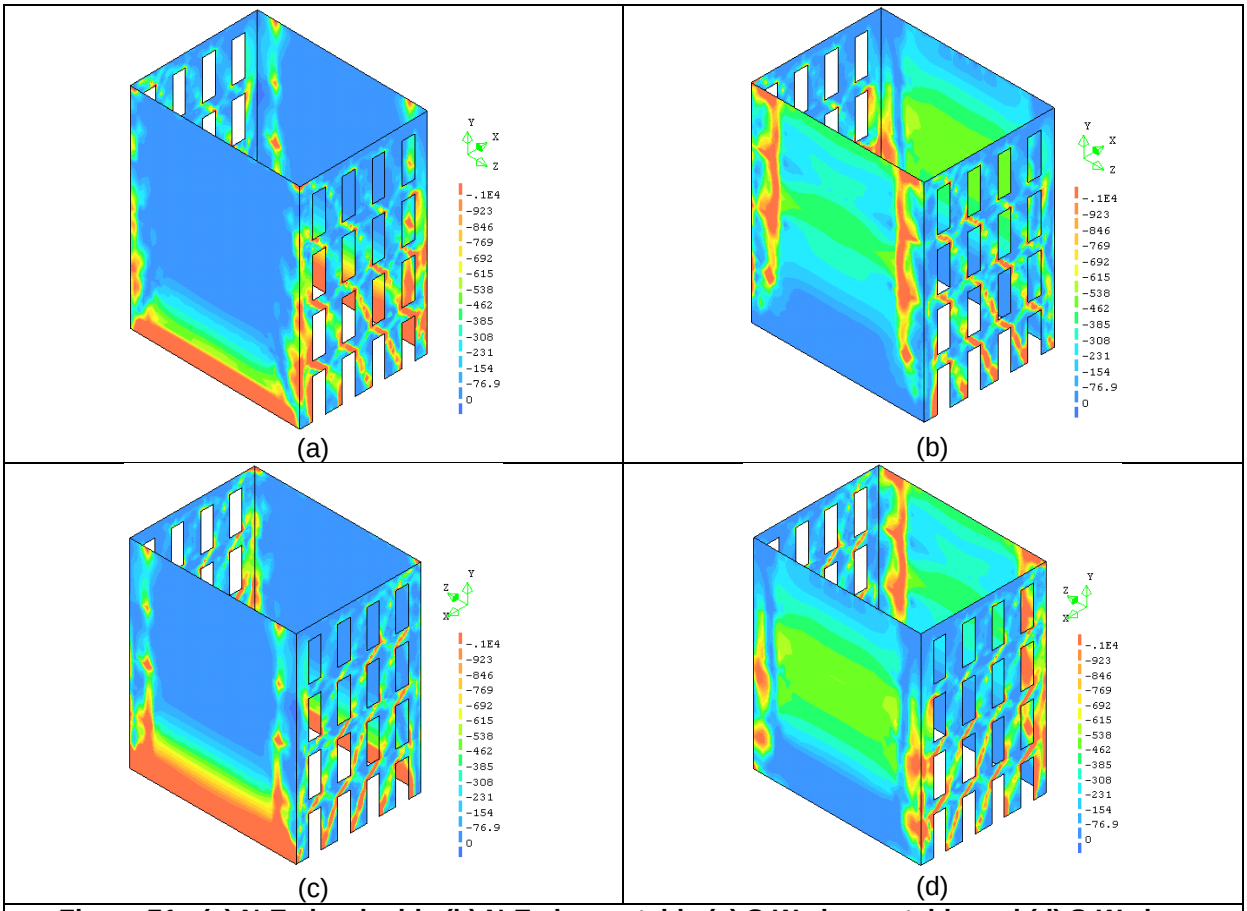

Figure 71 - (a) N-E view inside (b) N-E view outside (c) S-W view outside and (d) S-W view inside, units in kPa.

2xGft in N-S direction step 47

Deformed mesh

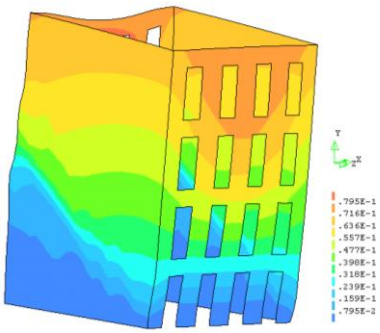

Figure 72 – deformed mesh, units in meters.

Strain states

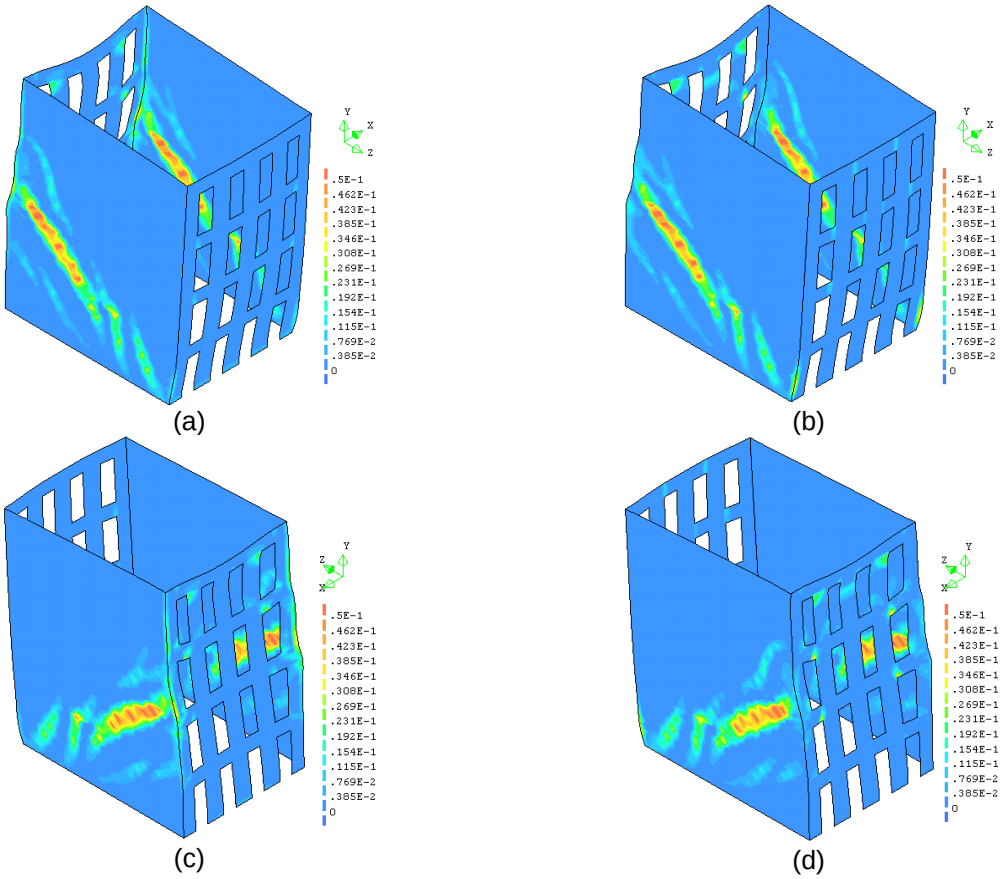

Figure 73 - (a) N-E view inside (b) N-E view outside (c) S-W view outside and (d) S-W view inside.

Stress states

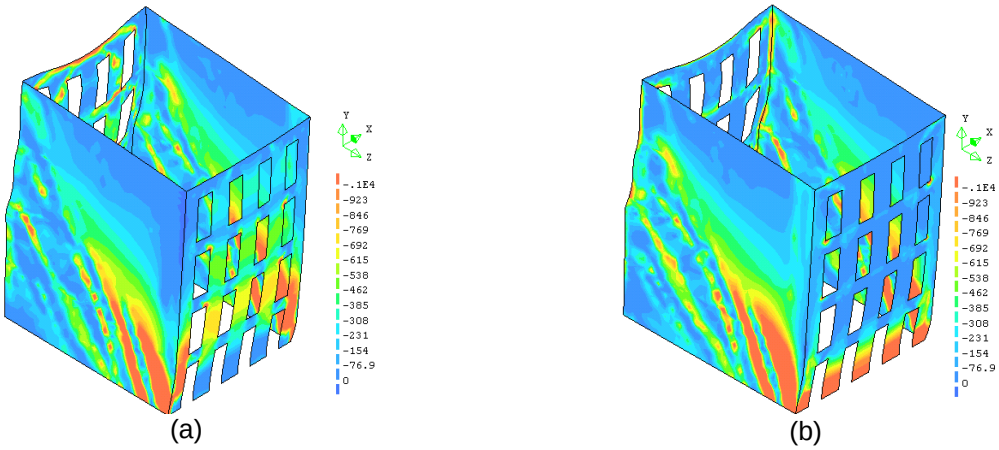

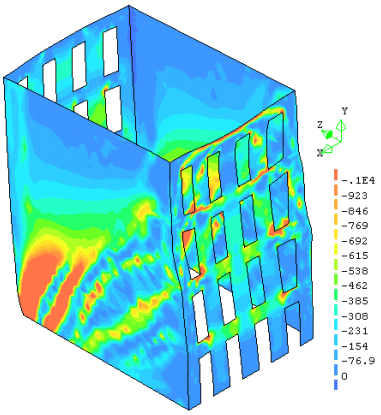

(c)

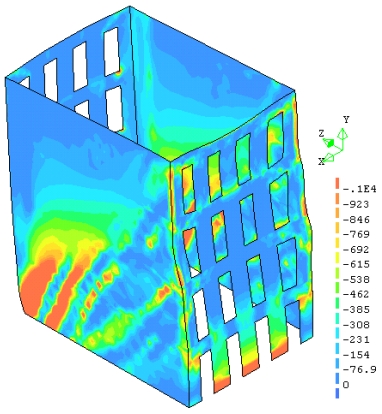

(d)

Figure 74 - (a) N-E view inside (b) N-E view outside (c) S-W view outside and (d) S-W view inside, units in kPa.

2 ANNEX B GRAPHICS FROM TIME HISTORY

2.1 Reference 100% PGA

2.1.1 Strain states envelopes

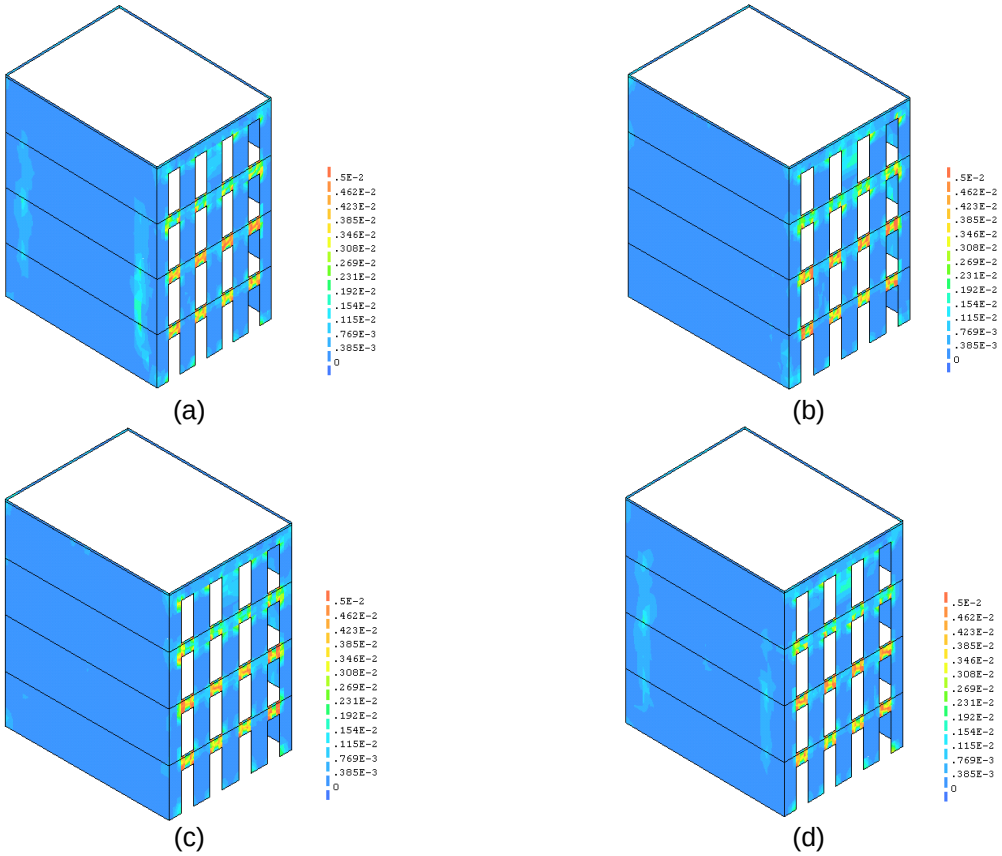

Figure 75 - (a) N-E view inside (b) N-E view outside (c) S-W view outside and (d) S-W view.

2.2 Reference 300% PGA

2.2.1 Strain states envelopes

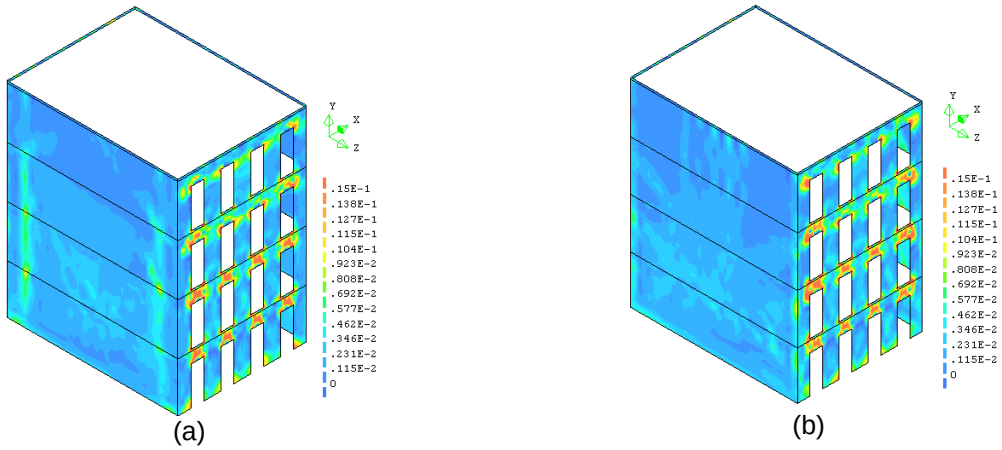

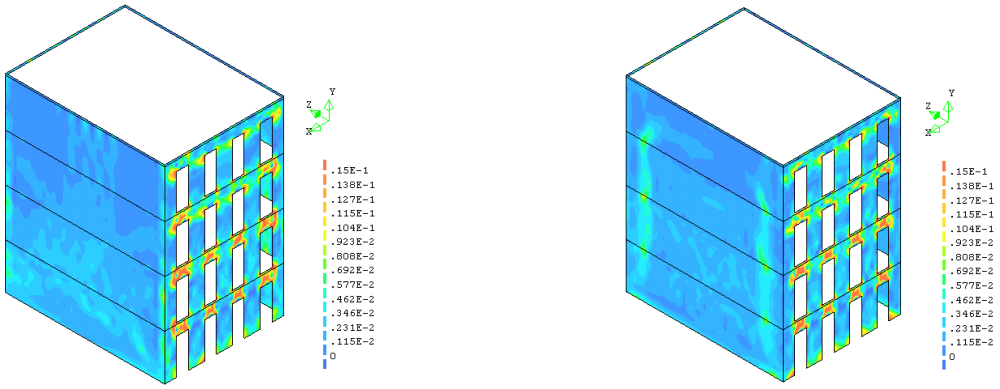

(c) (d)

Figure 76 - (a) N-E view inside (b) N-E view outside (c) S-W view outside and (d) S-W view.

2.2.2 Point A

Deformed mesh

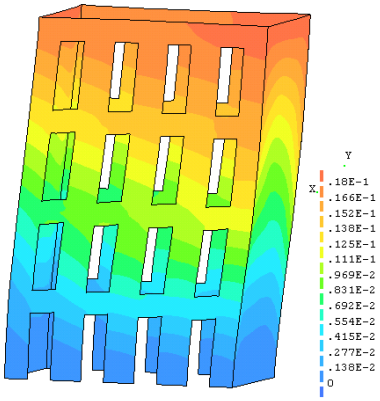

Figure 77 – deformed mesh, units in meters.

Strain states

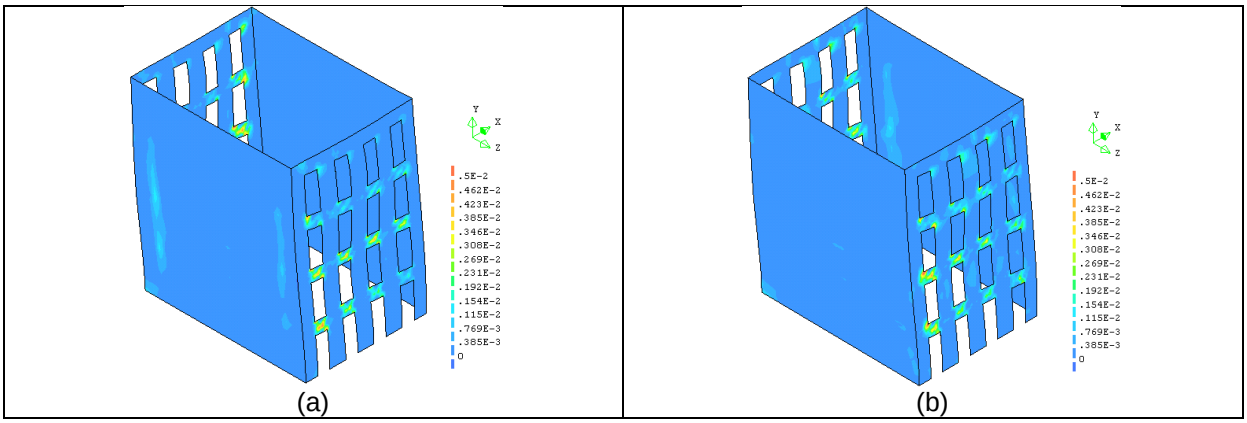

(a) (b)

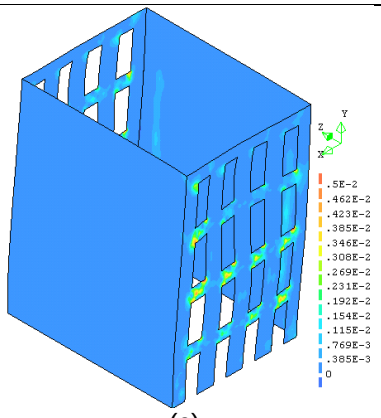

(c)

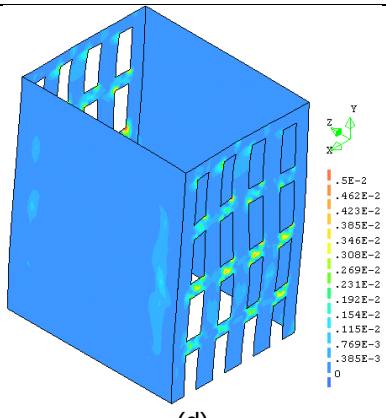

(d)

Figure 78 - (a) N-E view inside (b) N-E view outside (c) S-W view outside and (d) S-W view inside.

Stress states

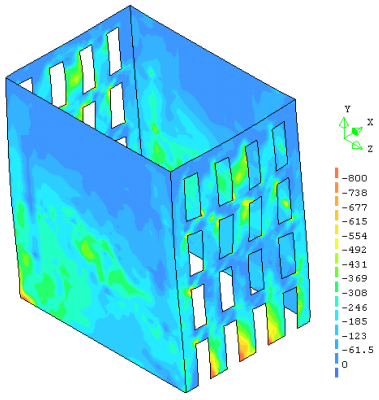

(a)

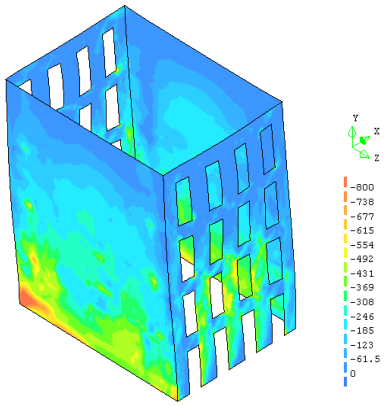

(b)

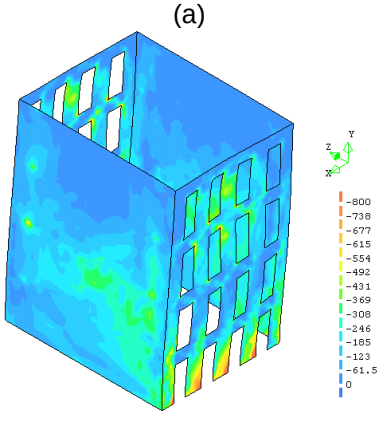

(c)

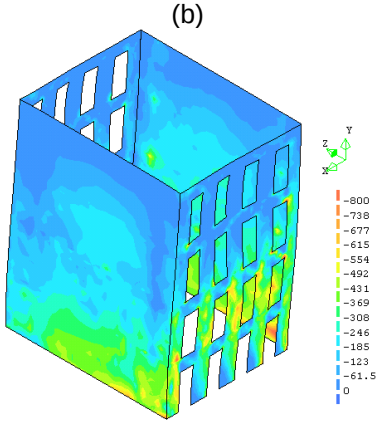

(d)

Figure 79 - (a) N-E view inside (b) N-E view outside (c) S-W view outside and (d) S-W view inside, units in kPa.

2.2.3 Point B

Deformed mesh

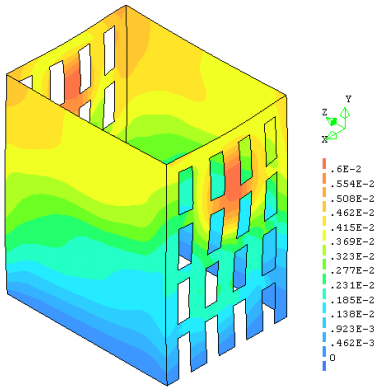

Figure 80 – deformed mesh, units in meters.

Strain states

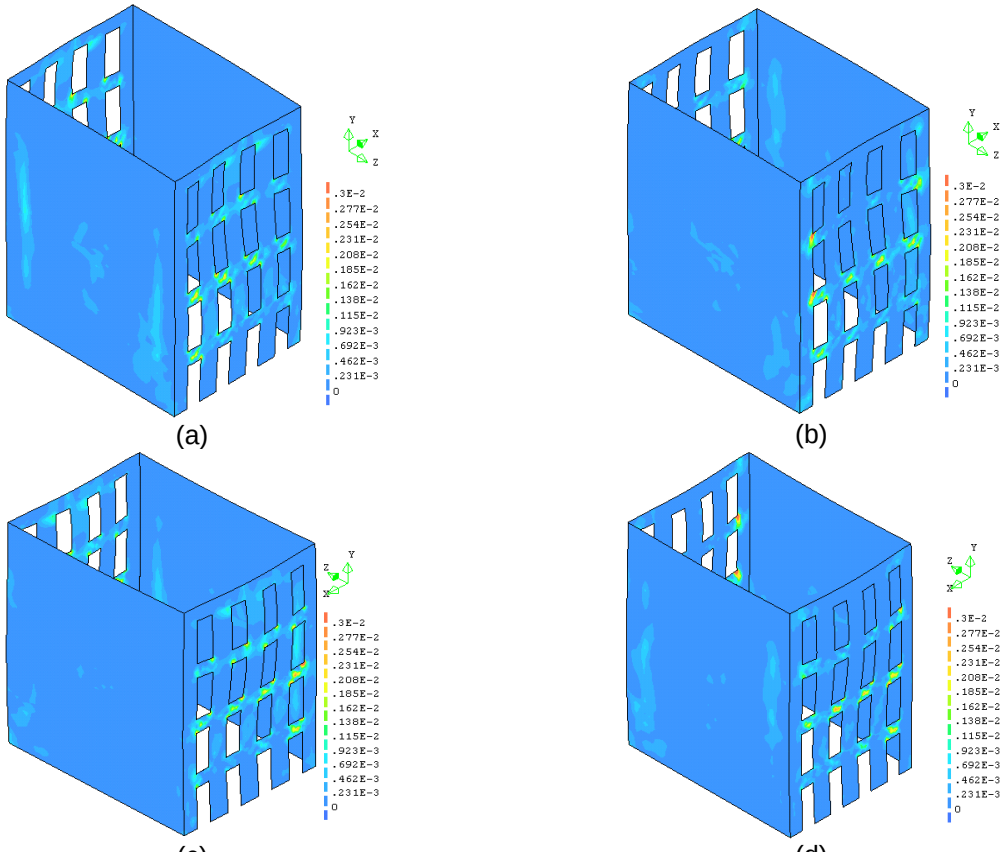

Figure 81 - (a) N-E view inside (b) N-E view outside (c) S-W view outside and (d) S-W view inside.

Stress states

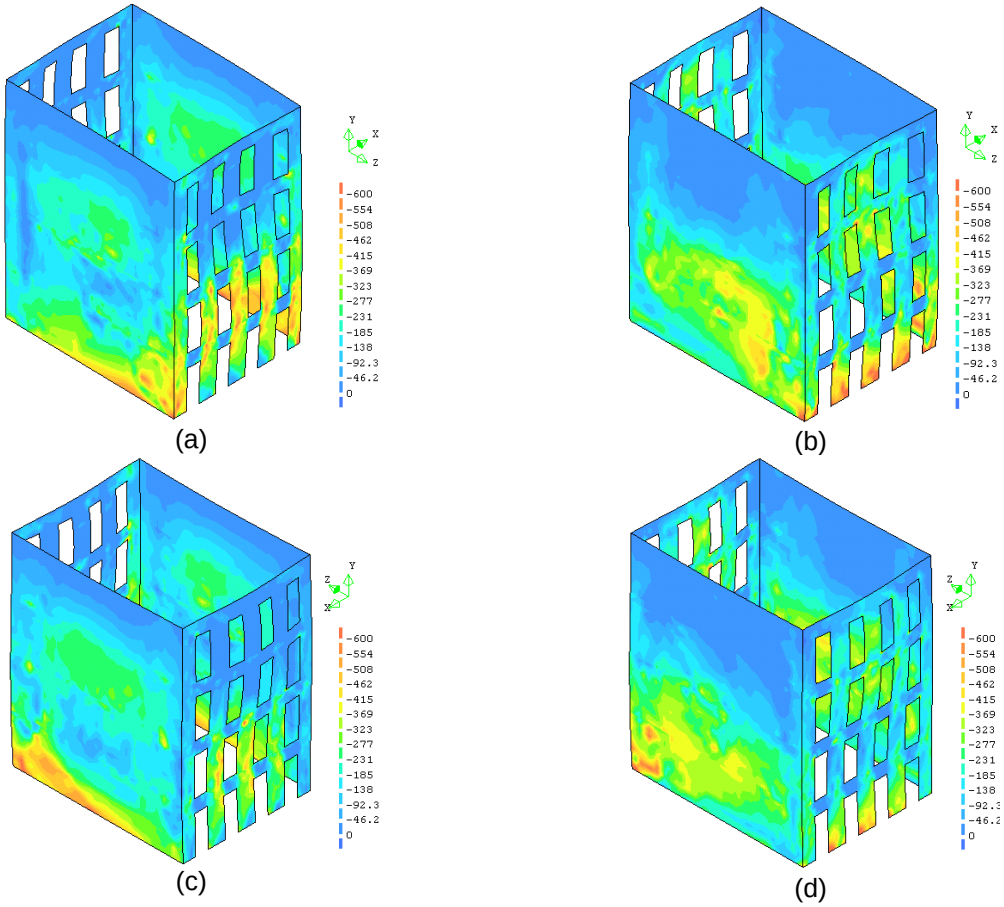

Figure 82 - (a) N-E view inside (b) N-E view outside (c) S-W view outside and (d) S-W view inside, units in kPa.

2.2.4 Point C

Deformed mesh

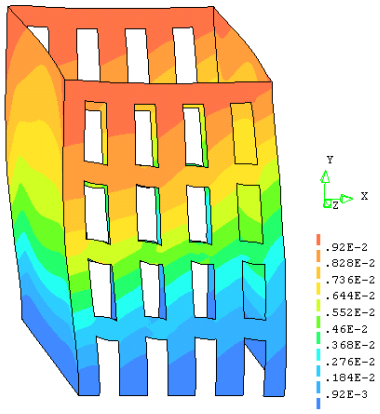

Figure 83 – deformed mesh, units in meters.

Strain states

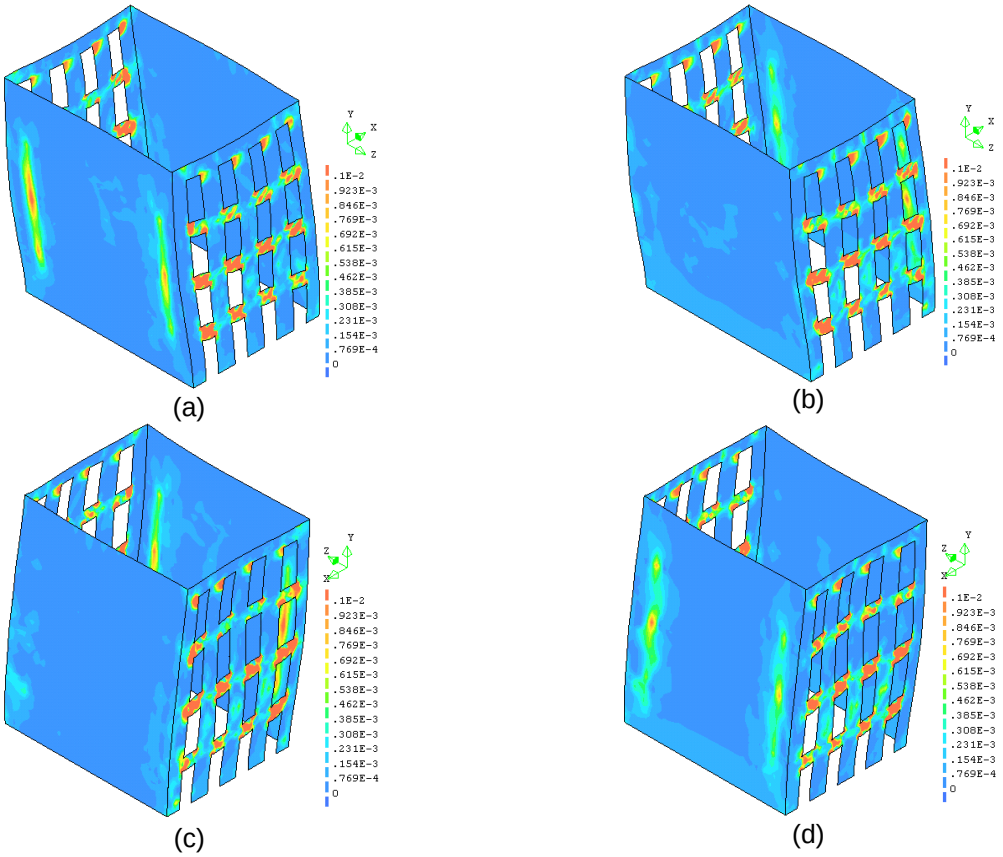

Figure 84 - (a) N-E view inside (b) N-E view outside (c) S-W view outside and (d) S-W view inside.

Stress states

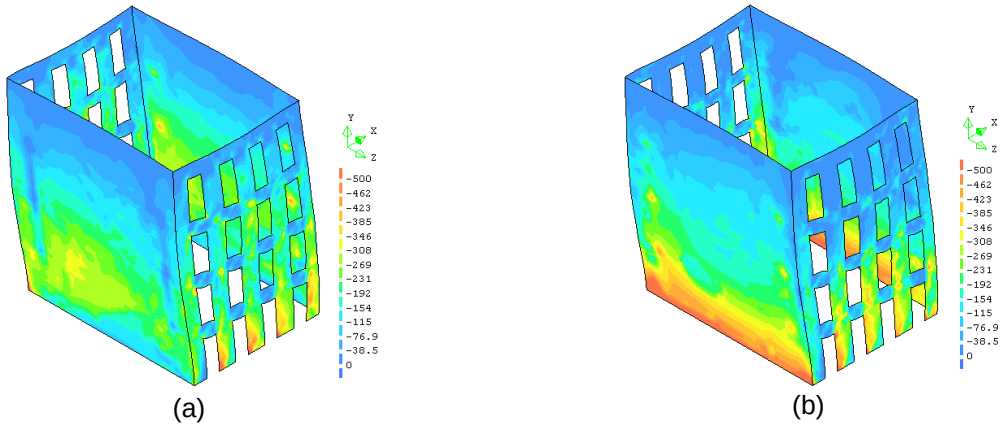

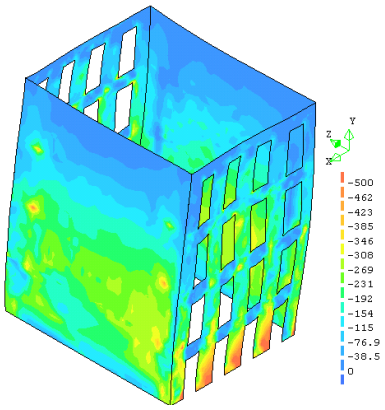

(c)

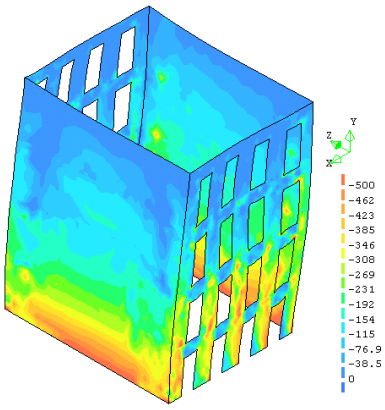

(d)

Figure 85 - (a) N-E view inside (b) N-E view outside (c) S-W view outside and (d) S-W view inside, units in kPa.

2.2.5 Point D

Deformed mesh

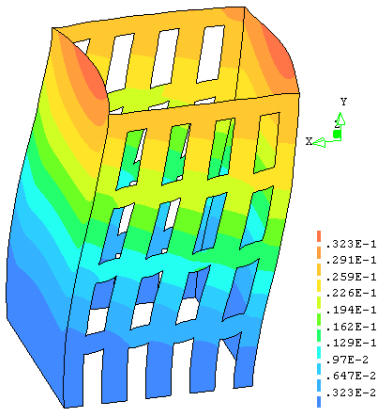

Figure 86 – deformed mesh, units in meters.

Strain states

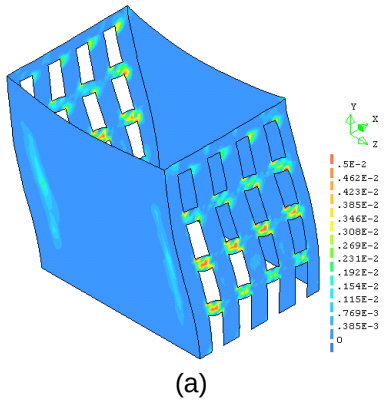

(a)

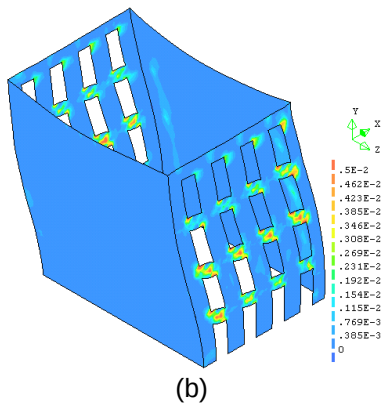

(b)

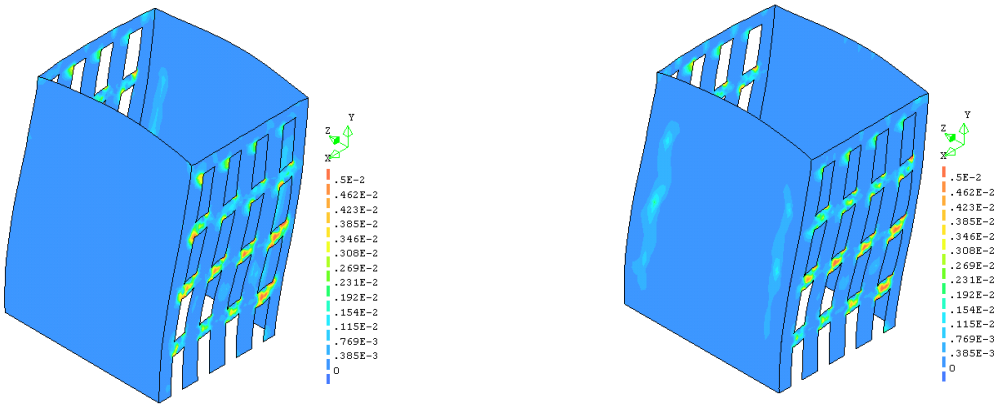

(c) (d)

Figure 87 - (a) N-E view inside (b) N-E view outside (c) S-W view outside and (d) S-W view inside.

Stress states

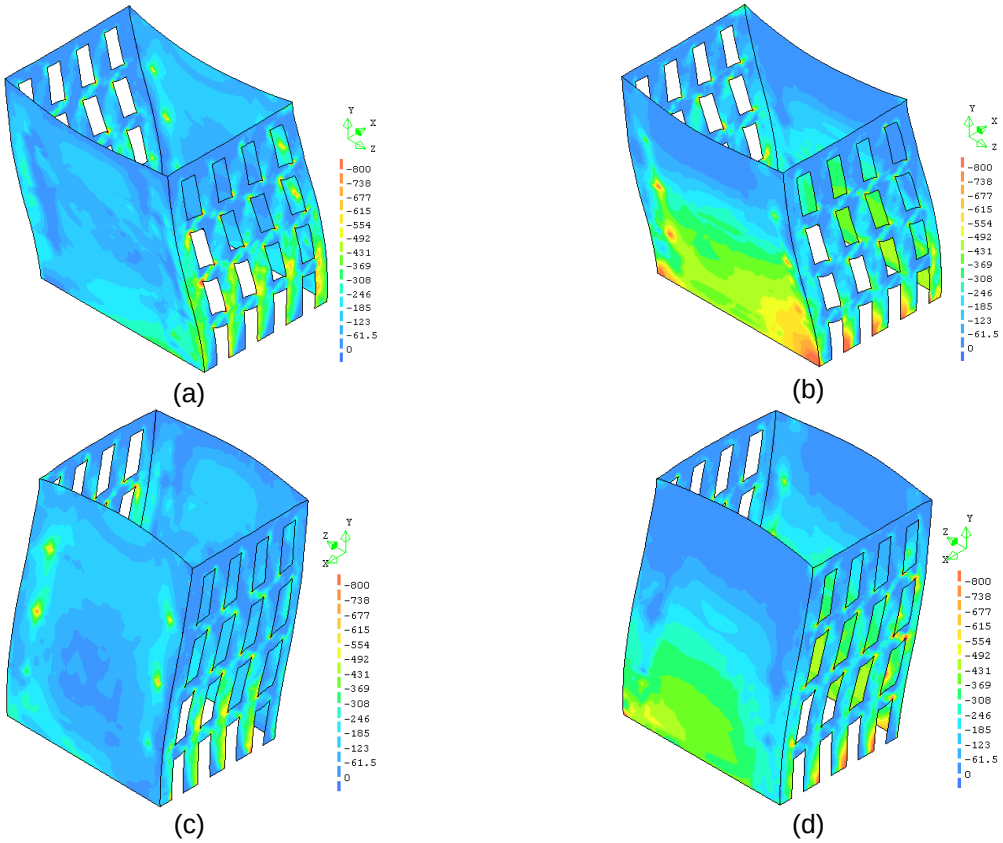

(a) (b)

(c) (d)

Figure 88 - (a) N-E view inside (b) N-E view outside (c) S-W view outside and (d) S-W view inside, units in kPa.

2.2.6 Point E

Deformed mesh

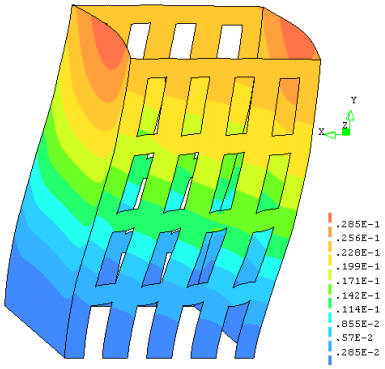

Figure 89 – deformed mesh, units in meters.

Strain states

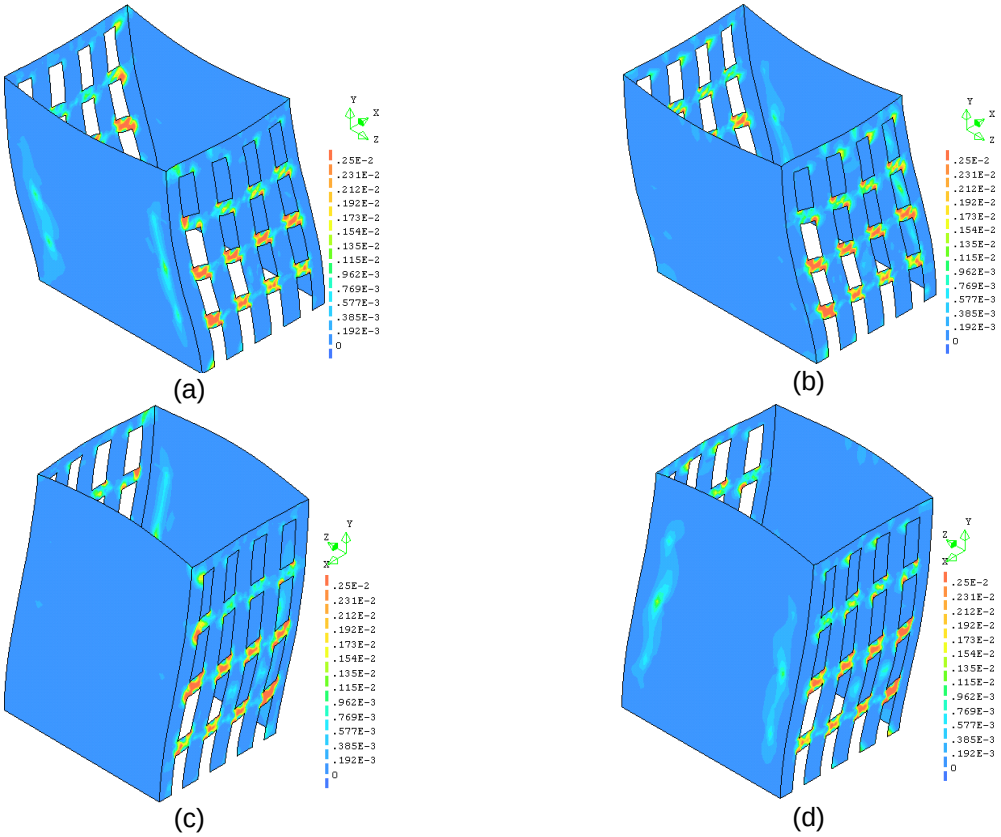

Figure 90 - (a) N-E view inside (b) N-E view outside (c) S-W view outside and (d) S-W view inside.

Stress states

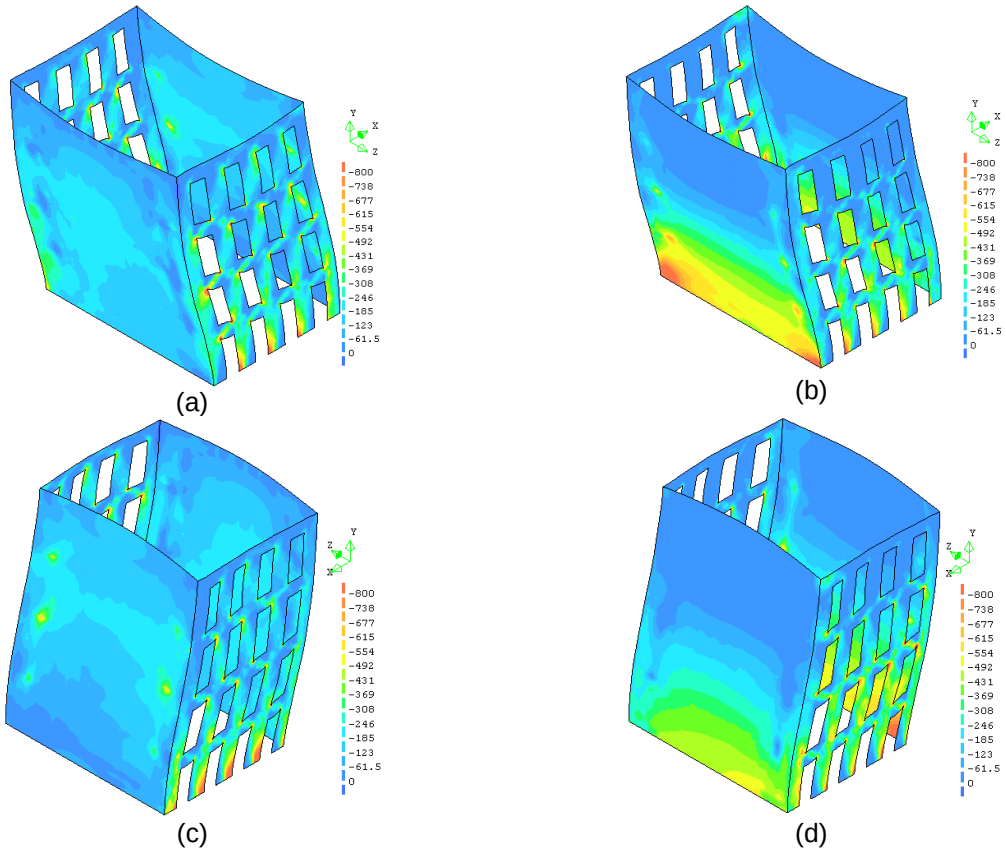

Figure 91 - (a) N-E view inside (b) N-E view outside (c) S-W view outside and (d) S-W view inside, units in kPa.

2.2.7 Point F

Deformed mesh

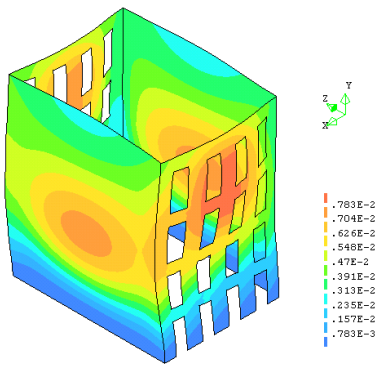

Figure 92 – deformed mesh, units in meters.

Strain states

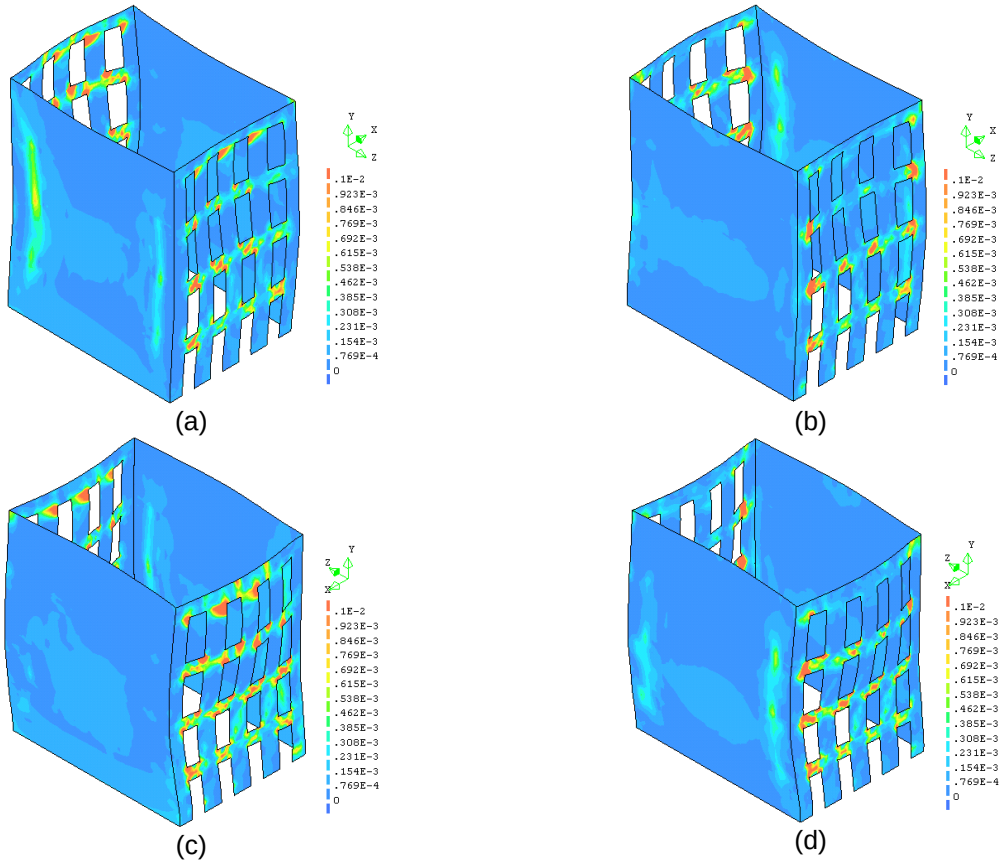

Figure 93 - (a) N-E view inside (b) N-E view outside (c) S-W view outside and (d) S-W view inside.

Stress states

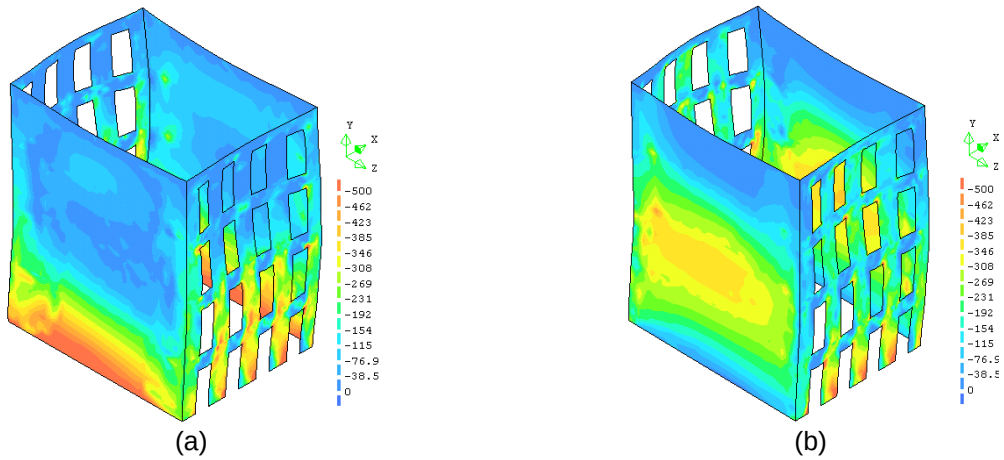

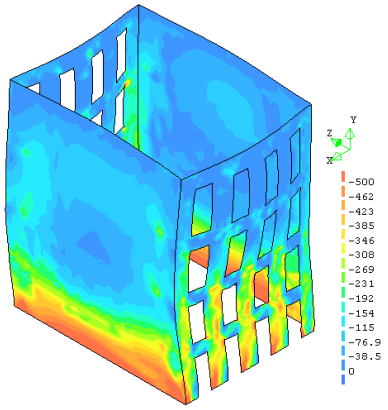

(c)

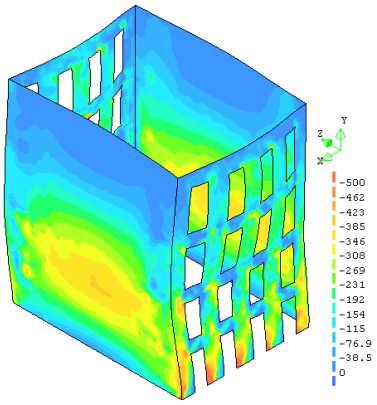

(d)

Figure 94 - (a) N-E view inside (b) N-E view outside (c) S-W view outside and (d) S-W view inside, units in kPa.

3 ANNEX C – SENSITIVITY ANALYSIS TIME HISTORY 100 % PGA

The parameters to be assessed in time history are the same than for pushover analyses: stiffness of the floor structures, and stiffness, damping ratio, tensile strength and tensile fracture energy of the masonry. In this section the earthquake from Lisbon area with variable parameters is compared with the reference results.

3.1 Stiffness of the MDF panels

The same range than for static analysis of Young's modulus are considered. The adopted values are 0.1xE, 10xE, 100xE and 100xE, being E the reference Young's modulus. The graphs used to compare the calculations are the envelopes of displacements versus seismic coefficient. The displacements are measured in the middle of the gabble walls at the top. The seismic coefficient is defined as the applied horizontal load divided by the total weight of the building.

In the Figure 95 and Figure 96 the comparison between reference and (a) 0.1xE, (b) 10xE (c) 100xE and (d) 1000xE in the X direction can be seen; first in the gabble walls and afterwards for the façade. Every graph has the same scale, for sake of simplicity in the comparison. The response for 0.1xE (a) is much different from the reference. Since the stiffness of the floor structure is very low the response of the gabble wall to perpendicular displacements is very irregular, with possible collapse. However, for the façade the structure responds in the same way. This is because the X direction corresponds to in-plane behaviour for the façade. For higher values of stiffness the response is very similar to the reference one, meaning that floor provides adequate connection between the main front and back façades.

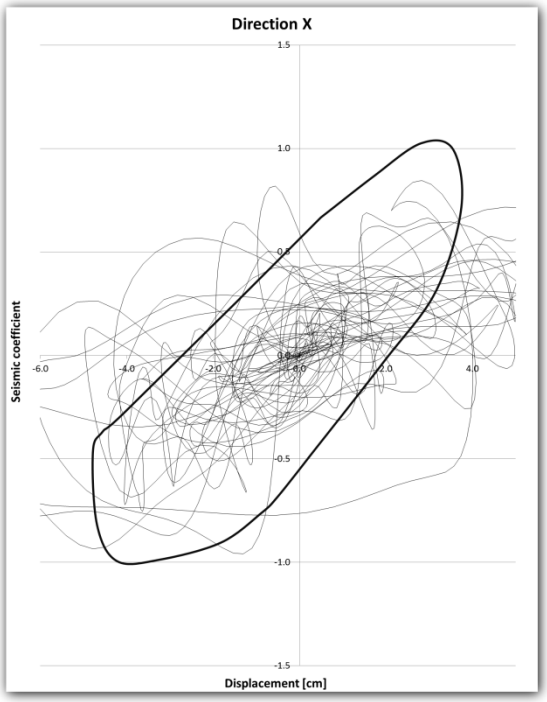

(a)

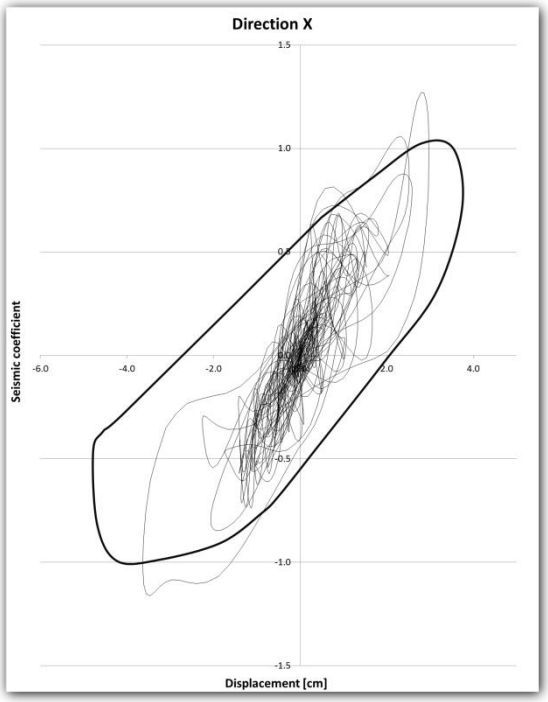

(b)

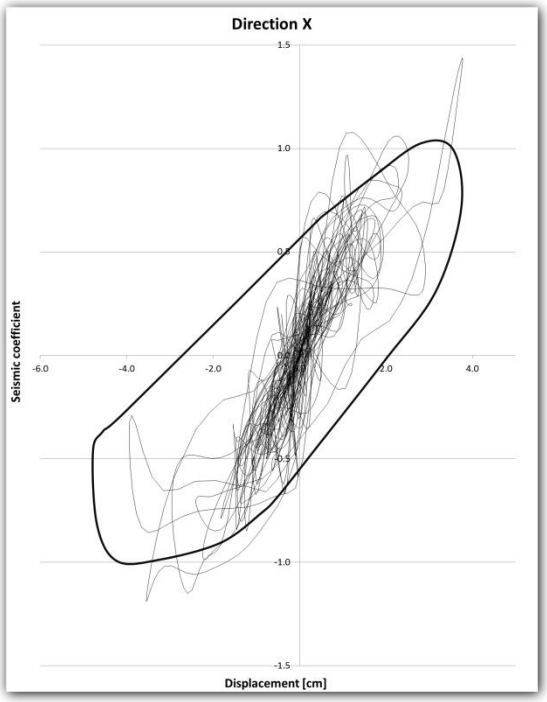

(c)

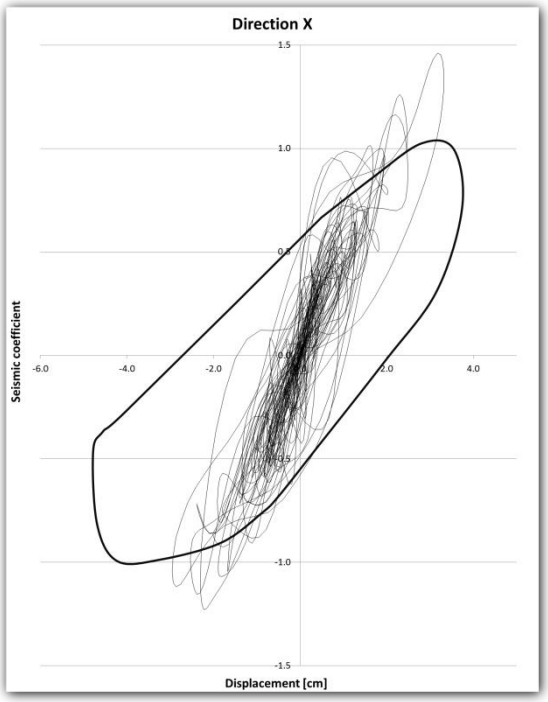

(d)

Figure 95 - Envelopes comparing the reference model with 0.1xE (a), 10xE (b), 100xE (c) and 1000xE (d) in direction X in the gabble wall.

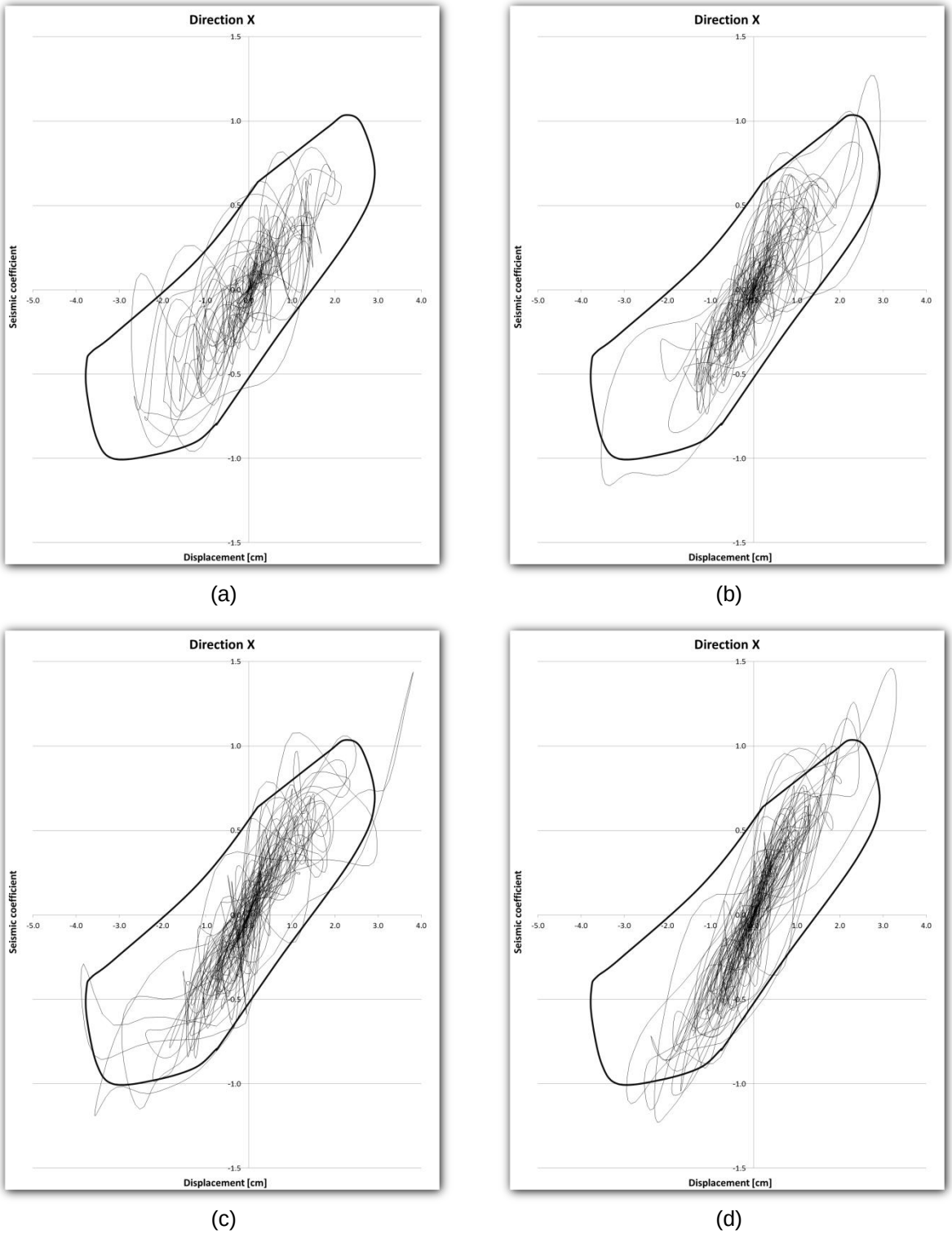

Figure 96 - Envelopes comparing the reference model with 0.1xE (a), 10xE (b), 100xE (c) and 1000xE (d) in direction X in the façade.

In the Figure 97 the comparison in the Z direction can be seen between the reference model and (a) 0.1xE, (b) 10xE, (c) 100xE and (d) 1000xE for the gabble wall. The 0.1xE model loses a bit its shape, being the peak values lower both in tension and in compression. The maximum values in terms of displacement and base shear capacity are larger as the stiffness of the floor structures increases. The response in the façade is shown afterwards, in the Figure 98. In this case, each response is different from the reference one. When the stiffness is low (a) the response gives very large displacements for a low seismic coefficient. This is because the Z direction is perpendicular to the façade, which is not able to bear much load when it is not connected to the gable walls. When the stiffness is increased the response of the façade is the expected response for the wall. It has the same shape that in X direction. The increment of stiffness in the floors gives to the structure the necessary global stiffness to respond as a whole, with box behaviour.

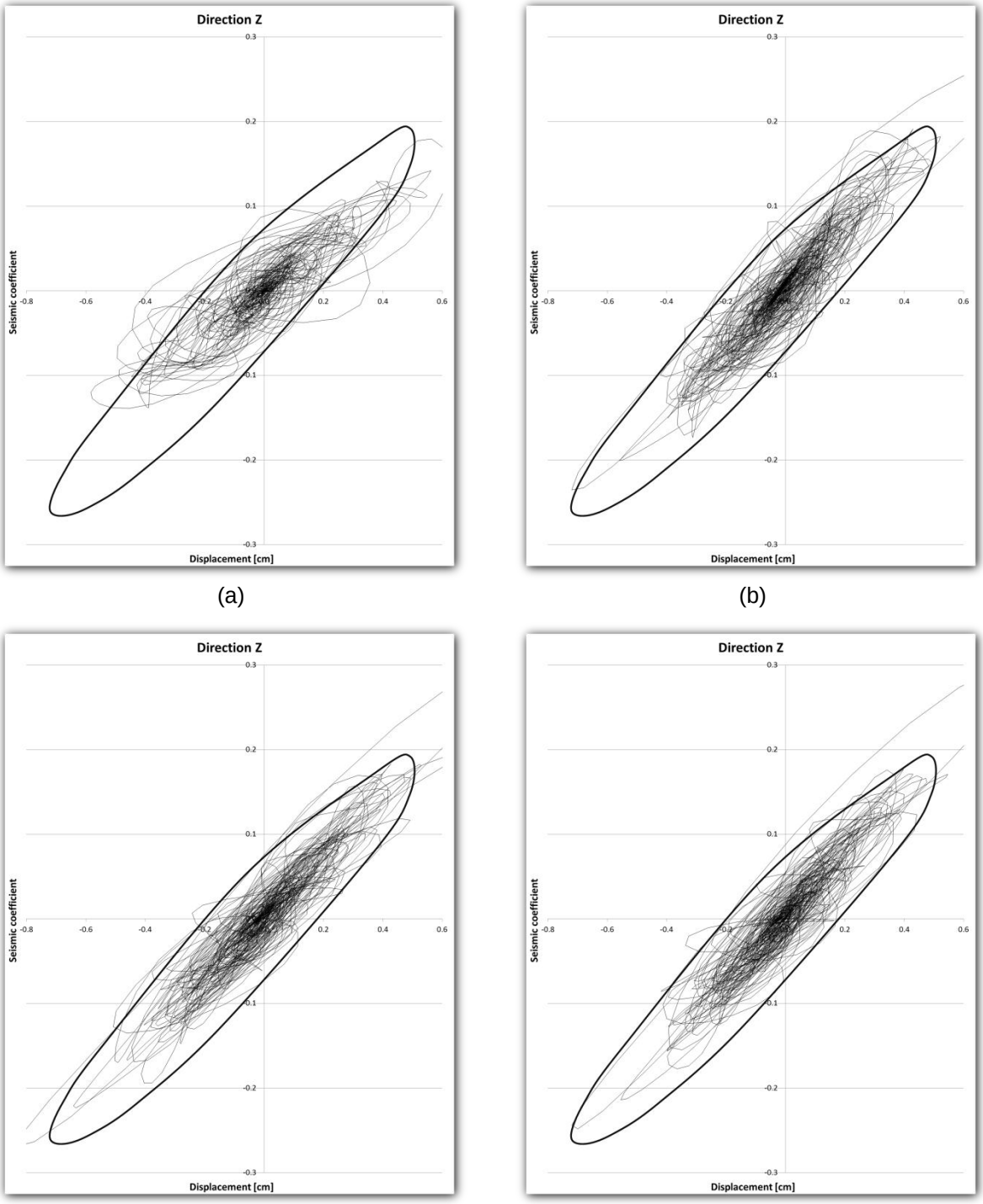

Figure 97 - Envelopes comparing the reference model with 0.1xE (a), 10xE (b), 100xE (c) and 1000xE (d) in direction Z in the gabble wall.

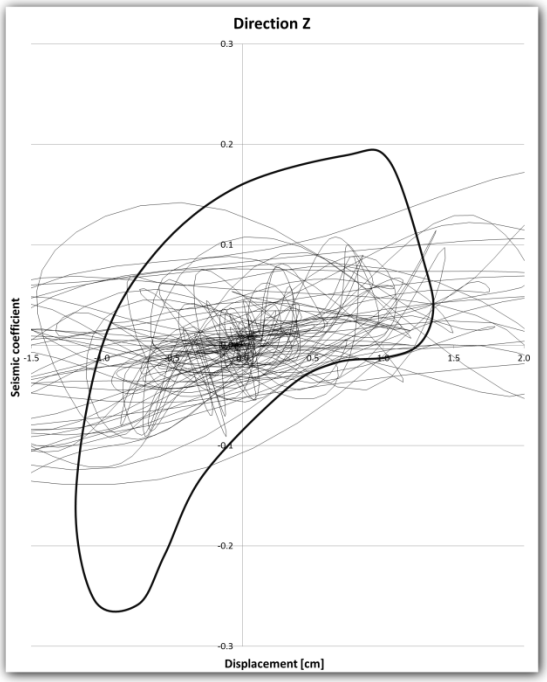

(a)

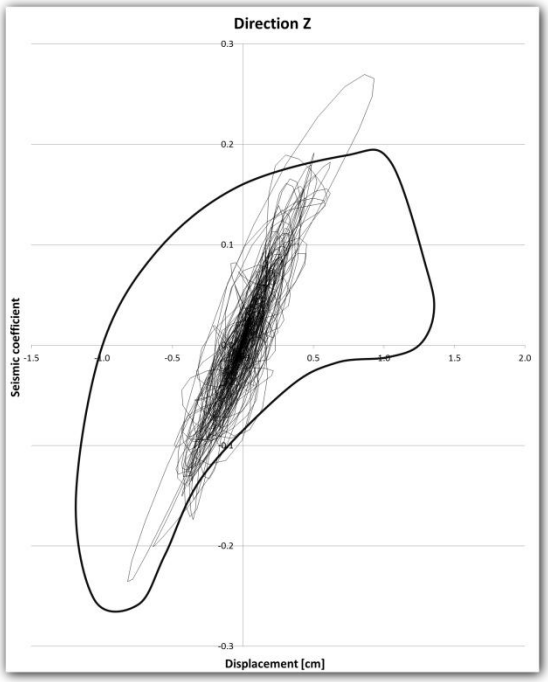

(b)

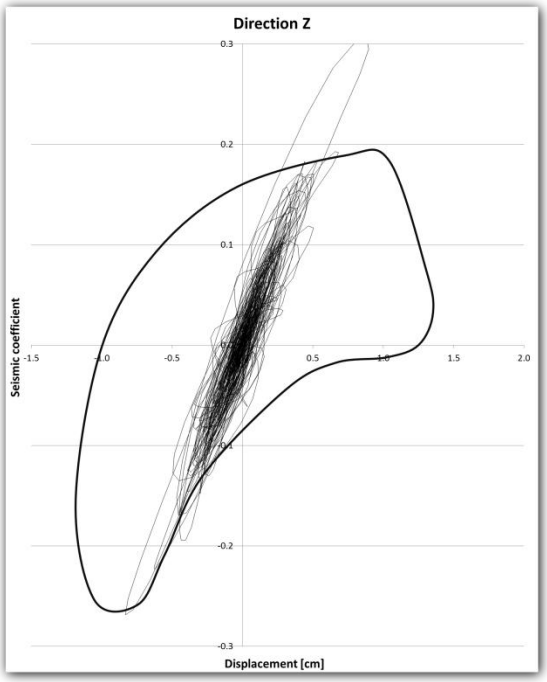

(c)

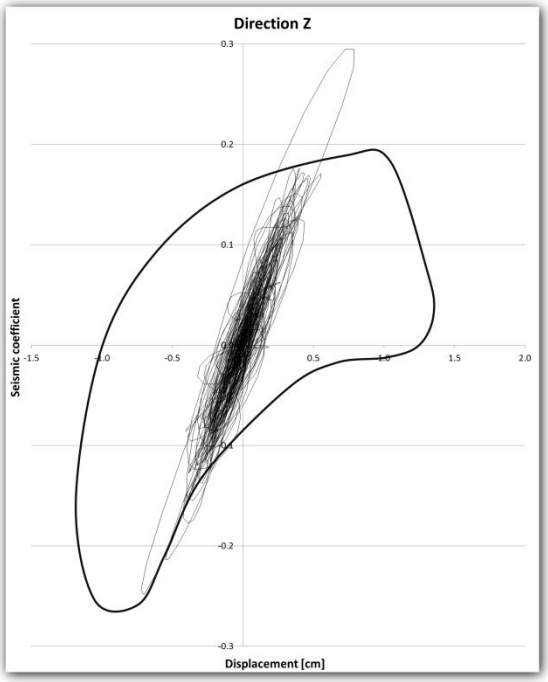

(d)

Figure 98 - Envelopes comparing the reference model with 0.1xE (a), 10xE (b), 100xE (c) and 1000xE (d) in direction Z in the façade.

3.2 Stiffness of masonry

As for the static analyses, two different calculations were performed. The Young's modulus was decreased to the half and increased to the double, obtaining thus the results for 0.5xE and 2xE. The characteristics of the graphs are the same as in the previous comparison. Again, the scale remains constant for the different calculations to make it easier to compare.

In the Figure 99 and Figure 100 the graphs of the envelopes in the X direction are shown, firstly in the gabble wall and then in the façade. The behaviours are very similar to the reference model. Only the peak values change moderately. When the masonry is less stiff there are more displacements and the seismic coefficient is lower, for the same demand. On the contrary, when the stiffness is larger the displacements are smaller and the seismic coefficient is slightly larger. As for the comparison of the stiffness of the MDF panels, the loads are too small to have more definitive conclusions.

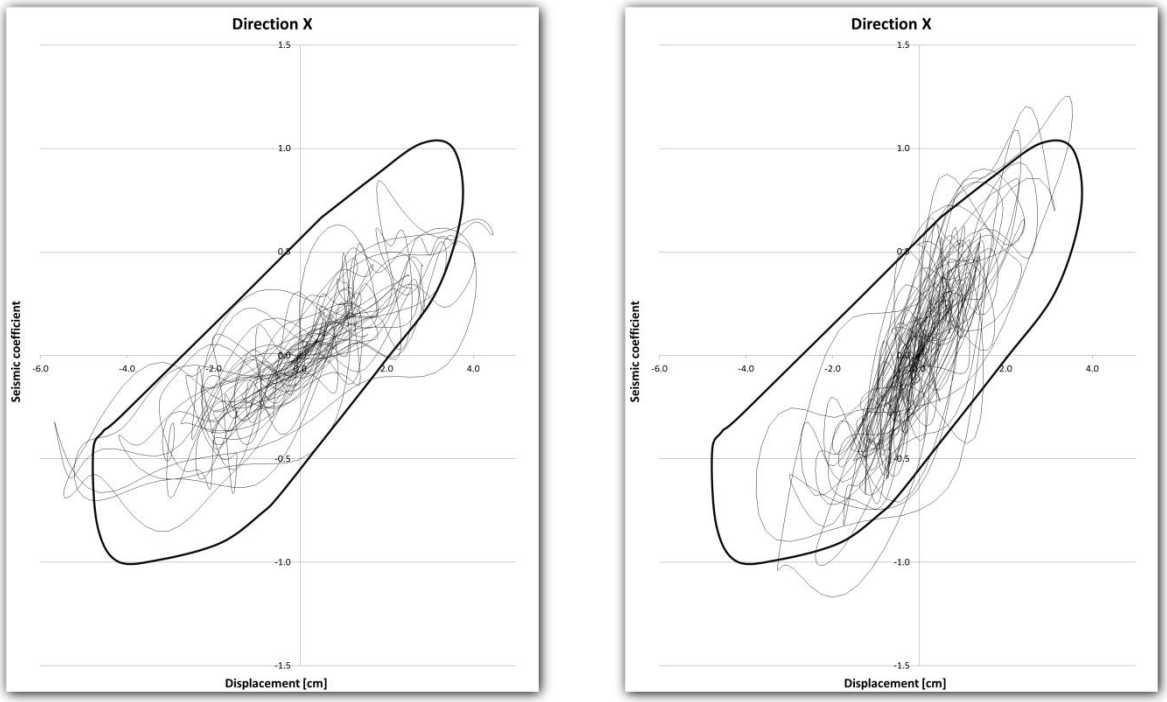

(a) (b)

Figure 99 - Envelopes comparing the reference model with 0.5xE (a) and 2xE (b) in direction X in the gabble wall.

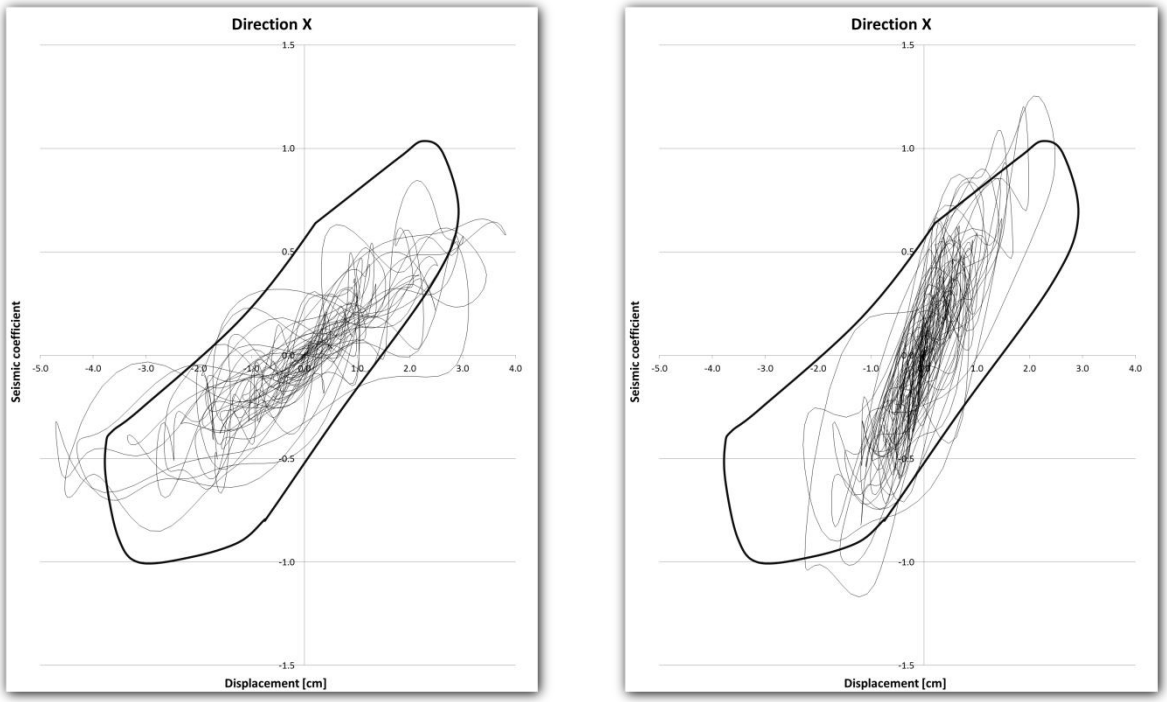

(a) (b)

Figure 100 - Envelopes comparing the reference model with 0.5xE (a) and 2xE (b) in direction X in the façade.

The comparison of the envelopes for the Z direction is shown in the Figure 101 for the gabble wall and in the Figure 102 for the façade. The stiffness of the masonry does not affect the way that the gabble wall responds to the earthquake; only changes in the peak values are noticeable. When the stiffness is reduced the displacements increase and they decrease when the value of the stiffness is augmented for very similar seismic coefficients. In the façade the behaviour has a regular shape for 0.5xE, with a significant increase of displacements. The wall is now able to bear large displacements without increment of seismic coefficient and lower energy dissipation. For 2xE the response changes, with slightly lower maximum displacements and considerable energy dissipation, which probably indicates larger damage.

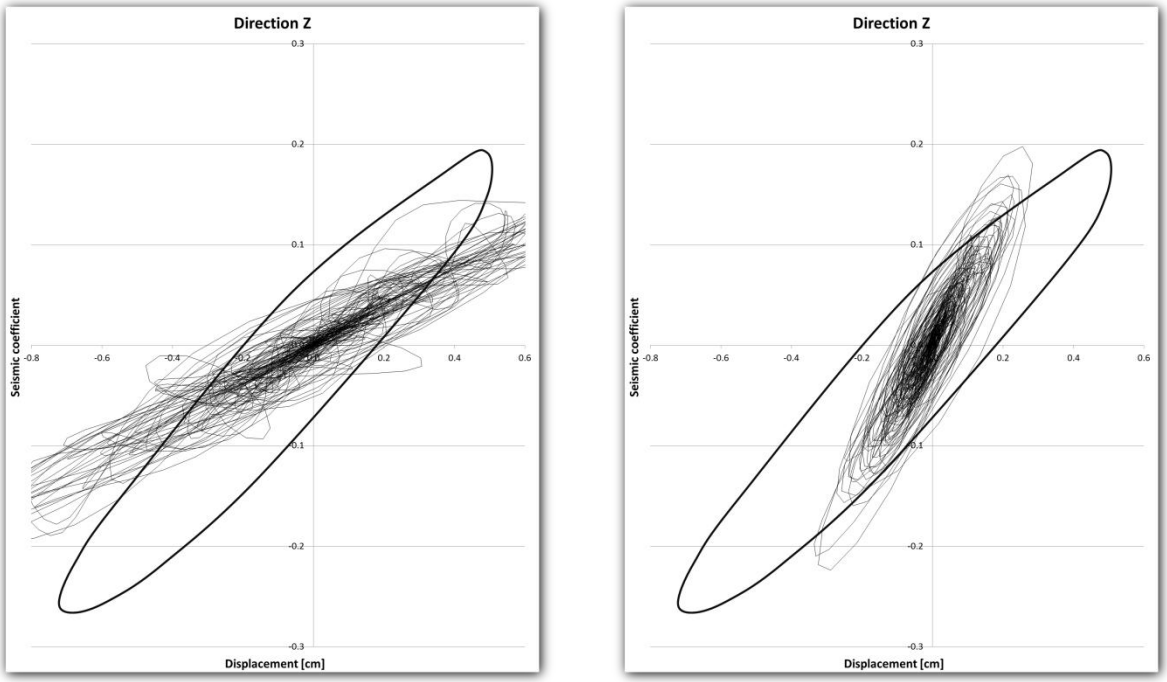

(a) (b)

Figure 101 - Envelopes comparing the reference model with 0.5xE (a) and 2xE (b) in direction Z in the gabble wall.

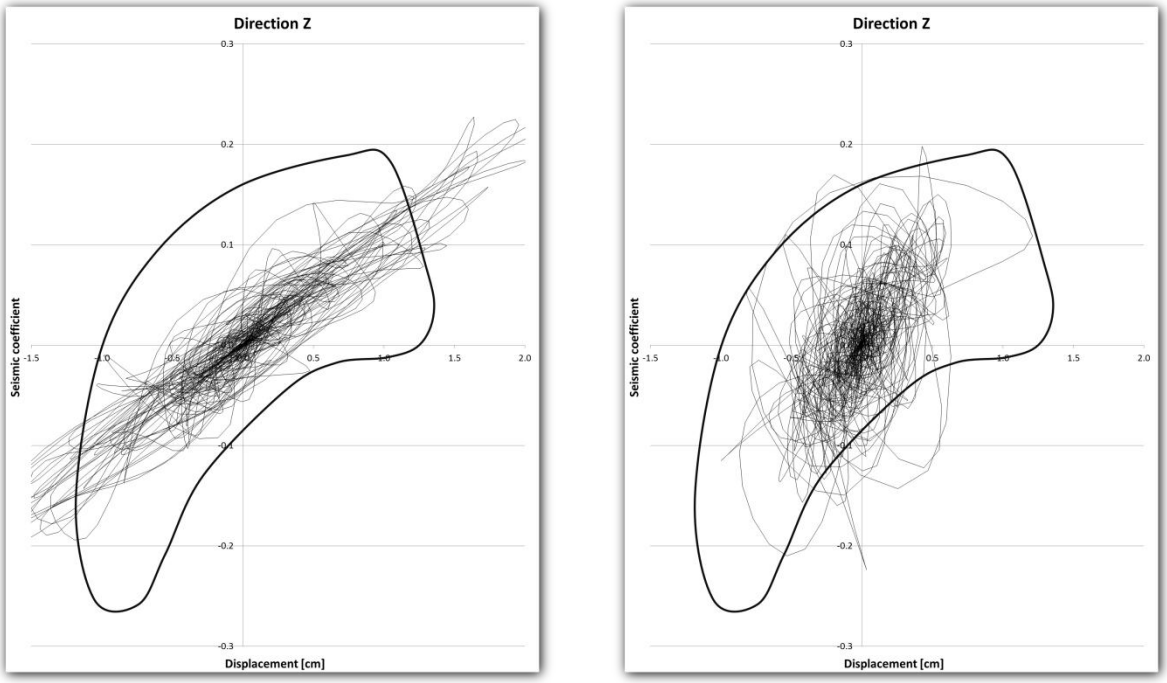

(a) (b)

Figure 102 - Envelopes comparing the reference model with 0.5xE (a) and 2xE (b) in direction Z in the façade.

3.3 Damping ratio.

The configuration of the graphs with the different damping ratios is similar to the previous examples. Two different calculations are shown to be compared with the reference model. Firstly, the damping parameters are changed in order to obtain the half (0.5xDamping) of the reference damping ratio and the double one (2xDamping). The envelopes for the X direction can be seen in the Figure 103 for the gabble wall and in the Figure 104 for the façade. Based on them, it is possible to say that the damping ratio has a small effect on the response of the structure. The shape of the envelope is pretty much the same and the maximum values do not vary a lot. The damping ratio produces a small variation of displacements and it does not affect the seismic coefficient. The reason could be, again, the low range of loads applied to the building, even if damping is also of influence for elastic results.

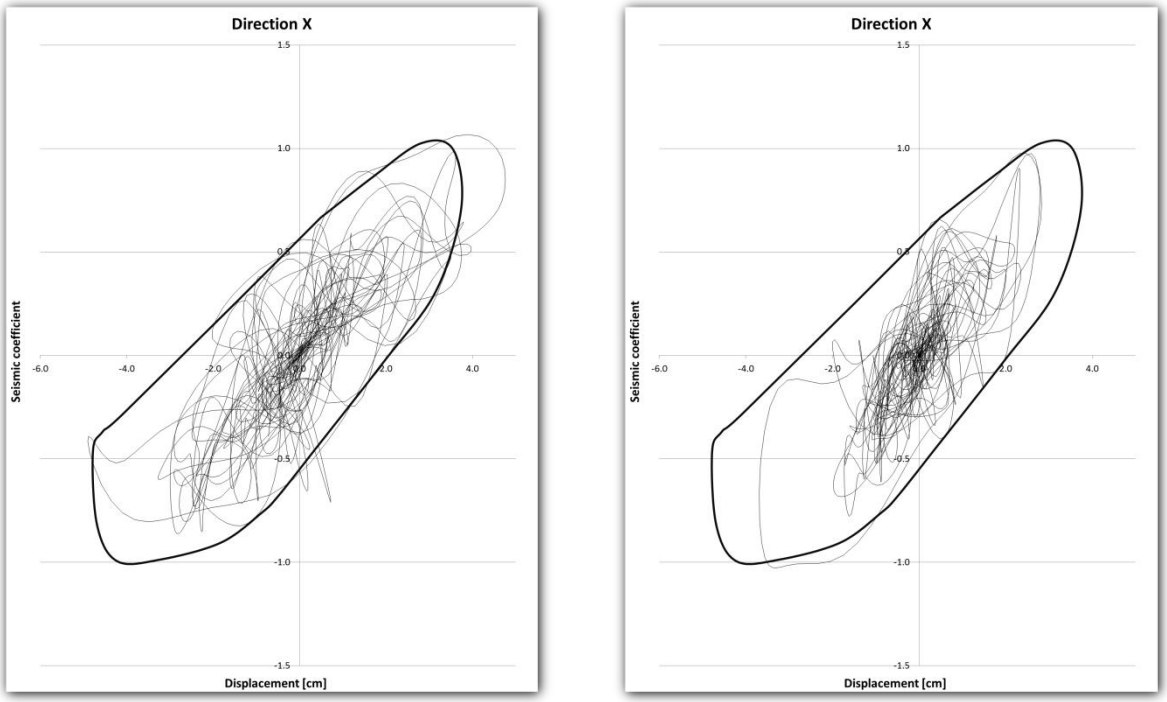

(a) (b)

Figure 103 - Envelopes comparing the reference model with 0.5xDamping (a) and 2xDamping (b) in direction X in the gabble wall.

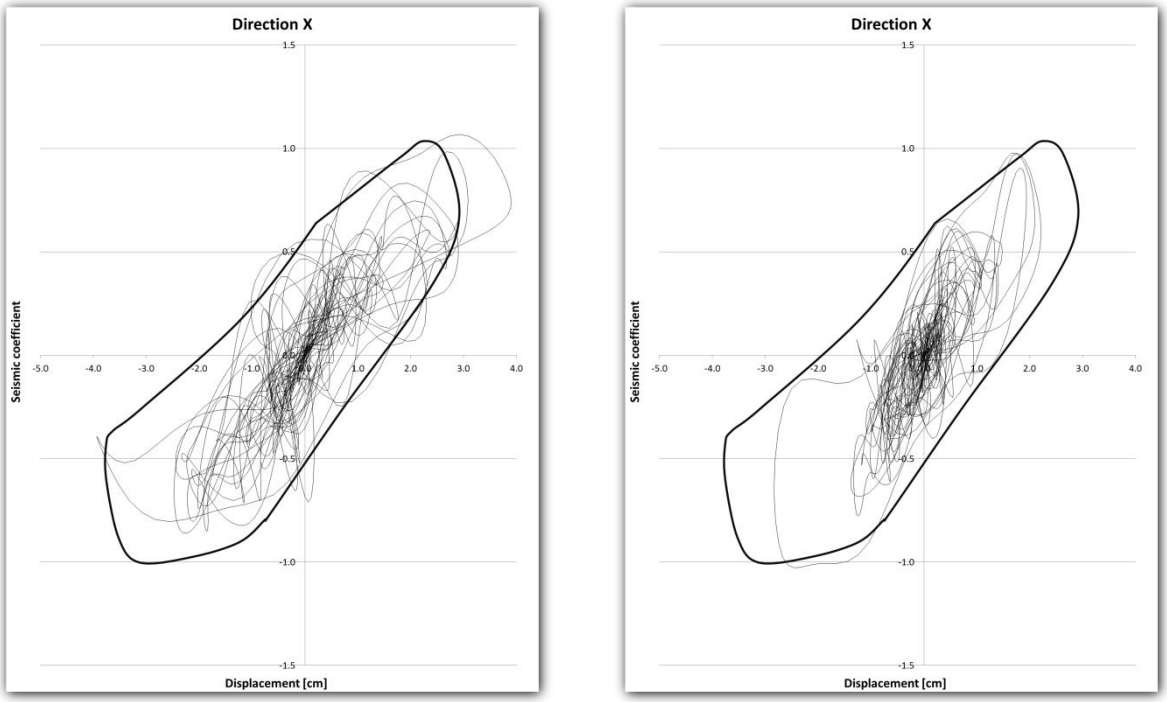

(a) (b)

Figure 104 - Envelopes comparing the reference model with 0.5xDamping (a) and 2xDamping (b) in direction X in the façade.

The envelopes in the direction Z are shown in the Figure 105 and Figure 106. The damping ratio has moderate influence in the results obtained from the calculations, but larger than in the X direction. The shape of the envelopes is the same and only the peak values vary a bit. When the damping ratio is half there is less dissipation with the movement of the building, so displacements and seismic coefficient are bigger. On the contrary, when the damping ratio is bigger more energy is dissipated by damping; displacements and seismic coefficient are smaller. The maximum displacement can reduce up to 35%, when damping is increased to the double.

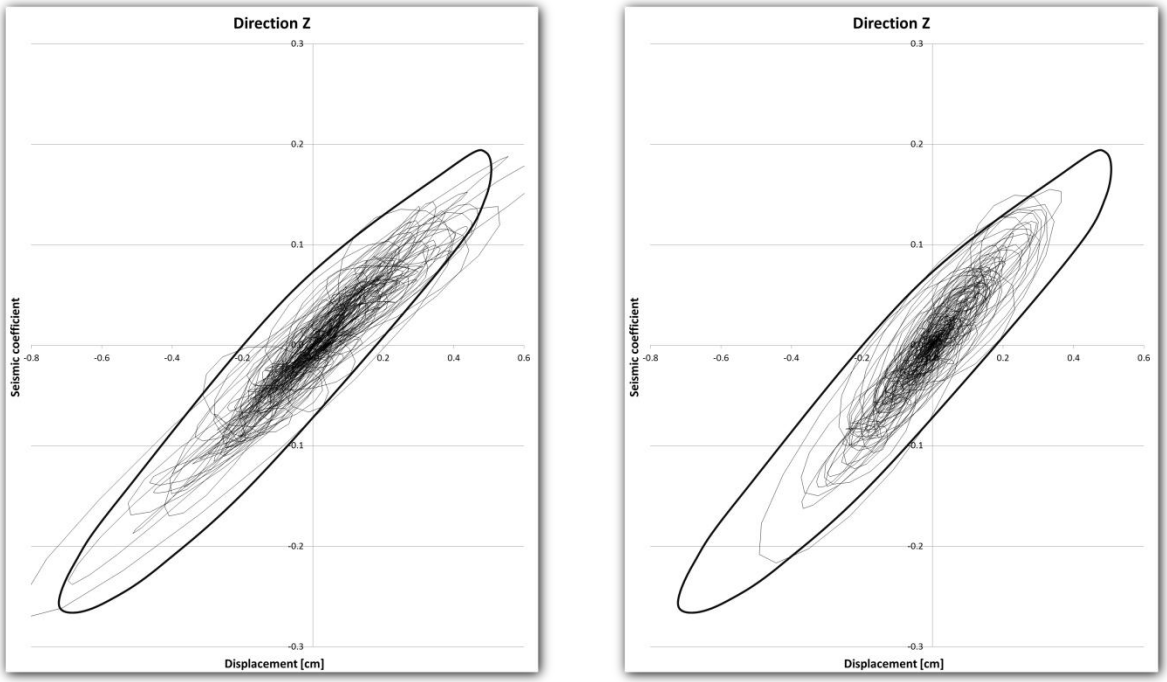

(a) (b)

Figure 105 - Envelopes comparing the reference model with 0.5xDamping (a) and 2xDamping (b) in direction Z in the gabble wall.

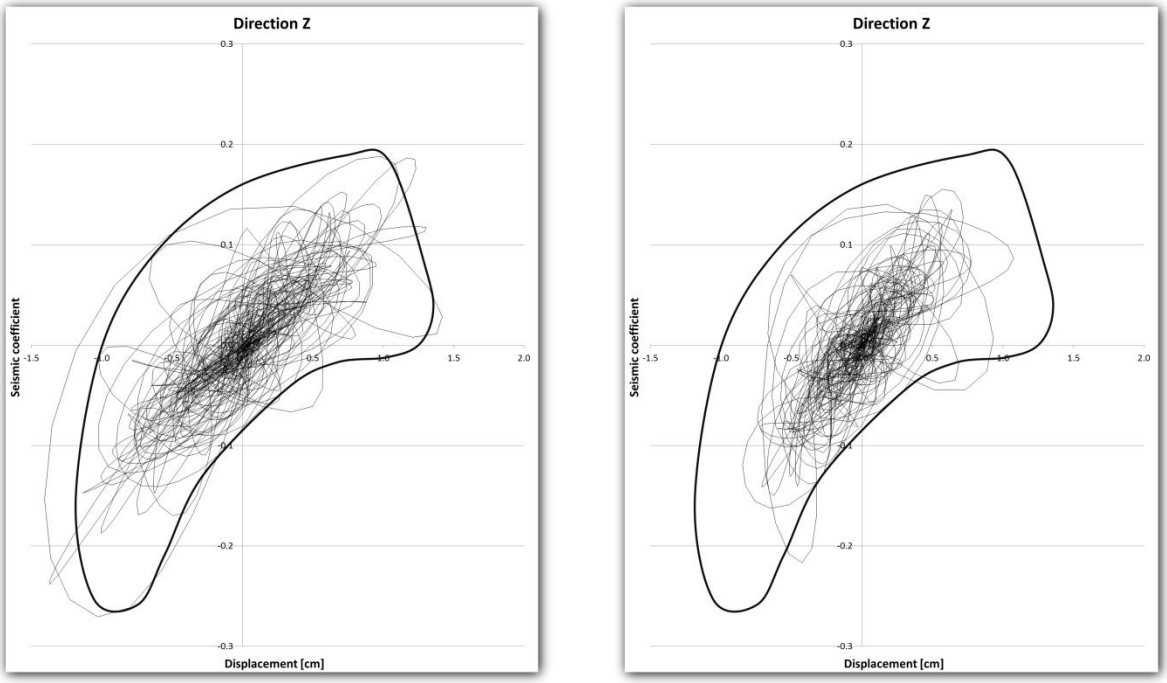

(a) (b)

Figure 106 - Envelopes comparing the reference model with 0.5xDamping (a) and 2xDamping (b) in direction Z in the façade.

3.4 Tensile strength

Two different calculation results are performed; with half strength (0.5xFt) and with double strength (2xFt). The comparison between reference model and 0.5xFt and 2xFt can be seen in the Figure 107, a and b respectively, for the direction X in the gabble wall. The graphs for the façade can be seen in the Figure 108. The variation of tensile strength has very moderate influence in the response of the building, due to the low range of loads applied to the structure. The response in this direction is basically the same than for the reference model, only the peak values vary a bit.

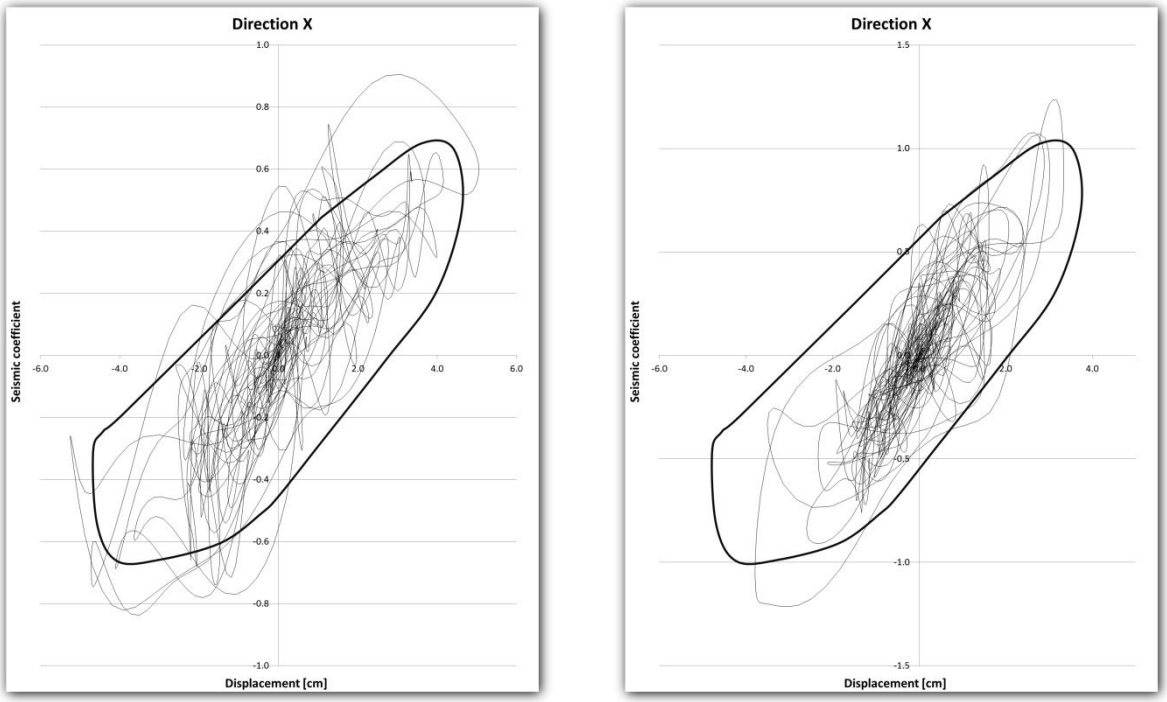

(a) (b)

Figure 107 - Envelopes comparing the reference model with 0.5xFt (a) and 2xFt (b) in direction X in the gabble wall.

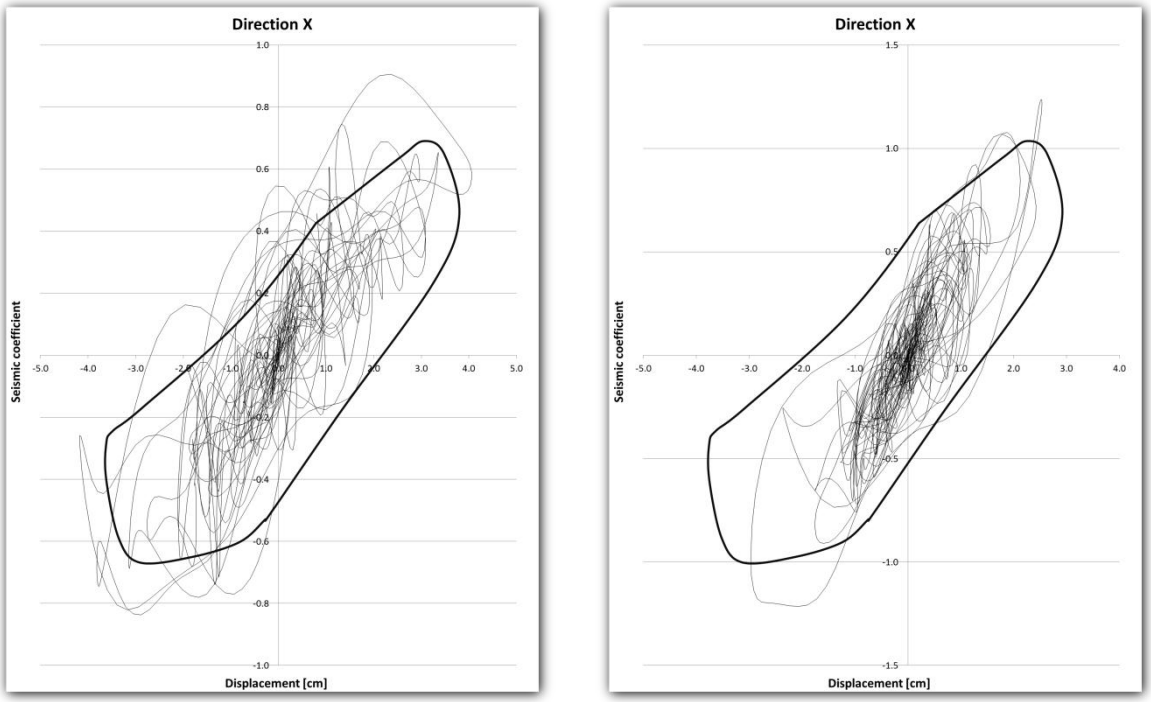

(a) (b)

Figure 108 - Envelopes comparing the reference model with 0.5xFt (a) and 2xFt (b) in direction X in the facade.

The envelopes showing the comparison between the reference model and the 0.5xFt and 2xFt can be seen in the Figure 109, a and b respectively in the Z direction for the gabble wall and in the Figure 110 for the façade. In this direction the influence of the tensile strength of the masonry is bigger than for the X direction, especially when it is decreased to the half, which seems rather strange but is partly corroborated in the results for the façade. In this case the displacements are smaller for a similar seismic coefficient.

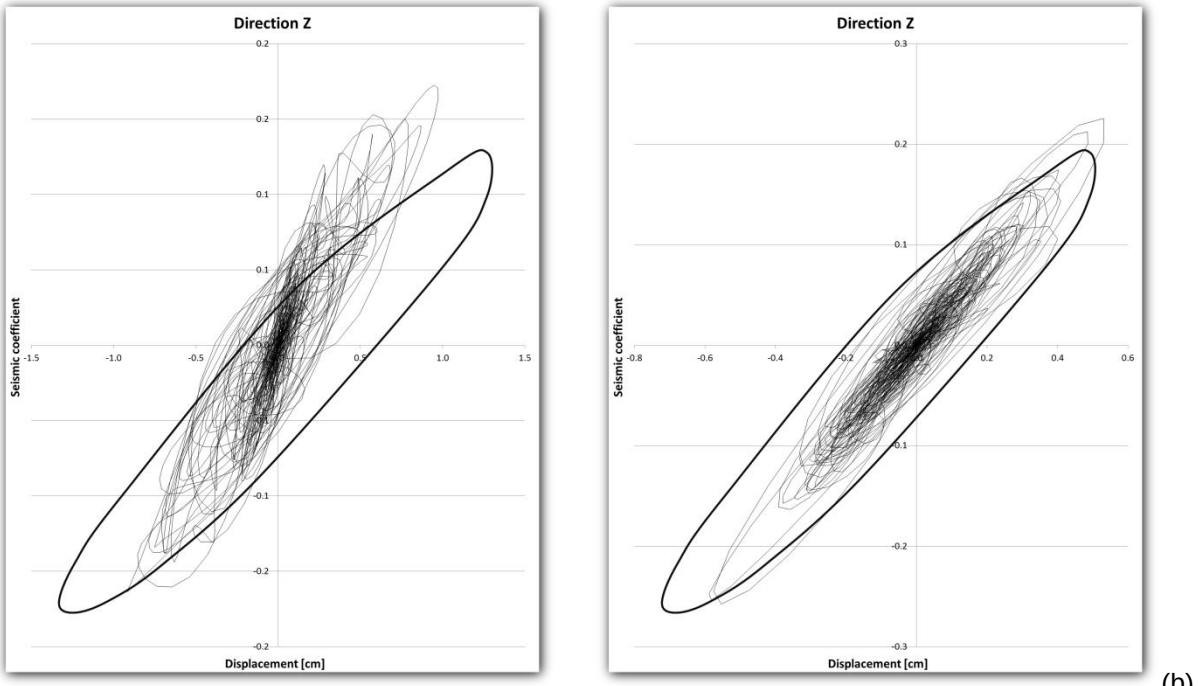

(a) (b)

Figure 109 - Envelopes comparing the reference model with 0.5xFt (a) and 2xFt (b) in direction Z in the gabble wall.

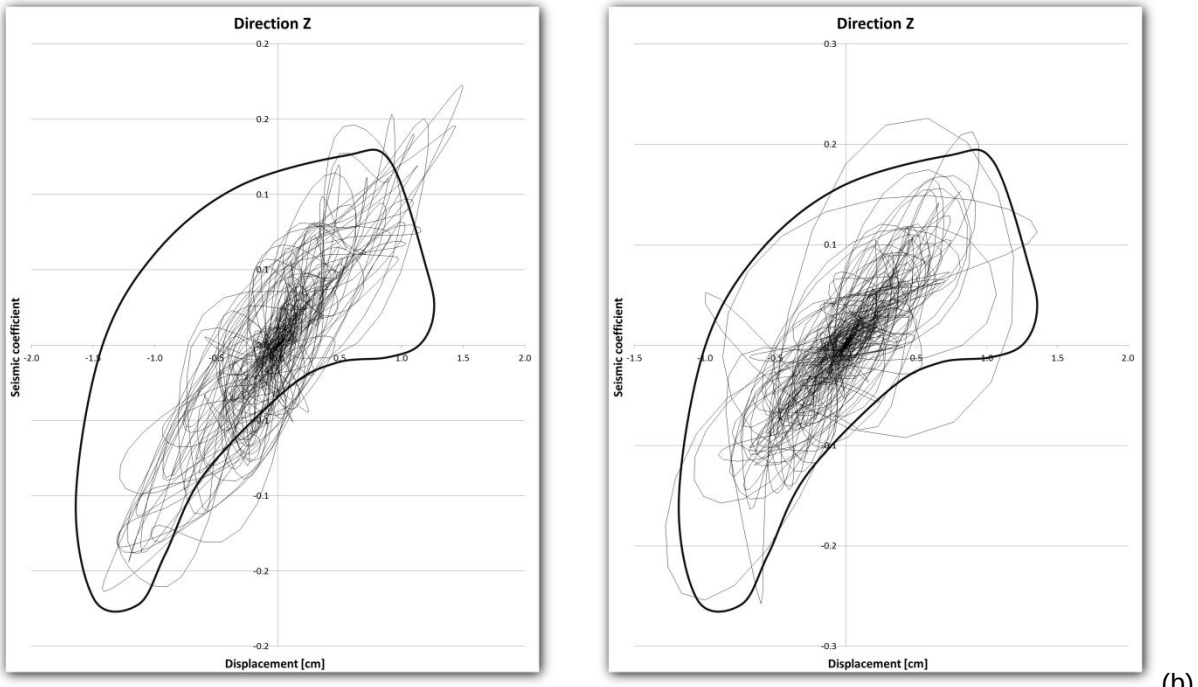

(a) (b)

Figure 110 - Envelopes comparing the reference model with 0.5xFt (a) and 2xFt (b) in direction Z in the gabble facade.

3.5 Fracture energy tensile.

Two different results are shown, one for half value of the fracture energy tensile (0,5xGft) and another one with double value (2xGft). The characteristics of the graphs are the same than for the previous results. The envelopes in the X direction in the gabble wall can be seen in the Figure 111 (a) for 0.5xGft and (b) for 2xGft. The same graphs for the façade can be seen in the Figure 112. The fracture energy tensile does not affect to the final behaviour, and a large variation is necessary. Both the shape and the peak values are almost exactly the same than for the reference. The loads should be increased more if some appreciable differences want to be obtained.

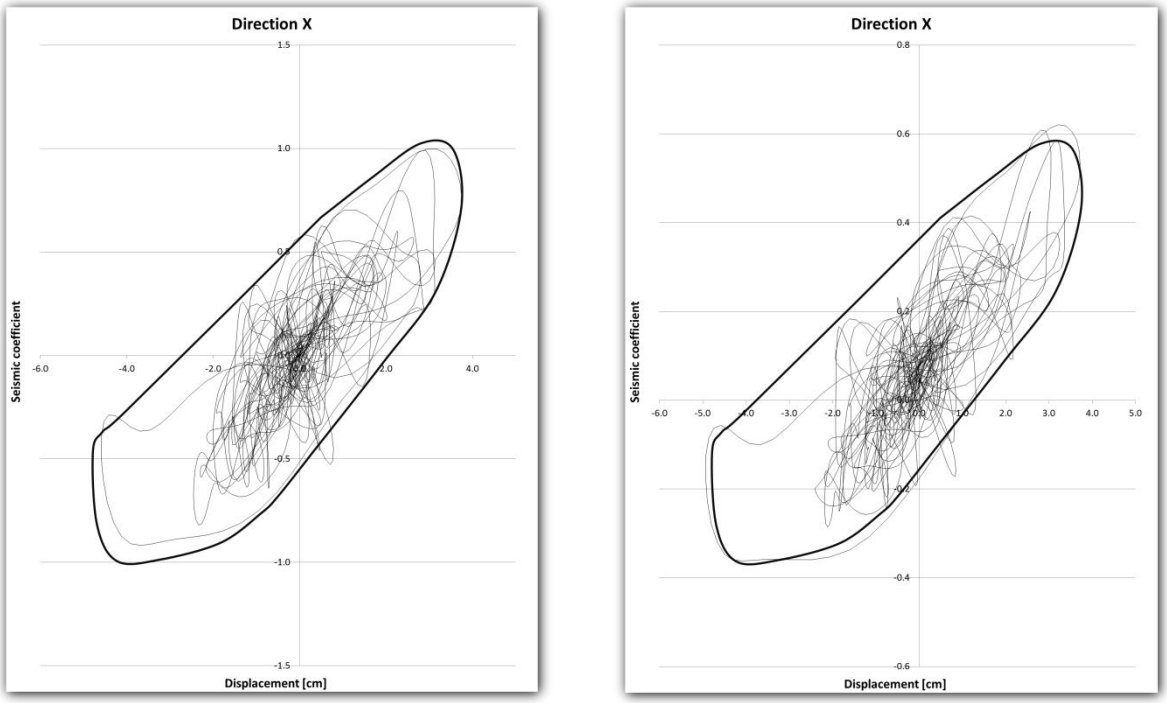

(a) (b)

Figure 111 - Envelopes comparing the reference model with 0.5xGft (a) and 2xGft (b) in direction X in the gabble wall.

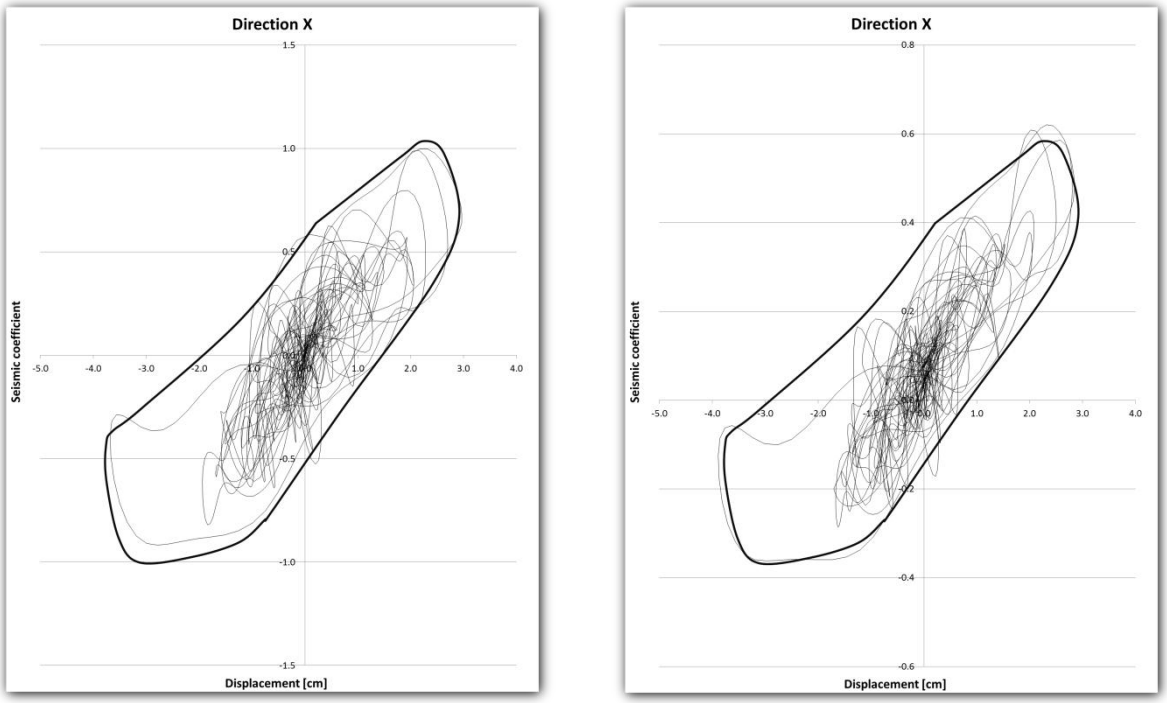

(a) (b)

Figure 112 - Envelopes comparing the reference model with 0.5xGft (a) and 2xGft (b) in direction X in the façade

The comparison in the direction Z between reference model and 0.5xGft (a) and 2xGft (b) can be seen in the Figure 113 for the gabble and in the Figure 114 for the façade. The decrease of fracture energy tensile does not have any effect in the response. However, when the fracture energy in augmented the influence is noticeable, which is again strange. The displacements are more less the same, but the seismic coefficient is reduced to the half.

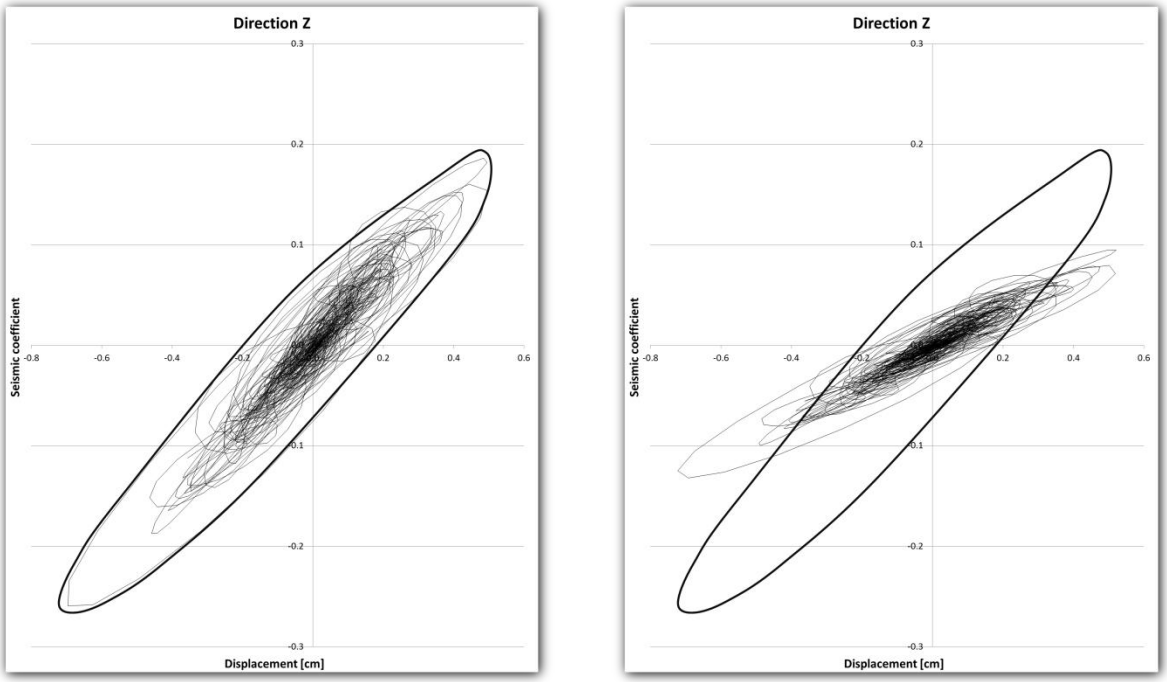

(a) (b)

Figure 113 - Envelopes comparing the reference model with 0.5xGft (a) and 2xGft (b) in direction Z in the gabble wall.

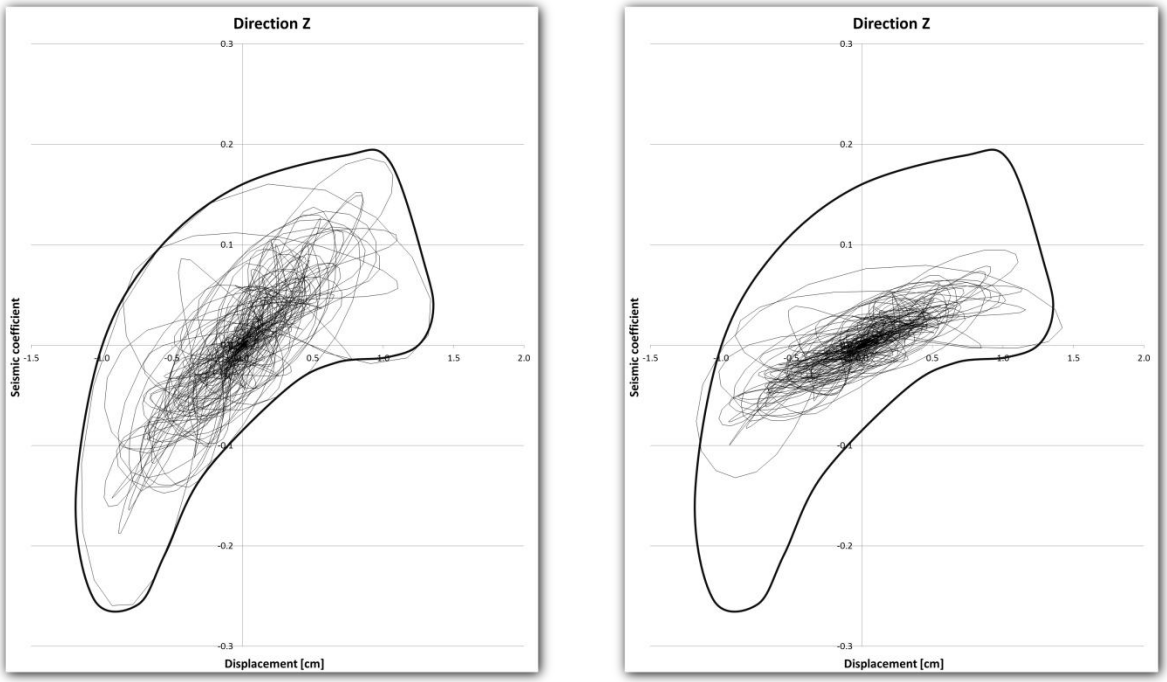

(a) (b)

Figure 114 - Envelopes comparing the reference model with 0.5xGft (a) and 2xGft (b) in direction Z in the façade.

4 ANNEX D – ENVELOPES FROM 300 % PGA EARTHQUAKE

4.1 Stiffness of the MDF panels

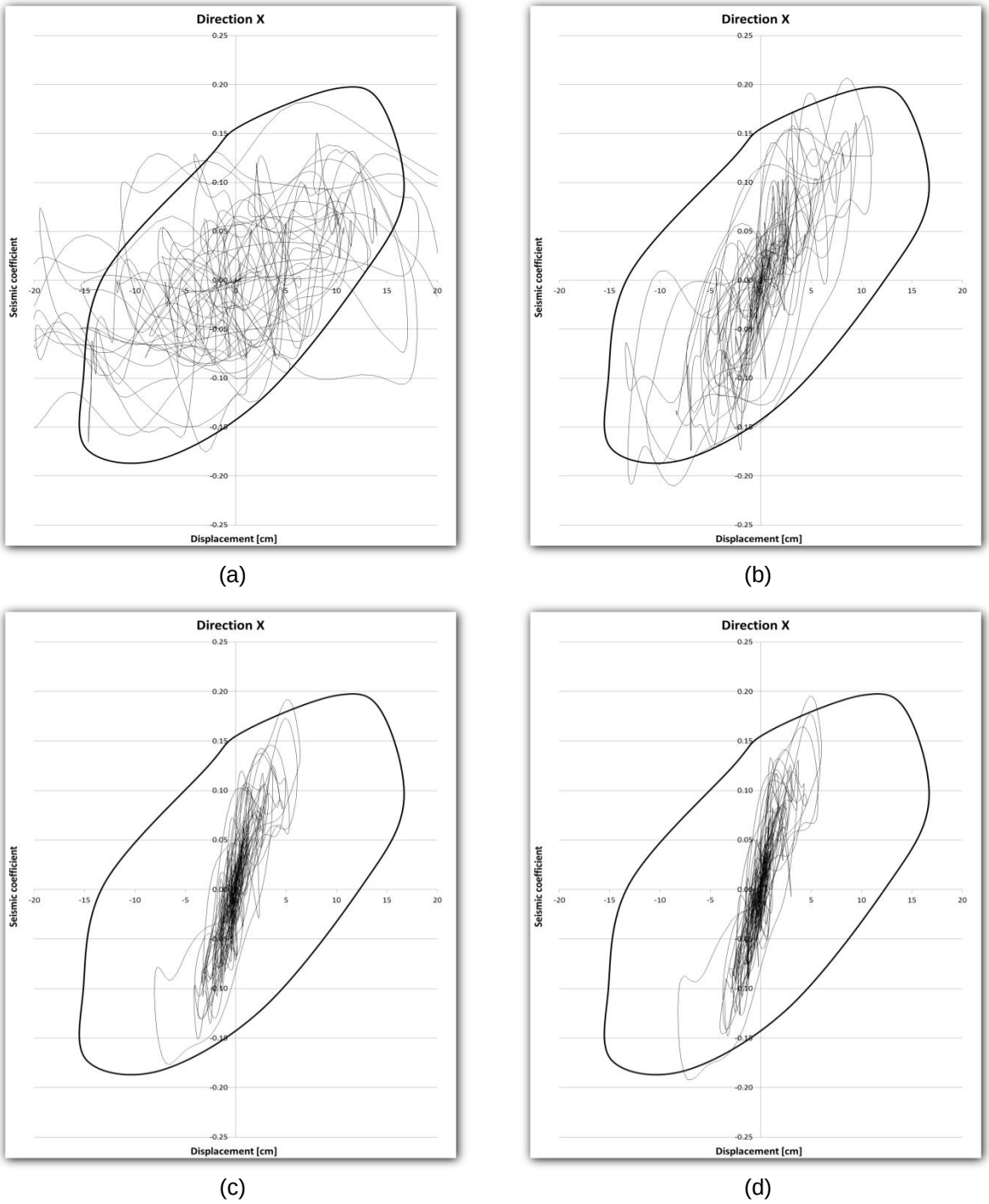

Figure 115 - Envelopes comparing the reference model with 0.1xE (a), 10xE (b), 100xE (c) and 1000xE (d) in direction X in the gabble wall.

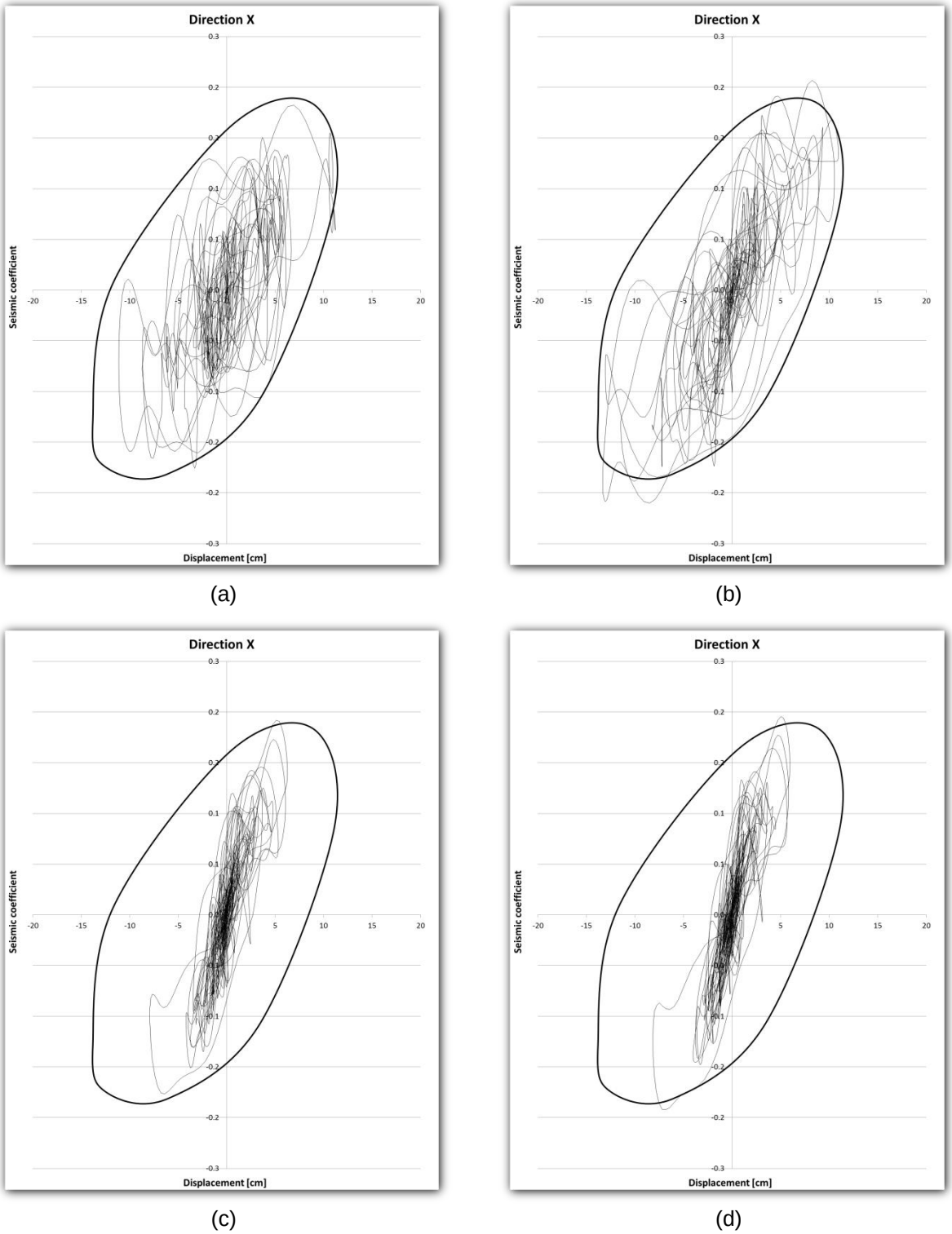

Figure 116 - Envelopes comparing the reference model with 0.1xE (a), 10xE (b), 100xE (c) and 1000xE (d) in direction X in the façade.

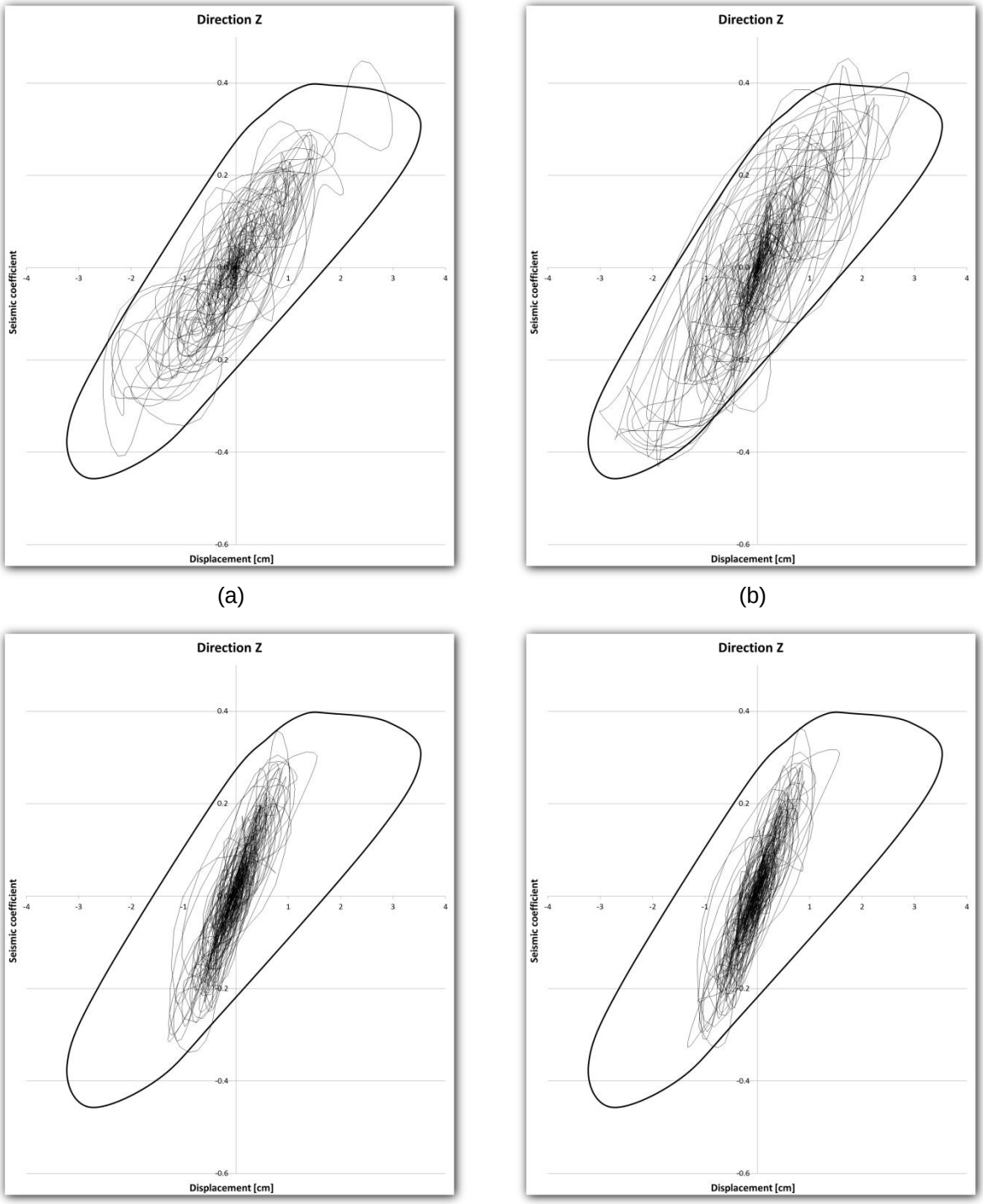

Figure 117 - Envelopes comparing the reference model with 0.1xE (a), 10xE (b), 100xE (c) and 1000xE (d) in direction Z in the gabble wall.

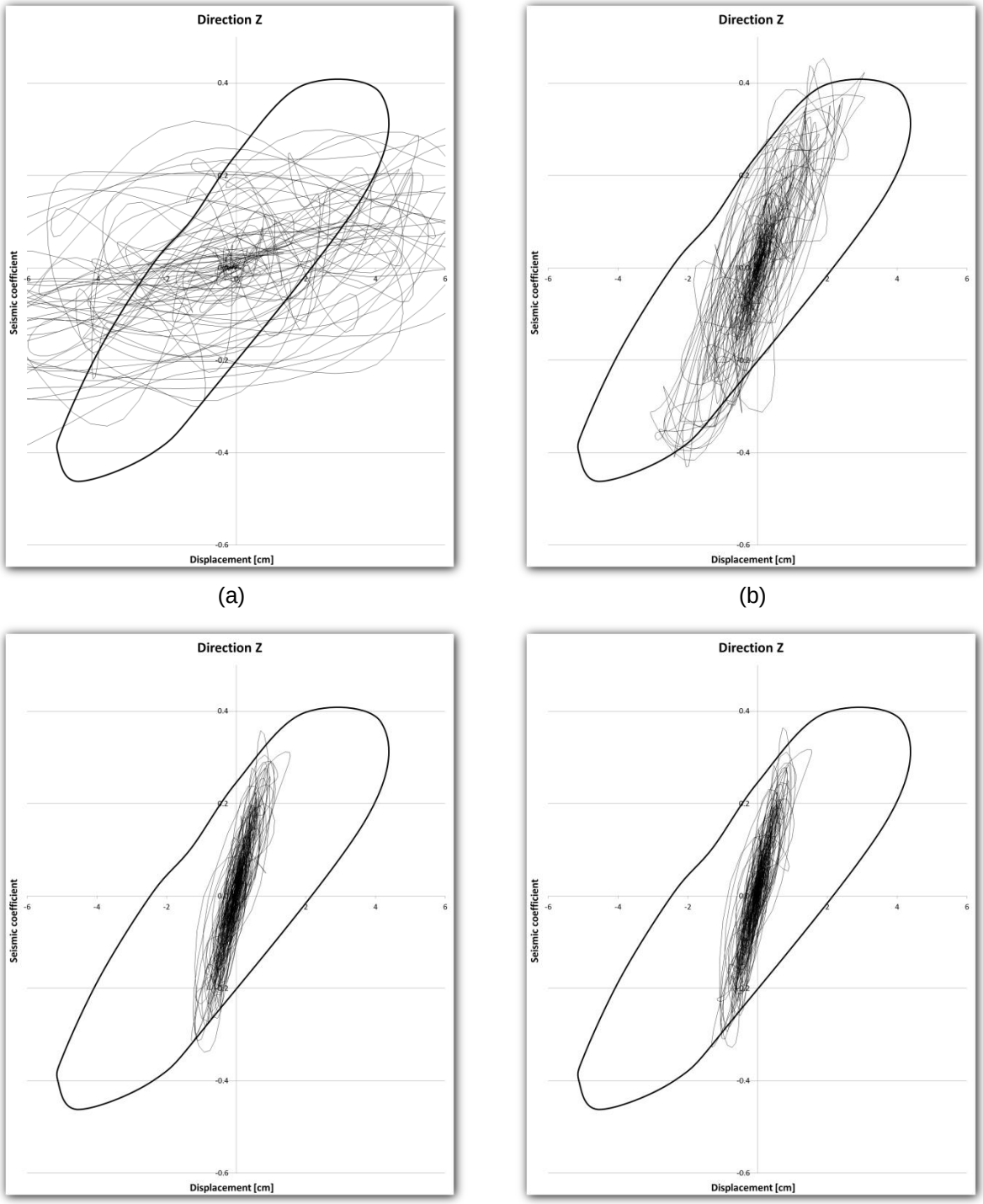

Figure 118 - Envelopes comparing the reference model with 0.1xE (a), 10xE (b), 100xE (c) and 1000xE (d) in direction Z in the façade.

4.2 Stiffness of the masonry

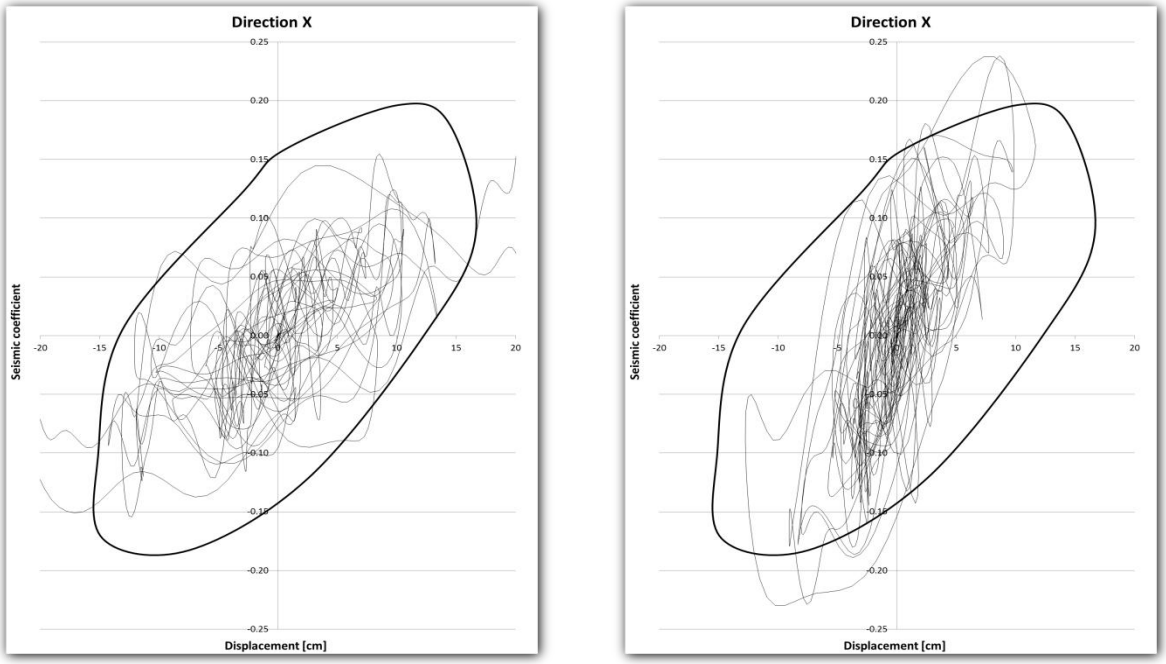

(a) (b)

Figure 119 - Envelopes comparing the reference model with 0.5xE (a) and 2xE (b) in direction X in the gabble wall.

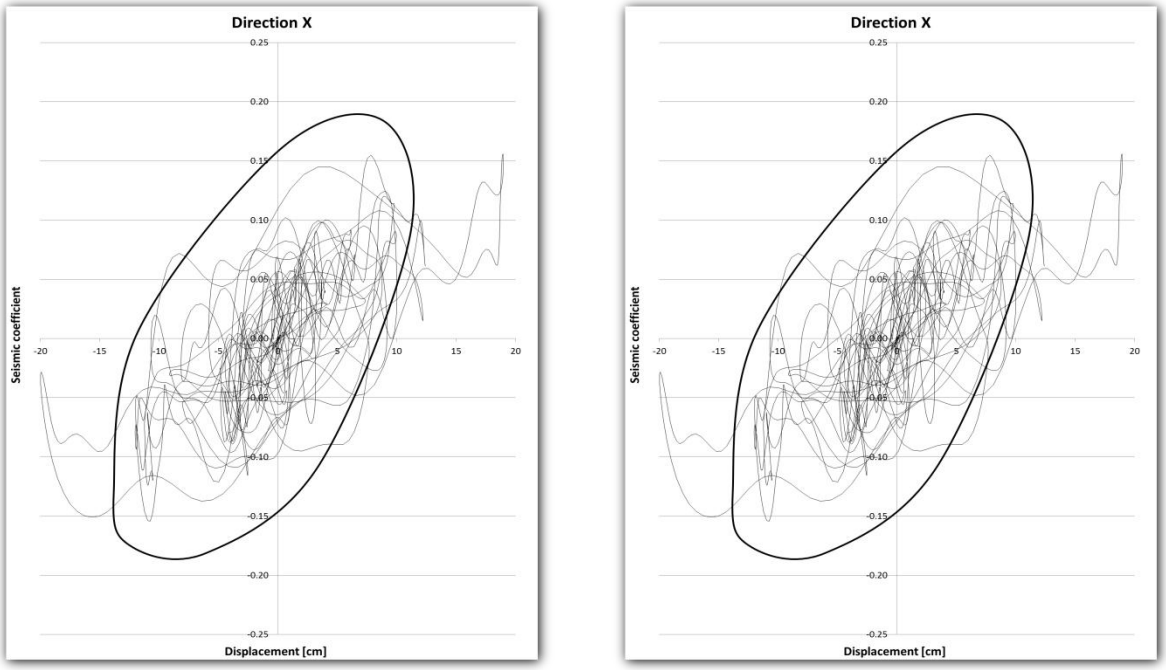

(a) (b)

Figure 120 - Envelopes comparing the reference model with 0.5xE (a) and 2xE (b) in direction X in the façade.

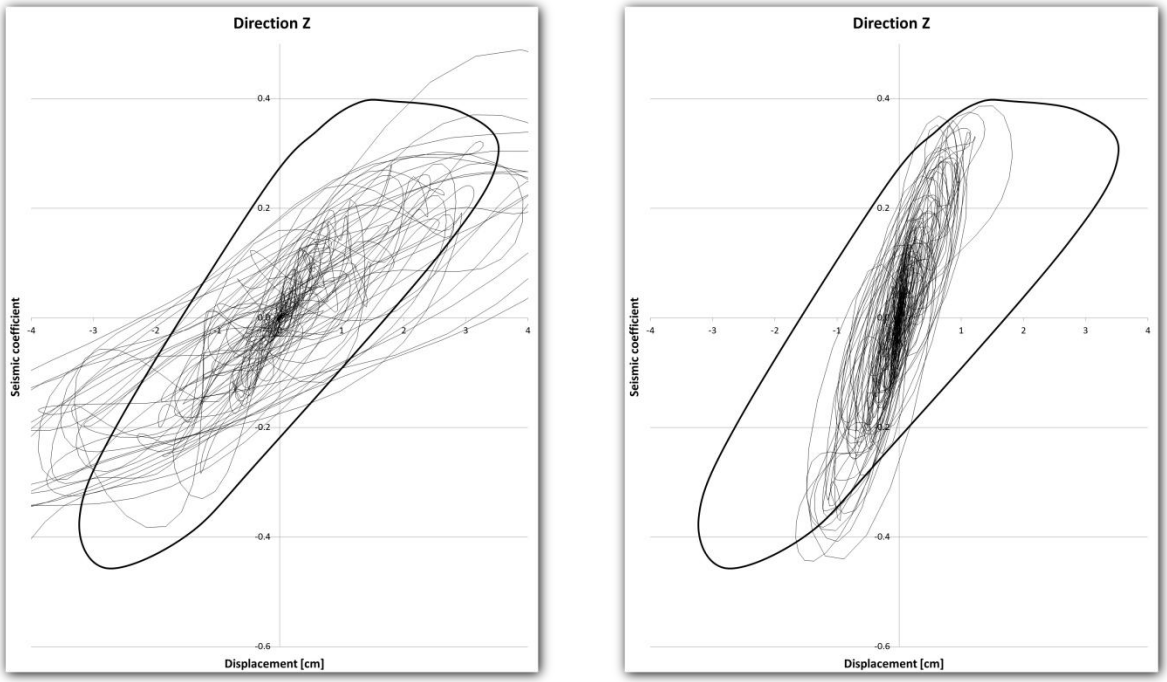

(a) (b)

Figure 121 - Envelopes comparing the reference model with 0.5xE (a) and 2xE (b) in direction Z in the gabble wall.

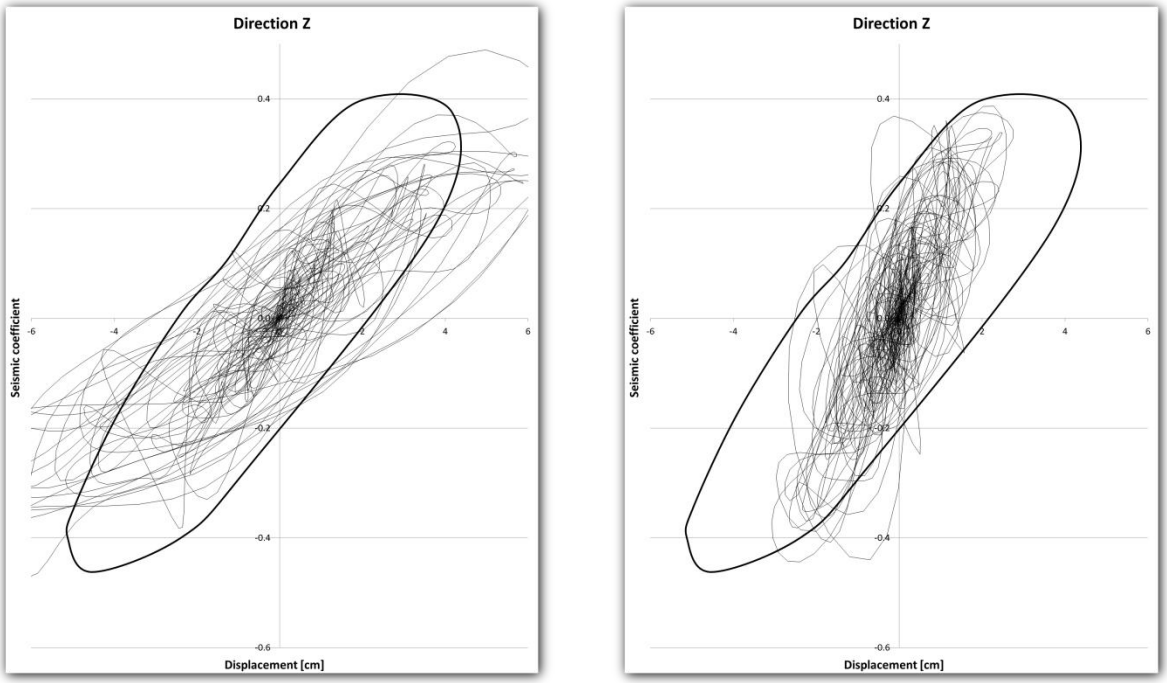

(a) (b)

Figure 122 - Envelopes comparing the reference model with 0.5xE (a) and 2xE (b) in direction Z in the façade.

4.3 Damping ratio

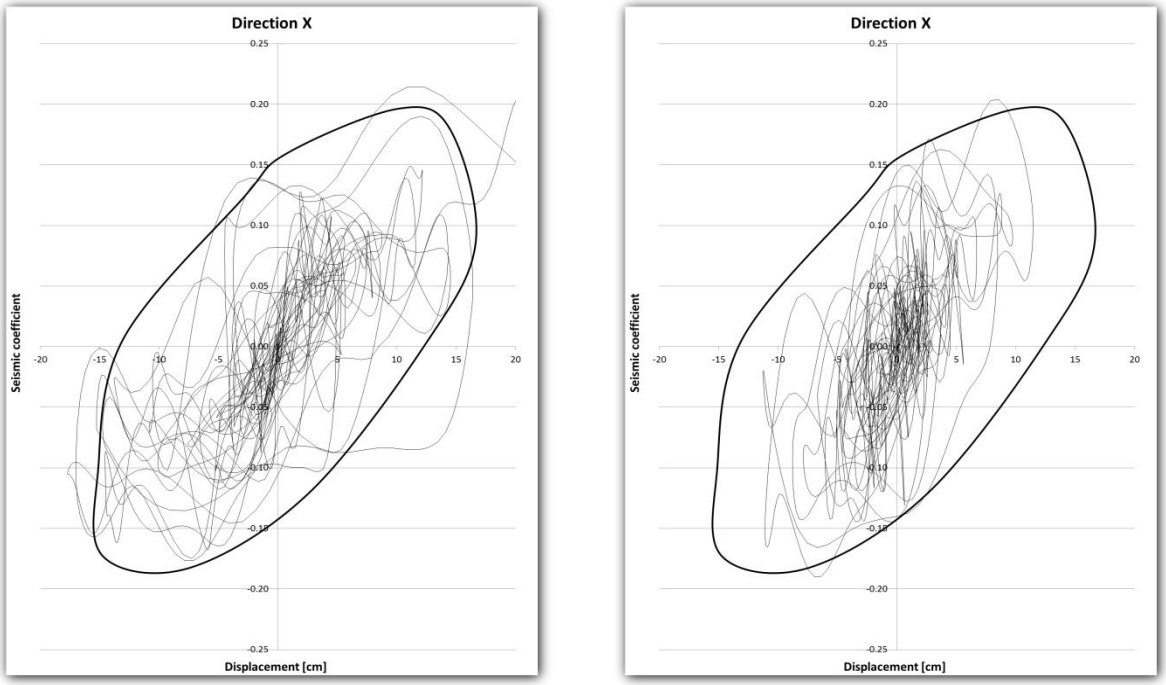

(a) (b)

Figure 123 - Envelopes comparing the reference model with 0.5xDamping (a) and 2xDamping (b) in direction X in the gabble wall.

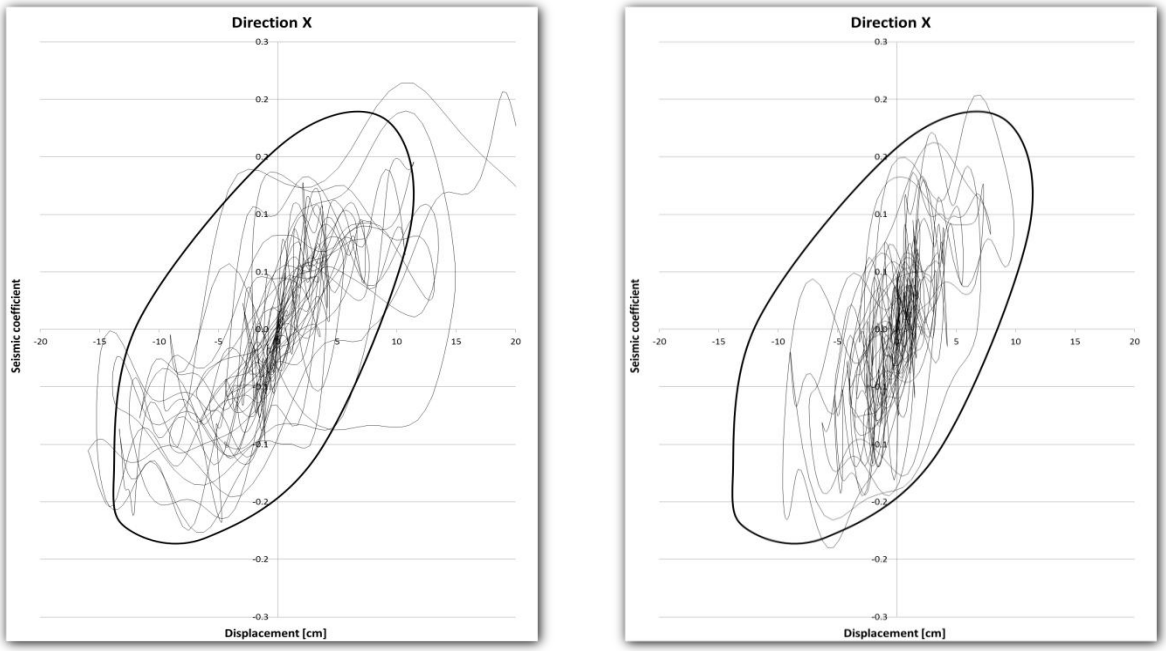

(a) (b)

Figure 124 - Envelopes comparing the reference model with 0.5xDamping (a) and 2xDamping (b) in direction X in the façade.

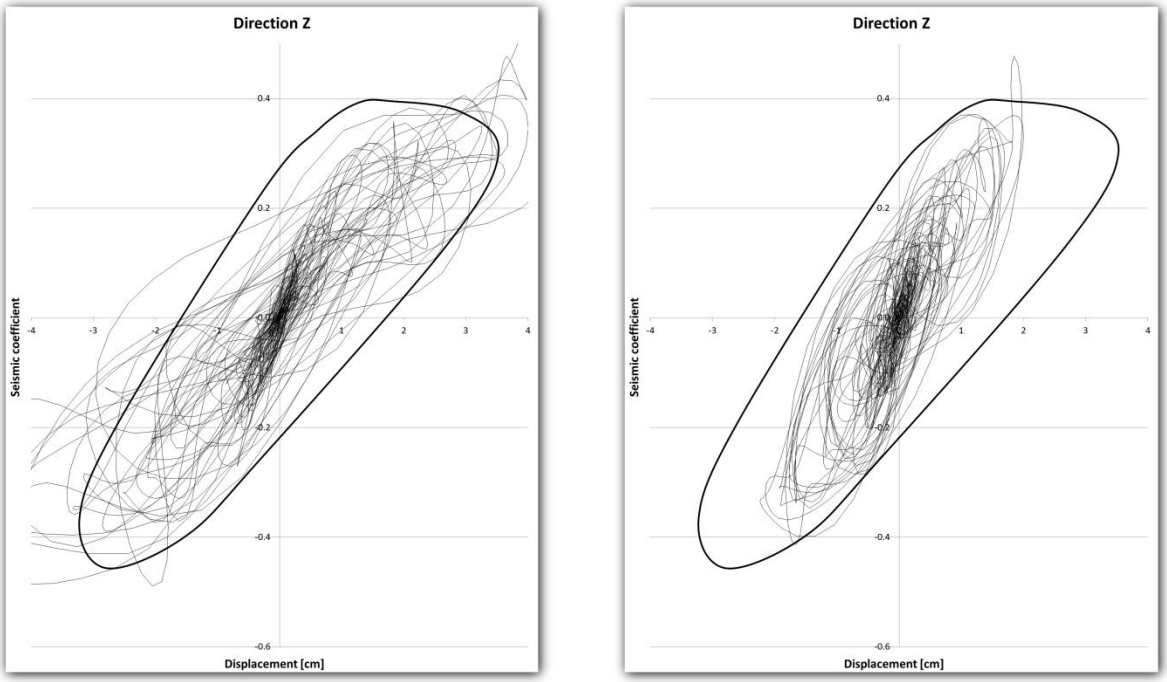

(a) (b)

Figure 125 - Envelopes comparing the reference model with 0.5xDamping (a) and 2xDamping (b) in direction Z in the gabble wall.

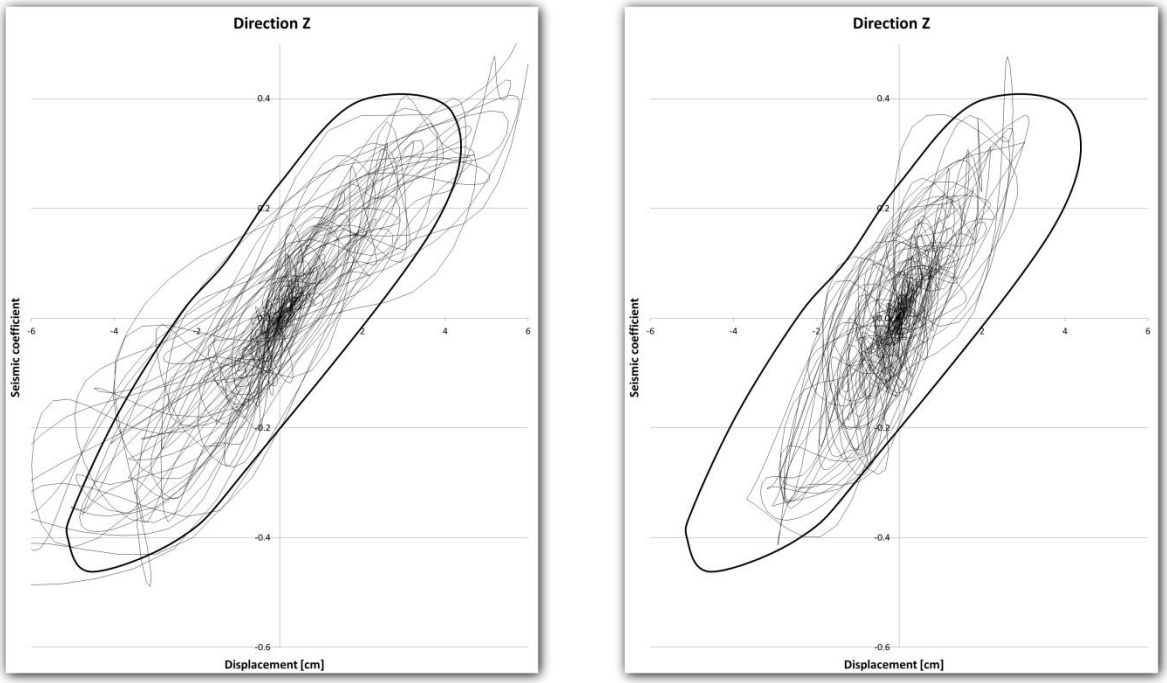

(a) (b)

Figure 126 - Envelopes comparing the reference model with 0.5xDamping (a) and 2xDamping (b) in direction Z in the façade.

4.4 Tensile strength

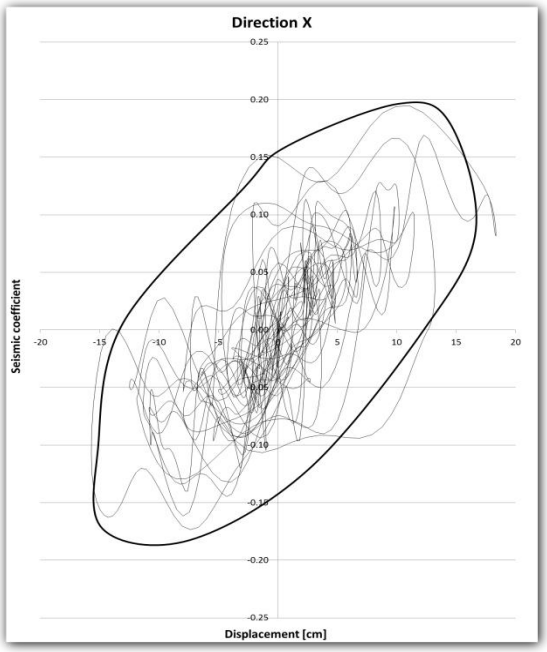

(a)

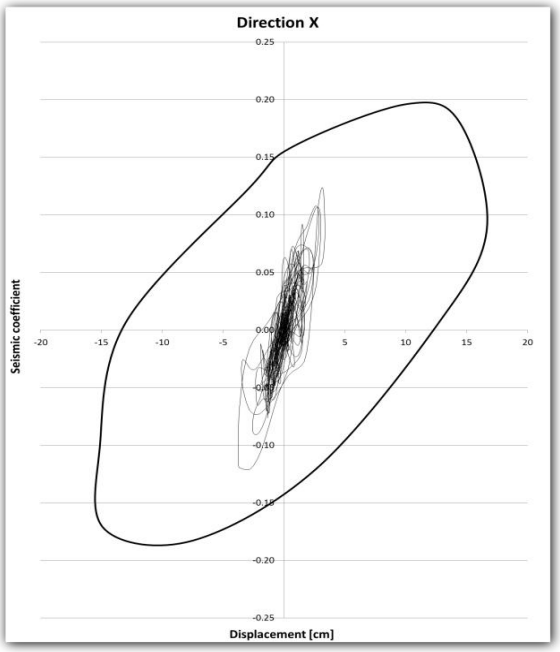

(b)

Figure 127 - Envelopes comparing the reference model with 0.5xFt (a) and 2xFt (b) in direction X in the gabble wall.

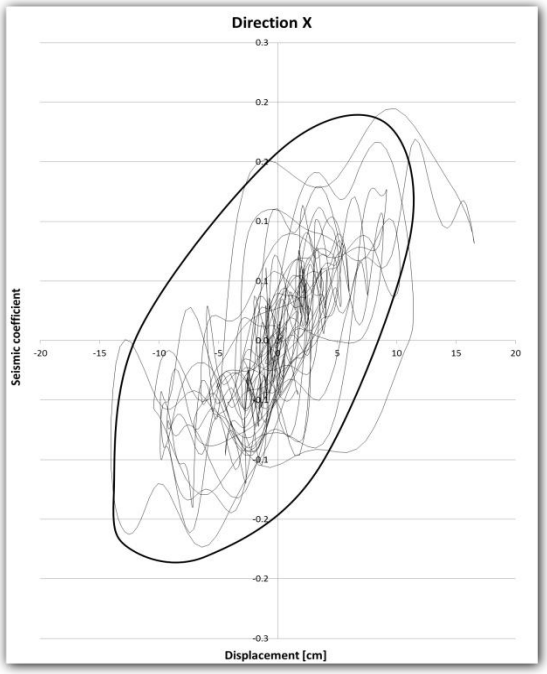

(a)

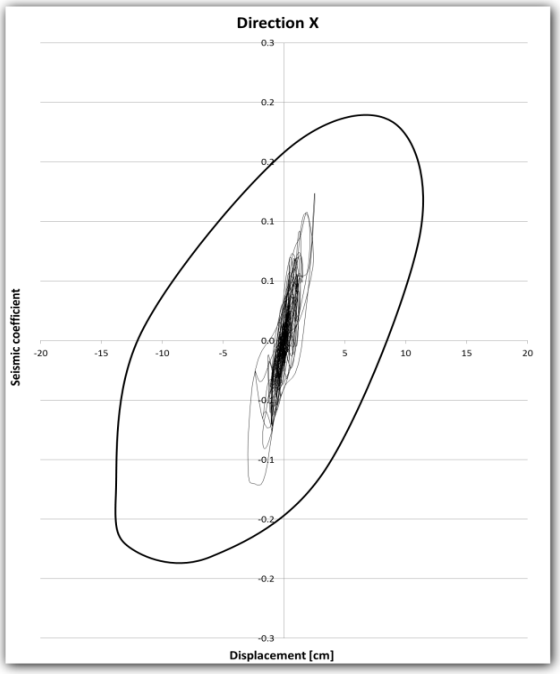

(b)

Figure 128 - Envelopes comparing the reference model with 0.5xFt (a) and 2xFt (b) in direction X in the façade.

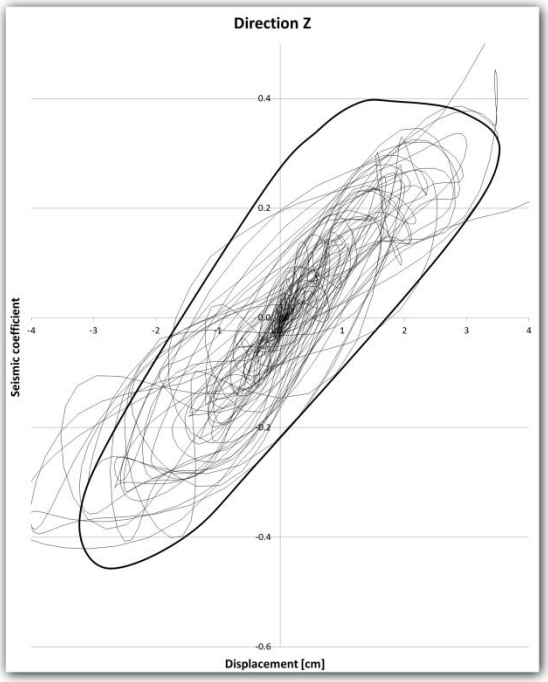

(a)

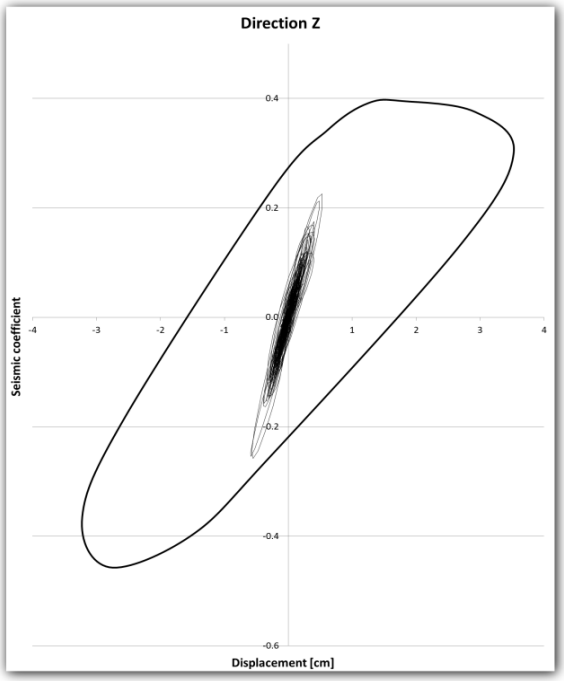

(b)

Figure 129 - Envelopes comparing the reference model with 0.5xFt (a) and 2xFt (b) in direction Z in the gabble wall.

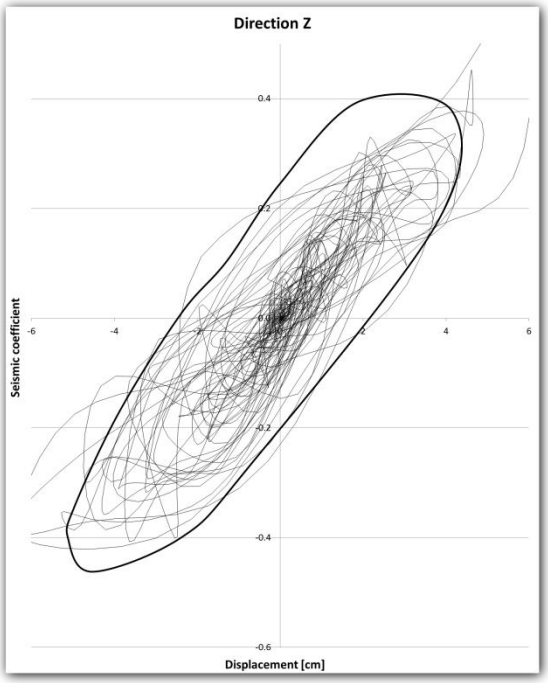

(a)

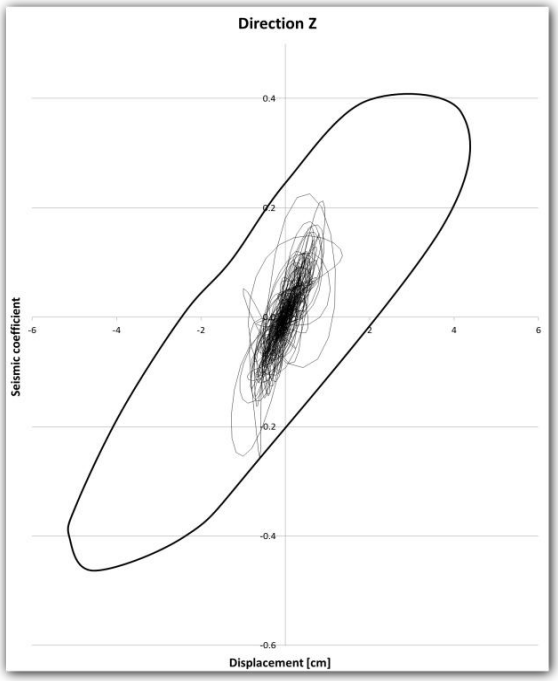

(b)

Figure 130 - Envelopes comparing the reference model with 0.5xFt (a) and 2xFt (b) in direction Z in the façade.

4.1 Fracture energy tensile

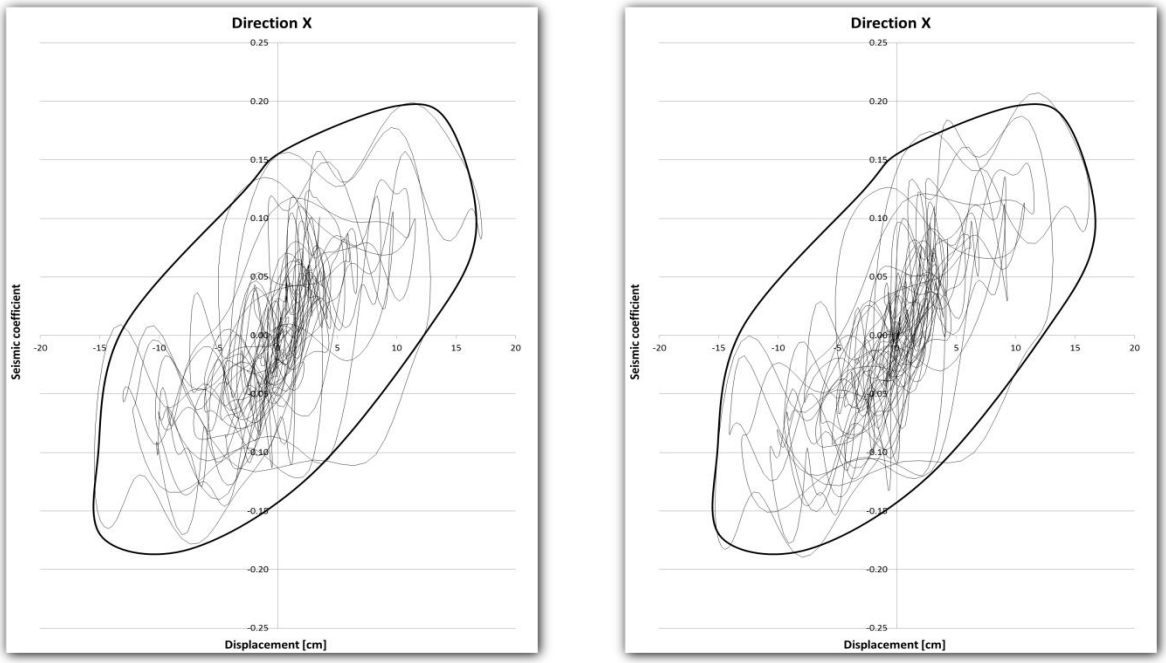

(a) (b)

Figure 131 - Envelopes comparing the reference model with 0.5xGft (a) and 2xGft (b) in direction X in the gabble wall.

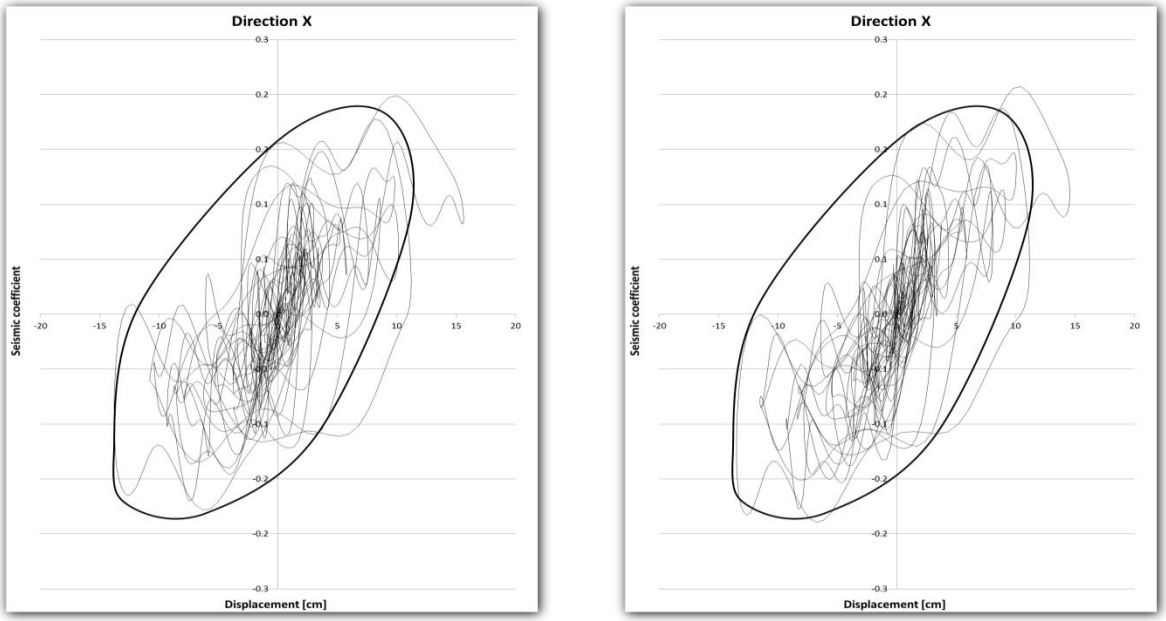

(a) (b)

Figure 132 - Envelopes comparing the reference model with 0.5xGft (a) and 2xGft (b) in direction X in the façade

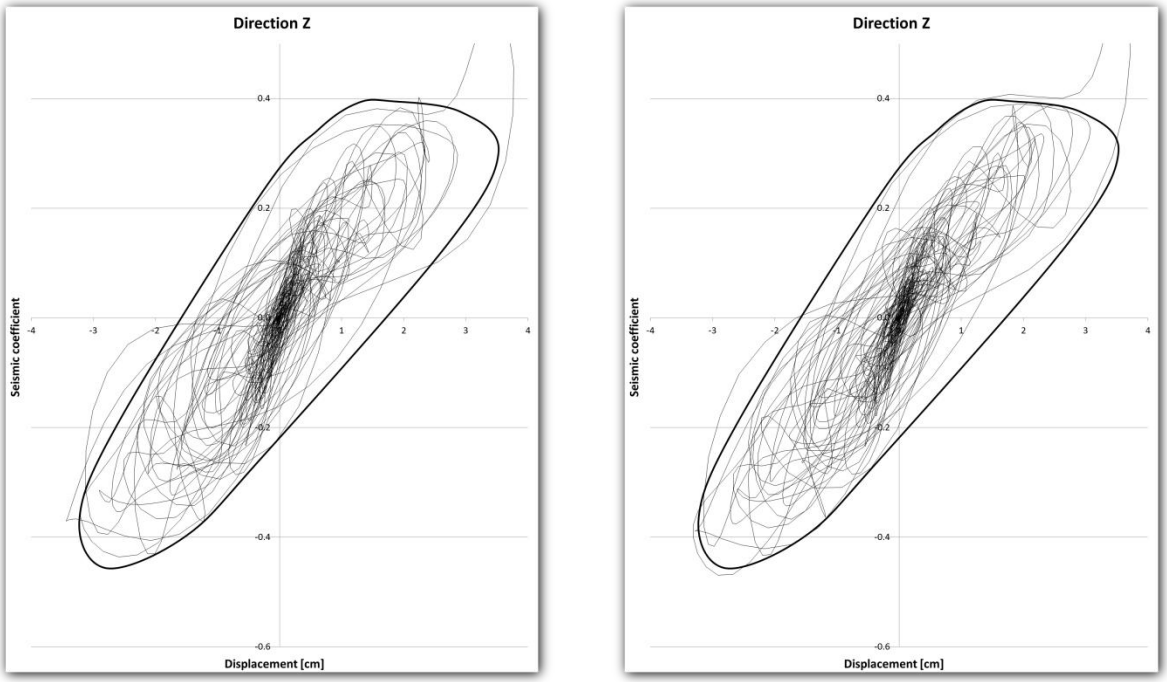

(a) (b)

Figure 133 - Envelopes comparing the reference model with 0.5xGft (a) and 2xGft (b) in direction Z in the gabble wall.

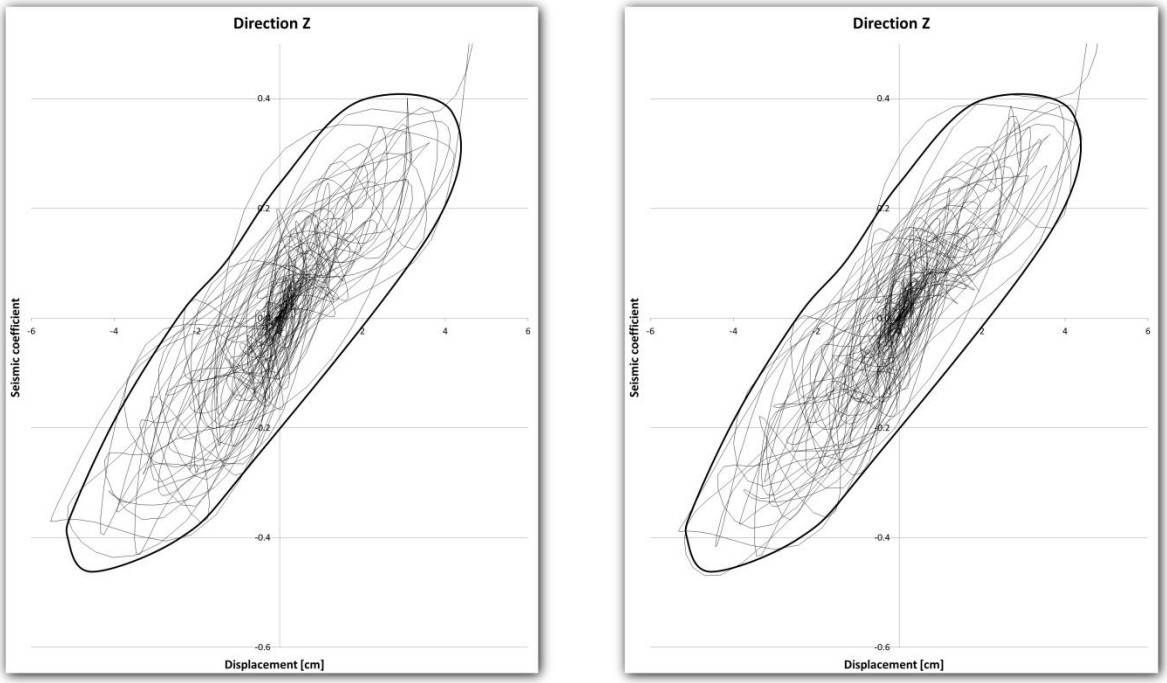

(a) (b)

Figure 134 - Envelopes comparing the reference model with 0.5xGft (a) and 2xGft (b) in direction Z in the façade.